1

AD-A134913

Department of Earth and Planetary Sciences
Massachusetts Institute of Technology
Cambridge, Massachusetts 02139

RESEARCH IN SEISMOLOGY

Semi-Annual Technical Report No. 5

Period Covered· 1 July 1977 - 31 December 1977

ARPA Order No. 1827

Program Code No. 5F10

Name of Contractor - M.I.T.

Effective Date of Contract - 1 June 1975

Contract Expiration Date: 30 September 1978

Amount of Contract: $500,000

Principal Investigators: M. Nafi Toksöz, 617/253-6382
Keiiti Aki, 617/253-6397
Sean C. Solomon, 617/253-3786

Program Manager - William J. Best, 202/694-5454

Short Title of Work - Research in Seismology

Sponsored by
Advanced Research Projects Agency
ARPA Order No. 1827

DTIC FILE COPY

DTIC
S ELECTE D
NOV 23 1983
E

APPROVED FOR PUBLIC RELEASE
DISTRIBUTION UNLIMITED

83 11 22 130

SUMMARY

The research completed under the contract F44620-75-C-0064 "Research in Seismology" during the period 1 July 1977 - 31 December 1977 falls within the two broad topics of (1) Seismic source mechanisms and (2) Seismic wave propagation. The specific research tasks within each category have broad applicability to the problem of discrimination of earthquakes from underground nuclear explosions, with particular emphasis on the Asian continent.

Source mechanism investigations included detailed studies of several earthquakes in eastern Turkey from the standpoint of field and teleseismic observations and of precursory phenomena (Toksöz et al., 1977, 1978; Toksöz and Arpat, 1977). Wave propagation work included studies of attenuation mechanisms in rock (Johnston et al., 1978) and the application of a technique for simultaneous inversion of surface wave attenuation and phase velocity information to data from several continental and oceanic paths (Lee, 1977; Lee and Solomon, 1978).

Details of these studies are given in the preprints and abstracts in the following sections. A list of publications completed under the contract during the reporting period is also included.

2. SEISMIC SOURCE MECHANISMS

STUDIES OF PREMONITORY PHENOMENA PRECEDING TWO LARGE EARTHQUAKES IN EASTERN TURKEY

M. Nafi Toksöz (Dept. of Earth and Planetary Sciences, Massachusetts Institute of Technology, Cambridge, Mass. 02139)
Esen Arpat (M.T.A. Institute, Ankara, Turkey)

Two destructive earthquakes occurred in Eastern Turkey on 5 September 1975 ($M_S = 6.7$) and 24 November 1976 ($M_S = 7.3$). On-site studies were carried out immediately after each earthquake. Both earthquakes had observable fault traces and many villages located directly over or very near the fault trace. The mechanism of the 1975 earthquake was a thrust (30 km fault length) and that of the 1976 earthquake was strike-slip (55 km fault length). There were no instruments in the epicentral region of either event.

Many villagers were interviewed to determine if there were noticeable pre-earthquake phenomena. Both events occurred at about mid-day. Many residents of affected villages raise livestock or have farm animals.

Before the 1976 earthquake there were corroborated reports of thunder-like noises (possibly due to very small foreshocks) at the epicenter. There was at least one case of increased water flow from a spring near the fault at least one day before the earthquake. Behavior of domestic and farm animals prior to the earthquake was investigated extensively by interviewing many villagers and shepherds. There were no confirmed observations of unusual behavior of farm animals, outdoors or indoors, prior to the earthquake. However, barking or howling of dogs a few hours to a few minutes before the earthquake was widely observed.

During the night preceding the 1975 earthquake, a brightening of the sky over a wide area was reported by observers both in the epicentral region and by geologists about 250 km away.

DTIC
COPY
INSPECTED

ssion For
GRA&I ☒
TAB ☐
Unannounced ☐
Justification
By
Distribution/
Availability Codes
Dist | Avail and/or Special
A-1

SOURCE PROPERTIES OF THE 1976 EARTHQUAKE IN E. TURKEY: A COMPARISON OF FIELD DATA AND TELESEISMIC RESULTS

M. Nafi Toksöz and John Nabelek

Department of Earth and Planetary Sciences
Massachusetts Institute of Technology
Cambridge, Massachusetts 02139

and

Esen Arpat

M.T.A. Institute
Ankara, Turkey

October 1977

Determining seismic moment and source parameters independently from geological observations in the field, and from seismic observations at teleseismic distances enables us to test the validity of source models.

The Eastern Turkey earthquake on 24 Nov. 1976 (O.T. 12:22:18.3 G.M.T., $M_S = 7.3$) had a clearly visible fault trace and measurable displacements. The seismic source properties of this earthquake can be determined from field observations and compared with those determined from teleseismic observations. In this paper we describe the earthquake source in terms of observed faulting and the source parameters based on body and surface waves.

Field Observations

The earthquake epicenter (39.3°N, 43.7°E) is to the north of a possible SE extension of the N. Anatolian fault trace through Lake Van. The connection of this earthquake fault with those in Iran is not clear, although there are a number of right-handed, strike-slip faults in Iran (branches of the North Tabriz fault) extending toward the Turkish border (Berberian, 1976).

The fault break was visible for about 55 km and was mapped (Fig. 1). Photographs in Fig. 2 illustrate the faulting. The motion was almost purely right-lateral, strike-slip. The surface trace has a strike of about N70°W in the central and western side and it bends somewhat east of Çaldiran and has an azimuth of about N45°W at the east end. The fault comes to an abrupt end under mountains in the west. At the eastern end the surface displacements become smaller gradually and the fault trace disappears toward the Iranian border. The observed horizontal displacements are more than 3 meters (330-350 cm) in the west, about 250 cm in the central regions and less to the east. The observed dip is nearly 90°. There are vertical displacements with inconsistent direction, generally about 50 cm, observed locally in several areas. The southward tilt of Lake Van, measured from water level marks, indicates a slight uplifting of the southern block. From the surface displacements, it appears that faulting may have started close to the west end and propagated to the east. The reported duration of severe shaking in Van (90 km to the SE, along an azimuth normal to the strike) was about 17 sec, consistent with a fault length of about 50-60 km.

Seismic moment and stress drop were calculated from the field observations. Taking the fault length $L = 55$ km, assuming fault width $W = 1/3\ L$ and the average observed displacement $D = 250$ cm, and rigidity $\mu = 4 \times 10^{11}$ dyne/cm^2, the seismic moment is $\bar{M} = 1.0 \times 10^{27}$ dyne/cm. The stress drop calculated using a strike-slip model is $\Delta\sigma = 35$ bars.

Source Parameters from Teleseismic Observations

Source mechanism and seismic moment of the earthquake were determined from analysis of P and surface waves. Data from WWSSN, Canadian network, and SRO stations were used in the analysis. The fault plane solution, obtained from both short and long period P-wave polarities, is shown in Fig. 3. The solution is well constrained with a strike: N73°W, dip: 78°S and slip angle: 4°. These are in excellent agreement with the field observations. Essentially they confirm the right-handed, strike-slip faulting with a very small thrust component. These results are further confirmed by the surface wave data.

The Rayleigh waves from 19 stations were analyzed to determine the seismic moment. Because of the large magnitude of the event, low-gain stations and SRO's were most suited for this study. The selection was made to obtain a good azimuthal coverage. In addition to R_1's, 5 R_2's were used. Station distributions and great circle paths are shown in Fig. 4.

Seismic moment was determined from the amplitude spectra and corrected for attenuation and geometric spreading. Theoretical amplitudes were calculated taking into account source finiteness, radiation pattern and layered earth models (Harkrider, 1964; Toksöz et al., 1965; Saito, 1967; Tsai and Aki, 1969, 1970; Canitez and Toksöz, 1971). A Gutenberg earth model was used for continental paths. The Q-values used were a combination of values given by Tsai and Aki (1969), Kanamori (1970), and Burton (1973). Most stations were located at nearly equal distances from the source. Thus the relative amplitudes at long periods are not affected appreciably by the velocity and Q-models chosen.

The observed and theoretical amplitudes at T = 100 sec period are shown in Fig. 5. Theoretical amplitudes were calculated using a focal depth = 15 km, and a source model given by P-wave first motion solution, with the seismic moment as a parameter. A very good fit is obtained with a seismic moment of $M_o = 7.5 \times 10^{26}$ dyne/cm. This is close to the value (10×10^{26} dyne-cm) calculated on the basis of fault length and surface displacements observed in the field. The effect of source finiteness and rupture velocity on spectra of long period waves was not observed. The source parameters are summarized in Table 1.

Conclusion

The Van earthquake provided excellent data for comparing source properties determined from field observations at the source and from seismic records at teleseismic distances. The surface faulting was very clear. The largest displacements were in the western half of the fault and the surface data suggested that fault rupture started in the west and propagated eastward. The fault plane solution agrees best with fault parameters in the western half.

The seismic moments calculated on the basis of observed fault length and displacements and determined from Rayleigh wave spectra were 1.0×10^{27} and 0.75×10^{27} dyne-cm, respectively. Considering the possible uncertainties in choice of parameters used in both calculations, the agreement is remarkable. It supports the idea that displacements at the surface were representative of those along the whole fault width.

The observed displacements and the stress drop ($\Delta\sigma = 35$ bars) are relatively high in comparison with other strike-slip earthquakes (Kanamori and Anderson, 1975) of 55 km fault length. This is probably due to the relatively young age of the fault, and the strength of the rocks that make up the fault zone.

Acknowledgements

This research was supported by the Advanced Research Projects Agency, monitored by the Air Force Office of Scientific Research under contract F44620-75-C-0064 and by NATO Science Grant No. 1162.

References

Berberian, M., 1976. Geol. Survey of Iran, Report No. 39.

Burton, P.W., 1974. Estimations of Q^{-1} from seismic Rayleigh waves. Geophys. J. R. astr. Soc., 36: 167-189.

Canitez, N. and Toksöz, M.N., 1971. Focal mechanism and source depth of earthquakes from body and surface wave data. Bull. Seism. Soc. Am., 61: 1369-1379.

Harkrider, D.G., 1964. Surface waves in multilayered elastic media, 1. Rayleigh and Love waves from buried sources in a multilayered elastic halfspace. Bull. Seism. Soc. Am., 54: 627-680.

Kanamori, H., 1970. Synthesis of long-period surface waves and its application to earthquake source studies, Kurile Islands earthquake of October 13, 1963. J. Geophys. Res., 75: 5011-5027.

Kanamori, H. and Anderson, D.L., 1975. Theoretical basis of some empirical relations in seismology. Bull. Seism. Soc. Am., 65: 1073-1095.

Saito, M., 1967. Excitation of free oscillations and surface waves by a point source in a vertically heterogeneous earth. J. Geophys. Res., 72: 3689-3699.

Toksöz, M.N., Harkrider, D.G. and Ben-Menahem, A., 1965. Determination of source parameters by amplitude equalization of seismic surface waves, 2. Release of tectonic strain by underground nuclear explosions and mechanisms of earthquakes. J. Geophys. Res., 70: 907-922.

Tsai, Y.B. and Aki, K., 1969. Simultaneous determination of the seismic moment and attenuation of seismic surface waves. Bull. Seism. Soc. Am., 59: 275-287.

Tsai, Y.B. and Aki, K., 1970. Precise focal depth determination from amplitude spectra of surface waves. J. Geophys. Res., 75: 5729-5743.

Table 1

Summary of Source Parameters

	Field Measurement (static)	Teleseismic
Strike	N70°W	N73°W
Dip	∿90°	78°S
Slip	--	4°
Fault Length	55 km	--
Magnitude (M_S)	--	7.3
Ave. Displacement	275 cm	--
Moment (dyne-cm)	1×10^{27}	0.8×10^{27}
Stress Drop	35 bars	--

Figure Captions

Fig. 1 - (a) Location of the earthquake within the seismotectonic setting of Turkey (inside the box), and (b) detailed map of the observed fault trace.

Fig. 2 - Photographs of the fault trace observed immediately after the earthquake. Photographs (a,b) show the western section and (b,c) the central section of the fault. The right-handed displacement is clearly visible by the 350 cm offset of the stream (b) and the 250 cm offset of a ditch (d).

Fig. 3 - Fault plane solution giving predominantly right-handed strike-slip motion in agreement with field observations shown in Fig. 2. Fault plane parameters: strike N73°W, dip 78°S, slip angle 4°.

Fig. 4 - Amplitude spectral density of Rayleigh waves at T = 100 sec. Circles and traingles signify values determined from R_1's and R_2's respectively. Line represents theoretical amplitude for a source model given by P-wave fault plane solution with seismic moment of $M_o = 7.5 \times 10^{26}$ dyne-cm.

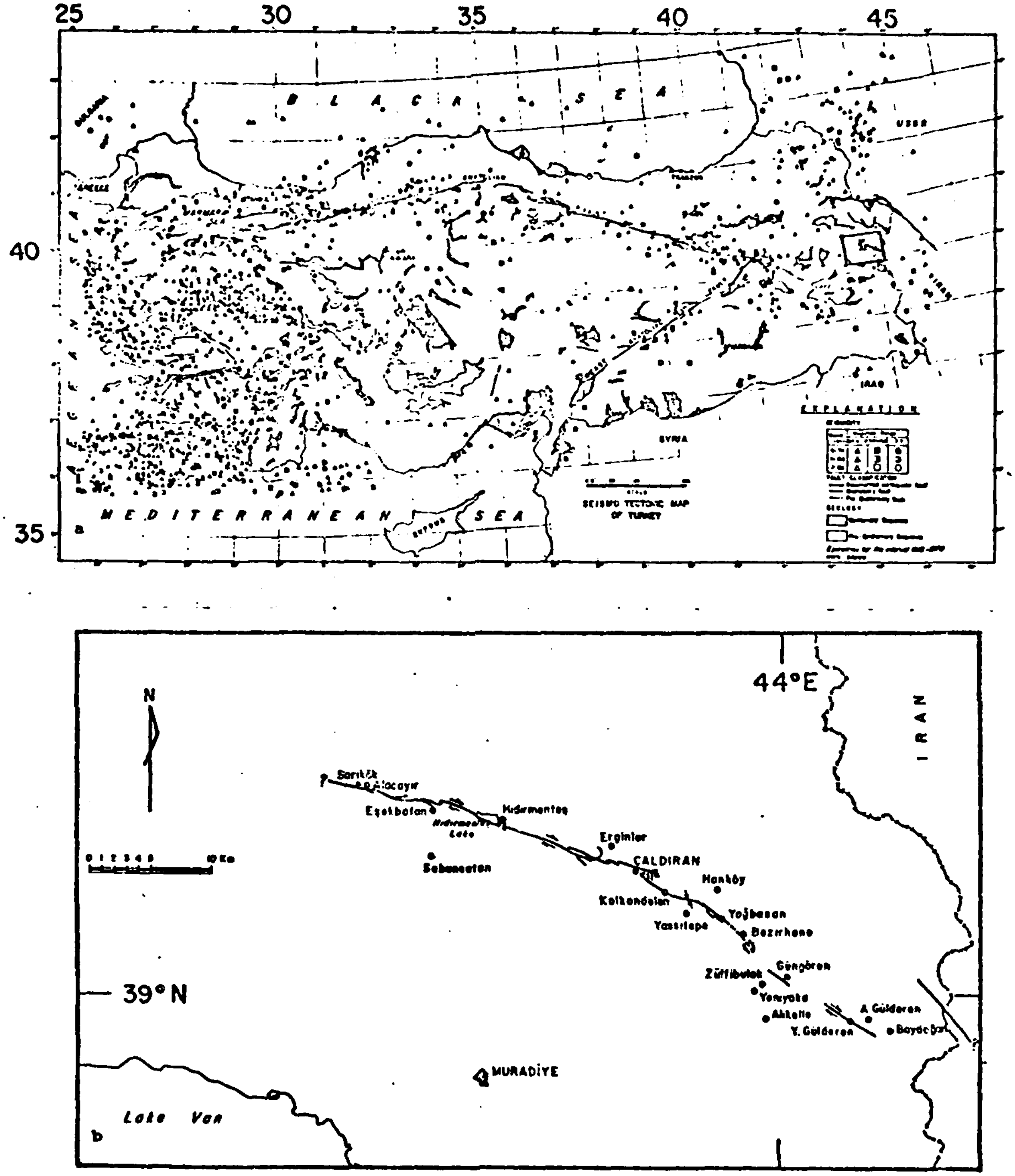
25
30
35
40
45
40
35
B L A C K S E A
M E D I T E R R A N E A N S E A
USSR
IRAQ
SYRIA
CYPRUS
SEISMO TECTONIC MAP OF TURKEY
EXPLANATION
a
N
44°E
IRAN
39° N
Sarıtök
Alocayır
Eşekbatan
Hıdırmenteş
Lake
Sebenoeten
Erginler
CALDIRAN
Hanköy
Kalkandelen
Yassıtepe
Yoğbasan
Bezirhane
Güngören
Züffibulak
Yeniyaka
Ahkelle
A. Gülderen
Y. Gülderen
Baydoğan
MURADİYE
Lake Van
b
10 Km

Fig.1

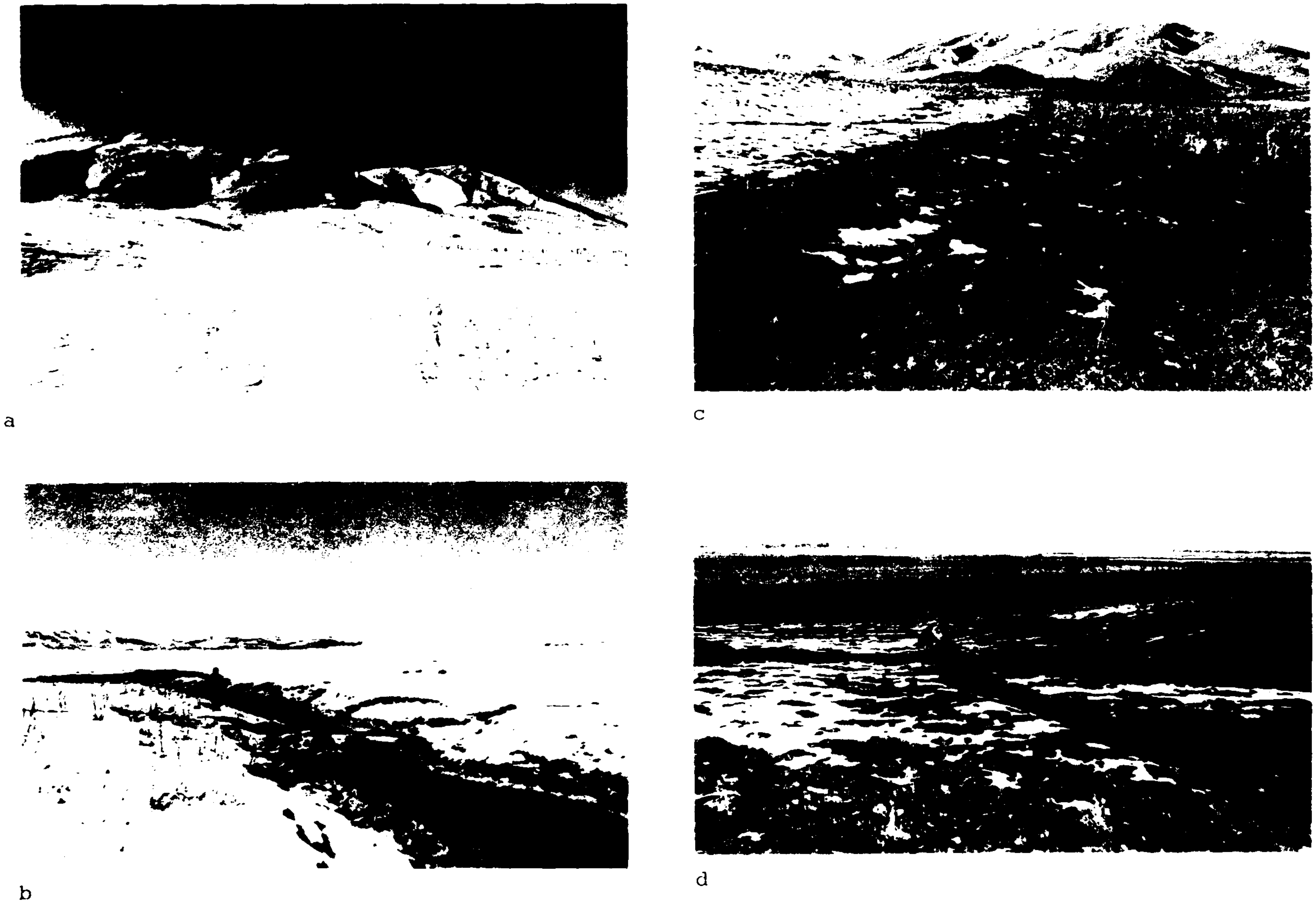

Fig. 2

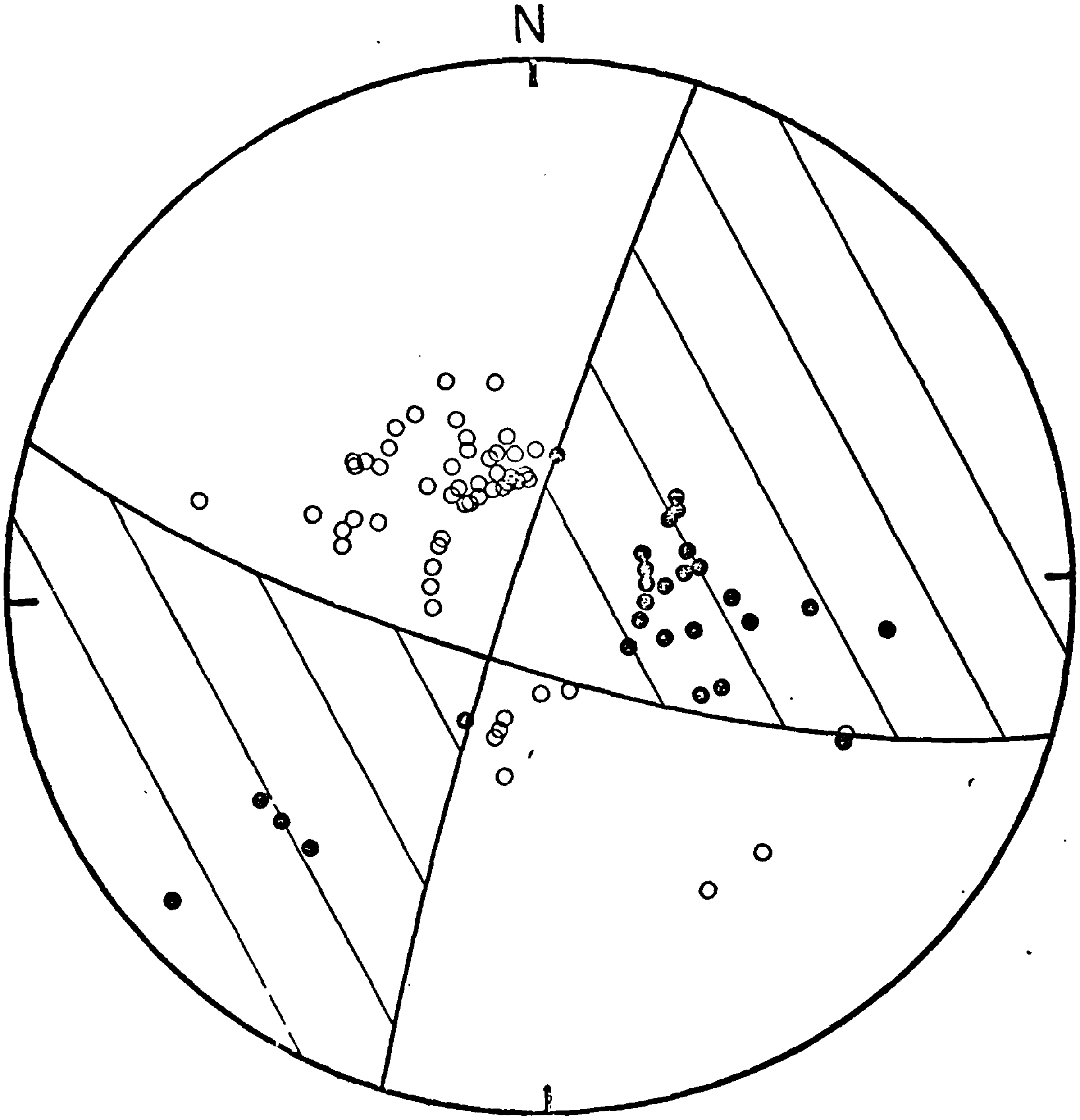

Fig. 3

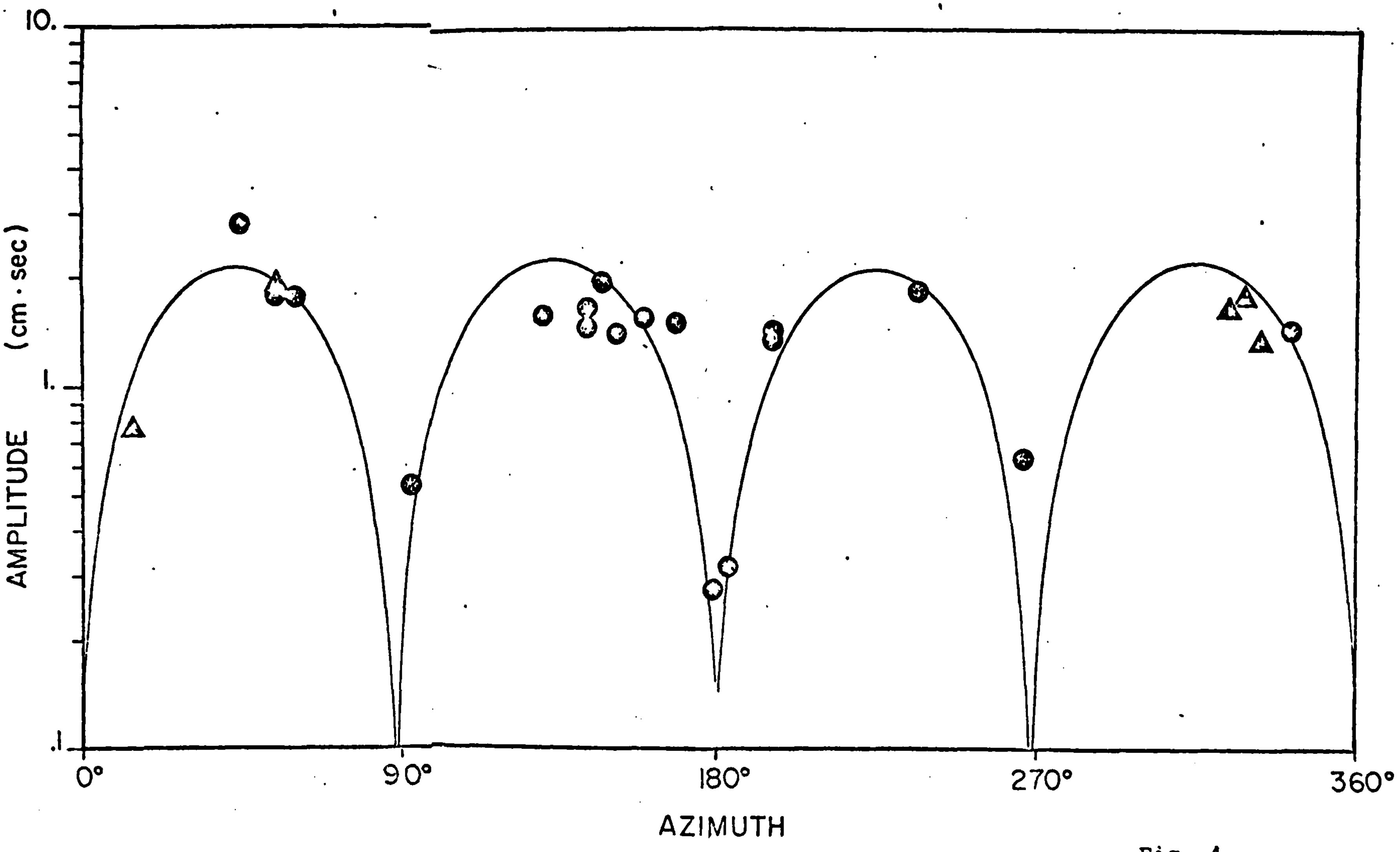

Fig. 4

3. SEISMIC WAVE PROPAGATION

Attenuation of Seismic Waves
in Dry and Saturated Rocks:
II. Mechanisms

David H. Johnston and M. Nafi Toksöz

Department of Earth and Planetary Sciences
Massachusetts Institute of Technology
Cambridge, Massachusetts 02139

and

Aytekin Timur

Chevron Oil Field Research Company
La Habra, California 90631

August 1977

Revised February 1978

ABSTRACT

Theoretical models based on several hypothesized attenuation mechanisms are discussed in relation to published data on the effects of pressure and fluid saturation on attenuation. These mechanisms include friction, fluid flow, viscous relaxation, and scattering. The application of these models to the ultrasonic data of Toksöz et al. (1978) indicates that friction on thin cracks and grain boundaries is the dominant attenuation mechanism for consolidated rocks under most conditions in the earth's upper crust. Increasing pressure decreases the number of cracks contributing to attenuation by friction thus decreasing the attenuation. Water wetting of cracks and pores reduces the friction coefficient, facilitating sliding and thus increasing the attenuation. In saturated rocks fluid flow plays a secondary role relative to friction. At ultrasonic frequencies in porous and permeable rocks, however, Biot-type flow may be important at moderately high pressures. "Squirting" type flow of pore fluids from cracks and thin pores to larger pores may be a viable mechanism for some rocks at lower frequencies. The extrapolation of ultrasonic data to seismic or sonic frequencies by theoretical models involves some assumptions, verification of which requires data at lower frequencies.

MATHEMATICAL NOTATION

a, a' = Biot flow structure constants

$c(\alpha_m)$ = pore-crack porosity

f = frequency

k = wavenumber

ℓ = crack half length

q = volume flow

r = radius of scattering inclusions

K, E, μ, ρ = matrix moduli and density

K', E', μ', ρ' = inclusion moduli and density

K^*, E^*, μ^*, ρ^* = effective moduli and density

K^*_A = frame bulk modulus

N/V_o = number of cracks per volume

P = pressure

P_c, P_f, P_d = confining fluid and differential pressures

Q, Q^{-1} = quality and dissipation factors

V = seismic velocity

α = attenuation coefficient

α_m = aspect ratio

δ = log decrement

ε = crack/pore porosity ratio

η = viscosity

θ = dilatation

κ = coefficient of friction

σ, σ^* = matrix and effective Poisson's ratios

τ = relaxation time

ϕ = total porosity

χ = permeability

ω = angular frequency

ω_c, ω_d = critical frequencies for squirting flow and shear relaxation

INTRODUCTION

In order to reasonably evaluate and interpret laboratory measurements generally made at ultrasonic frequencies (~1 MHz) and more importantly to extrapolate these results to seismic frequencies, a precise definition of the mechanisms involved in attenuation along with their pressure and frequency dependence is needed. Numerous mechanisms have been proposed and each may be considered to have a greater degree of importance to the overall attenuation under certain physical conditions. These mechanisms include: matrix anelasticity including frictional dissipation due to relative motions at the grain boundaries and across crack surfaces (Walsh, 1966); attenuation due to fluid flow including relaxation due to shear motions at pore-fluid boundaries (Walsh, 1968 and 1969; Solomon, 1973), dissipation in a fully saturated rock due to the relative motion of the frame with respect to fluid inclusions (Biot, 1956a,b; Stoll and Bryan, 1970); "squirting" phenomena (Mavko and Nur, 1975 ; O'Connell and Budianski, 1977); partial saturation effects such as gas pocket squeezing (White, 1975); energy absorbed in systems undergoing phase changes (Spetzler and Anderson, 1968); and a large category of geometrical effects including scattering off small pores and large irregularities and selective reflection from thin beds (O'Doherty and Anstey, 1971; Spencer et al., 1976). Of these mechanisms listed, all except the geometrical effects are dependent upon intrinsic rock properties and will be considered in this study. It is our purpose to evalute these mechanisms in terms of experimental data in order to determine under what conditions one or more may be dominant in causing the overall attenuations of both P and S waves.

In this paper we begin by examining the published data on seismic wave attenuation in rocks under varying physical conditions, highlighting important features that contribute to our understanding of the mechanisms involved. In the second section attenuation mechanisms along with available theoretical formulations are presented. In the final section, the theoretical models are compared to the data obtained by Toksöz et al. (1978, this issue). In Appendix A, the calculation of effective elastic moduli required for determining the attenuation is briefly discussed. Our main emphasis in this part will be to determine the relative importance of the mechanisms in contributing to the overall attenuation and to what extent laboratory data may be used to infer rock properties from seismic data obtained in the field. Our discussions will be limited primarily to fully saturated and completely dry competent rocks under pressures up to a few kilobars and relatively low temperatures as might be encountered in geophysical exploration.

ATTENUATION DATA

Seismic body wave attenuation has been measured for many rock types over wide ranges of physical conditions and frequencies, and by many techniques. Unfortunately, the systematics of attenuation behavior with pressure, temperature and saturation conditions has not been adequately measured nor is it well understood. With some exceptions, laboratory determinations of attenuation are limited to specific rocks under one physical state. However, an overview of these data can provide useful information on the nature and mechanics of attenuation in upper crustal rocks. In this section, individual determinations of attenuation will be briefly summarized, followed by a more extensive review of data that is pertinent to this paper.

The data examined in this paper have been obtained by numerous experimental techniques including pulse transmission of several types, resonant bars, and slow stress cycles. Each method determines a different measure of attenuation. The most commonly found quantities in the literature are the attenuation coefficient, α, for a plane propagating wave in an infinite medium; the logarithmic decrement, δ; and the dissipation factor, Q^{-1}, or its inverse, the "quality factor", Q. The relationships among these are given by:

$$Q = \frac{\pi f}{\alpha V} = \frac{\pi}{\delta} \tag{1}$$

where V = velocity and f = frequency. In this paper, we will deal with the parameters Q^{-1}, Q, and α exclusively.

A representative sample of individual attenuation measurements is listed in Table 1 along with other pertinent parameters. Another summary of individual measurements taken from the compilation of Bradley and Fort (1966) is shown graphically in Figure 1, where Q as a function of rock type and rock porosity is plotted. The values taken are generally at surface pressure although they cover a wide frequency range. Figure 1 shows the wide variability of attenuation in rocks and a general trend of Q inversely proportional to porosity. As noted by many investigators (Wyllie, et al., 1962; Knopoff, 1964, Bradley and Fort, 1966; and others), the accumulation of individual attenuation measurements has led to a series of generalities that may be applied to the nature of Q in crustal rocks. These are summarized below, with references to later sections of this paper where certain effects are discussed in more detail.

1. Frequency Dependence: Laboratory experiments show that Q may be independent of frequency (α proportional to f) over a broad frequency range (10^{-2}-10^{7}Hz) especially for some dry rocks (Birch and Bancroft, 1938; Born, 1941; McDonal et al., 1958; Peselnick and Outerbridge, 1961; Attwell and Ramana, 1966; Pandit and Savage, 1973; and others). Q^{-1} in liquids, however, is proportional to frequency (Pinkerton, 1947) so that in some highly porous and permeable rocks the total Q^{-1} may contain a frequency dependent component (Born, 1941; Wyllie et al., 1962). This component may be negligible at seismic frequencies even in unconsolidated marine sediments (Hamilton, 1972).

2. Strain Amplitude: Attenuation appears to be independent of strain amplitude for low strains such as those associated with seismic waves (Mason, 1958; Gordon and Davis, 1968). Some evidence exists (Winkler et al., 1977) that attenuation discontinuously increases above a strain of about 10^{-6}.

3. Fluid Saturation: Attenuation for fluid saturated rocks is higher than for dry rocks and depends on the degree of saturation, fluid type, and frequency in a complicated way. For rocks fully saturated with a low viscosity fluid (water, oil) it is generally found that at ultrasonic frequencies $Q_p \geq Q_s$. This topic will be further discussed in the next section.

4. Pressure and Stress Dependence. Observations show that attenuation decreases with increasing confining pressure. This is usually considered to be due to the closing of cracks in the rock matrix. Data supporting this and theoretical models of the pressure effects will be discussed in later sections of this paper. For applied nonhydrostatic stress, the attenuation appears to be anisotropic (Merkulova et al., 1972; Walsh et al., 1970). For shear waves polarized normal to the axis of maximum compression, attenuation is lowest due to the closure of cracks with faces normal to the axis (Lockner et al., 1977). At high differential stresses, the onset of dilatancy increases the attenuation (Lockner et al., 1977).

5. Temperature Dependence: The small amount of data on this topic (Volarovich and Gurevich, 1957; Gordon and Davis, 1968) indicate that Q is generally independent of temperature at temperatures low relative to the melting point.

An increase of attenuation in quartzite with temperatures above 150°C noted by Gordon and Davis (1968) may be due to thermal cracking of the rock. Near the boiling temperatures of pore fluids, attenuation may be affected strongly by temperature.

We will now consider in more detail data pertaining to the roles of fluid saturation and hydrostatic pressure in determining the attenuation of seismic waves in crustal rocks. In some cases the absolute determinations of attenuation reported by investigators are unreliable, yielding unreasonable values. Therefore, we generally present the data in terms of the relative change in α or Q^{-1}.

Attenuation as a Function of Saturation Conditions

Although of great interest to the exploration community, relatively little experimental work has been done on the nature of attenuation as a function of saturation conditions. Even the published data must be examined critically due to the inherent difficulties involved in partial saturation work. Unfortunately, little or no detailed description is given in the experimental literature about the techniques of fluid saturation. An important, yet experimentally difficult, aspect is maintaining a homogeneous distribution of the saturant in the bulk of the rock. We must also address the question as to what constitutes a "dry" rock. In most cases, samples are oven-dried prior to fluid injection. Heating the sample will cause some alterations of the matrix structure. In any event, it is nearly impossible to remove the fluid completely; at least a mono-molecular layer of fluid will probably remain in the thinnest cracks.

The degree of saturation and the type of saturant, characterized primarily by viscosity, appear to play an important role in attenuation. Studies of the effect of partial saturation by various fluids have been reported in Born (1941), Obert et al. (1946), Collins and Lee (1956), Wyllie et al. (1962), and Gardner et al. (1964). A summary of these results is shown in Figures 2-5, where Q or the fractional change in Q is plotted as a function of percent saturation. As pointed out in the preceding section, the overall Q of the rock may be considered to contain a frequency independent component plus a frequency dependent component due to the fluid inclusions. Thus the effect of partial saturation may be frequency dependent (Born, 1941). However, since the curves shown here were taken over a wide range of frequencies but exhibit similar behavior, fluid losses may not dominate frequency independent losses in most rocks at surface pressures.

Most of the rocks shown in Figures 2-5 are saturated with water, chemically active with intergranular material. The exception is the alundum (Al_2O_3) saturated with soltrol, a relatively inert petroleum naptha, shown in Figure 3. The behavior of attenuation as a function of water saturation is similar for all rocks. Q is sharply reduced at low saturations presumably due to the wetting effect of water entering the fine cracks, possibly reacting with intergranular material and softening the rock. Also note that the effect of pressure is to reduce the effect of saturation for both P and S waves as shown in

Figures 4 and 5 since the finer cracks are closed. In the case of soltrol saturation (Figure 3) the change in Q observed for water saturation is not seen. This implies that the effect observed for water saturation is primarily due to either chemical alteration of the intergranular material or a wetting phenomenon. Since it is unlikely that water reacts strongly with alundum, we favor the explanation that different wetting properties cause the different saturation effects observed. In real rocks, of course, a combination of the two mechanisms is likely.

The effect of fluid type, i.e. viscosity, has been discussed indetail by Wyllie et al. (1962) and Nur and Simmons (1969a). The dependence of attenuation on fluid viscosity is complicated and not at all obvious from results presented by Wyllie et al. (1962). Taking these data at face value, it would appear that very large viscosity fluids (eg. glycerol) result in small fluid contributions to attenuation. This makes sense for some attenuation mechanisms such as fluid flow in that higher viscosity fluids decrease the effective permeability. However, Nur and Simmons (1969a) have shown that the viscosity effect is frequency dependent, consistent with a relaxation type mechanism. In their experiment, a Barre granite (porosity =0.6%) was saturated with glycerol which has a viscosity extremely dependent on temperature. Thus by varying the temperature of the saturated sample, the effect of viscosity on velocities and relative attenuation of P and

S waves is measured. The attenuation of S waves as a function of pore fluid viscosity is shown in Figure 6. The relaxation peak occurs at a viscosity where the characteristic time is equal to the wave period. An experiment reported by Gordon (1974) shows similar results.

Attenuation as a Function of Pressure

The pressure dependence of attenuation has been generally neglected by most investigators yet the behavior of Q with pressure can yield as much information about mechanisms as the frequency dependence. When a rock is subjected to hydrostatic pressure such as overburden pressure, its elastic and anelastic properties will change. The behavior of elastic properties under pressure is well known and a theoretical treatment of it may be found in Toksöz et al. (1976). The most important factor causing changes in velocity is the change of porosity with pressure; in particular, the closing of thin cracks. This also holds true for changes in attenuation as will be discussed in the next section. In all cases, attenuation decreases (Q increases) with increasing pressure. Experimental data verifying this are found in Gardner et al. (1964), Klima et al., (1964), Levykin (1965), Gordon and Davis (1968), Al-Sinawi (1968), Walsh et al., (1970) and Toksöz et al. (1978). For these data and the theoretical models to be presented, the pressure given is the differential pressure, $P_d = P_c - P_f$, where P_c is the confining pressure and P_f is the fluid or pore pressure. This relationship holds for all rocks as demonstrated by laboratory tests (Wyllie et al., 1958; Nur and Simmons, 1969b).

The attenuation of P waves in diabase and greywacke were measured by Klima et al. (1964) up to a pressure of 4 kilobars (kb) by a pulse transmission method with a prevailing frequency of 0.9 MHz. Although not stated explicitly, the samples are assumed to be air dry. The results of this experiment are shown in Figure 7 which plots the change in the attenuation coefficient, α, as a function of pressure. In all cases a clear decrease in α is observed up to about 1 kb. The relative changes in attenuation are greater than those of the velocity measured in the same type rocks under the same conditions (Pros et al., 1962).

Levykin (1965) investigated the attenuation of both P and S waves in several igneous and metamorphic rock types up to pressures of about 4 kb. A pulse echo technique at a frequency of 1 MHz was used. Samples were air dry. The results of these experiments for several gneiss samples are shown in Figure 8. Again, the attenuation decreases rapidly with increasing pressure, leveling off after about 1 kb. Levykin attributes the differing extent to which attenuation is changed under pressure to be due to differences in the weathering of the rocks.

Gordon and Davis (1968) studied the effect of pressure (up to 4 kb) on a fluid saturated granite using slow stress cycles (f = 10 mHz). Their data are reproduced in Figure 9. The same features as seen in the previous works are evident here.

So far we have considered data only for low porosity rocks, either dry or completely saturated. However, the pressure effect for a partially saturated Berea sandstone has been studied by Gardner et al. (1964). Both extensional and torsional Q values were determined using resonance techniques at frequencies up to 30 kHz. External influences on the sample, such as losses into the pressure medium were considered. These data are shown in Figures 4 and 5. The same general behavior is seen for the data in Toksöz et al. (1978) for dry, methane, and water-saturated Berea sandstone at ultrasonic frequencies using the pulse transmission technique. The Q, however, levels off at a lower pressure than for the igneous and metamorphic rocks.

The variation of attenuation for P and S waves with pressure was also studied for a variety of rock types by Al-Sinawi (1968). A pulse transmission technique using 122 kHz transducers was used and the pressures for which measurements were taken were .5, 1, and 2 kb. All of the rocks studied were sedimentary except a granite gneiss and a volcanic tuff. Al-Sinawi found, as observed before, that both α_p and α_s decreased with pressure. In some rocks, particularly limestones, the pressure effect is different, however, this is not completely described.

ATTENUATION MECHANISMS

As a first approximation we will assume that attenuation mechanisms are independent of each other. Thus, we may consider each mechanism separately and then combine the results to determine the overall attenuation. More specifically, we will consider separately the relative effects of the matrix anelasticity, the viscosity and flow of saturating fluids and scattering from inclusions. The pressure dependence of these effects will be included. In all these cases the available theoretical formulations are not very rigorous. They are guided primarily by experimental observations and as a whole should be treated as empirical relationships. The calculation of effective elastic properties, necessary for the determination of attenuation, is discussed in Appendix A. The method used is that of Kuster and Toksöz (1974) and Toksöz et al. (1976).

Attenuation Due to Matrix Anelasticity

Attenuation of seismic waves in a rock matrix can be attributed to two factors: (1) intrinsic anelasticity of matrix minerals and (2) frictional dissipation due to relative motions at the grain boundaries and across crack surfaces. The intrinsic anelasticity of minerals is generally small. In individual crystals Q values are generally higher than a few thousand, while in the whole rock Q values are normally lower than a few hundred. Thus, in considering matrix attenuation, it is reasonable to neglect the intrinsic attenuation in minerals and to consider only the attenuation across grain surfaces and thin cracks.

The importance of frictional dissipation is supported by the observation that Q is generally independent of frequency as predicted by this mechanism. However, friction across crack surfaces cannot account for all the anelasticity of the matrix. As pointed out by Walsh (1966), rocks subjected to confining pressures high enough to close all cracks still exhibit non-zero attenuation. Thus it is necessary to consider in addition to dissipation across crack surfaces, an "intrinsic" anelasticity of the aggregate minerals.

The exact mechanism of grain boundary and crack dissipation is not known but frictional dissipation due to relative motions of the two sides may be the major factor (Walsh, 1966). If this is the case, then the attenuation should depend very strongly on the surface conditions that affect friction between grains. Among these are whether rocks are saturated or dry, the properties of saturating fluids, and the amount of clay or other soft components in the matrix.

From laboratory experiments and the lunar experience it is found that granular materials exhibit very high Q values when totally dry and in a vacuum. In the absence of atmosphere and water, the Coulomb forces across grains are very strong and friction coefficients are high. Hence, no sliding motion can take place across the surfaces. This accounts for very high Q values measured for seismic waves in the moon (Q = 2000-5000: Dainty et al., 1976; Nakamura et al., 1974; Latham et al., 1974; Toksöz et al., 1974) and in the laboratory under hard vacuum conditions (Pandit and Tozer, 1970; Warren et al., 1974; Tittmann et al., 1972, 1975). In the laboratory when a little water vapor was introduced into the vacuum chamber, Q values decreased significantly.

It is difficult to formulate attenuation due to grain boundary and "frame anelasticity" effects since this requires the detailed knowledge of crack and grain boundary properties.

Walsh (1966) formulated the problem by approximating the cracks as ellipsoids in plane strain. For random orientation of cracks, the Q values for compressional and shear waves were computed using the friction coefficient, κ, effective Poisson's ratio σ^*, matrix and effective rock moduli as parameters. The resulting expression for P waves in an infinite medium is too complicated to be presented conveniently but has the following form:

$$Q_p^{-1} = \frac{E^*}{E} \frac{(1-\sigma^*)}{(1-2\sigma^{*2})} \frac{\ell^3 N}{V_o} F(\kappa,\sigma^*) \tag{2}$$

when E^* and E are the effective and matrix Young's moduli respectively, and N is the number of cracks with half length, ℓ, in a volume, V_o. The function $F(\kappa,\sigma^*)$ is implicitly dependent on the angle between the normal to the crack plane and the direction of wave propagation. Only cracks of certain orientations, determined by κ and σ^*, will contribute to the attenuation.

A closed form solution for the attenuation of S waves is impossible to obtain, but again from the Walsh (1966) formulation we may write the general form as

$$Q_s^{-1} = \frac{E^*}{(1+\sigma^*)E} \frac{\ell^3 N}{V_o} F(\kappa) \tag{3}$$

where $F(\kappa)$ is a function of the friction coefficient.

For reasonable values of the friction coefficient and Poisson's ratio, Q_p/Q_s may be found by numerically evaluating equations 2 and 3 (Walsh, 1966). For κ between 0.0 and 0.5 and σ^* between 0.15 and 0.25, Q_p/Q_s is found to be between about 0.4 and 1.5. For most dry rocks $Q_p/Q_s < 1$, while for saturated rocks $Q_p/Q_s \sim 1.0$

at surface pressure (see Table 1).

Many data (Peselnick and Outerbridge, 1961; Peselnick and Zietz, 1959; Knopoff, 1964) can be explained by the frictional dissipation mechanism. This mechanism which yields a constant Q with frequency, also explains the "frame anelasticity" incorporated in Biot's (1956a,b) formulations.

Although friction explains much of the observed behavior of attenuation in rocks, the calculation of absolute values requires the specification of too many unknown parameters (friction coefficients, number and radii of cracks whose surfaces are in contact). Furthermore, these parameters most likely will change with saturation conditions. However, the Walsh formulation is useful in determining the effect of pressure on the frictional mechanism.

In order to formulate this pressure dependence we assume:

1. The cracks and grain boundaries that contribute to friction can be characterized by very thin spheroids with a small aspect ratio, α_m (where α_m = thickness/diameter). From equation A-3, the relative change of the fractional volume, c, for this family of cracks as a function of differential pressures is:

$$\frac{dc}{c} = \frac{-P}{K^*_A} \left[\frac{4}{3\pi\alpha_m} \frac{(1-\sigma^2)}{(1-2\sigma)} \right] \qquad (4)$$

where σ is the matrix Poisson's ratio and K^*_A is the effective static or frame bulk modulus.

2. The effective coefficient of friction, κ, is constant with pressure. Thus, $F(\kappa)$ in equation (3) is a constant. If we assume that the effective Poisson's ratio, σ^*, varies more slowly with pressure than c, then $F(\kappa,\sigma^*)$ in equation (2) is essentially a constant also.

Since the fractional volume of cracks with aspect ratio α_m is:

$$c(\alpha_m) = \frac{4\pi\alpha_m}{3} \frac{N(\alpha_m)\,\ell^3}{V_0} \qquad (5)$$

equation (2) may be written as:

$$Q_p^{-1} = \frac{3}{4} \frac{E^*}{E} \frac{(1-\sigma^*)}{(1-2\sigma^{*2})} \frac{c(\alpha_m)}{\pi\alpha_m} F(\kappa,\sigma^*) \qquad (6)$$

with a similar change for equation (3). Then:

$$\frac{dQ_p^{-1}}{Q_p^{-1}} = \frac{dE^*}{E^*} + \frac{dc}{c} + \varepsilon \tag{7}$$

where ε includes variations in σ^* and $F(\kappa,\sigma^*)$. Using assumption 2, $\varepsilon \to 0$. Substituting equation (4) into (7) and then integrating, we finally obtain :

$$Q_p^{-1} = Q_{p_o}^{-1} \frac{E^*}{E_o^*} e^{-AP/K_A^*} \tag{8}$$

where $A = \frac{4}{3\pi\alpha_m} \frac{(1 - \sigma^2)}{(1 - 2\sigma)}$ = constant. A similar expression is obtained for the attenuation of S waves. Q_p^{-1} and Q_s^{-1} at $P = 0$ are found empirically and thus the imaginary parts of the matrix moduli can be set as described in Appendix A. In fact, at each pressure, the imaginary parts are given by:

$$\begin{aligned} K_I &= (K_R + 4/3\mu_R) Q_p^{-1} - 4/3\mu_R Q_s^{-1} \\ \mu_I &= \mu_R Q_s^{-1} \end{aligned} \tag{9}$$

These results can then be used in equations (A-1) and (A-2) to determine the effective moduli, velocities and attenuation. Since α_m is arbitrary, the constant A is a free parameter and must be found empirically.

At first glance, the exponential decay of Q^{-1} with pressure predicted by equation (8) may not seem reasonable. As stated before, the attenuation of many rocks at high pressure is non-zero. However, equation (8) describes only the effects of cracks which control the behavior of the elastic and anelastic properties at relatively low pressures. If one considers a rock with an extremely low total porosity but moderate crack porosity such as a granite, then equation (8) may truly represent the pressure dependence of Q^{-1}. This is indeed observed in the data from Gordon and Davis (1968) shown in Figure 9. For rocks such as sandstones, however, we must consider the intrinsic aggregate anelasticity to contribute to the observed attenuation at pressures where the cracks are closed. In our models this is determined empirically and assumed to be constant with pressure.

One further consideration is the difference between surface pressure Q values for the dry Berea sandstone determined by the ultrasonic pulse method (Toksöz et al., 1978) and values obtained by dynamic resonance (Gardner et al., 1964 and unpublished data by the authors). Compared on a common basis, the Q_p value for the pulse technique is about 20 while for the resonance method it is higher than 50. The discrepancy is smaller for the saturated case. Two explanations are possible. Either the friction mechanism as we understand it does not provide a frequency independent Q or the attenuation is dependent on strain amplitude. Some evidence favors the latter. Winkler et al. (1977) have reported that Q discontinuously decreases at a strain of about 10^{-6}. This may be due to the presence of asperities in the cracks which inhibit sliding until a threshold amplitude is exceeded. The higher amplitude ultrasonic pulses (strain $>10^{-6}$) may thus be able to cause sliding on these rough surfaces and result in a higher attenuation. In the saturated case, crack surfaces are lubricated and the threshold amplitude is lower. Our own unpublished resonance data on the Berea sandstone and Plexiglass corroborate the amplitude threshold theory. As Winkler reported, a discontinuous increase in attenuation was observed in the sandstone. However, no such increase was observed in the crack and grain boundary free Plexiglass. This result further strengthens the idea that cracks with asperities in rocks result in an amplitude dependent frictional mechanism. It may therefore be valid to compare experimental and in situ results only when assured that factors such as strain amplitude are equivalent.

Attenuation Due to Viscosity and Flow of Saturating Fluids

All rocks in the upper crust are partially or completely saturated with some fluid. It is of special interest then to consider the effect of viscous fluids in a solid rock matrix. Some mechanisms by which fluids contribute to attenuation are illustrated in Fig. 10. These fluids in elongated pores and fine cracks contribute to attenuation in a complex manner. First, attenuation peaks due to viscous relaxation will develop at frequencies dependent both on pore geometry and fluid viscosity. For a rock with a wide spectrum of pore aspect ratios, the attenuation spectrum is of a complicated form. This problem has been discussed by Walsh (1968, 1969), Solomon (1973), and Kuster and Toksöz (1974) for spheroidal pores.

Second, fluid flow between pores, induced by the stress (seismic) wave, may cause attenuation. These flow mechanisms fall into two categories, inertial flow (Biot, 1956a,b), important at ultrasonic frequencies, and "squirting" flow (Mavko and Nur, 1975; O'Connell and Budiansky, 1977), more prominent at lower frequencies. We will consider each separately and our analysis of "squirting" flow will also include the formulation for viscous relaxation.

In highly porous and permeable rocks, relative motion may take place between the rock frame and the saturating fluid

as seismic waves propagate. Biot (1956 a,b and 1962a,b) derived a theory for acoustical wave propagation in an isotropic solid with interacting pores. This theory can be used to calculate both velocity and attenuation.
Biot theory predicts the existence of three types of body waves, two dilatational and one shear. One dilatational wave is highly attenuated and resembles a diffusion wave. The other is the P body wave that travels with little attenuation or dispersion. A formulation of Biot's theory has been developed by Stoll and Bryan (1970) and Stoll (1974 and 1977) and has been adopted for this study.

As with attenuation due to viscous shear relaxation, the viscous resistance to fluid flow is frequency dependent for oscillating motion. Below a certain frequency, dependent on the fluid properties and pore characteristics, this resistance is given by the ratio of the fluid viscosity, η, to the physical permeability, κ, and may be considered approximately constant, describing Poiseuille flow. At higher frequencies, turbulent flow develops in which the effects of viscosity are felt only in a thin boundary layer.

For frequencies at which Poiseuille flow is valid, the attenuation coefficient, α, for the P type body wave varies as the square of the frequency $(Q^{-1} \propto f)$. At higher frequencies, Biot derived a correction factor to the fluid viscosity and found that α is proportional to $f^{1/2}$ $(Q^{-1} \propto f^{-1/2})$. Shear attenuation involves only the idea that the moving solid frame drags the viscous fluid with it. Since the fluid motion is due only to inertial stresses, this mechanism must be treated in addition to the viscous relaxation model.

The Biot type loss mechanisms, pressure gradient flow and viscous drag, are schematically illustrated in Figure 10.

Biot theory and the numerical model of Stoll and Bryan (1970) require the following parameters: (following previous notations) the elastic moduli for the frame, $K_A{}^*$ and $\mu_A{}^*$ and matrix, K and μ; the bulk modulus and absolute viscosity of the fluid inclusions, K' and η; the porosity, ϕ, the physical permeability, χ; and the densities of the matrix and fluid, ρ and ρ'. All of these parameters are either known or can be calculated using the technique described by Kuster and Toksöz (1974) and Toksöz et al. (1976) (Appendix A). Two other free constants derived from Biot theory, a pore size parameter, a, and a structure constant, a', must be appropriately chosen or experimentally found for the material being considered. The choice of these values is discussed by Stoll and Bryan (1970).

The attenuation formulations, for the two dilatational waves after lengthy algebra, reduce to the solution of the following period equation (Stoll, 1974):

$$\begin{vmatrix} Hk^2 - \rho\omega^2 & \rho'\omega^2 - Ck^2 \\ Ck^2 - \rho'\omega^2 & m\omega^2 - Mk^2 - \dfrac{i\omega F\eta}{\chi} \end{vmatrix} = 0 \qquad (10)$$

where ω is the angular frequency and k is the wavenumber. $m = a'\rho'/\phi$ (with $a' \geq 1$). H,C and M are operators which are functions of the frame, matrix and fluid moduli, and F is a complex high frequency correction factor derived by Biot (1956b). The attenuation coefficient is obtained by solving for the complex roots ($k = k_R + ik_I$) of the period equation and using the imaginary part of the wavenumber, k_I. One root represents the diffusion wave and the other the propagating P wave. Another, more simple. period equation for k may be found for the S wave. Viscous drag at the pore-fluid interface results in greater loss than flow induced by pressure gradients. Thus, the model predicts that the attenuation of S waves is greater than for the P waves in the case of the fluid flow mechanism.

In general, the elastic moduli of the frame in this formulation may be complex, allowing for the anelasticity of the frame. Since this effect is considered separately in this study, the imaginary parts of the frame moduli are set to zero. Numerical calculations carried out by Stoll and Bryan (1970) indicate that frame anelasticity dominates over the fluid flow effects at lower frequencies ($f \leq 10^4$ Hz). At high frequencies, the fluid flow contribution could be detected for high porosity rocks if the permeability is also high. In this case the frequency dependence of the attenuation coefficient is f^2 at lower frequencies and $f^{0.5}$ at higher ($f \geq 10^5$Hz) frequencies. For most sedimentary rocks saturated with water, the effects of fluid flow are small at seismic frequencies ($f = 10 - 200$ Hz), but could become important at ultrasonic frequencies.

The pressure dependence of attenuation due to fluid flow depends primarily on the change in permeability in the rock due to compaction and pore collapse. The elastic moduli and total porosity are easily obtained as functions of pressure using the method of Toksöz et al. (1976). Furthermore, we may assume that the viscosity of the fluid inclusion remains relatively constant in the pressure range of interest.

Experimental determinations of permeability as a function of confining hydrostatic pressure have been made for several sandstones (Fatt and Davis, 1952), Westerly granite (Frangos, 1967), and Ottawa sand (Zoback and Byerlee, 1976). In general, permeability decreases with increasing pressure but the rate of decrease depends on the total porosity and fraction of crack porosity. In highly porous and permeable consolidated rocks, the bulk of the porosity and permeability is contained in the large aspect ratio pores which do not close under pressure. Fatt and Davis (1952) found a maximum reduction in permeability of 25% at 350 bars for the sandstones, while for a granite the reduction may be as much as an order of magnitude (Frangos, 1967). However, since the effect of fluid flow is negligible in all but the highly permeable rocks, we need only consider data on that type. Measurements of permeability in unconsolidated Ottawa sand (Zoback and Byerlee, 1976) show a slow reduction up to 800 bars where it drops off rapidly to level off again between 2000 and 3000 bars. The acceleration in permeability loss at 800 bars is presumably due to grain crushing and pore collapse. However, the applicability of this study to consolidated rocks is uncertain nor could it easily be modeled. We shall assume that the permeability of highly porous rocks is constant with pressure. The effect of this is to give an upper bound on the contribution due to fluid flow on attenuation.

Several investigators have proposed attenuation mechanisms by which flow is induced between two adjacent interacting cracks due to the relative volume change caused by the stress wave (Mavko and Nur, 1975; O'Connell and Budiansky, 1977). These are commonly known as "squirting" mechanisms and while they are not important at ultrasonic frequencies, they may be so at sonic or seismic frequencies. The elastic model of Toksöz et al. (1976) is particularly useful in treating these mechanisms in that a distribution of crack aspect ratios is uniquely determined and pressure gradients between cracks may be readily calculated.

Flow in any "squirting" mechanism is generally from small aspect ratio (thin) cracks to larger ones (pores). Thus the flow field within the crack may be approximated by the flow between two infinite plates as is done by Mavko and Nur (1975) and O'Connell and Budiansky (1977). Here we consider an approach to the problem consistent with the concepts and formulations introduced by Toksöz et al. (1976). The details of the calculations may be found in Appendix B. We assume that flow will take place between very thin cracks with $\alpha_m \simeq 0$ and pores with $\alpha_m = 1$ due to a differential volume change induced by the stress wave. The pressure difference, the equalized pressure after flow, the instantaneous flow, q, and the total flow, q_T. can be easily calculated. Assuming a relaxation of the form:

$$q_T = q \int_0^\infty e^{-t/\tau}\, dt = q\tau \qquad (11)$$

where τ is the relaxation time, we find that

$$\tau = 8\eta/\alpha_m^2 K'(1 + \varepsilon) \qquad (12)$$

where η is the viscosity, α_m the aspect ratio, K' the fluid bulk modulus and ε is the ratio of connected crack volume to pore volume. We can make the approximation $\varepsilon \approx 0$ for most porous rocks. Taking $K' = 2 \times 10^{10}$ dynes/cm^2, $\eta = 10^{-2}$ poise, with α_m ranging from 10^{-3} to 10^{-4}, we obtain relaxation times ranging from 4×10^{-6} to 4×10^{-4} sec.

The formulation of this mechanism in terms of complex moduli yields an expression that also includes the viscous relaxation mechanism in pores discussed earlier. This is a result of applying the correspondence principle for the shear modulus, $\mu' = i\omega\eta$ and expressing the bulk modulus as $K' = K_R' + i\omega g$, where g is considered an unknown to be determined from the relaxation time for the "squirting" flow. While this is a good approximation for high frequencies, at very low frequencies (<0.1 Hz) the fluid offers little resistance to flow and thus $K_R \approx 0$ (O'Connell and Budiansky, 1977). It is shown in Appendix B that the equations (A-1) and (A-2) for the effective moduli can be written in terms of two characteristic frequencies: $\omega_c = K/g$ and $\omega_d = 3K/4\eta$ (equation B-13). ω_d is recognized as the characteristic frequency for viscous relaxation (Walsh, 1969) and ω_c is the characteristic frequency for fluid flow from cracks. From the estimate of the relaxation time for this mechanism:

$$g = \frac{8\eta}{\alpha_m^2(1 + \varepsilon)} \frac{K}{K_R'} \qquad (13)$$

For example, with $\varepsilon = 0$, $\alpha_m = 10^{-3}$, $\eta = 10^{-2}$ poise, $K = 4 \times 10^{11}$ dynes/cm^2 and $K_R' = 2 \times 10^{10}$ dynes/cm^2 we find that $g = 1.6 \times 10^6$ poise or, more generally, $g = 1.6/\alpha_m^2$ poise. This mechanism is readily included in the elastic moduli formulations by finding g from eq. 13, and then substituting to find K' to be used in the elastic moduli calculations.

Other Sources of Attenuation

In many cases, rocks in the crust are partially saturated by two or more fluids - air and water, oil and brine, gas and oil to name a few. The effect of partial saturation on velocity is fairly well known; however, its effect on attenuation is not as well understood. Low seismic amplitudes from some gas-sands, though, imply that the effect can be large. One problem encountered is the distribution of the saturants in the rock frame. Not only are large scale irregularities in partial saturation found in rock formations but the distribution on a smaller scale, pore to pore, may change. Gas bubbles in water or oil are more likely to occupy space in the pores with larger aspect ratios than in the finer cracks, where the friction and relaxation mechanisms are more important. The latter effect is evident from the data at low saturations discussed earlier and shown in Figures 2-5.

Several mechanisms involving the presence of free gas in the pores may contribute to the attenuation in partially saturated rocks. This is illustrated in Figure 10. Gas bubbles have several effects. First, the pore fluid bulk modulus is reduced, facilitating flow even under very small pressure gradients. (Stoll (1977) has also suggested that in this case, conversion to Biot diffusion type waves at an interface can result in substantial energy loss.) "Squirt" flow would also be enhanced. Secondly, bubble squeezing and moving in particular may contribute to a decreased Q. Thus, in partially saturated rocks, the attenuation may be greater than in the fully saturated case. A small amount of fluid is required to lubricate cracks and grain boundaries to facilitate sliding and energy loss due to friction. The presence of gas bubbles on the other hand, enhances energy dissipation mechanisms operative at full saturation and further loss may result from motions of the bubbles themselves. This enhanced attenuation particularly concerns mechanisms dependent on pressure gradients induced by P waves.

An attenuation model describing the effects of large scale irregularities (on the order of 10 cm) in saturation conditions has been proposed by White (1975). The porous rock is modeled as containing spherical pockets saturated with gas with the rest of the volume saturated with liquid. Loss due to fluid flow is enhanced at the gas-liquid interfaces. White showed that for the particular model chosen, attenuation due to this mechanism can be important at seismic frequencies. There is some debate, however, as to the occurrence of the saturation irregularities.

Several other mechanisms for attenuation have been proposed although their applicability to upper crustal rocks is debatable. Several of these mechanisms may be operable in the upper mantle, however, such as grain boundary relaxation, relaxation caused by a phase change, and a "high temperature background" attenuation probably related to Nabarro diffusion (Jackson and Anderson, 1969).

Experimental evidence suggests little change in attenuation as a function of temperature at relatively low temperatures (Volarovich and Gurvich, 1957) when rock is not cracked and saturating fluids not altered. However, near phase changes, attenuation could change rapidly with temperature. High attenuation has been observed at critical points in multicomponent systems (Spetzler and Anderson, 1968; Wang and Meltzen, 1972). Energy is absorbed by a medium whose equilibrium is disturbed by a stress wave. The frequency at which this occurs is dependent on the rate at which phase equilibrium can follow the changes imposed on it by the wave (Spetzler and Anderson, 1968). This mechanism may result in high attenuation in certain geothermal areas.

We finally consider the effective attenuation due to scattering by inclusions in the rock. Although this is a geometrical effect, it can, in some cases, affect the observed attenuation. Yamakawa (1962) has analyzed the scattering of compressional waves by spherical pores. The equivalent attenuation coefficient, α, is given by:

$$\alpha = \phi \frac{12\pi^4 f^4 r^3}{V_p{}^4} \left[2B_o^2 + \frac{2}{3}(1 + \nu^3) B_1^2 + \frac{(2 + 3\nu^5)}{5} B_2^2\right] \qquad (14)$$

where $B_o = \dfrac{K - K'}{3k' + 4\mu}$

$B_1 = (\rho - \rho')/3\rho$

$B_2 = \dfrac{-20\mu^3}{3\mu(9K+8\mu)}$

and $\nu = V_p/V_s$, $\dot{r}$ = radius of inclusions, f = frequency. In the above, primed coefficients represent the inclusion properties. Although the effective attenuation of incident plane S waves has not been calculated, we may estimate this effect by noting that the energy loss due to SP reflections is equivalent to PS reflections because of the reciprocal theorem. While losses due to SS reflections are not the same as PP, they are close and we can reevaluate equation (19) for incident S waves assuming SS ≡ PP. Doing so, the only changes in the equation arethat V_p is replaced by V_s and $\nu = V_s/V_p$. Attenuation due to scattering is strongly dependent on frequency ($\propto f^4$). As will be shown in the next section, scattering effects can be important, if not dominant, at high ultrasonic frequencies (f >1 MHz). At seismic frequencies, scattering due to pores is negligible.

Another geometric effect is the apparent attenuation due to selective reflection of the short wavelength component of seismic waves in thin beds. Although of little importance with respect to laboratory measurements, this mechanism may, under certain conditions, contribute to observed amplitude loss in seismic sections. O'Doherty and Anstey (1971), Schoenberger and Levin (1974) and Spencer et al. (1977) have examined these cases in detail. In general, selective reflection due to cyclic stratification contributes a small but important part to the overall attenuation. If high reflection coefficients occur, the apparent attenuation can be high.

INTERPRETATION OF LABORATORY DATA

We shall now consider in more detail the relative effects of the various attenuation mechanisms in dry and saturated porous rocks. The methods and techniques discussed in the previous section will be applied to model the behavior of attenuation as a function of differential pressure for the ultrasonic data on the Berea sandstone presented in Toksöz et al., (1978). These models will then be extrapolated to other frequencies. The application of these models to previously reported data is difficult because absolute values of attenuation appear to be unreliable in some cases, and parameters needed in the calculations are unavailable in others.

The procecure taken involves first modeling the attenuation in the dry rock in order to establish the needed parameters for the friction mechanism and intrinsic attenuation in the absence of fluid associated mechanisms. These parameters will then be used in the modeling of the saturated sample data. An important but probably valid assumption made here is that all attenuation mechanisms that occur in dry rocks also occur in wet ones. Given the parameters obtained from the dry case, we may examine in more detail the relative importance of the mechanisms contributing to the attenuation in the brine-saturated case as a function of pressure. In particular, since the attenuation due to Biot-type fluid flow, squirting and scattering are readily calculable it remains to be seen what the contribution due to the presence of pore fluid is in terms of the friction mechanism and intrinsic aggregate anelasticity. The approach taken here is empirical and thus the models presented have no absolute predictive ability.

The elastic moduli, fluid and frame properties used in modeling the Berea sandstone are listed in Table II. The bulk modulus of brine as a function of pore pressure is given by Adams (1931) and Long and Chierici (1961). For the dry case, the bulk modulus of air is taken to be one bar and the pore pressure is assumed to be constant at one bar.

The surface pressure aspect ratio distribution listed in Table III is determined by fitting theoretically calculated elastic properties (equations A-1 and A-2) to the P and S wave velocity versus differential pressure data for both saturated and dry cases as described by Toksöz et al. (1976). The frequency is taken to be .5 MHz.

The contributions to attenuation in the dry case are assumed to be due to friction and the intrinsic aggregate attenuation only. Zero pressure Q's were taken as 23 for P waves and 26 for S waves based on the data from Toksöz et al. (1978). The pressure dependence of Q for the dry Berea sandstone may be reasonably modelled with $A = 0.2 \times 10^4$ (equation 8) and an intrinsic aggregate Q for both P and S waves of 120. The possible variations in the parameter A are not as wide as one might expect, ranging from 0.15×10^4 to 0.25×10^4. The results of this empirical model fitted to the data are shown in Figure 11.

The introduction of brine as the pore saturant results in no change in the parameter A, since the crack closing rate is the same as for the dry case, determined by the static rather than the dynamic effective bulk modulus.

In the preceding section the role of fluids in determining the attenuation was discussed. In particular, water may soften and lubricate the matrix resulting in a higher attenuation due to a friction type mechanism, especially for shear waves. Since the contributions due to Biot fluid flow, squirting flow, viscous shear relaxation and scattering are fairly well determined from the properties listed in Table II it remains to be seen in modeling the saturated data, what the contribution due to friction is. This must be determined empirically. One important constraint, however, is the low Q, especially Q_s, at high pressures. This implies that a mechanism which is relatively independent of pressure, such as Biot fluid flow, is required under those conditions.

The fluid flow contributions to the attenuation are calculated as described in the previous section. Given the attenuation due to all the mechanisms other than friction, it is found that to fit the data, one must choose a zero pressure Q_p for friction of 15 and a Q_s of 10. These low values of Q relative to the dry case indicate that brine saturation increases the attenuation due to friction by almost a factor of two. Although the data may be fit with a fluid viscosity of 1 cp, a better fit is obtained by allowing the effective viscosity to be 4 cp. This might be expected from experimental measurements of the viscosity of water in clay-water systems (Low, 1959). Such an effect would predict a higher attenuation in rocks with higher clay content. Furthermore, while not necessary, the best fit to the data, shown in Figure 12, is obtained by reducing the intrinsic aggregate Q for shear waves by 5%. It is perhaps no coincidence that the seismic velocities are best fit in the saturated case by reducing the matrix shear modulus 5% relative to the dry case. This may reflect the possibility of increased shear and thus higher attenuation at grain boundaries due to the presence of water as discussed earlier.

The relative contributions of the two important mechanisms, friction and Biot-type fluid flow, in the brine-saturated case are easily seen in Figure 13 showing Q_p^{-1} for each mechanism as a function of pressure. The small increase in the fluid flow contribution at low pressures is an artifact of the calculations. As would be expected, friction across cracks and grain boundaries is dominant at low pressures but becomes less important as cracks close. Since the bulk of the porosity and permeability is unaffected under the pressure conditions of interest, the fluid flow contribution to attenuation remains relatively constant with pressure and becomes an increasingly important mechanism. Obviously at some pressure, the porosity and permeability of the rock will break down and one should expect a rapid increase in Q.

Using the Berea sandstone properties from model calculations; we shall now examine in more detail the individual contributions of each mechanism for the fully saturated case and extrapolate these results to other frequencies. The interpretation of these models must remain strictly within the confines imposed upon them. That is, it is assumed that strain amplitudes are equivalent to those in the laboratory experiment and that no other mechanisms contribute to attenuation at frequencies other than those at 0.5 MHz.

A theoretical overview of the relative contribution of each mechanism considered is shown in Figure 14. Here, the P wave attenuation coefficients are plotted as functions of frequency for a surface pressure condition. Figure 14 was obtained by fixing the attenuation at 0.5 MHz based on the theoretical model of the pressure data (Figure 12). The resulting curves are theoretical extrapolations. A constant Q mechanism for friction is assumed. The same model is shown in Figure 15 except that the attenuation coefficients are calculated for a differential pressure equivalent to a depth of about 10000 feet. The corresponding aspect ratio distribution is listed in Table III.

Figures 14 and 15 clearly show the relative effects of friction, fluid flow, shear relaxation and scattering on the attenuation of P waves. Similar results are obtained for S waves. If friction is indeed a frequency independent attenuation mechanism, then it dominates the other mechanisms for this case. However, as seen before, friction is of somewhat less importance at higher pressures. As assumed in our models, the contribution of Biot fluid flow remains essentially unchanged between Figures 14 and 15. While never dominating in this case, it is of importance at about 10^5 Hz where Poisseuille flow breaks down. A striking change in the squirt flow and shear relaxation mechanism is apparent however. For surface conditions, the contribution due to these mechanisms is readily seen from Figure 16. Here, Q^{-1}

for both P and S waves is shown for the squirting and shear relaxation mechanisms only. Two peaks are evident, the lower frequency one corresponding to the flow mechanism and the other to viscous relaxation. The shape of the relaxation peaks are complicated, reflecting the spectrum of pore and crack shapes. The transition from flow to viscous relaxation takes place at about 50 KHz, below which $Q_p^{-1} > Q_s^{-1}$ and above which $Q_s^{-1} > Q_p^{-1}$. Even though viscous relaxation peaks at $f = 10^9$, Hz, it is clear from figures 14 and 16 that the contribution of these mechanisms to the attenuation in the Berea Sandstone is small in the frequency band of interest, even at surface pressure. Furthermore, the effect of pressure, as seen in Figure 15, is to close cracks contributing to both the squirt flow and viscous relaxation, thus lowering even further, their associated attenuations.

Scattering off inclusions produces a negligible effect except at very high frequencies where this mechanism clearly dominates. A larger scatterer radius will shift this curve to lower frequencies.

We finally combine both the frequency and pressure behavior of attenuation in our saturated Berea Sandstone model in Figure 17 where the total Q_p of the rock is shown. For low pressures, Q_p remains essentially unchanged as a function of frequency, reflecting the importance of the friction mechanism. Q_p increases with pressure and at high pressures and low frequencies ($<10^4$ Hz) Q_p is greater than 100. Q_p decreases with increasing frequency at higher pressures due to the increasing contribution of Biot flow. Finally, at very high frequencies (10^7 Hz), Q_p decreases sharply because of scattering.

While the ultrasonic attenuation data may be understood and modeled by several mechanisms, some problems exist in the extrapolation of these data to lower frequencies. As discussed earlier, the frequency dependence of the important friction mechanism is not clearly established. Furthermore, strain amplitudes at seismic exploration frequencies may not be the same as those used in ultrasonic measurements, thus invalidating the absolute estimates of Q. However, theoretical models, such as the ones presented in this paper, provide a method of comparing laboratory data taken under controlled conditions with in situ data. One has to be aware, however, that the contributions of mechanisms that may be important at low frequencies are difficult to establish from ultrasonic data unless supplementary information is available. Furthermore, it is obvious that from these models one would only obtain a point property of the rock. For in situ data, the intrinsic attenuation must be isolated from other amplitude reducing mechanisms such as scattering, spreading, or multiple reflections, before comparison with laboratory data.

CONCLUSIONS

The investigation of both published and new laboratory data on the attenuation of seismic waves in rocks, particularly sandstones, has shown that many of the same properties and processes that affect velocity also affect attenuation, many times to a greater extent. These properties include the number and distribution of cracks, the type and amount of fluid saturation and the mechanical properties of the rock matrix.

We have approached the problem of attenuation in dry and completely saturated rocks by examining a number of hypothesized mechanisms for which numerical models may be applied. The formulation of the pressure dependence of these models enables us to reasonably fit ultrasonic data for Q_p and Q_s in a Berea sandstone. The models for attenuation require the specification of several free parameters and thus limits their predictive abilities. Furthermore, assumptions involving the frequency and amplitude behavior of the friction mechanism must be considered if laboratory data are compared to in situ data. However, given the limitations of the models, several conclusions regarding the attenuation of seismic waves in rocks are possible:

1. At relatively shallow depths in the earth's crust, the primary mechanism for attenuation is friction on grain boundaries and thin cracks.

2. Increasing differential pressure decreases the number of cracks contributing to attenuation by friction. Since frictional loss depends on the number of cracks, the attenuation decreases with increasing pressure and eventually approaches a limiting value we call the intrinsic aggregate anelasticity. This is probably due to grain boundaries and fine structure relatively unaffected by pressure.

3. In totally dry rocks, the attenuation is less than wet or saturated rocks. The introduction of fluid into a dry rock will wet crack surfaces and grain boundaries. By this crack lubrication, frictional sliding is facilitated and the attenuation increases.

4. In a saturated porous rock, attenuation due to fluid flow plays a secondary role relative to friction. At low frequencies, squirting flow may be a viable mechanism, especially in the case of partial saturation. At ultrasonic frequencies, the Biot-type fluid flow mechanism, while not necessarily dominating, plays an important role in the overall attenuation at high pressures.

ACKNOWLEDGEMENTS

The authors thank Dr. Joseph Walsh and C.H. Cheng of MIT for their valuable assistance in preparing this manuscript. Professor Jan Korringa and Dr. Jim Spencer of COFRC provided beneficial discussions and comments on the paper. This research was supported in part by the Advanced Research Projects Agency, monitored by the Air Force Office of Scientific Research under contract F44620-75-C-0064. David Johnston was supported in part by a Chevron Fellowship.

APPENDIX A

ELASTIC MODULI FOR CALCULATING ATTENUATION

The calculation of attenuation requires the knowledge of several elastic moduli and their pressure dependence. Given the matrix or grain moduli and density, K, μ, and ρ, and the inclusion properties K', μ' and ρ', the effective properties of a composite medium may be found following the treatment of Kuster and Toksöz (1974). Cracks and large pores in the rock are represented by a discrete spectrum of various aspect ratio spheroids. Letting $c(\alpha_m)$ be the concentration of pores and cracks with aspect ratio α_m = thickness/diameter, the effective moduli are given by (Kuster and Toksöz, 1974):

$$\frac{K^* - K}{3K^* + 4\mu} = 1/3 \; \frac{K'-K}{3K + 4\mu} \sum_{m=1}^{M} c(\alpha_m) \; T_{iijj}(\alpha_m) \qquad \text{(A-1)}$$

$$\frac{\mu^* - \mu}{6\mu^*(K+2\mu) + \mu(9K+8\mu)} = \frac{\mu' - \mu}{25\mu(3K+4\mu)} \sum_{m=1}^{M} c(\alpha_m) \cdot \qquad \text{(A-2)}$$

$$[T_{ijij}(\alpha_m) - 1/3 \; T_{iijj}(\alpha_m)]$$

where '*' denotes effective properties, primed quantities refer to fluid properties and unprimed quantities are matrix properties. K and μ represent bulk and shear moduli and T_{iijj} and T_{ijij} are scalar quantities. The total porosity is:

$$\phi = \sum_{m=1}^{M} c(\alpha_m)$$

and the density is:

$$\rho^* = \rho(1 - \phi) + \rho'\phi$$

The effect of pressure on the crack and pore distributions and thus the effective moduli and velocities of rocks has been studied by Toksöz et al. (1976). The strain field around an ellipsoidal cavity is calculated as a function of the elastic moduli of the matrix and an applied strain field at infinity. The dilatation of the applied field is $-P/K_A^*$ where P is the applied hydrostatic differential pressure and K_A^* is the effective static bulk modulus or frame bulk modulus. From this, the fractional change in pore volume, dc/c may be found. For the particular case of very thin cracks (i.e. $\alpha_m \to 0$),

$$\frac{dc}{c} = - \frac{P}{K_A^*} \left\{ \frac{4}{3\pi\alpha_m} \frac{(1-\sigma^2)}{(1-2\sigma)} \right\} \tag{A3}$$

where σ = matrix Poisson's ratio. This relationship also provides the basis for calculating the change in attenuation due to friction under increasing hydrostatic or differential pressure.

Anelasticity may be introduced into the effective moduli formulations by employing the concept of complex moduli (Anderson et al., 1965 and Bland, 1960). This method is particularly useful in dealing with frequency independent Q mechanisms such as grain boundary and crack friction. Let the complex bulk and shear moduli be expressed as

$$K = K_R + iK_I$$
$$\mu = \mu_R + i\mu_I \qquad \text{(A-4)}$$

where subscripts R and I refer to real and imaginary parts. If the attenuation is small, then the velocities and attenuation coefficients can be expressed conveniently. For compressional waves,

$$V_p = \left[\frac{K_R + 4/3\ \mu_R}{\rho}\right]^{1/2}$$
$$Q_p^{-1} = \frac{K_I + 4/3\ \mu_I}{K_R + 4/3\ \mu_R} \qquad \text{(A-5)}$$

For shear waves,

$$V_s = [\frac{\mu_R}{\rho}]^{1/2} \qquad \text{(A-6)}$$
$$Q_s^{-1} = \frac{\mu_I}{\mu_R}$$

To determine the imaginary part of the moduli it is necessary to rely on observation and to follow an empirical approach. The magnitudes of K_I and μ_I should be chosen in each case to match observed Q values at appropriate conditions.

APPENDIX B

FLUID FLOW FROM CRACKS

FORMULATION AND ESTIMATION OF THE RELAXATION TIME

Flow will take place between thin cracks with aspect ratio $\alpha_m \simeq 0$ and pores with $\alpha_m \simeq 1$ due to a differential volume change induced by the stress wave. The fluid pressures and volume changes are given by:

$$P_0 = -K'\theta_0 \quad \text{and} \quad dC_0 = C_0\theta_0,\ \alpha_m \simeq 0$$

$$P_1 = -K'\theta_1 \qquad\qquad dC_1 = C_1\theta_1,\ \alpha_m \simeq 1 \tag{B-1}$$

where C is the volume concentration of cracks or pores and θ is the dilatation. The pressure difference is $\Delta P = P_0 - P_1$. Letting the equalized pressure after flow be $\overline{P}$, then the corresponding dilatation in both the crack and pore is $\overline{\theta} = -\overline{P}/K'$. The total liquid volume displaced in order to equalize the pressure is given by:

$$q_T = d\overline{C}_0 - dC_0 = dC_1 - d\overline{C}_1 \tag{B-2}$$

where $d\overline{C}_0 = C_0\overline{\theta}$ and $d\overline{C}_1 = C_1\overline{\theta}$. Solving for $\overline{\theta}$ we obtain:

$$\overline{\theta} = -\frac{\varepsilon\theta_0 + \theta_1}{1 + \varepsilon} \tag{B-3}$$

where $\varepsilon = C_0/C_1$, or the volumetric ratio of connected cracks to pores. Furthermore:

$$q_T = C_0 \left[\frac{\theta_1 - \theta_0}{1 + \varepsilon}\right] \qquad \text{(B-4)}$$

The instantaneous flow between two parallel plates (crack surfaces) separated by distance h is given by

$$q = \frac{h^2 A}{3\eta} \frac{dP}{dx} \qquad \text{(B-5)}$$

where A now becomes the cross sectional area of the crack and is equal to $\pi h^2/\alpha_m$ or $\pi h \ell$. If we let $dx = 2\ell$ (crack length) then from equation B-1 and B-5:

$$q = \frac{\pi h^3}{6\,\eta} K'(\theta_1 - \theta_0) \qquad \text{(B-6)}$$

Assuming a relaxation of the form:

$$q_T = q \int_0^{\infty} e^{-t/\tau}\, dt = q\tau \qquad \text{(B-7)}$$

where τ is the relaxation time, we obtain

$$\tau = \frac{C_o(\theta_1 - \theta_0)/(1 + \varepsilon)}{\pi h^3 K'(\theta_1 - \theta_0)/6\eta} \qquad \text{(B-8)}$$

Since the volume of the crack, $C_0 = \frac{4\pi h^3}{3\alpha_m^2}$:

$$\tau = 8\eta/\alpha_m^2 K'(1 + \varepsilon) \qquad \text{(B-9)}$$

Viscoelastic Formulation:

We will now show that by using the correspondence principle for both the shear and bulk moduli of the fluid phase that the equations for the effective moduli may be written in terms of real and imaginary parts and two characteristic frequencies. Rewriting equation A-1 for the effective bulk modulus by letting $\delta'' = (\frac{K'}{K} - 1)\frac{T_{iijj}}{3}$ (dropping the summation over aspect ratios we obtain:

$$K^* = \frac{K + \frac{4CK\mu\delta''}{3K + 4\mu}}{1 - \frac{3CK\delta''}{3K + 4\mu}} = K\left[\frac{1 + 4\mu C\delta'}{1 - 3KC\delta'}\right] \qquad \text{(B-10)}$$

where $\delta' = \delta''/(3K + 4\mu)$. Letting δ' be complex, i.e. $\delta' = a + ib$, then:

$$K^* = K\left[\frac{1 + 4\mu C(a + ib)}{1 - 3KC(a + ib)}\right] = K_R^* + K_I^*$$

where

$$K_R^* = K\left[\frac{(1 \quad 4\mu Ca)(1 - 3KCa) - 12K\mu C^2b^2}{(1 - 3KCa)^2 + (3KCb)^2}\right] \qquad \text{(B-11)}$$

and $$K_I^* = bK\left[\frac{4\mu C(1 - 3KCa) + 3KC(1 + 4\mu Ca)}{(1 - 3KCa)^2 + (3KCb)^2}\right]$$

Applying the correspondence principle we let $K' = K_R' + i\omega g$ and $\mu' = i\omega\eta$ where η is the viscosity and g is considered an unknown to be determined from the relaxation time for flow. We now show that the equations for the effective moduli can be written in terms of two characteristic frequencies and that the real and imaginary parts of δ' are uniquely determined. For small aspect ratios:

$$\delta' = \frac{1}{3K + 4\mu} \left(\frac{K'}{K} - 1\right) \frac{3K + 4\mu'}{3K' + 4\mu' + K_1} \qquad \text{(B-12)}$$

(Toksöz et al., 1976, equation C-4) where $K_1 = 3\pi\alpha_m\mu(3K + 4\mu)/(3K + 4\mu)$. Substituting the complex K' and μ' we obtain after some algebra:

$$\delta' = \frac{1}{3K + 4\mu} \left(K'' - 1 + \frac{i\omega}{\omega_c}\right) \frac{1 + i\omega/\omega_d}{(K''+K_2) + i\omega(1/\omega_c + 1/\omega_d)} \qquad \text{(B-13)}$$

where $K'' = K_R'/K$, $K_2 = K_1/3K$ with $\omega_c = K/g$ and $\omega_d = 3K/4\eta$. ω_d is recognized as the characteristic frequency for viscous relaxation in isolated cracks (Walsh, 1969) and ω_c is the characteristic frequency for fluid flow from cracks. Finally, it can be shown that the real and imaginary parts of $\delta' = a + ib$ can be written as:

$$a = \frac{1}{A} \left[(K''-1)\left(K''+K_2+\frac{\omega^2}{\omega_d}\left(\frac{1}{\omega_c}+\frac{1}{\omega_d}\right)\right) - \frac{\omega^2}{\omega_c}\left(\frac{K''+K_2}{\omega_d} - \frac{1}{\omega_c} - \frac{1}{\omega_d}\right) \right]$$

$$b = \frac{1}{A} \left[\omega \left(\frac{K''+K_2}{\omega_d} - \frac{1}{\omega_c} - \frac{1}{\omega_d}\right)(K''-1) + \frac{\omega}{\omega_c}(K''+K_2) + \frac{\omega^3}{\omega_c\omega_d}\left(\frac{1}{\omega_c} + \frac{1}{\omega_d}\right) \right] \qquad \text{(B-14)}$$

where $A = [(K''+K_2)^2 + \omega^2(\frac{1}{\omega_c} + \frac{1}{\omega_d})^2]/(3K + 4\mu)$. The equivalent result is obtained for the effective shear modulus.

From equation (B-9) we have

$$\frac{1}{\omega_c} = \frac{8\eta}{\alpha_m^2 K_R'(1 + \varepsilon)} \qquad \text{(B-15)}$$

so that

$$g = \frac{8\eta}{\alpha_m^2(1 + \varepsilon)} \frac{K}{K_R'} \qquad \text{(B-16)}$$

References

Adams, L.H., 1931, Equilibrium in binary systems under pressure; I. An experimental and thermodynamic investigation of the system, NaCl-H_2O at 20°, Am. Chem. Soc. J., 53, 2769-3785.

Al-Sinawi, S., 1968, An investigation of body wave velocities, attenuation on elastic parameters of rocks subjected to pressure at room temperature, Ph.D. thesis, St. Louis University, Geophysics.

Anderson, D.L., Ben-Menahem, A., and Archambeau, C.B., 1965, Attenuation of seismic energy in the upper mantle, J. Geophys, Res., 70, 1441-1448.

Attewell, P.B., Ramana, Y.V., 1966, Wave attenuation and internal friction as functions of frequency in rocks, Geophysics, 31, 1049-1056.

Biot, M.A., 1956a, Theory of propagation of elastic waves in a fluid-saturated porous solid I. Low frequency range, J. Acoust. Soc. Am., 28, 168-178.

Biot, M.A., 1956b, Theory of propagation of elastic waves in a fluid-saturated porous solid II. High frequency range, J. Acoust. Soc. Am., 28, 179-191.

Biot, M.A., 1962a, Mechanics of deformation and acoustic propagation in porous media, J. Appl. Phys., 33, 1482-1498.

Biot, M.A., 1962b, Generalized theory of acoustic propagation in porous dissipative media, J. Acoust. Soc. Am., 34, 1254-1264.

Birch, F. and Bancroft, D., 1938, Elasticity and internal friction in a long column of granite, Bull. Seis. Soc. Am., 28, 243-254.

Bland, D.R., 1960, The Theory of Linear Viscoelasticity, New York, Pergamon Press.

Born, W.T., 1941, Attenuation constant of earth materials, Geophysics, 6, 132-148.

Bradley, J.J. and Fort, A.N., Jr., 1966, Internal friction in rocks in Handbook of Physical Constants, S.P. Clark, Jr. (ed.), Geol. Soc. Am. Pub., 175-193.

Collins, F. and Lee, C.C., 1956, Seismic wave attenuation characteristics from pulse experiments, Geophysics, 21, 16-40.

Dainty, A.M., Goins, N.R., and Toksöz, M.N., 1976, Seismic investigation of the lunar interior, Lunar Science VII, Lunar Science Institute, Houston, 181-183.

Fatt, I. and Davis, D.H., 1952, Reduction in permeability with overburden pressure, Trans. AIME, Pet. Branch, 195, 329.

Frangos, W.T., 1967, The effect of continuing pressure on the permeability of westerly granite, B.S. thesis, Mass. Inst. Tech., Cambridge.

Gardner, G.H.F., Wyllie, M.R.J., Droschak, D.M., 1964, Effects of pressure and fluid saturation on the attenuation of elastic waves in sands, J. Petroleum Tech., 16, 189-198.

Gordon, R.B., 1974, Mechanical relaxation spectrum of crystalline rock containing water, J. Geophys. Res., *79*, 2129-2131.

Gordon, R.B. and Davis, L.A., 1968, Velocity and attenuation of seismic waves in imperfectly elastic rock, *J. Geophys. Res.*, *73*, 3917-3935.

Hamilton, E.L., 1972, Compressional wave attenuation in marine sediments, *Geophysics*, *37*, 620-646.

Jackson, D.D. and Anderson, D.L., 1970, Physical mechanisms of seismic wave attenuation, *Rev. Geophys. Space Phys.*, *8*, 1-63.

Klima, K., Vanek, J., and Pros, Z., 1964, The attenuation of longitudinal waves in diabase and greywacke under pressures up to 4 kilobars, *Studia Geoph. et Geod.*, *8*, 247-254.

Knopoff, L., 1974, Q, *Rev. Geophys.*, *2*, 625-660.

Kuster, G.T. and Toksöz, M.N., 1974, Velocity and attenuation of seismic waves in two-phase media, Part I. Theoretical formulations, *Geophysics*, *39*, 587-606.

Latham, G.V., Nakamura, Y., Lammlein, D., Dorman, J. and Duennebier, F., 1974, Structure and state of the lunar interior based upon seismic data (abstr.), *Lunar Science V*, Lunar Science Institute, Houston, 434.

Levykin, A.I., 1965, Longitudinal and transverse wave absorption and velocity in rock specimens at multilateral pressures up to 4000 km/cm^2, *USSR Geophys. Ser.* (Engl. transl.), *1*, Physics of the Solid Earth, 94-98.

Lockner, D., Walsh, J.B. and Byerlee, J., 1977, Changes in seismic velocity and attenuation during deformation of granite, submitted to J. Geophys. Res.

Long, G., and Chierici, G., 1961, Salt content changes compressibility of reservoir brines, Pet. Engineer, July, B-25,B26,B-31.

Low, P.H., 1959, Viscosity of water in clay systems, in Eighth National Conference on Clays and Clay Minerals, Pergamon Press, New York, 170-182.

Mason, W.P., 1958, Physical Acoustics and the Properties of Solids, Van Nostrand Co., Princeton.

Mavko, G. and Nur, A., 1975, Melt squirt in the aesthenosphere, J. Geophys. Res., 80, 1444-1448.

McDonal, F.J., Angona, F.A., Mills, R.L., Sengbush, R.L., Van Nostrand, R.G., and White, J.E., 1958, Attenuation of shear and compressional waves in Pierre Shale, Geophysics, 23, 421-439.

Merkulova, V.M., Pigulevskiy, E.D., and Tsaplev, U.M.,1972, Sound absorption measurements in uniaxially compressed rocks, USSR, Physics of the Solid Earth, 3, 166-167.

Nakamura, Y., Dorman, J., Duennebier, F., Ewing, M., Lammlein, D. and Latham, G., 1974, High frequency lunar teleseismic events, Geochim. Cosmochim. Acta, Suppl. 5, 2883-2890.

Nur, A. and Simmons, G., 1969a, The effect of viscosity of a fluid phase on velocity in low porosity rocks, Earth Planet. Sci. Lett., 7, 99-108.

Nur, A. and Simmons, G., 1969b, The effect of saturation on velocity in low porosity rocks, Earth Planet. Sci. Lett., Obert, L., Windes, S.L., and Duvall, W.I., 1946, Standardized tests for determining the physical properties of mine rock, U.S. Bur. Mines, R.I. 3891.

O'Connell, R.J. and Budiansky, B., 1977, Viscoelastic properties of fluid saturated cracked solids, submitted to J. Geophys. Res.

O'Doherty, R.F. and Anstey, N.A., 1971, Reflections on amplitudes, Geophys. Prospecting, 19, 430-458.

Pandit, B.I. and Savage, J.C., 1973, An experimental test of Lomnitz's theory of internal friction in rocks, J. Geophys. Res., 78, 6097-6099.

Pandit, B.I. and Tozer D.C., 1970, Anomalous propagation of elastic energy within the Moon: Nature, 226, 335.

Peselnick, L. and Zietz, I., 1959, Internal friction of fine-grained limestones at ultrasonic frequencies, Geophysics, 24, 285-296.

Peselnick, L. and Outerbridge, W.F., 1961, Internal friction and rigidity modulus of Solenhofen limestone over a wide frequency range, U.S. Geol. Surv. Prof. Paper No. 400B.

Pinkerton, J.M.M., 1947, An pulse method for the measurement of ultrasonic absorption in liquids, results for water, Nature, 160, 128-129.

Pros, Z., Vanek, J. and Klima, K., 1962, The velocity of elastic waves in diabase and greywacke under pressures up to 4 kilobars, Studia Geoph. et Geod., 6, 347-367.

Solomon, S.C., 1973, Shear wave attenuation and melting beneath the mid-Atlantic Ridge, J. Geophys. Res., 78, 6044-6059.

Spencer, T.W., Edwards, C.M. and Sonnad, J.R., 1976, Seismic wave attenuation in non-resolvable cyclic stratification, submitted to Geophysics.

Spetzler, H. and Anderson, D.L., 1968, The effect of temperature and partial melting on velocity and attenuation in a simple binary system, J. Geophys. Res., 73, 6051-6060.

Stoll, R.D., 1974, Acoustic waves in saturated sediments, in Physics of Sound in Marine Sediments, L. Hampton (ed.), Plenum, New York.

Stoll, R.D., 1977, Acoustic waves in ocean sediments, Geophysics, 42, 715-725.

Stoll, R.D. and Bryan, G.M., 1970, Wave attenuation in saturated sediments, J. Acous. Soc. Am., 47, 1440-1447.

Tittmann, B.R., Abdel-Gawad, M. and Housley, R.R., 1972, Elastic velocity and Q factor measurements on Apollo 12, 14, and 15 rocks, Proc. 3rd Lunar Sci. Conf., 3, 2565-2575.

Tittmann, R.B., Housley, R.M., and Abdel-Gawad, M., 1975, Internal friction quality factor - 3100 achieved in lunar rock 70215,85, Lunar Science VI, Lunar Science Institute, Houston, 812-814.

Toksöz, M.N., Dainty, A.M., Solomon, S.C., and Anderson, K.R., 1974, Structure of the moon, Rev. Geophys. Space Phys., 12, 539-567.

Toksöz, M.N., Cheng, C.H., and Timur, A., 1976, Velocities of seismic waves in porous rocks, Geophysics, 41, 621-645.

Toksöz, M.N., Johnston, D.H., and Timur, A., 1978, Attenuation of seismic waves in dry and saturated rocks, I. laboratory measurements, submitted to Geophysics.

Volarovich, M.P. and Gurevich, G.I., 1957, Investigation of dynamic moduli of elasticity for rocks in relation to temperature, Bull. Acad. Sci. USSR, Geophys. 4, 1-9.

Walsh, J.B., 1966, Seismic wave attenuation in rock due to friction, J. Geophys. Res., 71, 2591-2599.

Walsh, J.B., 1968, Attenuation in partially melted material, J. Geophys. Res., 73, 2209-2216.

Walsh, J.B., 1969, New analysis of attenuation in partially melted rock, J. Geophys. Res., 74, 4333-4337.

Walsh, J.B., Brace, W.F. and Wawersik, W.R., 1970, Attenuation of stress waves in Ceder City quartz diorite, Air Force Weapons Laboratory Tech. Rep. AFWL-TR-70-8.

Wang, C. and Meltzen, M., 1972, Propagation of elastic waves in a rock undergoing phase transitions, Cordilleran Section, 68th Annual Meeting, Geol. Soc. Am. Abst. 4, 256-257.

Warren. N., Trice, R., and Stephens, J, 1974, Ultrasonic attenuation: Q measurements on 70215, 29, Geochim. Cosmochim. Acta, Supp. 5, 2927-2938.

White, J.E., 1975, Computed seismic speeds and attenuation in rocks with partial gas saturation, Geophysics, 40, 224-232.

Winkler, K., Gladwin, M., and Nur, A., 1977, The dependence of seismic attenuation on effective stress, Abst., Trans. Am. Geophys. Union (EOS), 58, 1183.

Wyllie, M.R., Gregory, A.R. and Gardner, G.H.F., 1958,An experimental investigation of factors affecting elastic wave velocities in porous media, Geophysics, 23, 459-493.

Wyllie, M.R.J., Gardner, G.H.F. and Gregory, A.R., 1962, Studies of elastic wave attenuation in porous media, Geophysics, 27, 569-589.

Yamakawa, N., 1962, scattering and attenuation of elastic waves, Geophysical Magazine (Tokyo), 31, 63-103.

Zoback, M.D. and Byerlee, J.D., 1976, Effect of high pressure deformation on permeability of Ottawa sand, Am. Assoc. Pet. Geol. Bull., 60, 1531-1542.

Table 1. Measured Body Wave Q For Several Rock Types

Rock	Q	Frequency, Hz	Method	Reference
Quincy Granite	125	(.14-4.5) x 10^3	long resonance	Birch and Bancroft (1938)
	166		tors. resonance	
Solenhofen Limestone	112	(3-15) x 10^6	P wave pulses	Peselnick and Zietz (1959)
	188		S wave pulses	
I-1 Limestone	165	(5-10) x 10^6	P wave pulses	Peselnick and Zietz (1959)
Hunton Limestone	65	(2.8-10.6) x 10^3	long. resonance	Born (1941)
Amherst Sandstone	52	(.930-12.8) x 10^3	long. resonance	Born (1941)
Berea Sandstone (brine saturated)	10	(.2-.8) x 10^6	P and S wave pulses	Toksöz et al. (1977)
Navajo Sandstone	21	50 - 120	flexural vibrations	Bruckshaw and Mahanta (1954)
Pierre Shale	32	50 - 450	P wave in situ	McDonel et al. (1958)
	10		S wave in situ	

Table II

Physical Properties Used for Modeling the Berea Sandstone

Matrix: $K = 35 \times 10^{10}$ dynes/cm^2
$\mu = 25 \times 10^{10}$ dynes/cm^2
$\rho = 2.61$ g/cm^3

Inclusion: $K' = 2.6 \times 10^{10}$ dynes/cm^2
$\eta = 4 \times 10^{-2}$ poise
$\rho' = 1.0$ g/cm^3

Frame: $\phi \approx 0.16$
$\chi = 75$md

Fluid Flow Structure Constants: $a = 1.0 \times 10^{-4}$, $a' = 3.0$

TABLE III

Aspect Ratio Distributions

	Concentration, c	Aspect ratio, α
Surface	0.12	1.00
	0.04	0.10
	0.10×10^{-3}	0.17×10^{-2}
	0.10×10^{-3}	0.14×10^{-2}
	0.20×10^{-3}	0.10×10^{-2}
	0.15×10^{-3}	0.60×10^{-3}
	0.75×10^{-4}	0.30×10^{-3}
	0.30×10^{-4}	0.10×10^{-3}
	0.90×10^{-5}	0.30×10^{-4}
	0.30×10^{-5}	0.10×10^{-4}
10000 feet	0.119	1.00
	0.395	0.98×10^{-1}
	0.152×10^{-1}	0.258×10^{-3}

Figure Captions

Figure 1. Q as a function of porosity. Data for igneous and metamorphic rocks (triangles), limestones (squares), and sandstones (circles) are taken from Bradley and Fort (1966).

Figure 2. Change in Q as a function of saturation. Data from Obert et al. (1946) and Martin (1956).

Figure 3. Change in Q as a function of soltrol and water saturation in alundum at about 10 kHz. Data from Wyllie et al. (1962). Samples 7915-B and 7928-B for soltrol and water, respectively.

Figure 4. Q as a function of saturation and differential pressure in Berea sandstone, extensional mode. Data from Gardner et al. (1964).

Figure 5. Q as a function of saturation and differential pressure in Berea sandstone, torsional mode. Data from Gardner et al. (1964).

Figure 6. Relative attenuation of S waves as a function of pore fluid viscosity in Barre granite. Data from Nur and Simmons (1969a).

Figure 7. Change in the attenuation coefficient as a function of pressure for several rocks. Data from Klima et al. (1964).

Figure 8. Change in the attenuation coefficients of P and S waves as functions of pressure for several gneisses. Data from Levykin (1965).

Figure 9. Q^{-1} as a function of differential pressure in a granite. Data from Gordon and Davis (1968).

Figure 10. Schematic illustration of several proposed attenuation mechanisms for saturated and partially saturated rocks.

Figure 11. Model fit (solid and dashed lines) to data from Toksöz et al. (1978, Figure 7) dry Berea sandstone. Pore pressure is assumed to be 1 bar (14.7 psi).

Figure 12. Model fit to data from Toksöz et al. (1978, Figure 11), brine-saturated Berea sandstone.

Figure 13. Relative contributions of the friction and fluid flow mechanism for P waves from the model of Figure 12 as function of differential pressure.

Figure 14. P-wave attenuation coefficients at surface pressure as functions of frequency, for several mechanisms considered in the saturated Berea sandstone model. Model parameters are listed in Tables II and III and the text. The viscous shear relaxation mechanism is included on the line labeled "squirt" flow.

Figure 15. P-wave attenuation coefficients as functions of frequency for the saturated Berea model as in Figure 14. Here, the contributions for each mechanism are calculated at a differential pressure equivalent to about a 10000 ft. depth.

Figure 16 Q_p^{-1} and Q_s^{-1} for the "squirt" flow and viscous shear relaxation mechanisms in the saturated Berea sandstone model at surface pressure as functions of frequency.

Figure 17. Total Q_p for the saturated Berea model as a function of frequency and differential pressure based on the results presented in Figures 12, 14, and 15.

Fig

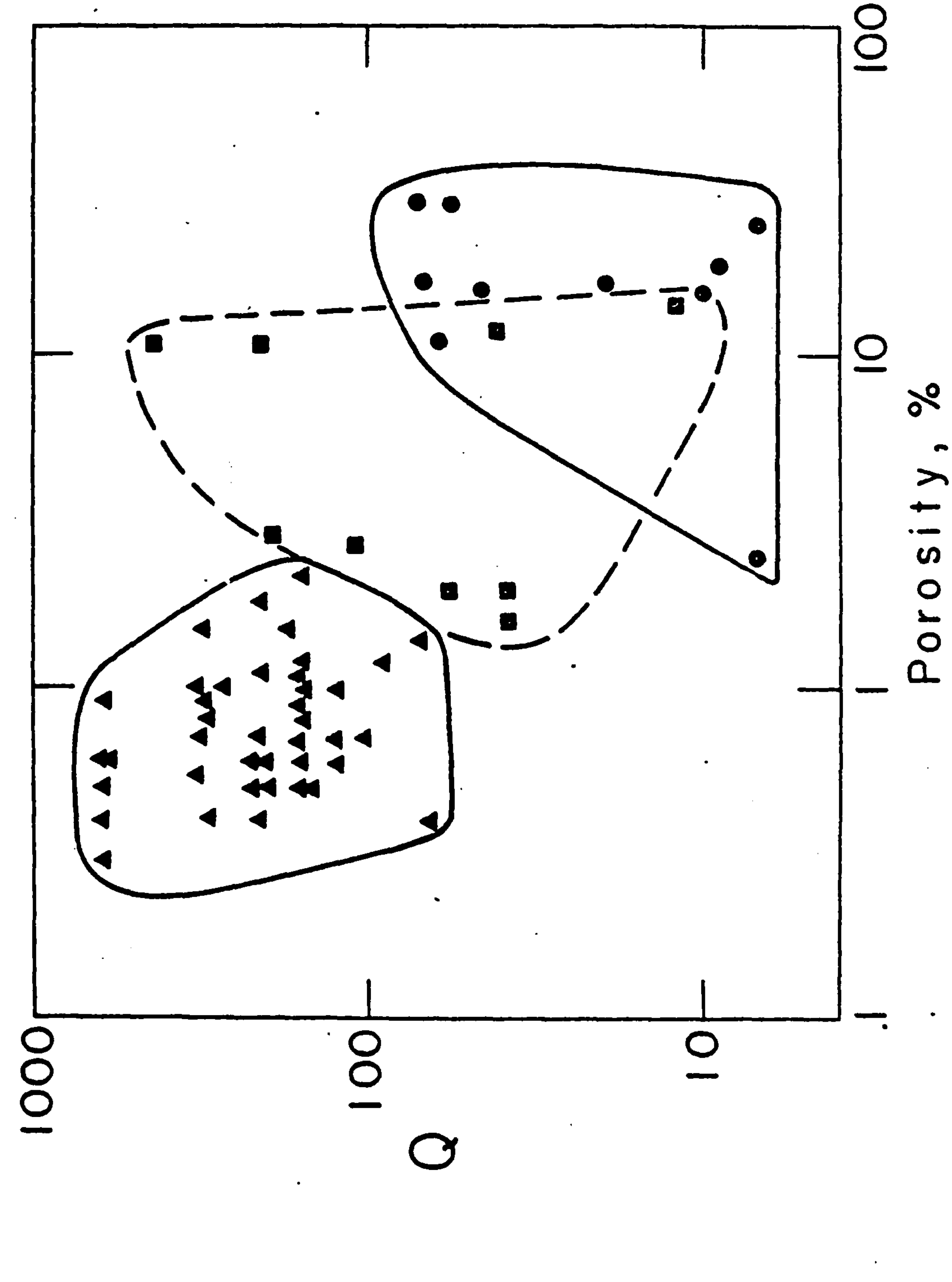

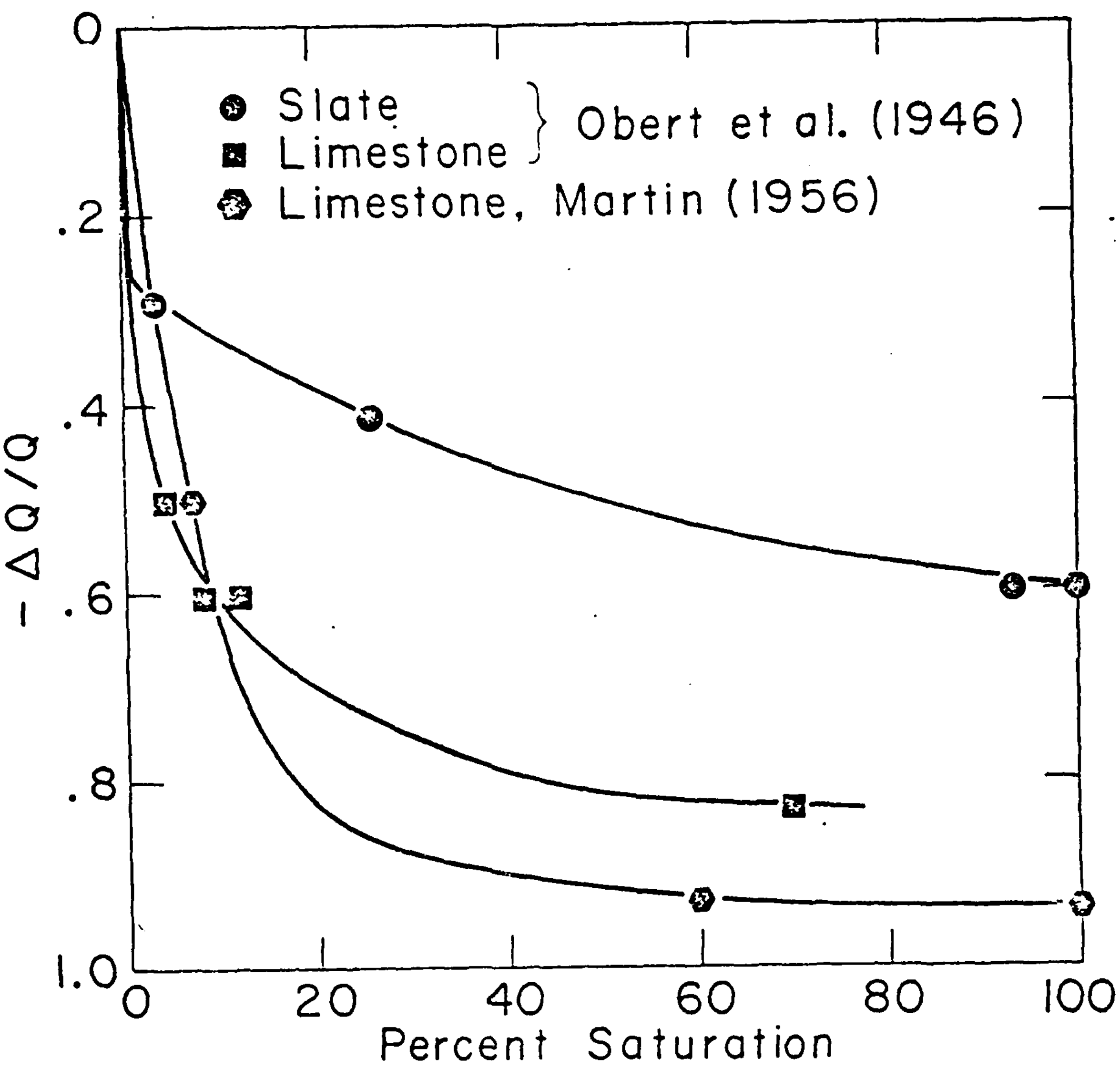
Slate
Limestone
Obert et al. (1946)
Limestone, Martin (1956)
0
.2
.4
.6
.8
1.0
- ΔQ/Q
0
20
40
60
80
100
Percent Saturation

Fig. 2

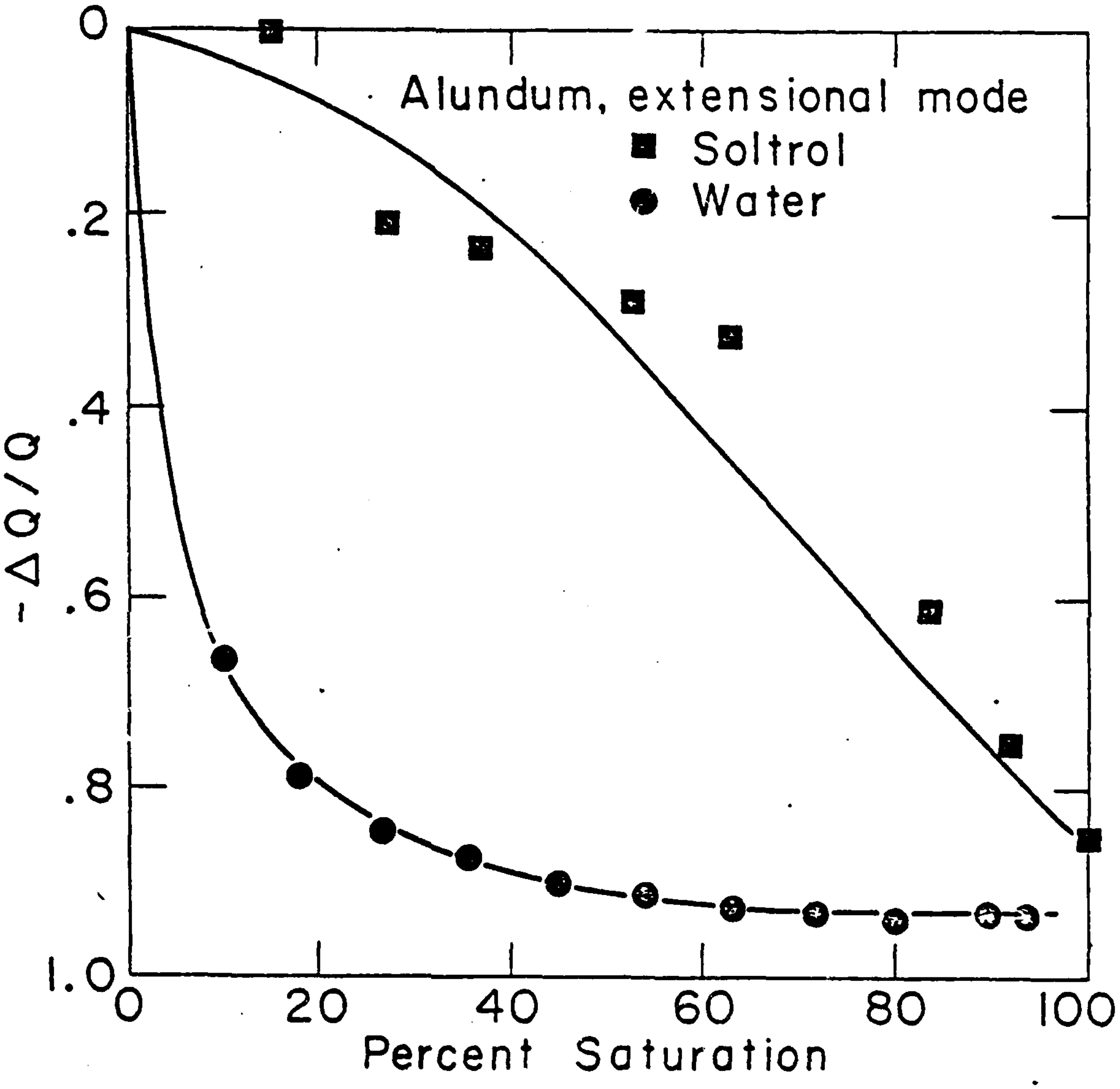
Alundum, extensional mode
■ Soltrol
● Water
0
.2
.4
.6
.8
1.0
-ΔQ/Q
0
20
40
60
80
100
Percent Saturation

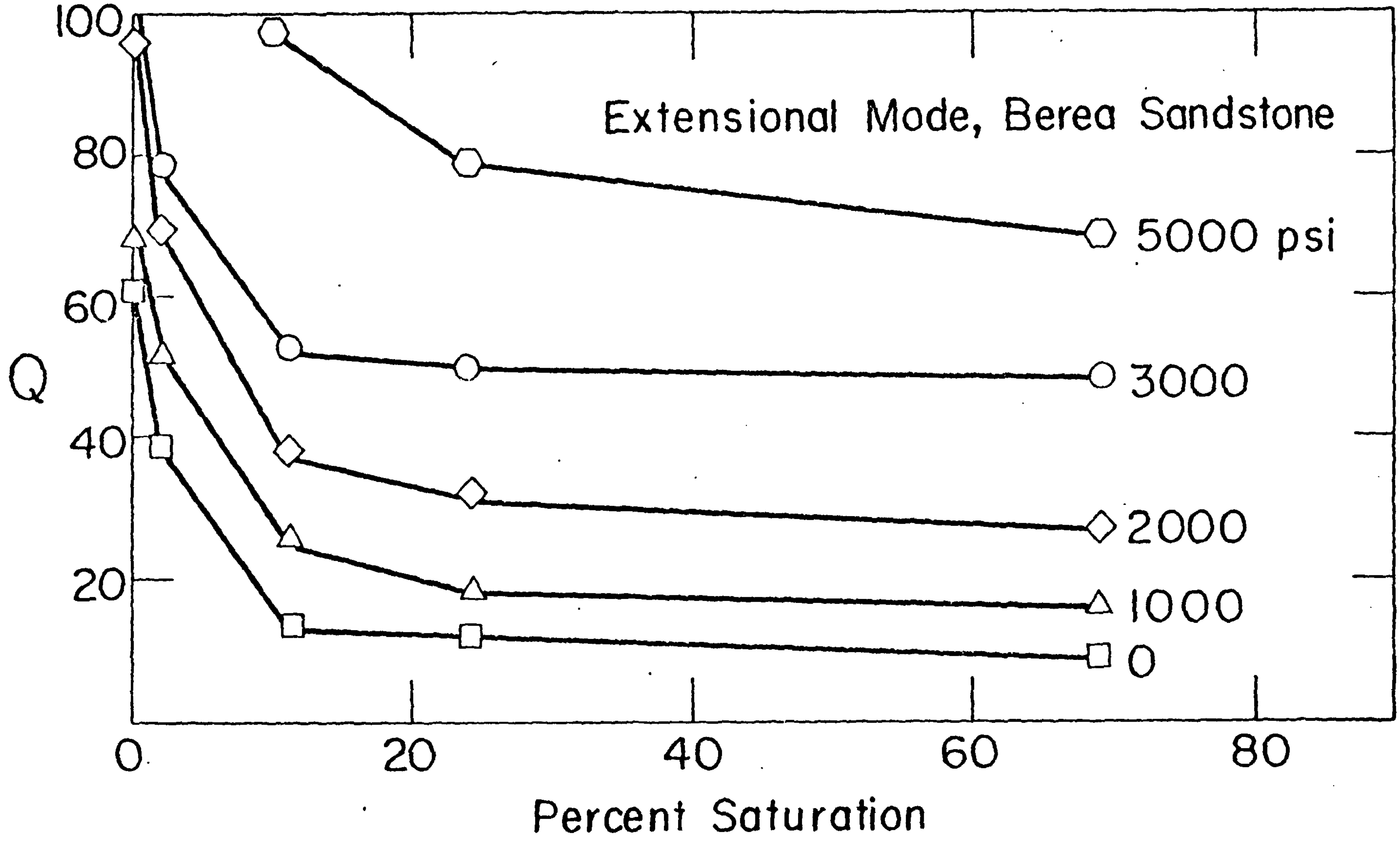
Extensional Mode, Berea Sandstone
5000 psi
3000
2000
1000
0
Q
100
80
60
40
20
0
20
40
60
80
Percent Saturation

Fig. 4

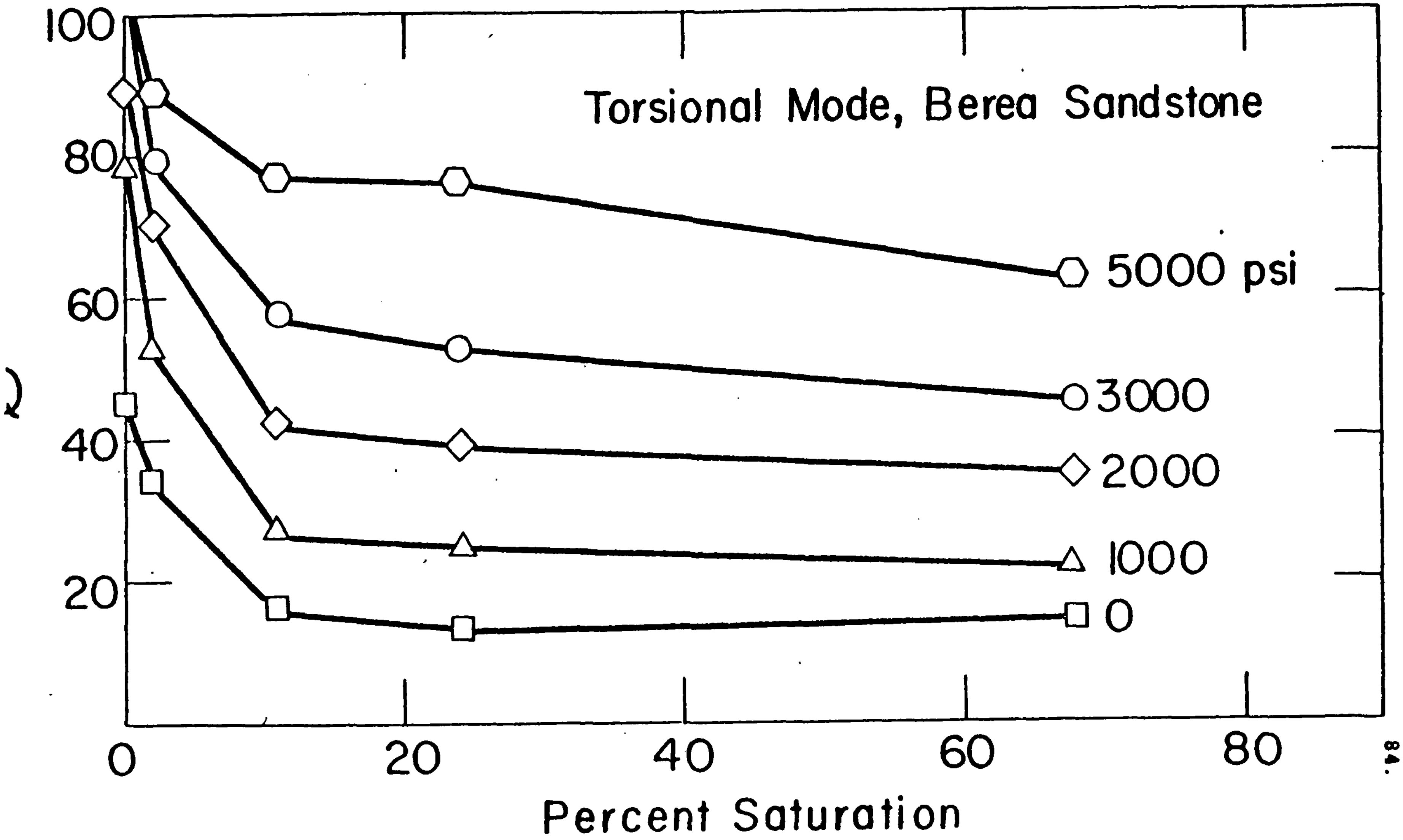
Torsional Mode, Berea Sandstone
100
80
60
40
20
0
20
40
60
80
Percent Saturation
5000 psi
3000
2000
1000
0

Fig. 5

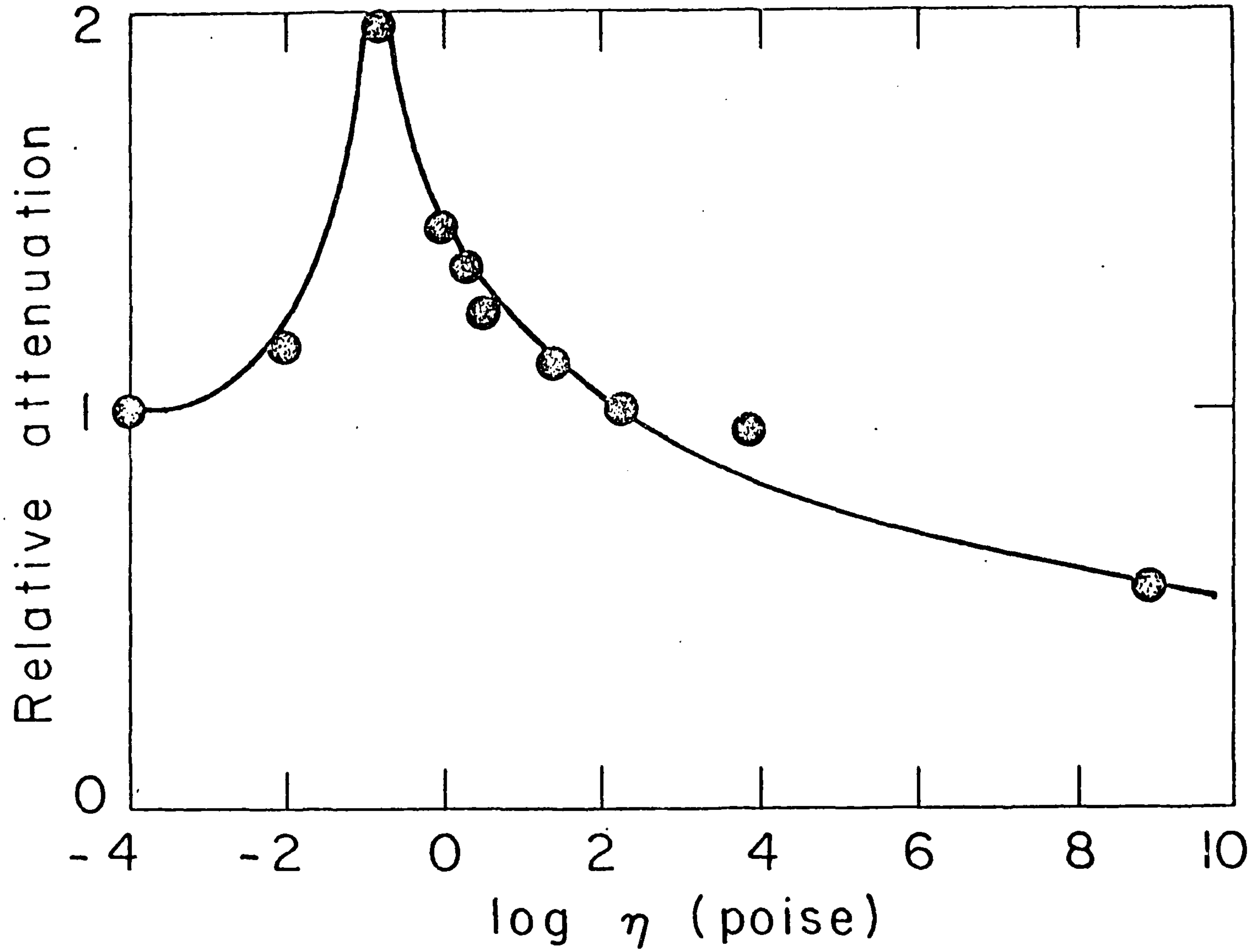

Fig. 6

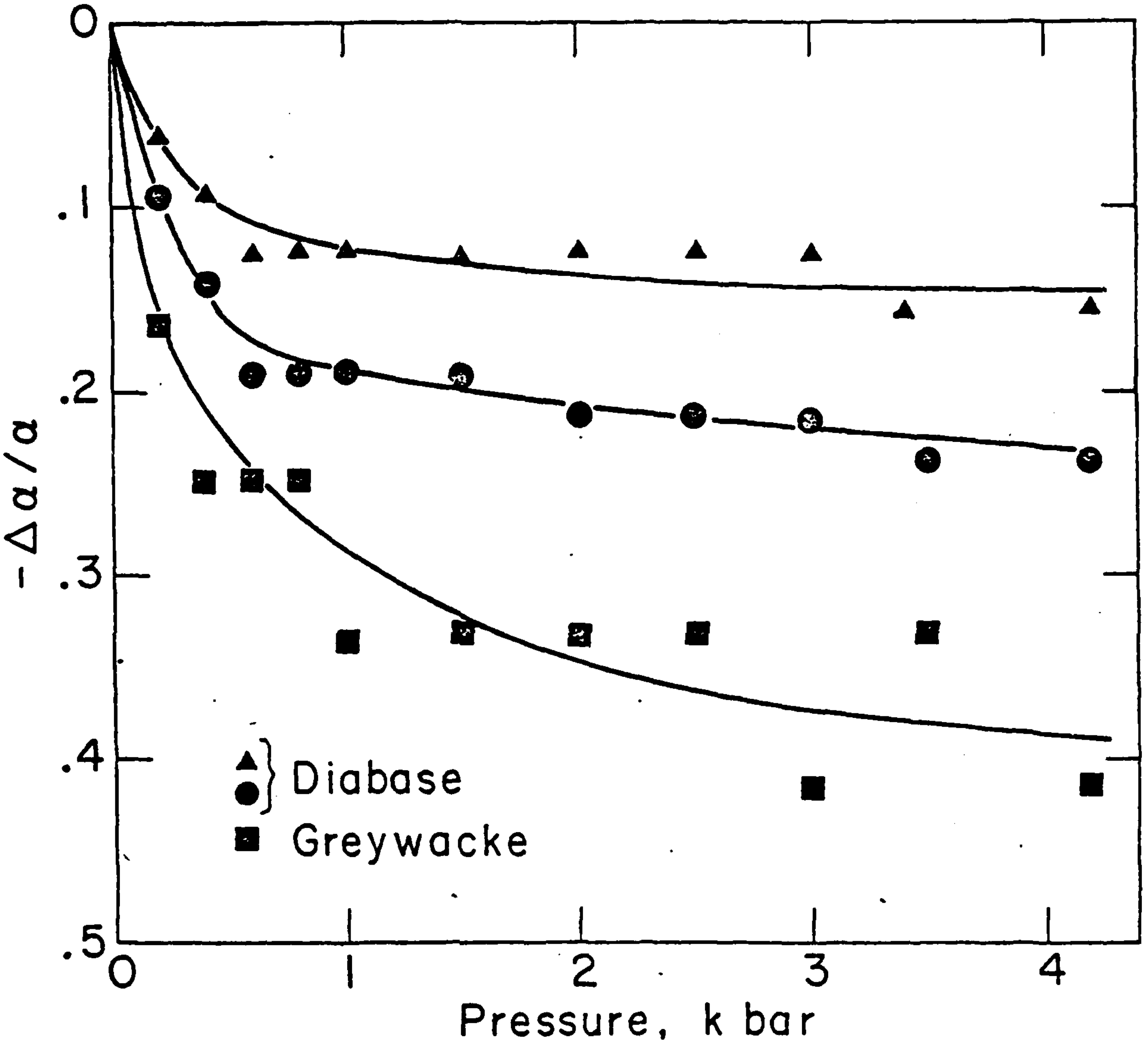

Fig. 7

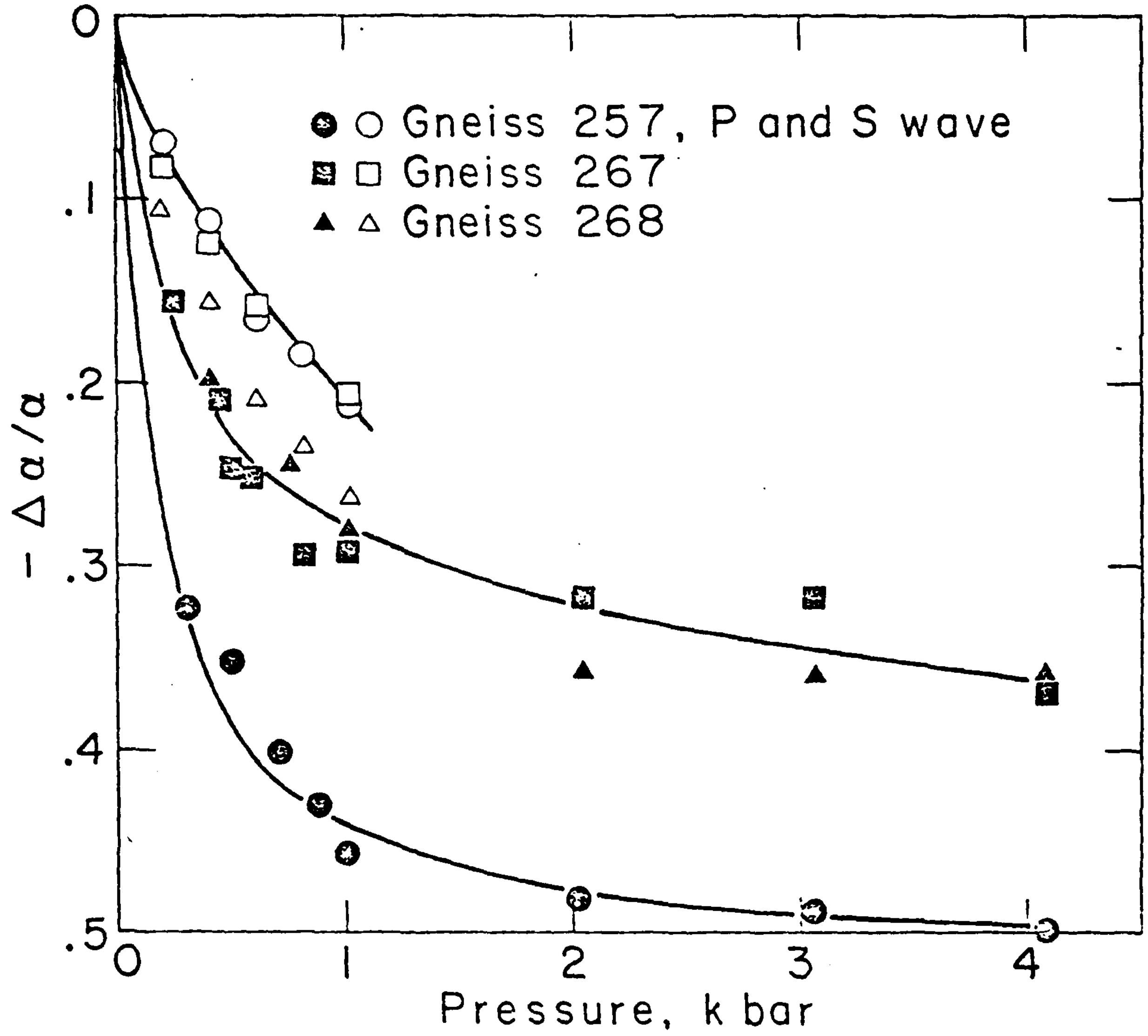
● ○ Gneiss 257, P and S wave
▨ □ Gneiss 267
▲ △ Gneiss 268
0
.1
.2
.3
.4
.5
- Δa/a
0
1
2
3
4
Pressure, k bar

Fig. 8

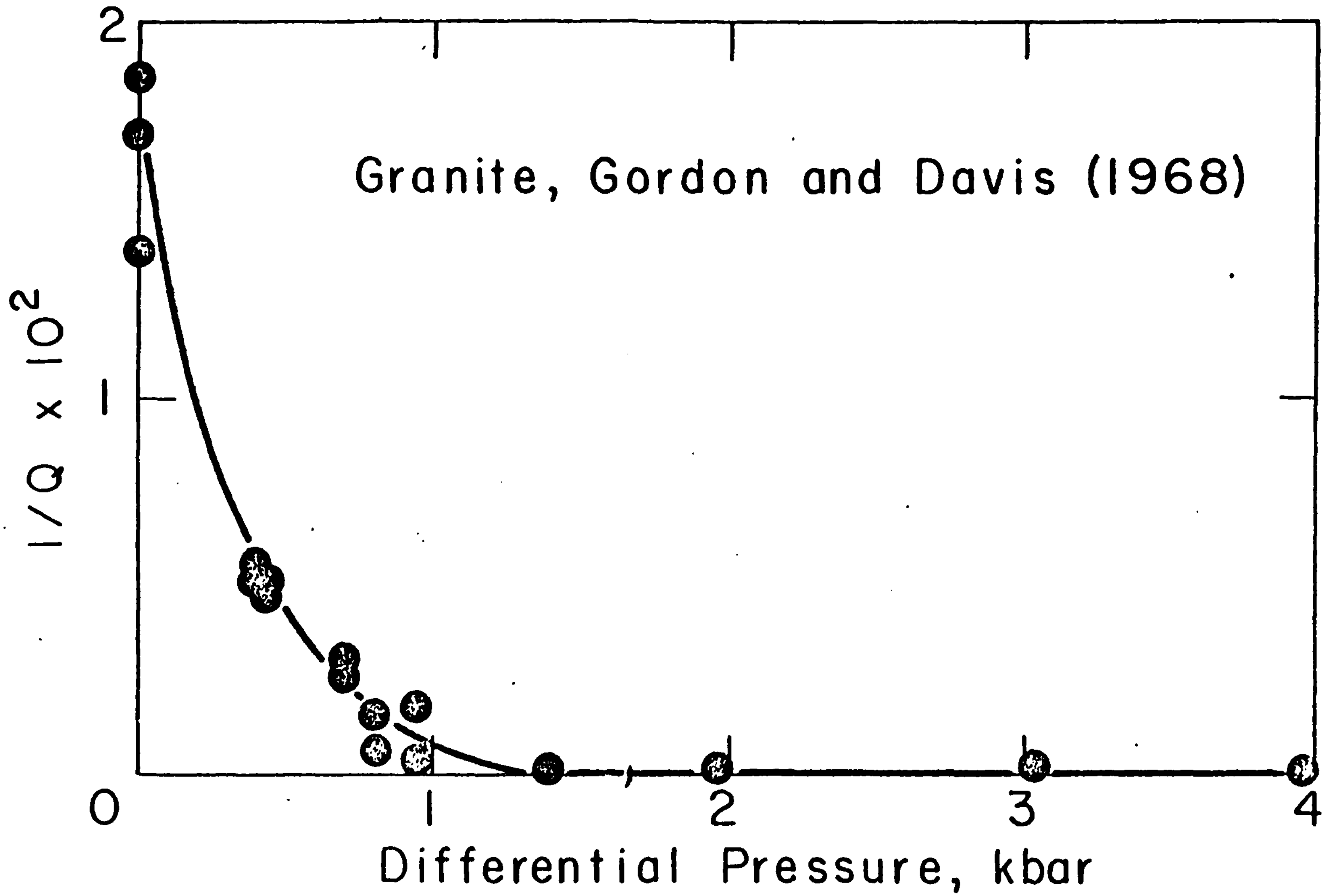
Granite, Gordon and Davis (1968)
$1/Q \times 10^2$
2
1
0
1
2
3
4
Differential Pressure, kbar

Fig. 9

Effects of Fluid Saturation

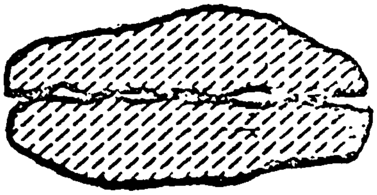

Crack Lubrication
Facilitating Friction

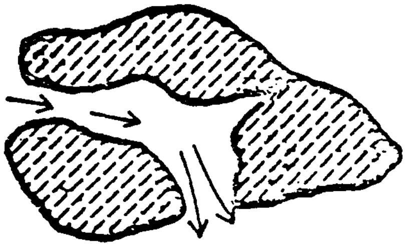

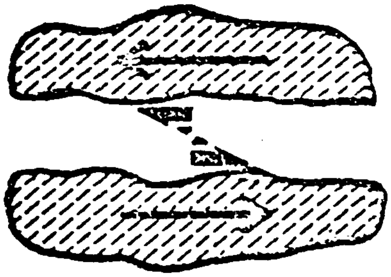

Biot Fluid Flow with
Boundary Shear

Squirting Flow

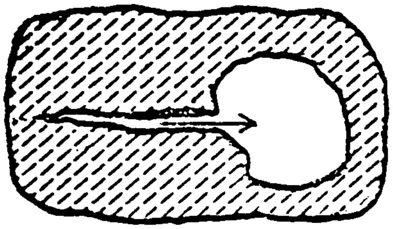

crack to pore

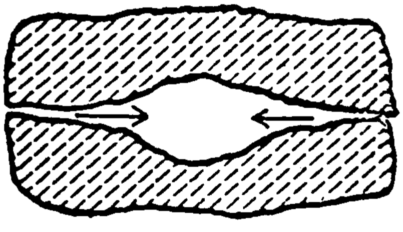

edge to center

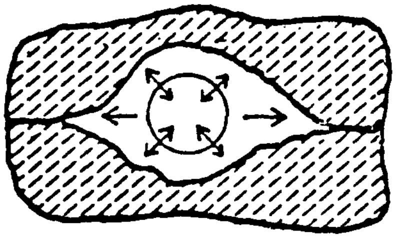

Gas Bubble Motion
and Squeezing

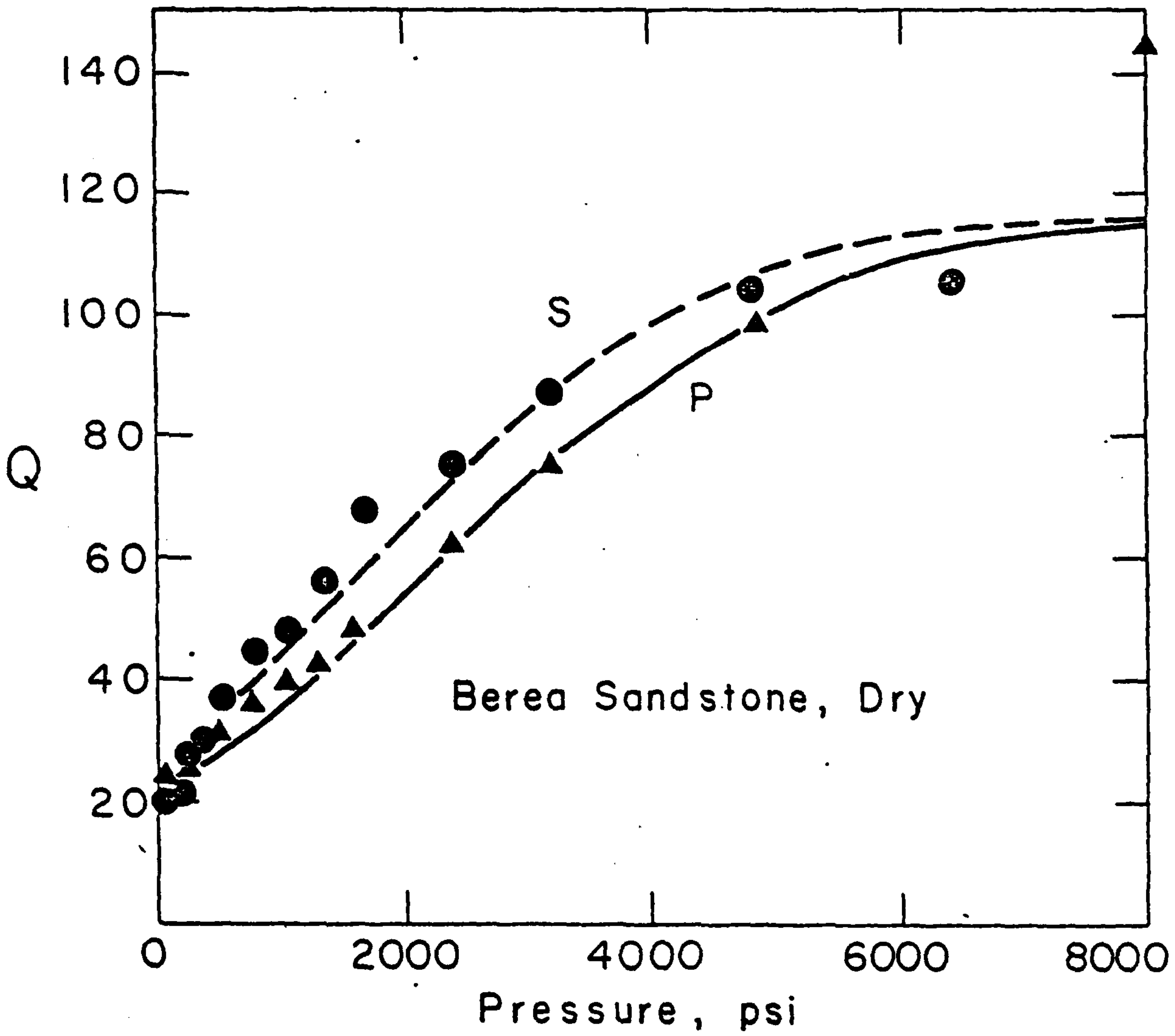
140
120
100
80
60
40
20
Q
S
P
Berea Sandstone, Dry
0
2000
4000
6000
8000
Pressure, psi

Fig. 11

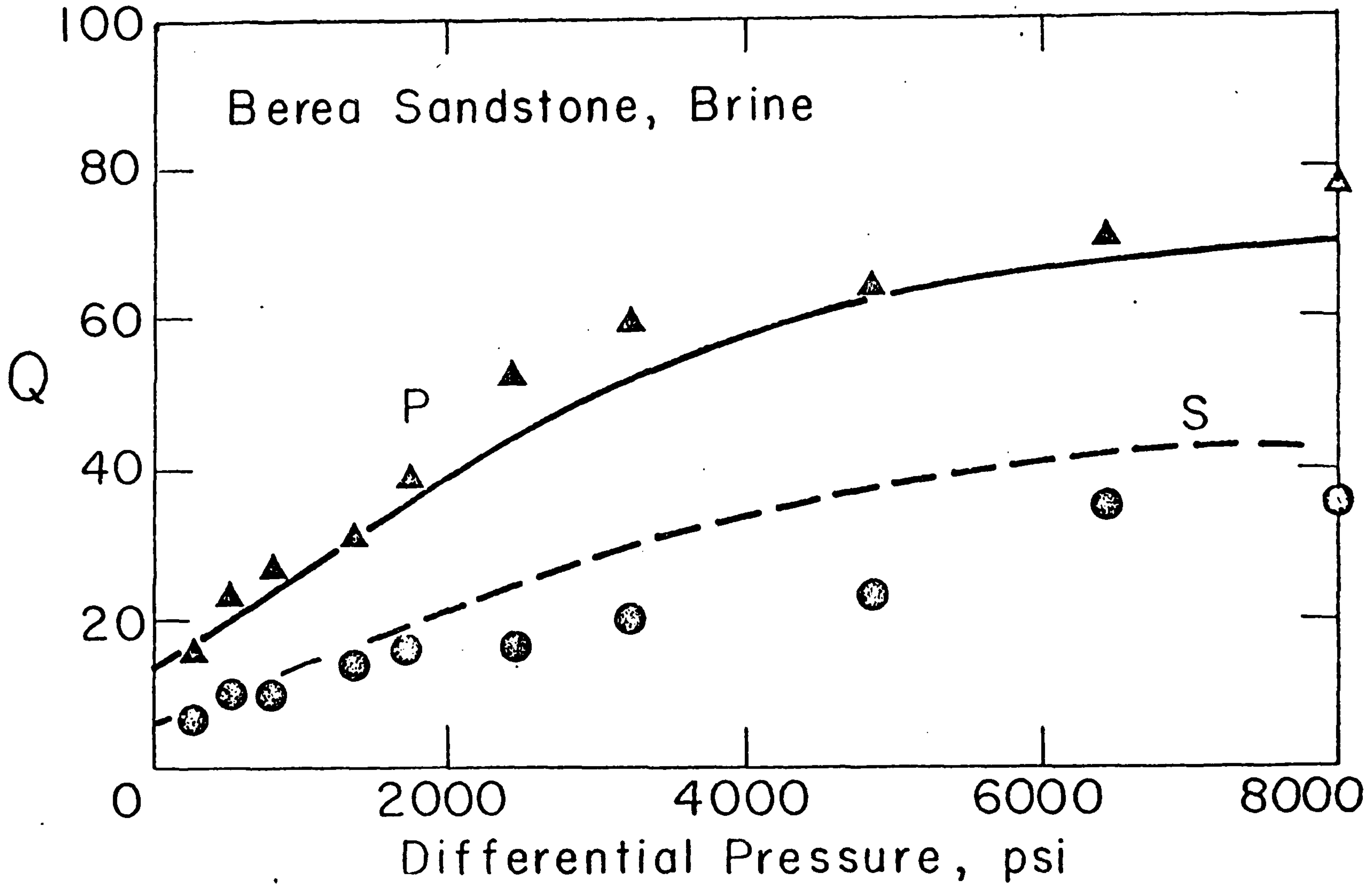
Berea Sandstone, Brine
Q
100
80
60
40
20
0
2000
4000
6000
8000
Differential Pressure, psi
P
S

Fig. 12

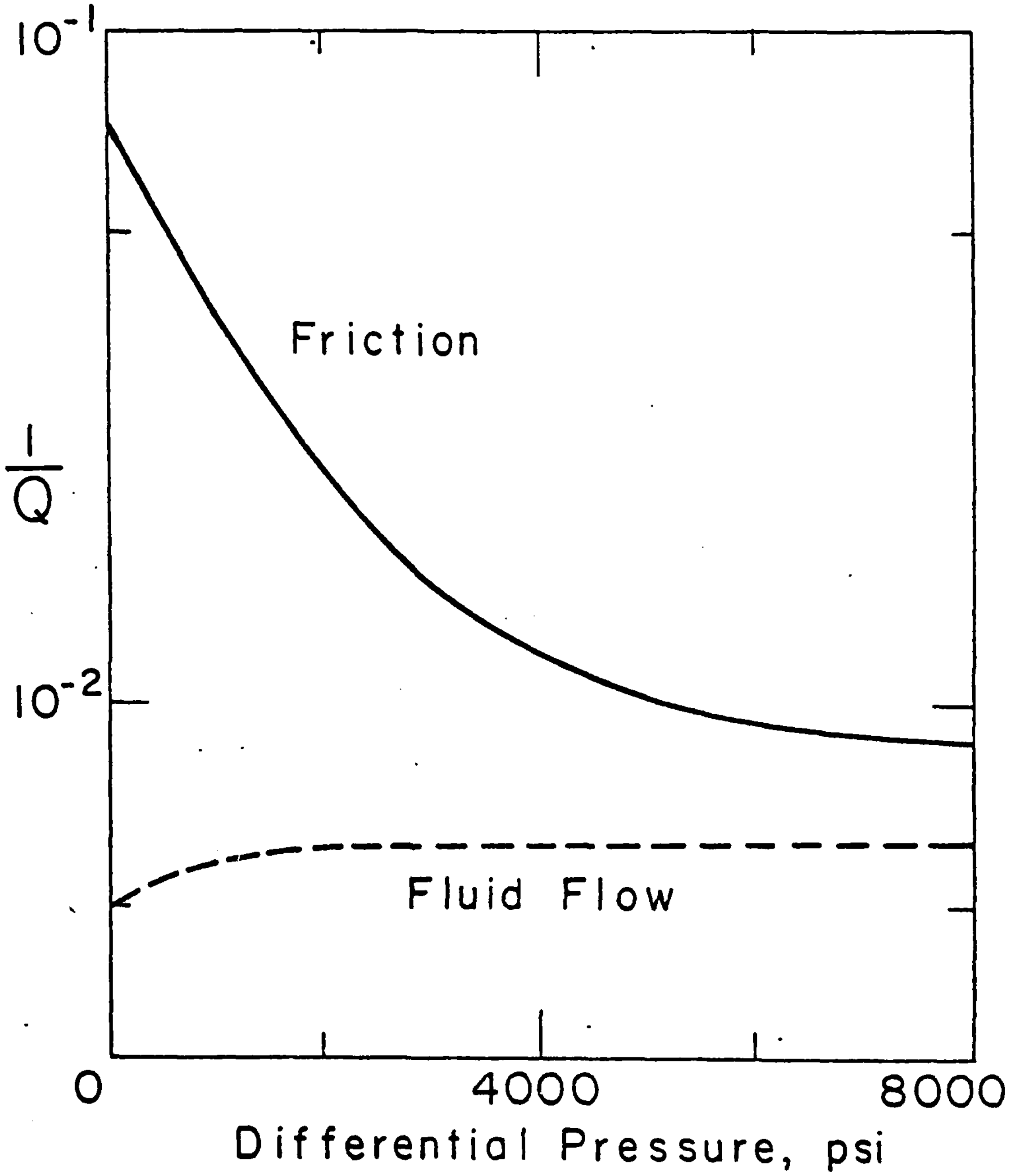
10^{-1}
10^{-2}
$\frac{1}{Q}$
Friction
Fluid Flow
0
4000
8000
Differential Pressure, psi

Fig. [illegible]

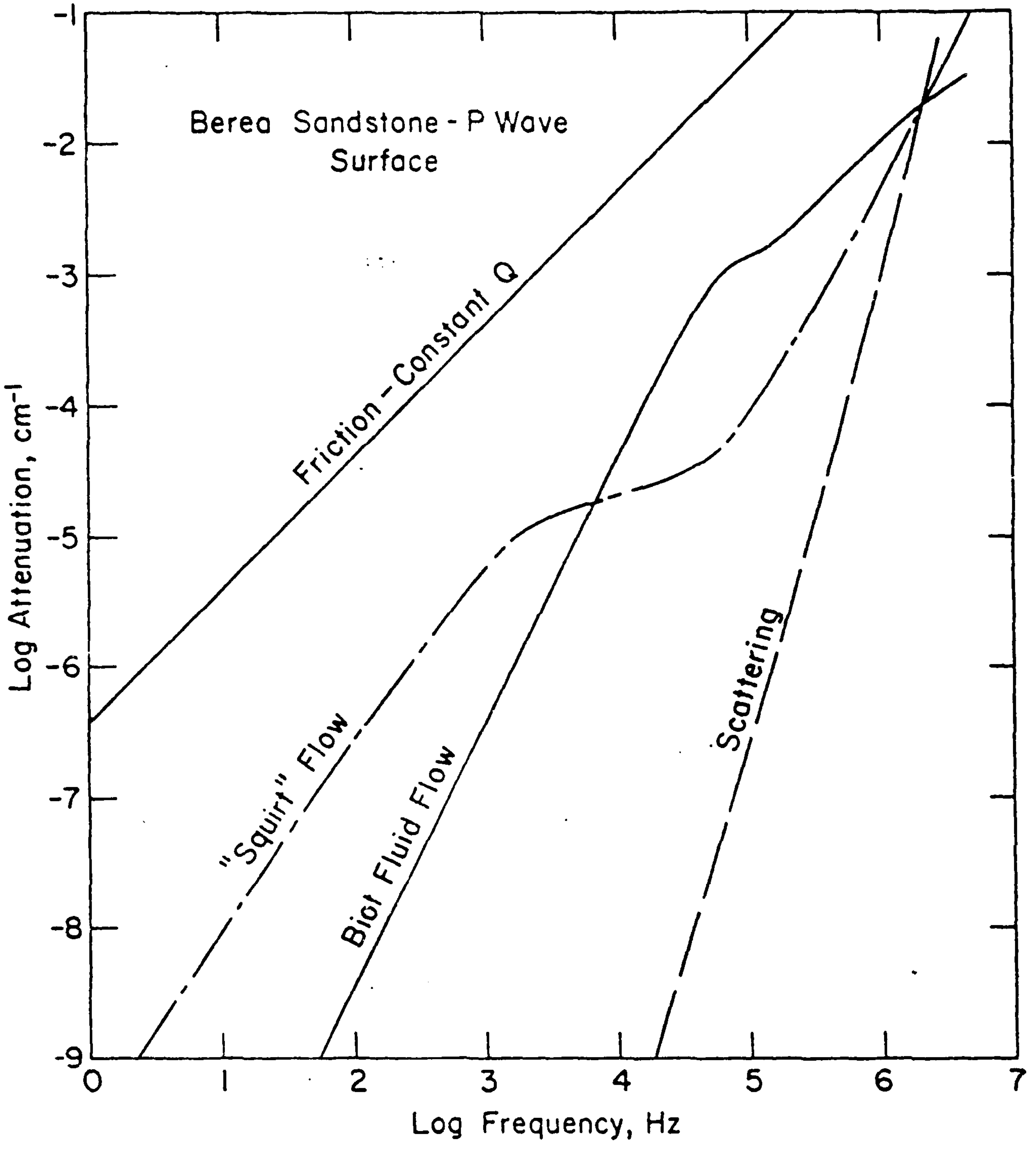
Berea Sandstone - P Wave
Surface
Friction - Constant Q
"Squirt" Flow
Biot Fluid Flow
Scattering
Log Attenuation, cm^{-1}
Log Frequency, Hz
-1
-2
-3
-4
-5
-6
-7
-8
-9
0
1
2
3
4
5
6
7

Fig. 14

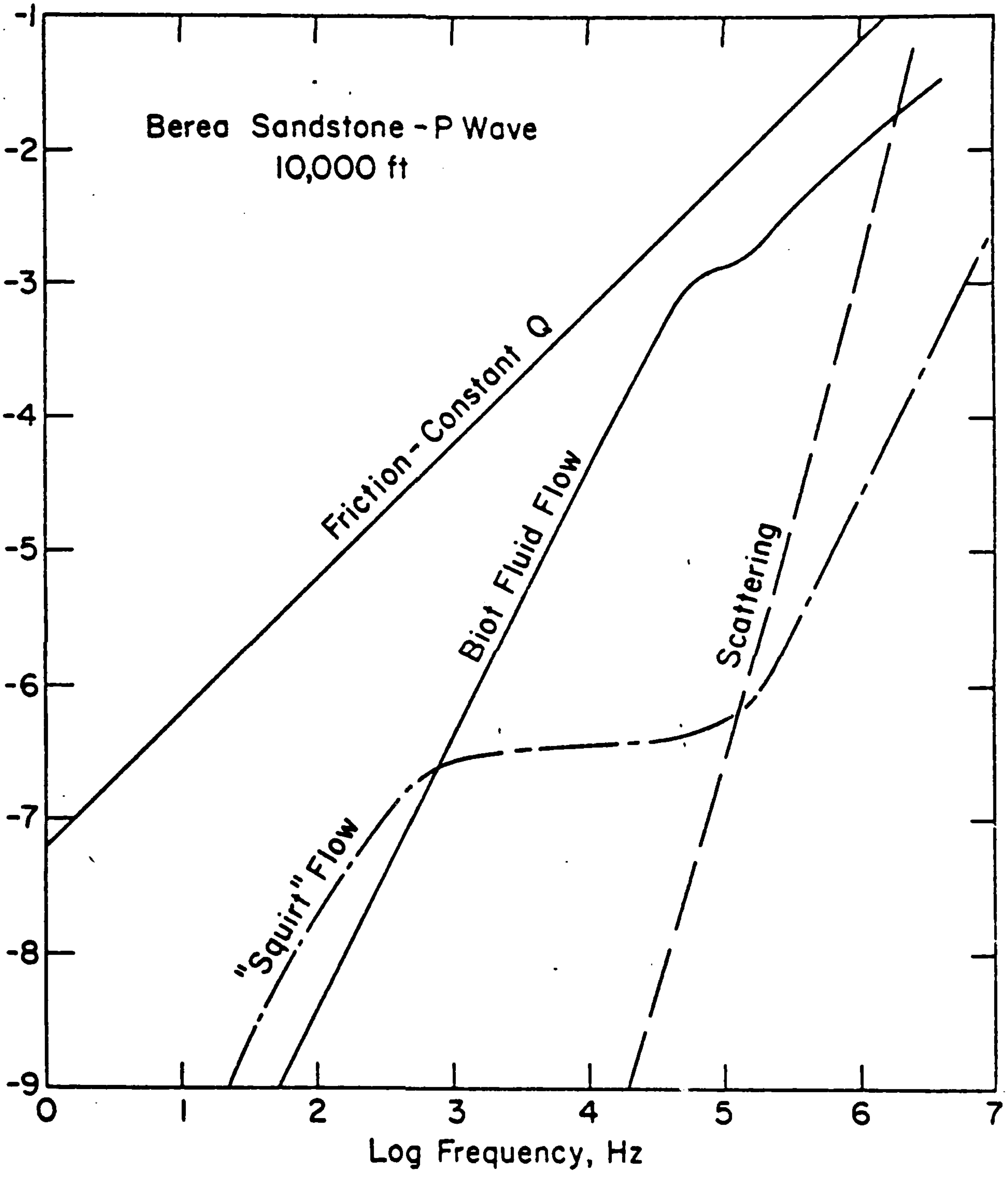
Berea Sandstone - P Wave
10,000 ft
Friction - Constant Q
Biot Fluid Flow
Scattering
"Squirt" Flow
Log Attenuation, cm⁻¹
Log Frequency, Hz
-1
-2
-3
-4
-5
-6
-7
-8
-9
0
1
2
3
4
5
6
7

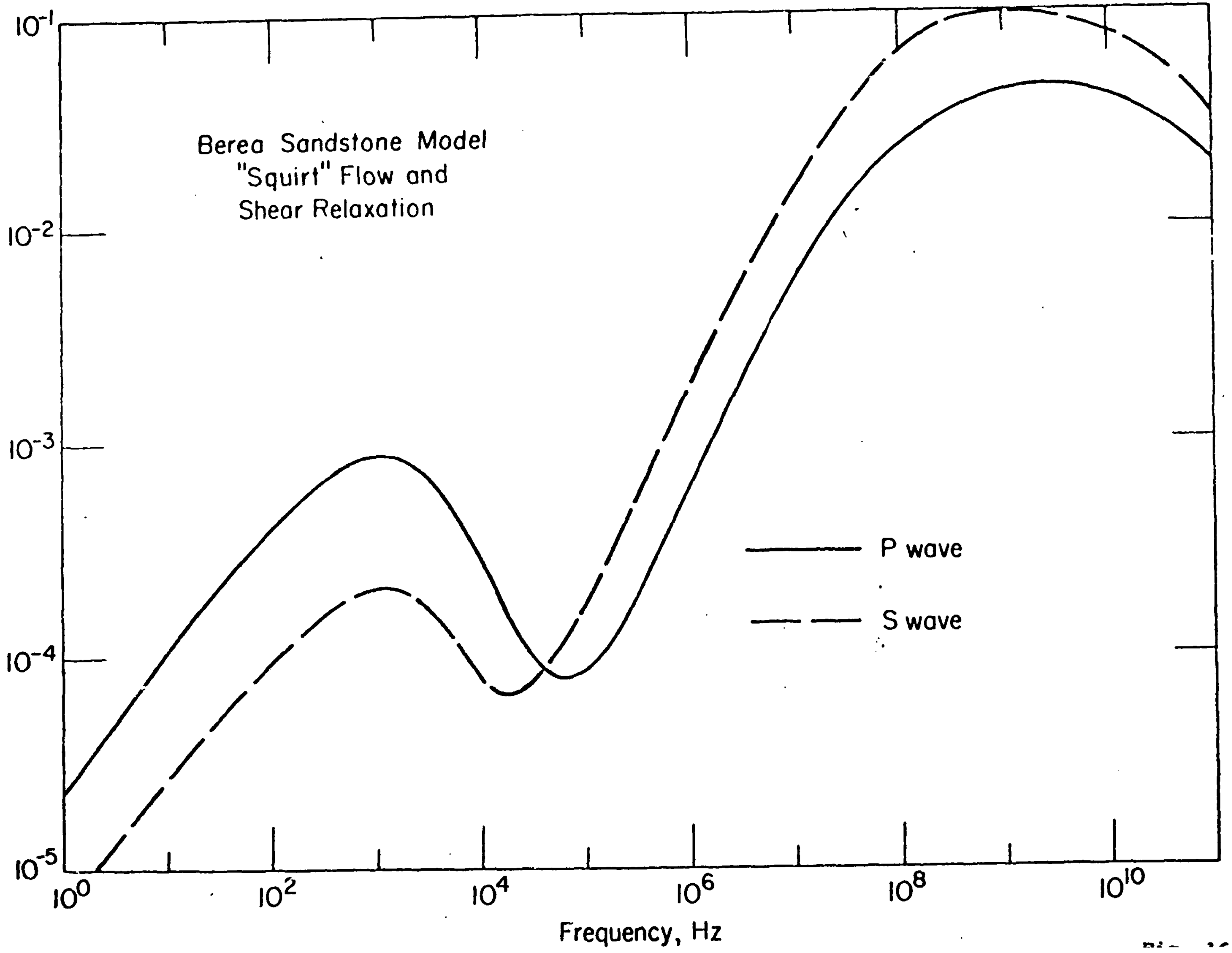
Berea Sandstone Model
"Squirt" Flow and
Shear Relaxation
P wave
S wave
10^-1
10^-2
10^-3
10^-4
10^-5
10^0
10^2
10^4
10^6
10^8
10^10
Frequency, Hz

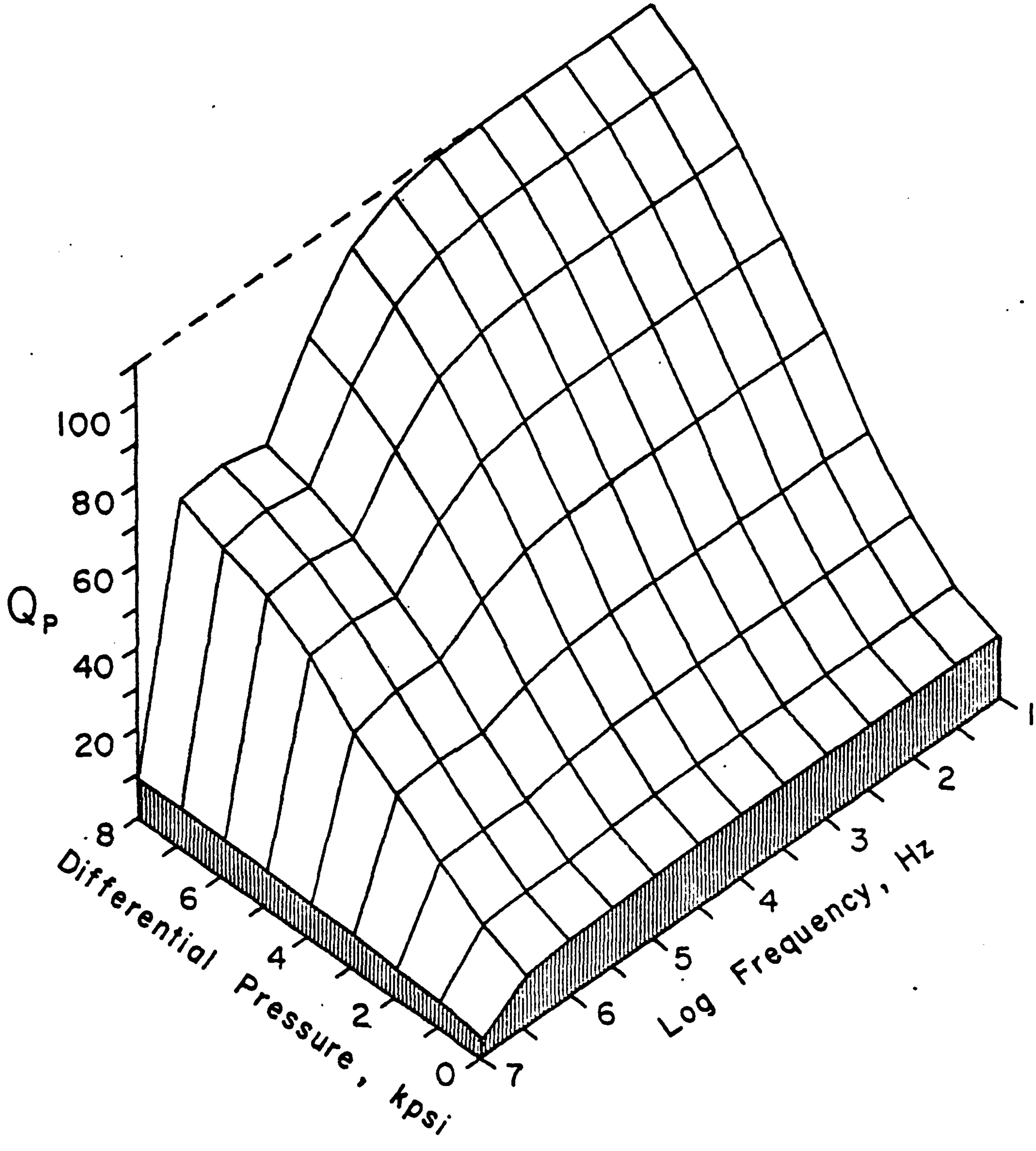
Q_P
100
80
60
40
20
8
6
4
2
0
Differential Pressure, kpsi
1
2
3
4
5
6
7
Log Frequency, Hz

Fig. 17

SIMULTANEOUS INVERSION OF SURFACE WAVE PHASE VELOCITY AND ATTENUATION FOR CONTINENTAL AND OCEANIC PATHS

by

Wook Bae Lee

B.S., Seoul National University
(1966)
M.S., Indiana University
(1972)

SUBMITTED IN
PARTIAL FULFILLMENT
OF THE REQUIREMENTS FOR THE
DEGREE OF DOCTOR OF PHILOSOPHY

at the

MASSACHUSETTS INSTITUTE OF TECHNOLOGY

November, 1977

Signature of Author.. Wook Bae Lee ....
Department of Earth and Planetary Sciences, 4 November 1977

Certified by......... Sean C. Solomon ....
Thesis Supervisor

Accepted by..
Chairman, Departmental Committee on Graduate Students

ABSTRACT

Simultaneous Inversion of Surface Wave Phase Velocity and Attenuation for Continental and Oceanic Paths

by

Wook Bae Lee

Submitted to the Department of Earth
and Planetary Sciences on 4 November 1977
in partial fulfillment of the
requirements for the degree of
Doctor of Philosophy

An inversion study of surface wave attenuation and dispersion has been conducted to investigate the vertical and lateral variations of shear attenuation and shear velocity structure in the earth's mantle. Variation of lithosphere thickness and of shear attenuation in the asthenosphere can be related to temperature variations, partial melting and even some indications of the tectonic history of the earth. Possible attenuation mechanisms in the earth's mantle are expected to be thermally activated relaxation mechanisms. The relatively small strains associated with seismic wave amplitudes satisfy linearity at least approximately for such mechanisms. The linearity assumption is particularly important because of its

computability. Causality and superposition principals are the main characteristic of linearity. Anelastic dispersion, which arises from linearity, is an important consequence due to causality. In a viscoelastic medium, anelastic dispersion (due to causality) is considered by a given dispersion-attenuation relation and implemented into the inversion schemes.

A formalism for simultaneous inversion is developed and applied to data from North America and the Pacific. The simultaneous inversion approach is formally different and gives a different result from the approximate inversion scheme of Anderson and Hart (1976). The L_1 norm concept in the inversion process is particularly advantageous for the sparse and inaccurate seismic attenuation data. The set theoretical approach (Lee and Solomon, 1975), which includes the square matrix inverse and linear programming (L_1 norm inversion) was used for the actual inversion.

Inversion results show: (1) a distinctive low-Q zone everywhere in North America and the Pacific; (2) a varying thickness for the high-Q lid; 60±20 km (Pacific); 80±20 km (western North America), 130±30 km (east-central North America); (3) the LVZ and LQZ coincide in western North America and the Pacific, and overlap in eastern North America; (4) anisotropy may be a problem in western North America but is not a problem in east-central North America; (5) the data do not discriminate

among possible dispersion relations because errors in Q^{-1} data are too large; (6) the predicted dispersion in the low velocity zone varies from region to region and according to the intrinsic dispersion relation assumed.

Thesis Supervisor: Sean C. Solomon

Title: Associate Professor of Geophysics

Acknowledgements

My deepest gratitude goes to Professor Sean C. Solomon for his guidance, constructive criticism, and enthusiasm. Plus he improved this manuscript to a readable form.

I appreciate helpful discussions with Professor Aki and my thanks to Professor Jackson who let me out of my post-doctoral duties at U.C.L.A. to finish this work.

I owe thanks to Dr. Brian Mitchell who sent me his attenuation data in a tabulated form and the station information on Q^{-1} measurements in the Pacific. I also owe thanks to Dr. J. Weissel, who sent me his up-to-date results on the marginal basins in the western Pacific.

I also appreciate Howard Patton's efforts which helped my attempts at searching the long-period Rayleigh wave data in the western United States and George Zandt who let me use his matrix decomposition program.

I wish to mention office mates Mike Fehler and Steve Taylor, who helped me in many ways in the last stage of this work. I would like to thank Ms. Dorothy Frank and Ms. Ellen Loiselle for their typing efforts. And last, I extend special gratitude to my wife, Heiyoung, whose patience, sacrifice, cheer, and even complaint, helped to finish this work.

This investigation was supported by the Advanced Research Projects Agency and monitored by the Air Force Office of Scientific Research under contracts F44620-71-C-0049 and F44620-75-C-0064.

Table of contents

Page

Abstract 1

Acknowledgements 4

List of Figures 9

List of Tables 13

I. Introduction 14

II. Set theoretical approach: Inversion schemes

2.1 Resume 27

2.2 Uniqueness, resolution and errors 29

2.3 L_1 and L_2 norms 30

2.4 Classification of inversion schemes 32

2.4a Single ('best') model and extreme models 33

2.4b Model and data statistics 33

1. Stochastic inverse 34

2. Weighted least square inverse 36

3. Set theoretical approach 38

2.5 Set theoretical approach 38

2.5a Square matrix method 39

2.5b Linear programming technique 41

2.5c Ellipsiods: Edgehog method 42

2.6 Q^{-1} models in North America: Set theoretical approach

2.6.1 Data 43

Page

2.6.2 Resolution 52

2.6.3 Correlation and incompatibility 64

2.6.4 Linear programming procedure 69

2.6.5 Results and discussion 71

III. Attenuation mechanisms in the upper mantle

3.1 Resume 87

3.2 Seismic and laboratory observations 88

3.3 Non-linear or linear attenuation process? 92

3.4 Solid friction and viscous damping 93

3.5 Hysteresis, resonance, scattering and relaxations 95

3.6 The distribution function of relaxations 98

3.6a Box distribution - Becker theorem 99

3.6b Log-normal distribution (Gaussian) 101

3.7 Q frequency dependent or independent ? 103

IV. Anelastic dispersion

4.1 Resume 107

4.2 Superposition and causality 106

4.3 Anelastic dispersion 110

4.3a Importance of anelastic dispersion in seismic studies 111

4.3b Reasons for neglect of anelastic dispersion in the past 112

Page

4.4 Dispersion-attenuation relations 113

    4.4a Frequency independent Q 114

    4.4b Frequency dependent Q 116

V. Formulation of simultaneous inversion of surface wave phase velocity and attenuation

5.1 Resume 119

5.2 Forward problem 119

5.3 Inverse problem 122

5.4 Resolution analysis 132

5.5 Inversion procedure at a reference frequency 135

VI. Applications

6.1 Data 138

    6.1a North America 138

    6.1b The central Pacific 141

6.2 Inversions:

    6.2a Love waves in western North America 151

    6.2b Love and Rayleigh waves in western North America 172

    6.2c Love and Rayleigh waves in east-central North America 185

    6.2d Rayleigh waves in the central Pacific 205

Page

6.3 Discussion:

6.3a Love waves in western North America 224

6.3b Love and Rayleigh waves in western North America 229

6.3c Love and Rayleigh waves in east-central North America 230

6.3d Rayleigh waves in the central Pacific 231

VII. Conclusions 233

References 241

Appendices

I. Kramers-Krönig relations 258

II. Dispersion relations: Frequency domain approach 263

III. Dispersion relations: Time domain approach 266

IV. Partial derivatives at a reference frequency 269

V. Comparison between simultaneous inversion and the correction technique of Anderson and Hart 272

List of Figures

Page

2.1 Paths of two-station Q^{-1} measurements in North America 50

2.2a Resolving kernels of surface wave attenuation, western United States(1) 55

2.2b Resolving kernels of surface wave attenuation, east-central United States(2) 56

2.2c Resolving kernels of surface wave attenuati east-central United States(3) 57

2.3 Constraints in two-dimensional solution space of Q^{-1} 61

2.4 Correlation length D_{ij} between i-th and j-th observations 67

2.5a Envelope of attenuation model for western United States(1) 73

2.5b Envelope of attenuation model for east-central United States(2) 74

2.5c Envelope of attenuation model for east-central United States(3) 75

2.6a Love wave attenuation predicted by Q^{-1} model, western United States(1) 78

2.6b Rayleigh wave attenuation predicted by Q^{-1} model, western United States(1) 79

2.6c Love wave attenuation predicted by Q^{-1} model, east-central United States(2) 80

Page

2.6d Rayleigh wave attenuation predicted by Q^{-1}, east-central United States (2) 81

2.6e Love wave attenuation predicted by Q^{-1}, east-central United States (3) 82

2.6f Rayleigh wave attenuation predicted by Q^{-1}, east-central United States (3) 83

6.1 Pacific area map with the earthquake (April 26, 1973, $20^h 26^m 30.8^s$, latitude 19.9°N, longitude 155.13°W, $m_b = 6.0$), stations and paths. 143

6.2 Rayleigh wave dispersion, central Pacific: observations and predictions 147

6.3 Rayleigh wave group velocity, central Pacific 145

6.4 The initial model of density, shear wave velocity and shear attenuation, western North America (a) 153

6.5 Love wave dispersion, western North America (a): observations and predictions 156

6.6 Love wave attenuation, western North America (a): observations and predictions 158

6.7a Partial derivatives of Love waves: real and imaginary parts, western North America ($\nu = o$) 161

6.7b Partial derivatives of Rayleigh waves: real and imaginary parts, western North America ($\nu = o$) 163

Page

6.8a Resolving kernels for shear wave velocity, western North America (a) 170

6.8b Resolving kernel of shear attenuation, western North America (a) 171

6.9 Envelopes of shear velocity and attenuation, models S1 and E1, western North America (a) 174

6.10 Envelopes of shear velocity and attenuation, models S4 and E1, western North America (a) 176

6.11 'Best' fitting earth models, S11 and QC11 comparison, western North America (a) 178

6.12a Resolving kernels of shear velocity, western North America (b) 182

6.12b Resolving kernels of shear attenuation, western North America (b) 184

6.13 Envelopes of shear velocity, shear attenuation and density, models S31W, S32W and S33W, western North America (b) 187

6.14 Love wave dispersion, western North America (b): observations and predictions 189

6.15 Rayleigh wave dispersion, western North America (b): observations and predictions 191

6.16 Love wave attenuation, western North America (b): observations and predictions 193

6.17 Rayleigh wave attenuation, western North America (b): observations and predictions 195

6.18a Resolving kernels of shear velocity, east-central North America 197

Page

6.18b Resolving kernels of shear attenuation, east-central North America 199

6.19 Envelopes of shear velocity, shear attenuation and density, models S31E and S32E 201

6.20 Love wave dispersion, east-central North America: observations and predictions 207

6.21 Rayleigh wave dispersion, east-central North America: observations and predictions 209

6.22 Love wave attenuation, east-central North America: observations and predictions 211

6.23 Rayleigh wave attenuation, east-central North America: observations and predictions 213

6.24a Resolving kernels of shear velocity, the central Pacific 215

6.24b Resolving kernels of shear attenuation, the Central Pacific 217

6.25 Envelopes of shear velocity and attenuation, model S21P 219

6.26 Rayleigh wave attenuation, the central Pacific: observations and predictions 221

List of Tables

Page

2.1 Love wave and Rayleigh wave propagation parameters, western United States 44

2.2 Love wave and Rayleigh wave propagation parameters, east-central United States 46

2.3 Focusing indices of three-layered Q_β^{-1} model: Love wave data, western United States 63

2.4 Correlation length D_{ij} between selected Q_L^{-1} data, western United States 68

2.5 Envelopes of attenuation model, $100/Q_\beta$, western United States and east-central United States 76

5.1 Expressions for the quantities $F_{ijkl}^{(m)}$ 128

6.1 Events examined for long period Rayleigh waves, LON to TUC 140

6.2 Great circle paths in each age group for the 26 April 1973 Pacific event 145

6.3 Ages of marginal basins in the Pacific 150

6.4 Starting Q^{-1} models for inversion of Love wave data, western North America 154

6.5 Envelopes of shear velocity and shear attenuation at 0.01 Hz for selected simultaneous inversions 165

Page

6.6 Envelopes of shear velocity and shear attenuation at 0.1 Hz for selected simultaneous inversions 166

6.7 Envelopes of shear velocity and shear attenuation at 1 Hz for selected simultaneous inversions 167

6.8 Envelopes of shear velocity and shear attenuation for simultaneous inversion for Solomon (1972a) - type relaxation model 168

6.9 Starting model for inversion of combined Love and Rayleigh phase velocity and attenuation in western North America 179

6.10 Envelopes of shear velocity and shear attenuation at 1 Hz and density (models S31W, S32W, S33W) 202

6.11 Starting model for inversion of east-central North America data (ν = o) 203

6.12 Envelopes of shear velocity and shear attenuation at 1 Hz, and density in east-central North America 204

6.13 Starting model for the central Pacific 222

6.14 Envelopes of shear velocity and shear attenuation at 1 Hz in the Pacific 223

6.15 Envelopes of shear velocity (at 1 Hz) and shear attenuation for frequency independent Q models by various inversion procedures, for Love waves in western North America. 225

CHAPTER I

Introduction

Seismic wave amplitudes attenuate while propagating through the earth. This fact provides information to understand the interior of the anelastic earth. Anelastic properties (seismic attenuation, viscosity, etc.) can be more sensitive to composition, temperature, pressure, microstructure and the presence of fluid phases than are the elastic properties (seismic velocities, density). Therefore, knowledge of the anelastic properties of the upper mantle is complementary to knowledge of the elastic properties and would improve our understanding considerably of the state of the mantle and the tectonic history of the earth. Toward this goal, this thesis presents the solution to the inverse problem of surface wave attenuation over continental and oceanic paths. While solving the inverse problem and determining seismic attenuation as a function of depth is important to problems of seismic wave propagation, earthquake source mechanisms, and the discrimination of nuclear explosions from earthquakes, the main motivation of this study is to better define physically realizable anelastic earth models, to characterize the lateral variation of seismic properties, and ultimately to provide clues to the sublithospheric mantle convection flow patterns. In this study, we will suggest an inversion scheme which is appropriate for the characteristics (sparse and inaccurate) of seismic attenuation data. Relating the seismic observations and linear attenuation mechanisms, the inverse problem will be recast to take account of the intrinsic dispersion that arises from linearity, which has been often neglected.

The concepts of lithosphere and asthenosphere (Daly 1940) form an essential basis for plate tectonics (Isacks, Oliver and Sykes 1968). In strictest terms, the major distinction between lithosphere and asthenosphere is in their differing long-term deformation in response to non-hydrostatic stresses. A common alternative distinction amenable to ready quantification using seismic waves is that the seismic anelasticity, as measured by the reciprocal Q^{-1} of the specific quality factor, is greater by roughly an order of magnitude or more in the asthenosphere than in the lithosphere. There is no theoretical basis for believing that these two different viewpoints will give, for instance, the same value for the thickness of the lithosphere. Nonetheless, the mechanisms of viscous deformation and seismic wave attenuation are both probably thermally activated and might be expected to show a qualitatively similar dependence on the temperature distribution in the mantle. More convincingly, it was the contrast in seismic attenuation that led to the idea (Oliver and Isacks 1967; Utsu 1966) that lithosphere is subducted on a grand scale in island arc regions.

The advantages of the surface wave method for studying Q in the earth were summarized by Anderson et al. (1965): the long period waves suffer less inhomogeneities, more readily sample the depths in the mantle where the most seismic energy is dissipated, and allow the geometrical spreading factor to be evaluated more accurately. Since surface waves are often the most visible portion of seismograms, it is convenient to measure their amplitudes.

In a linear, perfectly elastic medium, the amplitude of a stress wave propagating a distance x is proportional to $e^{i(kx-\omega t)}$, where ω is the angular frequency, k is the wave number, and t is time. In a linearly viscoelastic medium, the wave number of a travelling wave may be considered complex, so that amplitude is proportional to $e^{-k^*x+i(kx-\omega t)}$, where k^* is the imaginery part of k. Then the dimensionless quality factor Q and its inverse Q^{-1}, which are the most common measures of attenuation in seismology, are defined as

$$Q = \frac{k}{2k^*} , \qquad Q^{-1} = \frac{2k^*}{k} \qquad (1.1)$$

These quantities will be used as the measure of attenuation for most sections of this thesis.

In this thesis we will first consider in Chapter II the classical linear inverse problem based on the Anderson and Archambeau theory (1964). Although this traditional theory will be supplanted in Chapter V, it provides a framework to investigate an inversion scheme for highly inaccurate and sparse attenuation data. In Chapter II, observations of surface wave attenuation in two different regions of North America are inverted to determine Q^{-1} as a function of depth z in the crust and upper mantle.

In the traditional theory of Anderson and Archambeau (1964), the dissipation Q^{-1} of surface waves over a layered medium at a given period is equal to the sum of the dissipation in each layer if we assume $Q^{-2}(z)$ is small:

$$\left.\begin{aligned} Q_L^{-1} &= \sum_{j=1}^{M} \frac{\beta_j}{c_L} \frac{\partial c_L}{\partial \beta_j} Q_{\beta_j}^{-1} \\ Q_R^{-1} &= \sum_{j=1}^{M} \{ \frac{\beta_j}{c_R} \frac{\partial c_R}{\partial \beta_j} Q_{a_j}^{-1} \} . \end{aligned}\right\} \tag{1.2}$$

where the subscript j is the layer index; the subscripts L, R, α and β associated with Q^{-1} identify the wave types Love, Rayleigh, P and S, respectively; α_j and β_j are the compressional- and shear-wave velocity in layer j; and c_L and c_R are Love- and Rayleigh-wave phase velocities. With the additional assumption that the losses under purely compressive stress are negligible, so that

$$Q_a^{-1} = \frac{4}{3} \left(\frac{\beta}{a}\right)^2 Q_\beta^{-1}$$

(Anderson, Ben Menahem and Archambeau 1965), equation (1.2) can be expressed as the linear equations

$$\sum_{j=1}^{M} a_{ij} x_j = b_i \quad , \quad i = 1, 2, \ldots, N \tag{1.3}$$

or, in matrix notation,

$$\underline{\underline{A}}\,\underline{x} = \underline{b} \tag{1.4}$$

where $b_i = Q_L^{-1}$ or Q_R^{-1} at the ith frequency and $x_j = Q_{\beta j}^{-1}$ in the jth layer.

It is usually assumed that Q_β^{-1} is independent of frequency, though there are several grounds for believing otherwise (Tsai and Aki 1969; Jackson and Anderson 1970; Jackson 1971; Solomon 1972a,b). Suppose, therefore, that $Q_{\beta j}^{-1}$ in layer j is a function of frequency f. Then $Q_{\beta j}^{-1}$ may be approximated as a polynomial in f (Backus and Gilbert 1968) in the restricted range of frequencies:

$$Q^{-1}\ (f) = x_j(1 + c_j'/f + c_j''f)$$

where c_j' and c_j'' are constants. If we can estimate these constants by physical reasoning, $Q_{\beta j}^{-1}$ is still linear in the unknowns x_j. Define, for fixed c_j' and c_j'',

$$P_{ij} = a_{ij}(1 + c_j'/f + c_j''f)$$

where f_i is the frequency of the ith surface wave. Then equation (1.4) can be written as

$$\underline{\underline{P}}\,\underline{x} = \underline{b} \tag{1.5}$$

The goal of the inverse problem is to determine a linear estimator, $\underline{\underline{L}}$, that operates on $\underline{b}$ so as to provide a solution $\hat{\underline{x}}$ so that the error $\underline{x}_{true}-\hat{\underline{x}}$ is minimized in some sense:

$$\hat{\underline{x}} = \underline{\underline{L}}\,\underline{b}$$

Therefore, equations (1.4) or (1.5) are N linear algebraic equations with M unknowns, valid if $x_j^2 \ll 1$. Hereafter, we will discuss our problem in terms of N linear equations with M unknowns.

Three alternative inversion schemes for treating such a problem are briefly discussed in Chapter II: 1) the stochastic inverse, 2) the weighted least-square inverse, and 3) the set theoretical approach, which includes the square matrix inverse and the linear programming method.

It is ideal for a discrete linear inverse problem with inaccurate observations to be considered by a stochastic process, as long as the statistical structure of the model parameters and of the noise are known. If these statistical properties are not well defined or cannot be reasonably estimated, however, other inversion techniques must be sought. The weighted least-square inverse applied to inaccurate surface-wave attenuation data is the most straightforward approach but often gives a physically implausible negative solution for Q^{-1} (Knopoff 1964). The set theoretical approach does not share these disadvantages in that the model parameters and the noise are constrained to be elements of prespecified sets.

Since the attenuation data presently available for most surface wave paths are determined by only a few observations (sometimes two or three), the uncertainties are usually large and the error co-variance matrix is not at all well known. In general, geophysical properties are not perfectly resolvable vertically even though the data are error free (Backus and Gilbert, 1968). With large errors, the resolution obviously degrades (Backus and Gilbert, 1970; Der, Masse, and Landisman, 1970). In modelling the attenuation of surface waves in the crust and mantle, the resolution is not fine enough to allow more than a few layers (three or four). In such a circumstance, an important question, addressed in Chapter II, is the extent of correlation and incompatibility among the data. Most likely the observed values of attenuation are contaminated by effects other than anelasticity and by imprecise measurements. Since a small deviation in the value of an observation at a certain frequency will cause a relatively larger error in the solution space near that frequency than at very different frequencies, a reasonable criterion for the correlation of the data must be defined. Correlation and incompatability of the data may be possible causes of the negative solutions that result from the least-square sense inversion. Because of this possibility, we also want to make rules for incompatible solutions to be excluded. Such conditions as positiveness of the solution and that the solution curve fit within error bounds can be a reasonable filter for the weighted least square inverse to be successful.

These conditions are fulfilled in terms of the square matrix inverse by requiring:

$$\hat{x}_i \geq 0$$

$$|b_i - \hat{b}_i| \leq \sigma_i \qquad \text{for all } i$$

where $\hat{\underline{x}}$ is a vector of solution parameter space, $\underline{b}$ is the vector of observed values, $\hat{\underline{b}}$ is the vector of values predicted by the model $\hat{\underline{x}}$, and $\underline{\sigma}$ is the vector of data standard deviations. Moreover, the square matrix idea plays an important role in choosing layer thicknesses for the model. In a discrete linear inversion problem, with N equations and M unknowns, each equation represents an M-1 dimensional hyperplane in M dimensional solution space. By choosing appropriate thicknesses, N hyperplanes can be focused to intersect within a small volume in solution space.

Since the data now available have large uncertainties and, as we shall see, often show a discrepancy between Love wave and Rayleigh wave data, it is often better to seek an envelope of possible attenuation models than to look for a single 'best' model. To construct such an envelope of models we use the linear programming method, which has been developed mathematically by Dantzig (1963), adapted for geophysical problems by Johnson (1972) and discussed in theoretical terms by Sabatier (1977a,b). We mention in passing that other techniques for finding such an envelope, based on trial-and-error searches of either a continuous or discrete model parameter space, have been applied to the surface-wave attenuation problem by Burton and Kennett (1972) and Burton (1977).

In Chapter III, attenuation mechanisms in the Earth's mantle are reviewed. A particular interest of this chapter is to reexamine the linearity assumption of attenuation mechanisms with the results of laboratory experiments and seismic observations. Although the assumption of linearity in attenuation is the most powerful computational tool for non-harmonic waveforms, there have been objections to the linearity assumption for two reasons. (1) Some laboratory experiments on hysteresis loops for strain show that linear theories are valid only at strain amplitudes less than 10^{-6}. This shows that seismic strain amplitude is marginal in this regard. For example, a wave of displacement amplitude 1 cm and wavelength 100 km gives its strain amplitude of 6×10^{-7} ($= 2\pi A/\lambda$). (2) Knopoff (1959) argued that most suggested viscoelastic linear mechanisms of attenuation in the mantle show a strong frequency dependence which is not observed in any composite earth material in laboratory or in any seismic observations. However, Orowan (1967) and recently Liu et al. (1976) showed that the frequency independence of Q is possible by a superposition (distribution) of linear viscoelastic mechanisms of relaxation using a box distribution function. So far, many such distribution functions have been suggested to explain various laboratory observations by metallurgists and polymer scientists. On the occasion of this development, we should look thoroughly into a linear theory.

In Chapter IV, the linear theory for attenuation is discussed in phenomenological (mathematical) terms rather than physical terms. The basic assumptions of linearity are the superposition and causality principles. The superposition principle allows us to treat Fourier components which can be reconstructed into a waveform. The causality principle amounts to no 'signal before stimulus'.

The fact has been repeatedly stressed (Lomnitz, 1957; Futterman, 1962; Jeffreys, 1965, 1975; Carpenter and Davies, 1966; Randall, 1976; Liu et al., 1976), but not always heeded, that linear dissipation in solids gives rise to phase velocity dispersion of first order in Q^{-1} and that this intrinsic dispersion is significant for the inversion of surface wave phase velocities and of normal mode periods. The dispersion-attenuation relation over a frequency band in which Q^{-1} is independent of frequency has been derived by somewhat different routes by Kolsky (1956), Lomnitz (1957), and Futterman (1962). Most physical mechanisms proposed to account for dissipation in the earth are of the form of a thermally activated shear relaxation (Jackson and Anderson, 1970); the dispersion-attenuation relation for a relaxation is given by Zener (1948). When a continuous distribution of relaxations is superposed to produce a Q^{-1} independent of frequency within a finite frequency band, the dispersion-attenuation relation agrees with the constant Q^{-1} models (Liu et al., 1976). Because of a growing body of data suggesting that Q increases with frequency above about 1 Hz in the earth (see Solomon, 1972; Der and McElfresh 1977), it is also useful to consider dispersion attenuation relations in which Q has a power-law dependence on frequency (Jeffreys, 1958, 1965, 1975; Lamb, 1962). In Chapter V, a formulation for simultaneous inversion of surface wave phase velocity and attenuation is developed. Such a simultaneous treatment is preferable to the traditional separate treatment for several reasons. The two problems are intrinsically coupled because of a dependence of phase velocity on the anelastic structure and a sensitivity of surface wave attenuation to changes in elastic structure. Further, if linearity holds, the body wave phase velocity and attenuation at each depth in the earth are related by integral transforms and in general are frequency dependent. Finally, the elucidation of the physical mechanisms governing dissipation is made easier by treating the intrinsic phase velocity and Q^{-1} in the earth as dependent in the analysis of resolution and in the inversion process.

The forward and inverse problems of surface wave dispersion (or normal mode periods) and attenuation for an anelastic earth have been treated by several workers. Schwab and Knopoff (1971, 1972, 1973) developed the formalism for computation of dispersion and attenuation for surface waves or free oscillations in a lossy earth and applied their formalism to several earth models with frequency-independent velocity and Q^{-1}. Earth models for frequency dependent shear velocity and Q^{-1} based on an assumed set of relaxation mechanisms and seismic data taken over a broad frequency band were considered by Nur (1971) and Solomon (1972a). Carpenter and Davies (1966), Randall (1976), and Liu et al. (1976) have given an approximate correction to surface wave phase velocities to account for the intrinsic dispersion introduced by dissipation. Using the correction appropriate to Q^{-1} independent of frequency in the seismic wave band, Anderson et al. (1977), Anderson and Hart (1976) and Hart et al. (1976, 1977) used Q^{-1} model MM8 of Anderson et al. (1965) to adjust observed eigenfrequencies, and inverted the corrected normal mode data sets to obtain earth models.

In Chapter V, we outline the formalism, based on a generalization of Haskell's matrix treatment, for simultaneous inversion of surface wave phase velocity and attenuation to obtain a complex, frequency dependent earth model. The approach is mathematically more complete, and gives different results, than the techniques mentioned above and allows specification of the intrinsic disperion-attenuation relation in the earth as an adjustable input. Resolution analysis is extended for the above formalism using the two variable treatment of Der and Landisman (1972).

In Chapter VI, resolving length analysis and extremal inversion are applied to Love and Rayleigh wave data in North America, and Rayleigh wave data in the eastern Pacific. To compare the simultaneous inversion with the data-corrected, separate inversion of Anderson and Hart (1976), weighted least-square inversion is performed for Love wave data in western North America. The results are sensitive to the dispersion-attenuation relation in the low-Q zone and point toward future experiments that might define the relation better.

CHAPTER II

Set Theoretical Approach: Inversion Schemes

2.1 Resume

The geophysical inverse problem aims to find out possible models of earth structure consistent with gross earth data. Gross earth data consist of mass, moment of inertia, body wave travel times and attenuation, surface wave phase velocity, group velocity and attenuation, free oscillation periods, etc. The earth models we are interested in are density, S-wave velocity, P-wave velocity, Q_β^{-1} and Q_α^{-1}. Most times, we are interested in an inverse problem for a linear system, starting with a reasonable guess about one or more structural parameters inside the earth. The perturbation of a structural parameter is linearly related to small changes in observables. The relationship between observables and model can be specified by giving the kernels $G_i(r)$ for the initial model $m(r)$ as

$$d_i = \int_0^1 G_i(r)\, m(r)\, dr$$

where $d_i (i = 1, \ldots N)$ is the difference between an observed and predicted datum and r is the radial coordinate.

In practice, since the data available are finite, the data are inaccurate, and our mathematical formulation is approximate, the solution of the problem is non-unique. This is the most serious problem in geophysical inverse theory. Therefore, an important task is to represent the degree of non-uniqueness in a meaningful way. Backus and Gilbert (1967, 1968, 1970) showed the optimal way of inferring an earth model from a given data set. They introduced the useful concepts of spatial resolution and trade-off between resolution and error in the solution due to errors in the data. For non-linear inverse problems, mainly searching and testing have been used to represent solutions. The Monte Carlo search (Keilis-Borok and Yanovskaya, 1967; Press, 1970) and Hedgehog search (Keilis-Borok and Yanovskaya, 1967; Press, 1970)

are two approaches in this category. Jackson (1973) presented the Edgehog method to quasi-linear problems to estimate extreme models. Besides the limitations of linearity, the assumption of Gaussian statistics of errors may not be valid for a geophysical data set. The least square criterion is based on the Gaussian distribution of errors. If this assumption is invalid, the minimization of the so-called L_2-norm is meaningless. Claerbout and Muir (1973) explored the application of the L_1-norm to geophysical data analyses. In the L_1-norm criterion, the sum of absolute values is minimized, instead of the sum of squares as in the L_2-norm. A big advantage of L_1-norm analysis is that, by taking the median, the effect of a large error in a datum is effectively eliminated. The linear programming approach adapted by Johnson (1972) to inversion of regionalized earth models is an L_1-norm analysis. Lee and Solomon (1975) extended this idea as the set theoretical approach, combining square matrix inversion and the linear programming method.

2.2 Non-uniqueness, resolution and errors

All geophysical inverse problems involve some degree of non-uniqueness. Often it is more serious than we believe. The source of non-uniqueness is the finiteness of data in number and extert, random errors in data, and some arbitrariness of our physical assumptions. The resolving power approach of Backus and Gilbert (1968, 1970) provides an excellent tool for challenging this non-uniqueness. They showed that we can determine only a smoothed version of the solution (loss in resolution). By calculating the resolving length by Backus and Gilbert theory, we could estimate how the details of a model parameter could be pursued and how reliable they are. Details smaller than the resolving length are invisible to an observer with only M data. When we introduce random errors in data, the situation becomes worse. Backus and Gilbert (1970) and Der et al. (1970) dealt with the question of resolving length with inaccurate data, in which the variance of solution parameters and resolution (deltaness) are competing objectives. More than one variable is invovled in an inversion process, including the depth resolution of the desired variable, errors in the solution, and the separation between the desired and undesired variables. Backus (1970) and Der et al. (1972) discussed the two variable case with some examples.

One of the main objectives of the inverse problem is to resolve some important features in the structure, for example, a low velocity zone. Certainly such an objective is a competing concept against uniqueness of the solution. At the same time, we may lose the stability of the problem. For this reason, for example in the generalized inverse, small eigenvalues of the kernel matrix are avoided to get a smoother solution.

2.3 L_1 and L_2 norm

In measure theory, the definition of the L_p norm is given by (Reiz and Nagy, 1965)

$$\|m\|_p = \begin{cases} \left(\int |m(r)|^p \, dr\right)^{1/p} \\ \text{or } \left(\sum_{i=1}^{N} |m_i|^p\right)^{1/p} \end{cases}$$

$$p = 1, 2, \quad \ldots \quad , \infty$$

which must be finite for valid members of L_p. The reason for introducing this norm is the intriguing property of the norm that a certain statistical distribution of error and its statistical average is related to a certain norm. We define $\|m\|_2$ by the value of m which minimizes the sum of squared differences between m and x (called the L_2 norm):

$$\|m\|_2 = m \text{ such that } \sum_{i=1}^{N} (m - x_i)^2 \text{ is minimum.}$$

Taking the derivative with respect to m and setting it equal to zero, we find $\|m\|_2$ is given by the definition of the arithmatic mean. Now let us define $\|m\|_1$ by minimizing the summed absolute values (called the L_1 norm).

$$\|m\|_1 = m \text{ such that } \sum_{i=1}^{N} |m - x_i| \text{ is minimum.}$$

Again setting the derivative with respect to m equal to zero:

$$0 = \sum_{i=1}^{N} \operatorname{sgn}(m - x_i)$$

Here the sign function is +1 when the argument is positive, -1 when the argument is negative. This defines $\|m\|_1$ as a median. One other norm which is of use with geophysical data, is L_∞ (Chebyshev norm) (Parker, 1972). The average defined by Chebyshev norm as

$$\|m\|_\infty = m \text{ such that } \lim_{p\to\infty} \left(\sum_{i}^{N} (m - x_i)^p\right)^{1/p} \text{ is min.}$$

The midpoint $\|m\|_\infty$ bisects the distance between the extreme data points, thus minimizing the maximum error. The significance of the L_1 norm in the above argument is that a blunder in data is cast off. The basic assumption behind L_2 norm is the Gaussian statistics of error. If this assumption is broken as in some geophysical data, least square modelling is not an effective one. When some event is unpredictable and gives a big error, L_1 norm modelling has an advantageous robust effect (Claerbout and Muir, 1973). In many problems the L_2 norm is the natural norm. Most physical quantities are defined in Hilbert space which is also an L_2-norm vector space. On the other hand, it is often unnatural to square variables which are already positive, like energy, temperature, density, Q, etc. When such quantities occur as measurements, the asymmetric L_1 norm may be the natural norm. Asymmetry comes from the positivity condition. In this case, we have the usual linear programming technique. The least-square type inversion methods are based on L_2 norm statistics.

2.4 Classifications of Inversion Schemes

Inversion schemes which are in practice so far can be classified in many different ways. If the system is completely linear, or nearly linear (i.e., a linearized perturbation is valid), most of the schemes belong to linear inversion. Non-linear schemes include the searching techniques, such as Monte Carlo search and Hedgehog search. The gradient method (Marquart, 1963) is another scheme for non-linear systems. Jackson (1973) showed a remedy for quasi-linearity by letting the data residual and 'smoothness criterion' go to extremes (Edgehog method). In general, extreme model approaches have a much wider range of linearity.

The single 'best' model has been an ultimate objective in many inverse problems. However, suppose the number of measurements is so small that the resolution length exceeds the radius of the earth; then we must abandon the original objective. Instead we only can pursue the possible range of the model. If data have a large uncertainty, a single best model may not be meaningful. Searching procedures, such as Monte Carlo, do not have a single 'best' criterion, but rather produce extreme models (envelopes).

2.4a Single 'best' Model and Extreme Model Approach

In an inversion process, we desire to recover a best model from currently available geophysical data. The L_1 norm approach may give an upper and lower bound to the solution space (envelopes). The least-square approach would force such a case to have unique answer. The linear programming technique is a specific L_1 norm approach. Extreme model approaches such as Monte Carlo, Hedgehog, Edgehog and linear programming give the advantages of exploring the possible range of solutions and giving some indication of the degree of uniqueness for a given data set. If there is a large uncertainty in the data, such as Q^{-1} data, the best model may not be meaningful.

2.4b Model and Data Statistics

In a discrete linear inverse problem, we have, in matrix notation:

$$\underline{\underline{A}}\,\underline{x} = \underline{c}$$

where $\underline{\underline{A}}$ is a N x M matrix, and $\underline{x}$ and $\underline{c}$ are column vectors with M and N rows, respectively. In practice, we cannot measure $\underline{c}$ exactly, but rather observe $\underline{b} = \underline{c} + \underline{n}$, where $\underline{n}$ is some random noise accounting for errors of measurement. Accordingly the form of the problem is

$$\underline{\underline{A}}\underline{x} + \underline{n} = \underline{b} \tag{2.1}$$

where $\underline{\underline{A}}$ and $\underline{b}$ are knowns, but $\underline{x}$ and $\underline{n}$ are unknowns.

1) Stochastic inverse

Suppose we have a priori knowledge of the statistical nature of $\underline{x}$ and $\underline{n}$, where $\underline{x}$, $\underline{n}$ and $\underline{b}$ are assumed to be random variables related to signal, noise and data processes, so that:

$$\begin{aligned} E\{\underline{x}\} &= \underline{m}_x \\ E\{\underline{n}\} &= 0 \\ E\{\underline{x}\underline{x}^T\} &= \underline{\underline{R}}_{xx} \\ E\{\underline{n}\underline{n}^T\} &= \underline{\underline{R}}_{nn} \end{aligned}$$

where $E\{\underline{x}\}$ denotes the expected value of $\underline{x}$, and $\underline{x}^T$ denotes the transpose of $\underline{x}$. If the signal and noise processes are independent, then $E\{\underline{x}\underline{n}^T\} = E\{\underline{n}\underline{x}^T\} = 0$ and the linear estimator $\underline{\underline{L}}$ is (Jordan and Franklin, 1971)

$$\underline{\underline{L}} = \underline{\underline{R}}_{xx}\underline{\underline{A}}^T (\underline{\underline{A}}\,\underline{\underline{R}}_{xx}\underline{\underline{A}}^T + \underline{\underline{R}}_{nn})^{-1} \qquad (2.2)$$

With $\underline{\underline{L}}$ defined above, the relations

$$\underline{x} = \underline{m}_x + \underline{\underline{L}}(\underline{b} - \underline{\underline{A}}\,\underline{m}_x)$$

$$\underline{x} = \underline{\underline{L}}\,\underline{b} \quad \text{for } \underline{m}_x = 0 \qquad (2.3)$$

yield a minimum-error covariance matrix $\underline{\underline{S}}$:

$$\underline{\underline{S}} = E \left\{ (\underline{x} - \hat{\underline{x}})(\underline{x} - \hat{\underline{x}})^T \right\}$$

$$E \left\{ \underline{x} \right\} = \underline{m}_x \qquad (2.4)$$

From the above two equations, $E\{\underline{x}\} = E\{\hat{\underline{x}}\}$, so $\hat{\underline{x}}$ is unbiased. Therefore, the estimator $\underline{\underline{L}}$ provides a global minimum of $\underline{\underline{S}}$. One other important fact is that the above discussion is valid for a non-Gaussian error as well as Gaussian. This estimator is the stochastic inverse which was introduced to geophysical problem by Franklin (1970) and by Jordan and Franklin (1971). The construction of correlation operators $\underline{\underline{R}}_{xx}$ and $\underline{\underline{R}}_{nn}$ was discussed by Jordan and Franklin (1971) and Wiggins (1972). For the noise correlation, $\underline{\underline{R}}_{nn}$, it is rather easy to form a covariance matrix if the observational errors are uncorrelated. In such a case, the covariance matrix has the following representation:

$$\underline{\underline{R}}_{nn} = \begin{pmatrix} \sigma_1^2 & 0 & 0 & \cdots & 0 \\ 0 & \sigma_2^2 & 0 & \cdots & 0 \\ 0 & 0 & \sigma_3^2 & \cdot\cdot & 0 \\ & & & \cdot\cdot & \\ 0 & 0 & 0 & \cdot\cdot & \sigma_N^2 \end{pmatrix} \qquad (2.5)$$

where the diagonal element σ_i^2 is the variance of the i-th noise component. The construction of the solution covariance matrix is, however, rather subtle. In a sense, $\underline{\underline{R}}_{xx}$ acts as a filtration operator which discards unreasonable solutions on the basis of physical constraints defined by the resolving power of the data. If equation (2.1) is written as a perturbation equation, then $\underline{\underline{R}}_{xx}$ converges to a scalar times the identity matrix for perfect resolving power (Franklin, 1970). Wiggins (1972) introduced an N x N weighting matrix $\underline{\underline{W}}$ assumed to be a diagonal matrix with each element w_{ii} proportional to the dimension of the i-th solution parameter.

2) Weighted least square inverse

Suppose we do not have a prior knowledge of the statistics of the solution, but we do have a noise covariance matrix. Then consider

$$E\left\{\underline{n}\right\} = 0$$

$$E\left\{\underline{n}\,\underline{n}^T\right\} = \underline{\underline{R}}_{nn} = \begin{pmatrix} \sigma_1^2 & 0 & 0 & \cdot\cdot & 0 \\ 0 & \sigma_2^2 & 0 & \cdot\cdot & 0 \\ 0 & 0 & \sigma_3^2 & \cdot & 0 \\ & & & \cdot\cdot & \\ 0 & 0 & 0 & \cdot & \sigma_N^2 \end{pmatrix}$$

Choose $\underline{x}$ that minimizes

$$J(\underline{x}) = (\underline{b} - \underline{\underline{A}}\underline{x})^T R_{nn}^{-1}(\underline{b} - \underline{\underline{A}}\underline{x})$$

Such a solution is given by

$$\frac{\partial J(x)}{\partial x} = 2\underline{\underline{A}}^T \underline{\underline{R}}_{nn}^{-1}\,(\underline{b} - \underline{\underline{A}}\underline{x}) = 0$$

$$\underline{x} = (\,\underline{\underline{A}}^T \underline{\underline{R}}_{nn}^{-1}\,\underline{\underline{A}}\,)^{-1}\,\underline{\underline{A}}^T \underline{\underline{R}}_{nn}^{-1}\,\underline{b} \qquad (2.6)$$

providing that $(\underline{\underline{A}}^T \underline{\underline{R}}_{nn}^{-1}\underline{\underline{A}})^{-1}$ exists. For $(\underline{\underline{A}}^T \underline{\underline{R}}_{nn}^{-1}\underline{\underline{A}})^{-1}$ to exist it is necessary that the dimension of $\underline{b}$ is not smaller than that of $\underline{x}$. The weighted least square inverse $\underline{\underline{L}}$ yields the minimum error covariance matrix $\underline{\underline{S}}$ where

$$\underline{\underline{L}} = (\underline{\underline{A}}^T \underline{\underline{R}}_{nn}^{-1} \underline{\underline{A}})^{-1} \underline{\underline{A}}^T \underline{\underline{R}}_{nn}^{-1}$$

and

$$\underline{\underline{S}} = E \left\{ (\underline{x} - \underline{\hat{x}}) (\underline{x} - \underline{\hat{x}})^T \right\} = (\underline{\underline{A}}^T \underline{\underline{R}}_{nn}^{-1} \underline{\underline{A}})^{-1}$$

In the case of $M > N$, $\underline{\underline{S}}$ does not exist. For this situation, Lanczos's (1961) analysis and Gilbert's (1971) minimum solution could be used to solve the underdetermined problem.

3) Set theoretical approach

Suppose, unlike the previous cases, the statistical structure of neither $\underline{x}$ nor $\underline{n}$ is known, but rather $\underline{x}$ and $\underline{n}$ are constrained to lie in specified sets:

$$\underline{x} \in \Omega_x$$

$$\underline{n} \in \Omega_n$$

where Ω_x and Ω_n are sets in M- and N-dimensional spaces, respectively. In particular, these sets can be polyhedrons for L_1 norm modelling and ellipsoids for L_2 norm modelling. The latter case is the Edgehog method presented by Jackson (1973). The former case is square matrix inverse and linear programming technique (Lee and Solomon, 1975).

2.5 Set theoretical approach for attenuation

Let $\underline{x}$ and $\underline{n}$ be constrained to lie in specified sets:

$$\begin{aligned} \underline{x} \in \Omega_x &= \left\{ \underline{x};\ x_j > 0,\ j=1,2,\ ..\ ,M \right\} \\ \underline{n} \in \Omega_n &= \left\{ \underline{n};\ n_i < \sigma_i,\ i=1,2,\ ..\ ,N \right\} \end{aligned} \qquad (2.7)$$

where Ω_x and Ω_n are sets in M- and N-dimensional spaces, respectively. These constraints amount to the condition that the solution be positive and that the data lie within the error bounds. The observations $\underline{b}$ specify N hyperplanes in M-dimensional solution space. These hyperplanes provide a set of solutions which is required to be constrained by Ω_n such that

$$\underline{x} \in \Omega_{x/b} = \left\{ \underline{x};\ \underline{b} - \underline{\underline{A}}\underline{x} \in \Omega_n \right\} \qquad (2.8)$$

Since the solution set must satisfy the positiveness condition, $\underline{x}$ must lie in the intersection of Ω_x and $\Omega_{x/b}$. Let Ω_{sol} denote this intersection:

$$\underline{x} \in \Omega_{sol} = \Omega_x \cap \Omega_{x/b} \qquad (2.9)$$

Two alternative views of the constraints (2.8) lead to two different but complementary set theoretical approaches. If we use mean hyperplanes as constraints, the approach is via the square matrix inverse. If we use extremal hyperplanes as constraints. it is via the linear programming method.

2.5a Square matrix method. The linear problem expressed in the following (1.3) equation may be regarded as one for which there are N constraints, or equations, and M unknowns.

$$\sum_{j}^{M} a_{ij}x_j = b_i , \quad i = 1, 2, .. ,N$$

Each constraint represents an M-1 dimensional hyperplane. In M-dimensional space, M constraints will provide a point which is the intersection of M hyperplanes. There are ${}_{N}C_{M}$ (M combinations out of N) number of such points in M-dimensional space. In matrix terms, from the N x M original matrix, we can choose ${}_{N}C_{M}$ square matrices which will provide ${}_{N}C_{M}$ sets of solutions, i.e.

$$\underline{\underline{H}}_k \underline{x} = \underline{b}_k , \quad k = 1,2, .. , {}_{N}C_{M} \tag{2.10}$$

where $\underline{\underline{H}}_k$ and $\underline{b}_k$ are an M x M matrix and M-dimensional column vector, respectively. The solutions that satisfy equation (2.10) and fit the data to within the error bars will form a set $\Omega_{x/b}$. Therefore, the solution domain is defined as the intersection between $\Omega_{x/b}$ and Ω_x. By (2.10) the estimate of the vector $\underline{x}$ is defined as a set, not as a single vector. We need a specific way of determining which vector within the solution domain, Ω_{sol}, is the proper estimate of $\underline{x}$. Naturally a reasonable choice of such an estimate is to define $\underline{x}$ as a center of Ω_{sol}, where the center can be defined in the way of averaging the elements of the set. The set of solutions must not be empty if our hypotheses on the system are correct. Therefore, this technique can be used for hypothesis testing. The term 'hypothesis' here includes the parameterizations and the assumptions used to construct the model. The most sensitive such hypotheses are the determination of layer thickness and an adequate assumption of frequency dependence of Q^{-1}.

2.5b Linear programming method. The linear programming technique (Dantzig 1963) is similar in concept to the square matrix inverse but differs in motivation. The philosophy is to build an envelope of possible models rather than a best model as in the other approaches discussed. To get maxima and minima of the model parameters, constraints are obtained from inaccurate observations such that the true value for each data point is within some tolerance, e.g. the standard deviation. From each of our original equations (1.3) we get two constraints:

$$\begin{aligned} \sum_{j=1}^{M} a_{ij}x_j &\geq b_i - \sigma_i \,, \quad i = 1,2, \ldots ,N \\ \sum_{j=1}^{M} a_{ij}x_j &\leq b_i + \sigma_i \,, \quad i = 1,2, \ldots ,N \end{aligned} \qquad (2.11)$$

where σ_i is the standard deviation of ith observation. Each inaccurate datum restricts possible solutions to the space sandwiched between the hyperplanes defined by the equations:

$$\begin{aligned} \sum_{j=1}^{M} a_{ij}x_j^{min} &= b_i - \sigma_i \\ \sum_{j=1}^{M} a_{ij}x_j^{max} &= b_i + \sigma_i \\ i = 1,\ 2,\ &\ldots ,N \end{aligned} \qquad (2.12)$$

The region of space containing points satisfying all 2N constraints will be the intersection of all these sandwiched regions and of Ω_x. This intersection will be referred to as the solution domain Ω_{sol}. This set Ω_{sol} is a convex set, in that all points lying on a line connecting any two interior points also must lie within the set. Further discussions of this technique may be found in the original development of Dantzig (1963) and in Johnson's (1972) adaptation of the method to inversion of regionalized earth models.

2.5c Ellipsoids: Edgehog

Now assume that Ω_x and Ω_n are ellipsoids:

$$\Omega_x = \left\{ \underline{x};\ (\underline{x} - \underline{m}_x)^T (\underline{x} - \underline{m}_x) \leq 1 \right\}$$

$$\Omega_n = \left\{ \underline{n};\ (\underline{n}^T \underline{\underline{R}}^{-1} \underline{n}) \leq 1 \right\}$$

Then

$$\Omega_{x/b} = \left\{ \underline{x};\ (\underline{b} - \underline{\underline{A}}\underline{x})^T \underline{\underline{R}}^{-1} (\underline{b} - \underline{\underline{A}}\underline{x}) \leq 1 \right\} \qquad (2.13)$$

$$\Omega_{sol} = \Omega_x \cap \Omega_{x/b}$$

where

$$\underline{\underline{R}} = \begin{pmatrix} \sigma_1^2 & 0 & 0 & .. & 0 \\ 0 & \sigma_2^2 & 0 & .. & 0 \\ & & & .. & \\ 0 & 0 & 0 & & \sigma_N^2 \end{pmatrix}$$

With a weighting matrix $\underline{\underline{R}}$, Ω_{sol} is generally an ellipsoid. If the principal axis system is used, $\Omega_{x/b}$ is represented by an ellipsoid because each axis direction is weighted by eigenvalues.

2.6.1 Data

The surface wave attenuation observations we shall use to infer Q^{-1} structure come from two different regions in North America. The first set of data, given in Table 2.1, and referred to as data set 1 below comes from two-station measurements of Love-wave and Rayleigh-wave attenuation between WWSSN stations at Longmire, Washington and Tucson, Arizona (Solomon 1971, 1972a). The reciprocal of the group velocity U and the attenuation coefficient $k^*(= f/QU)$ are each the average of independent determinations using southward and northward travelling waves. Standard deviations are shown at frequencies for which more than one measurement was possible in each direction. Earthquake sources, all lying approximately on the great circle through LON and TUC, are in Alaska (5), Asia (2), Mexico (2) and Chile (1). The LON-TUC path samples primarily the tectonically active Basin and Range physiographic province (Fig. 2.1).

The second set of data, given in Table 2.2 is for east-central United States and comes from two sources. The first source consists of two-station measurements (Solomon 1971, 1972b) of Q_L^{-1} and Q_R^{-1} between Rapid City, South Dakota and Atlanta, Georgia (one direction only) for earthquakes in the Aleutians (5) and the Caroline Ids. (1).

TABLE 2.1

Love wave and Rayleigh wave attenuation, western United States (Solomon 1971)

f Hz	T sec	U_L km/sec	k^*_L $10^{-4}km^{-1}$	$100/Q_L$	Q_L	U_R km/sec	k^*_R $10^{-4}km^{-1}$	$100/Q_R$	Q_R
.0121(1)[a]	82.52	4.12	2.31	2.50±(.96)[b]	40				
.0135	73.84	4.11	2.57	2.48±(.88)	40				
.0150(2)	66.80	4.10	2.65	2.31±(.54)	43				
.0164	60.99	4.02±.04[c]	2.58±.68[c]	2.01±.53[c]	50				
.0178	56.12	3.97±.02	2.65±.65	1.88±.46	53				
.0192(3)	51.96	3.94±.04	2.90±.65	1.89±.42	53				
.0207	48.38	3.91±.05	3.02±.70	1.81±.42	55				
.0221	45.26	3.87±.07	3.02±.84	1.68±.41	59				
.0235	42.51	3.83±.09	2.88±.84	1.49±.44	67	3.55	1.62	.78±(.30)[b]	128
.0249(4)	40.08	3.79±.11	2.65±.90	1.28±.44	78	3.50±.03[c]	1.42±.96[c]	.63±.43[c]	158
.0264	37.92	3.77±.08	2.65±.68	1.21±.31	83	3.44±.04	1.22±.92	.51±.38	197
.0278	35.97	3.69±.11	2.38±.64	1.01±.27	99	3.41±.06	1.0±1.2	.37±.49	270
.0292	34.22	3.66±.12	2.18±.67	.87±.27	115	3.40±.05	1.6±1.3	.58±.47	172
.0307	32.62	3.65±.15	2.04±.87	.77±.33	129	3.36±.04	2.1±1.4	.72±.48	138
.0321(5)	31.18	3.61±.18	1.9±1.2	.69±.43	144	3.32±.06	2.3±1.3	.75±.42	134
.0335	29.85	3.53±.22	1.1±2.0	.35±.68	283	3.29±.08	2.0±1.0	.64±.31	156
.0349	28.63	3.55±.23	0.9±2.4	.28±.76	360	3.28±.09	1.54±.62	.46±.19	217
.0364	27.51	3.51±.22	0.7±2.7	.22±.81	450	3.22±.12	0.84±.80	.24±.23	420
.0378(6)	26.47	3.47±.21	0.5±2.9	.14±.85	700	3.20±.11	0.3±1.2	.08±.32	1200

TABLE 2.1 CONTINUED

.0392	25.51	3.36±.13	-1.6±0.4			3.17±.11	0.08±1.4	.02±.37	5000
.0406	24.61	3.34±.15	-1.8±0.9			3.13±.09	0.01±1.4	.00±.35	
.0421	23.78	3.34±.13	-1.9±1.6			3.09±.07	0.2±1.5	.05±.35	2000
.0435	23.00	3.36±.12	-1.9±2.1			3.06±.06	0.6±1.6	.13±.36	790
.0449	22.27	3.39±.15	-1.8±2.3			3.00±.06	0.8±1.8	.16±.37	600
.0463	21.58	3.40±.16	-1.6±2.3			2.93±.04	0.3±1.6	.07±.33	1500
.0478	20.94	3.40±.17	-1.2±2.1			2.92±.07	0.9±1.6	.17±.31	580
.0492	20.33	3.39±.17	-0.7±2.0			2.92±.09	1.4±1.4	.26±.27	380
.0506	19.76	3.39±.15	-0.1±1.9			2.94±.10	1.6±1.3	.30±.24	340
.0520(7)	19.22	3.39±.12	0.3±1.7	.06±.36	1600	2.95±.11	1.7±1.1	.31±.20	320
.0535	18.70	3.38	0.15	.03±(.38)	3400	2.95±.12	1.83±.94	.32±.17	310
.0549	18.22	3.34	0.27	.05±(.30)	1900	2.94±.12	1.83±.71	.31±.12	320
.0563	17.76	3.33	0.36	.07±(.27)	1500	2.93±.12	1.78±.55	.29±.09	340
.0577	17.32	3.33	0.44	.08±(.24)	1230	2.92±.10	1.68±.42	.27±.07	370
.0592	16.90	3.34	0.52	.09±(.23)	1070	2.91±.09	1.51±.25	.24±.04	420
.0606(8)	16.50	3.35	0.66	.12±(.19)	870	2.88±.08	1.64±.41	.25±.06	400
.0620	16.12	3.37	0.80	.14±(.12)	730	2.85±.09	1.80±.80	.26±.12	380
.0634	15.76	3.39	0.88	.15±(.30)	670	2.88	2.14	.31±(.15)	320
.0649	15.42	3.38	0.98	.16±(.30)	615	2.91	2.27	.32±(.19)	310
.0663(9)	15.08	3.35	1.16	.19±(.30)	540	2.92	2.69	.38±(.21)	270

a used in square matrix inverse treatment of layer parameterization and data correlation and incompatibility

b assumed uncertainty -

c standard deviation

TABLE 2.2

Love wave and Rayleigh wave attenuation, east-central United States

f Hz	T sec	U_L km/sec	k^*_L $10^{-4}km^{-1}$	$100/Q_L$	Q_L	U_R km/sec	k^*_R $10^{-4}km^{-1}$	$100/Q_R$	Q_R
From Solomon (1971, 1972b)									
.0164	60.99	4.00±.02^a	1.13±.10^a	.88±(.30)^b	114				
.0178	56.12	3.95±.01	.76±.01	.54±(.30)	185				
.0192	51.96	3.92±.02	.55±.14	.36±(.30)	280	3.80±.03^a	1.6±1.2^a	.98±.78^a	102
.0207	48.38	3.92±.06	.16±.53	.10±.32^a	1000	3.76±.07	1.1±1.4	.63±.79	160
.0221	45.26	3.84±.04	.00±.8			3.68±.04	1.0±1.3	.53±.69	190
.0235	42.51	3.76±.02	-.05±.9			3.61±.04	.8±1.3	.40±.63	250
.0249	40.08	3.71±.02	.09±1.2	.04±.58	2400	3.54±.05	.7±1.2	.31±.54	320
.0264	37.92	3.67±.02	.3±1.5	.13±.66	780	3.47±.05	.5± .9	.23±.40	440
.0278	35.97	3.63±.02	.5±1.7	.22±.70	460	3.41±.04	.4± .7	.16±.28	610
.0292	34.22	3.60±.02	.8±1.9	.30±.74	330	3.37±.02	.4± .6	.13±.22	760
.0307	32.62	3.57±.03	1.1±2.0	.39±.75	260	3.34±.01	.3± .8	.10±.28	970
.0321	31.18	3.55±.03	1.3±2.1	.47±.74	210	3.28±.04	.2±1.2	.05±.40	1900
.0335	29.85	3.54±.03	1.5±2.1	.52±.71	200	3.23±.07	.1±1.6	.02±.48	4500
.0349	28.63	3.58	.2	.06±(.30)	1700	3.20±.10	.1±1.8	.03±.53	3900
.0364	27.51					3.17±.12	.1±2.0	.04±.57	2400
.0378	26.47					3.10±.06	.1±2.8	.03±.73	3400
.0392	25.51					3.07±.04	.4±3.1	.10±.77	960
.0406	24.61					3.04±.01	-1.1± .9		

TABLE 2.2 CONTINUED

.0421	23.78					3.04±.02	-.7±.9		
.0435	23.00					3.05±.02	-.3±.9		
.0449	22.27					3.07±.01	.1±.9	.01±.19	7600
.0463	21.58					3.08±.01	.4±.8	.09±.17	1150
.0478	20.94					3.08±.01	.8±.6	.16±.13	610
.0492	20.33					3.06	1.5	.29±(.15)[b]	340
.0506	19.76					3.05	1.7	.33±(.15)	310
From Mitchell (1973a, b)									
.0200	50.0					(3.83)[c]	1.84	1.12±(.3)[b]	89
.0222	45.0					(3.77)	1.36	.73±(.3)	136
.0250	40.0	(3.78)[c]	1.5	.72±(.3)[b]	139	(3.67)	1.31	.61±(.3)	163
.0286	35.0	(3.66)	1.1	.45±(.3)	222	(3.53)	0.50	.20±(.3)	510
.0333	30.0	(3.55)	1.5	.51±(.3)	196	(3.32)	0.55	.18±(.3)	571
.0400	25.0	(3.47)	1.4	.39±(.3)	256	(3.09)	0.60	.15±(.3)	667
.0500	20.0	(3.43)	1.4	.31±(.3)	323	(2.98)	0.26	.05±(.3)	2041
.0571	17.5	(3.42)	1.2	.23±(.3)	437	(2.99)	0.43	.07±(.3)	1389
.0667	15.0	(3.43)	2.7	.44±(.3)	227	(3.03)	1.1	.16±(.3)	629
.0833	12.0	(3.44)	2.6	.36±(.3)	281	(3.08)	1.6	.20±(.3)	510
.1000	10.0	(3.45)	3.8	.42±(.3)	239	(3.13)	1.9	.19±(.3)	329
.1111	9.0	(3.46)	5.7	.57±(.3)	177	(3.15)	3.7	.33±(.3)	299
.1250	8.0	(3.47)	9.8	.87±(.3)	116	(3.16)	4.2	.34±(.3)	295
.1429	7.0	(3.47)	11.9	.92±(.3)	109	(3.18)	6.0	.43±(.3)	235

TABLE 2.2 CONTINUED

.1667	6.0	(3.48)	11.2	.74±(.3)	134	(3.19)	6.8	.42±(.3)	240
,2000	5.0	(3.48)	13.4	.74±(.3)	135	(3.20)	9.0	.46±(.3)	218
.2500	4.0	(3.48)	17.6	.78±(.3)	128	(3.21)	10.4	.43±(.3)	235

a standard deviation

b assumed uncertainty

c assumed, from McEvilly (1964)

Fig. 2.1. Paths used for two-station surface wave Q^{-1} measurements, shown superposed on the outlines of the physiographic provinces of the United States. The shaded region is approximately the area represented by Mitchell's (1973a,b) measurements.

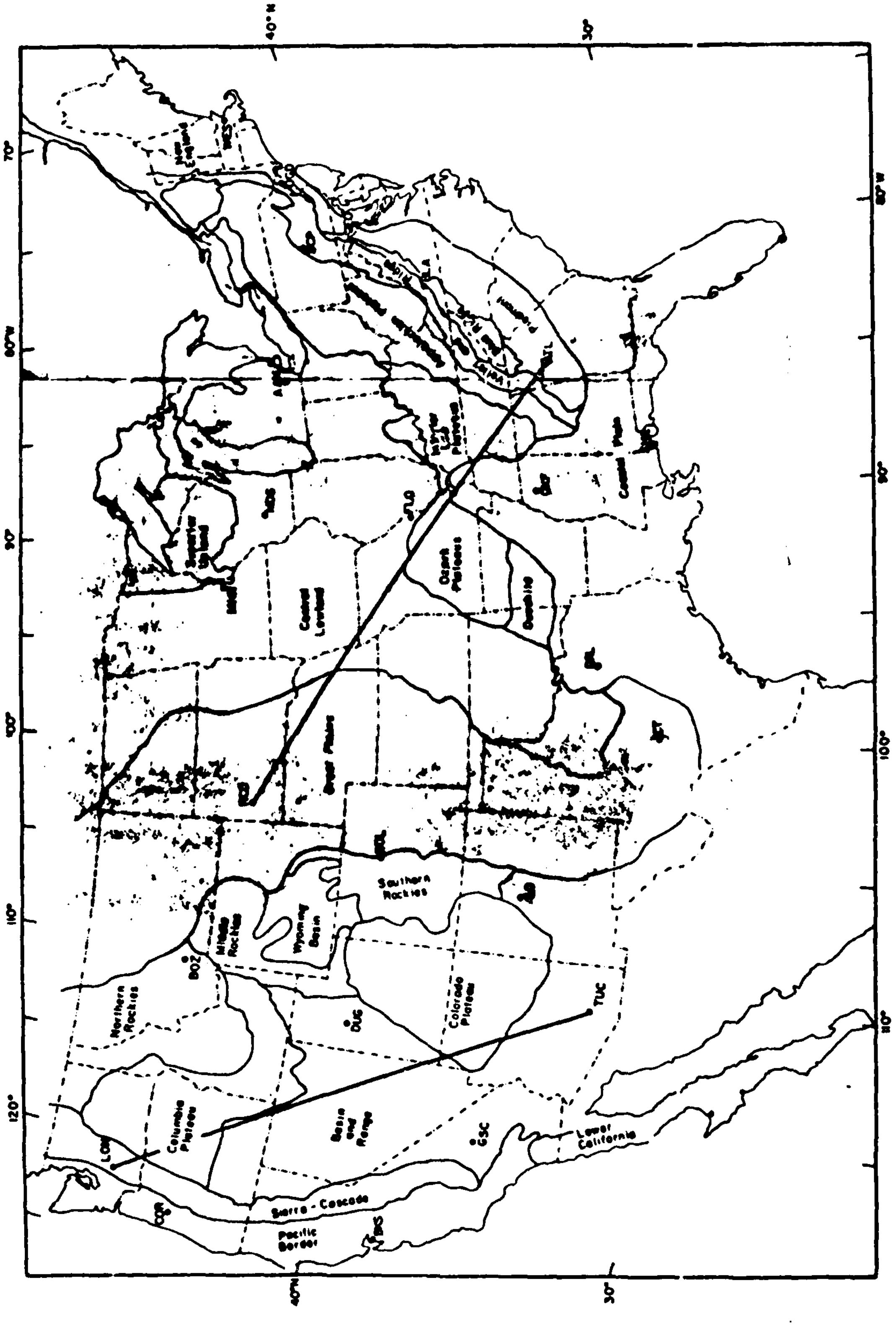
40° N
30°
70°
80° W
90°
100°
110°
120°
New England
Interior Low Plateaus
Coastal Plain
Superior Upland
Central Lowland
Ozark Plateaus
Ouachita
Great Plains
Southern Rockies
Wyoming Basin
Middle Rockies
Northern Rockies
BOZ
DUG
Colorado Plateau
TUC
Columbia Plateau
Basin and Range
GSC
LON
COR
BKS
Sierra - Cascade
Pacific Border
Lower California

Standard deviations are shown where repeated measurements were made. The RCD-ATL path samples primarily the stable platform region of the Great Plains and Central Lowland physiographic provinces (Fig. 2.1). The second source of data is Mitchell's (1973a,b) measurement of Rayleigh wave and Love wave attenuation from the southeastern Missouri earthquake of 1965 October 21. The determinations of Q_L^{-1} and Q_R^{-1} were derived from amplitude measurements at a number of seismograph stations between the Rocky and Appalachian mountains and between the Gulf coast and the Canadian shield, based on the assumption that the properties of individual surface-wave paths are approximately uniform over the area sampled (Fig. 2.1). Uncertainties are assumed for Mitchell's reported values of k*, and Q^{-1} was calculated using the surface wave group velocities from McEvilly's (1964) model for central United States. The measurements of Solomon (1971, 1972b) are referred to as data set 2 below. A third data set is formed by combining Solomon's observations with the shorter-period measurements ($f \geq 0.04$ Hz for Q_L^{-1}, $f \geq 0.0286$ Hz for Q_R^{-1}) of Mitchell (1973a,b).

The phase velocity partial derivatives a_{ij} (equations 1.2 and 1.3) were calculated using computer programs written by Harkrider (1964). For western United States, the plane-layered velocity-density model used for these calculations were taken from model 35CM2 of Alexander (1963) above 125 km and from models NTS N3 of Julian (1970) and US 26 of Anderson and Julian (1969) below that depth. For east-central United States, the (isotropic) velocity-density model of McEvilly (1964) was adopted.

To apply the inversion techniques of the preceding section to those observations of surface wave attenuation, resolving power analysis is an essential step. We then have to establish criteria to obtain independent information about the model and to detect incompatible observations. Finally we may solve the inverse problem.

2.6. 2 Resolution

Study of the resolution and error of observational measurements is useful in selecting the manner in which a continuous function of depth $Q^{-1}(z)$ can be approximated by a function constant within a small number of layers, so that our linear system is overdetermined. Such a study can also yield criteria for estimating the reliability of the inversion results. In the set theoretical approach, it is required that solution vectors be independent. An excessive number of layers can cause instability of the inversion and an interdependence of solution vectors. Backus and Gilbert (1967, 1968) have treated the general problem of vertical resolution from a finite set of error-free observations. If we take the large observational errors into consideration, the resolution is considerably worsened. The relationship between observational errors and resolution has been discussed by Der et al. (1970), Backus and Gilbert (1970) and Wiggins (1972).

In the scheme of Der et al. (1970), the idea is to minimize simultaneously both the variance of the linear combination x_k of observations that gives the best estimate of some physical parameter of interest in a certain layer k and the dependence of x_k on the parameters for layers other than the kth. This is accomplished by minimizing the function

$$E_k = \beta \text{ var } x_k + \sum_{j=1}^{M} w_j e_{jk}^2 , \quad j \neq k \qquad (2.14)$$

subject to

$$e_{kk} = \sum_{i=1}^{N} c_{ki} a_{ik} = 1$$

where

$$e_{jk} = \sum_{i=1}^{N} c_{ki} a_{ij} , \quad j = k$$

and where w_j is a layer thickness, a_{ik} is the partial derivative of the ith observation with respect to the parameter of interest in layer k, normalized with respect to the layer thickness, e_{kk} is delta-function-like and e_{jk} is the deviation from a delta function, and the c_{ki} are constants to be

Fig. 2.2 Resolution of surface wave attenuation data at selected depths for (a) data set 1 (western United States), (b) data set 2 (east-central United States), (c) data set 3 (east-central United States). The letter v shows the center of the layer k for which equation (2.14) is evaluated.

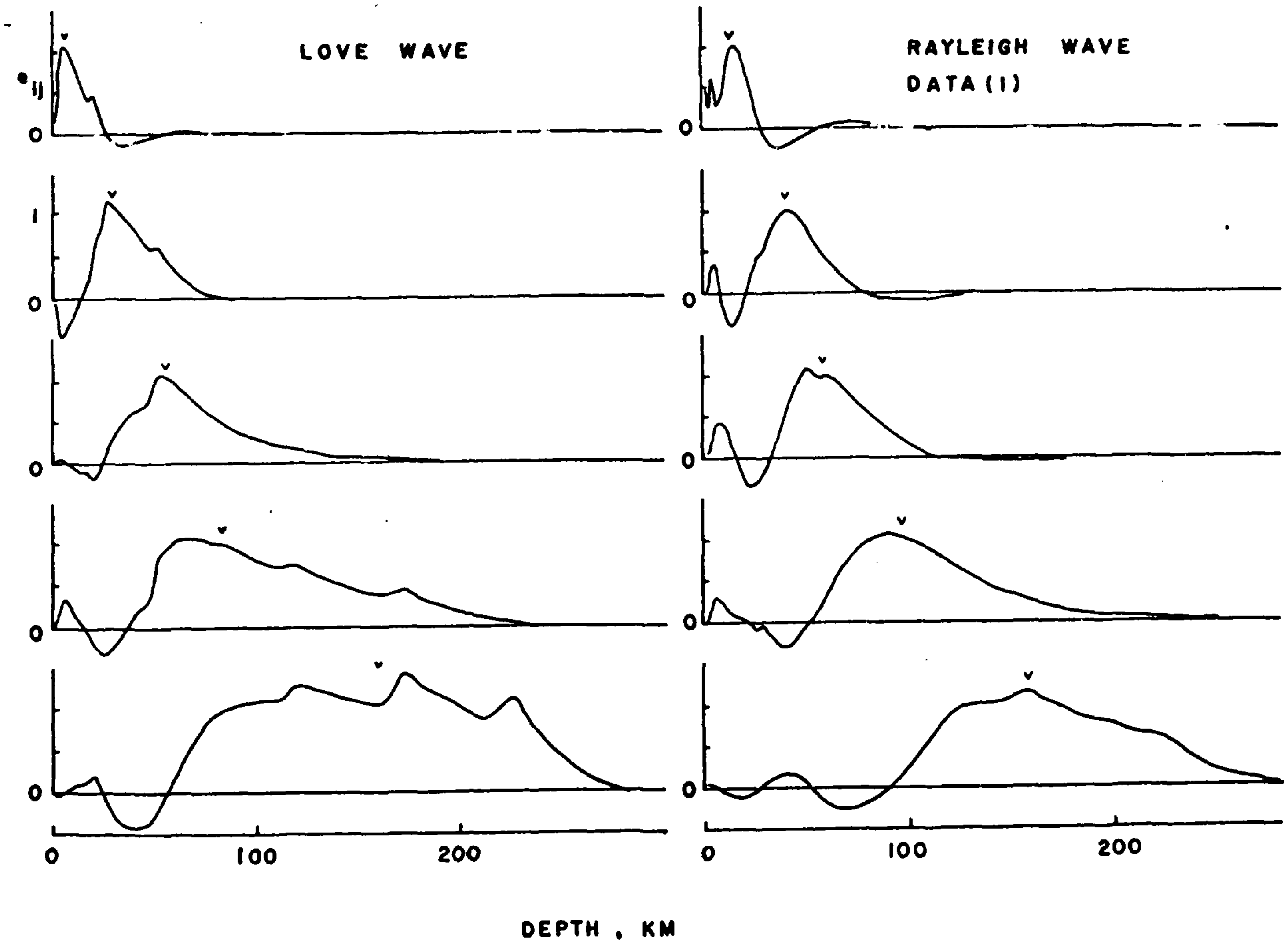
LOVE WAVE
RAYLEIGH WAVE
DATA (1)
e_{ij}
1
0
0
100
200
DEPTH , KM

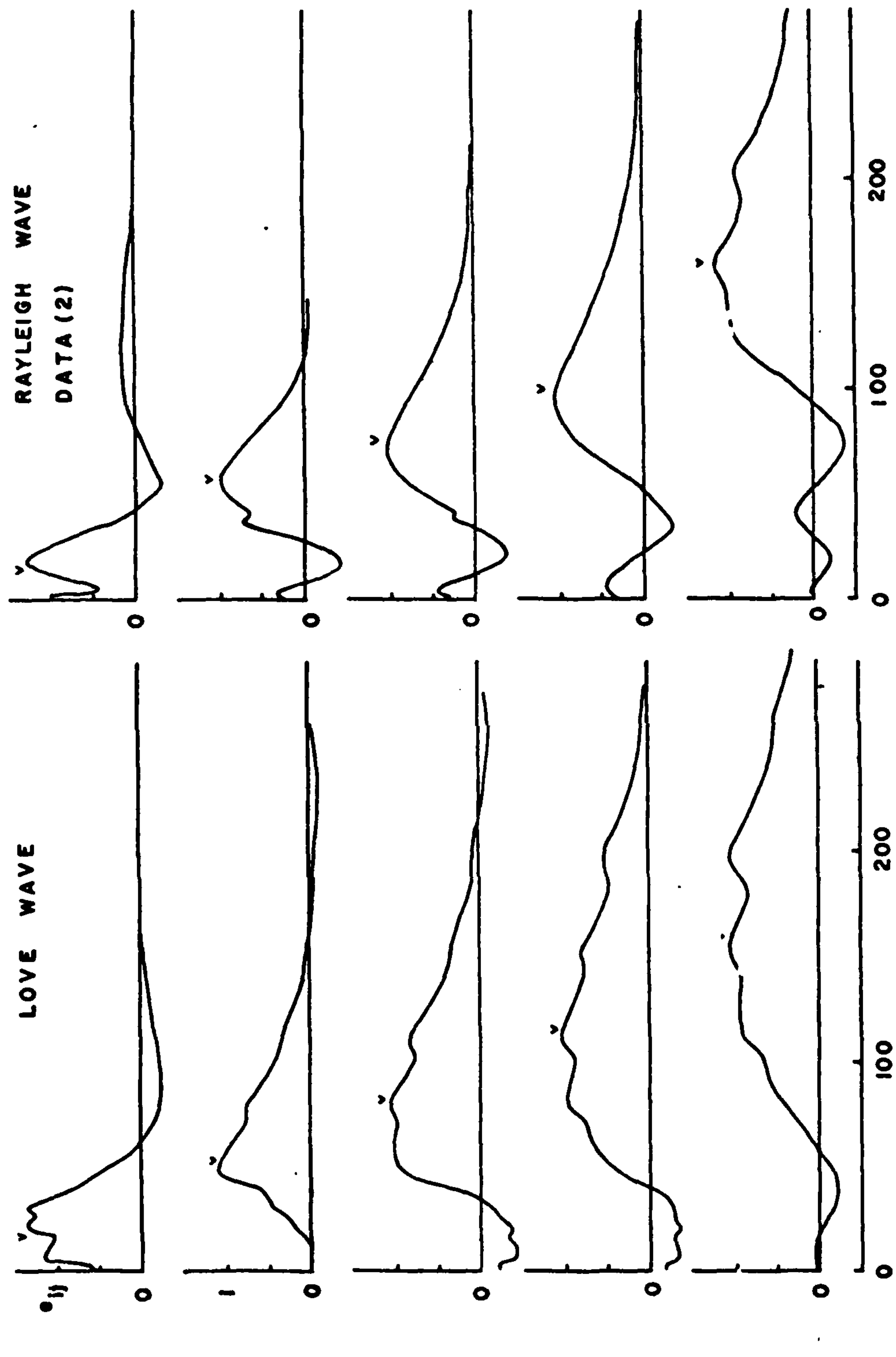
LOVE WAVE
RAYLEIGH WAVE
DATA (2)
e_{ij}
1
0
0
100
200
DEPTH , KM

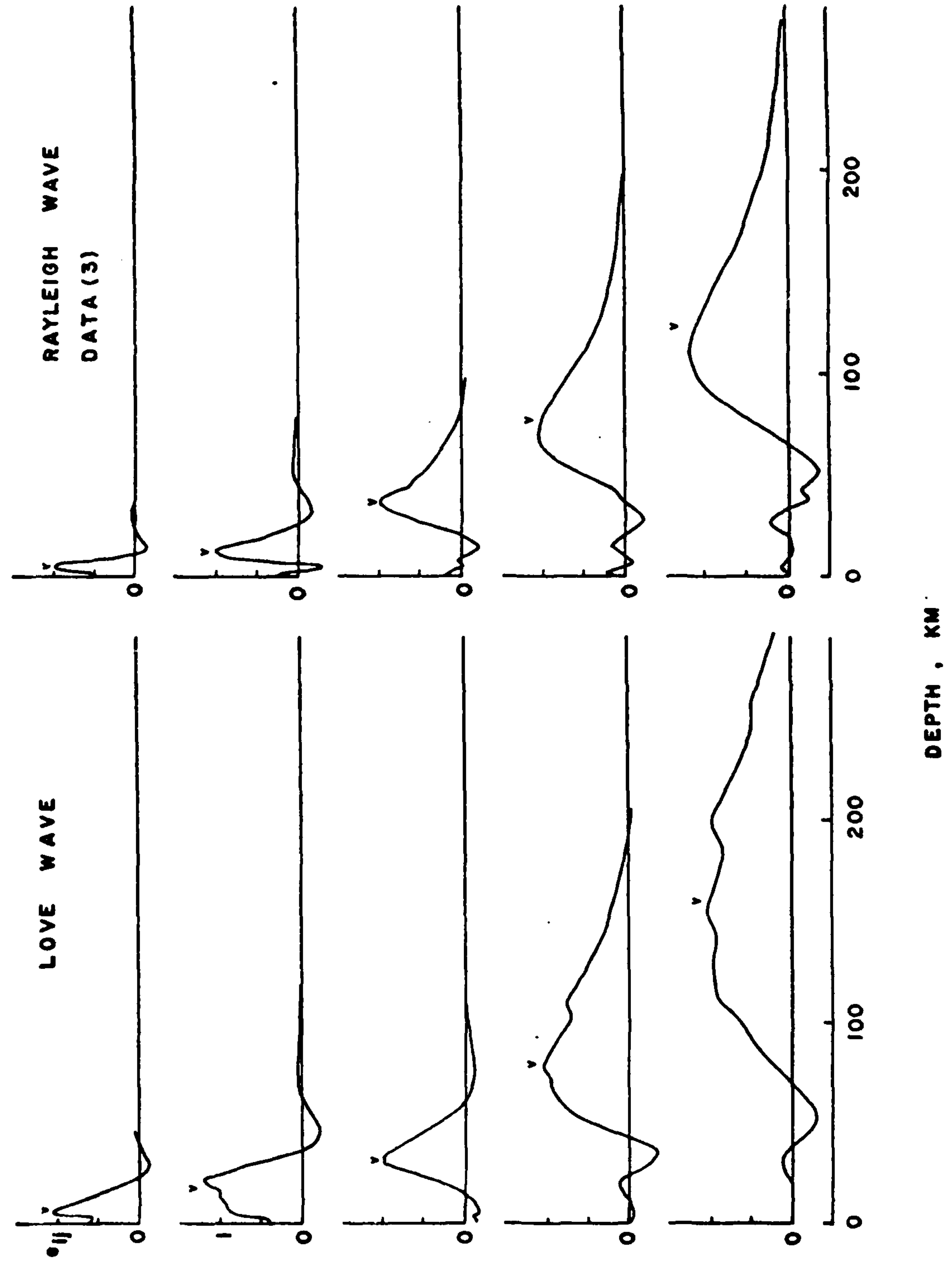
LOVE WAVE
RAYLEIGH WAVE
DATA (3)
e_{ij}
1
0
0
100
200
DEPTH , KM

determined subsequently. The quantity β is an adjustable parameter that determines which of the two minimizations is to be more effective. If the desired value for var x_k is too small or too large, i.e. β is chosen to be too small or too large for the two minimizations to balance, the result will not be physically meaningful. When β is zero, the problem corresponds to the case of error-free observations.

The resolution analysis of Der et al. (1970) applied to the surface wave observations introduced above allows us to assess the vertical resolving length of the data. The functions e_{jk} are plotted for selected layers k in Fig. 2.2a for data set 1, Fig. 2.2b for data set 2, and Fig.2.2c for data set 3. The parameter β in 2.14 is adjusted so that the variance of x_k is 0.5. From Fig. 2.2 it may be observed that the resolving power of Q_L^{-1} data is generally poorer than for Q_R^{-1} data. We estimate from the suite of resolving lengths that the allowable number of layers in a model for Q^{-1} is 3 or 4 for Love and Rayleigh waves, respectively, in data sets 1 and 3, and 2 or 3 for Love and Rayleigh waves, respectively, in data set 2.

Because the above analysis is valid only for independent observations, we can get only a rough idea about the layer thicknesses without knowing the co-variance matrix of error. Since the number of layers is few, determination of the layer thicknesses is very important. Therefore, it will be interesting to consider the limitations on layer thicknesses imposed by the set theoretical constraints.

A simple example will serve to show the utility of a geometrical picture of the constraints. In M-dimensional space, these constraints are in general hyperplanes. For ease of visualization, let us imagine a 2-dimensional solution space, which is not all that unreasonable since there is only one significant jump in the value of Q_β^{-1} at the boundary between lithosphere and asthenosphere. In that case the constraints are straight lines in the solution plane. The slope of a family of lines is determined by the matrix elements and the axis-intersections are determined by the observations.

To illustrate this idea, we take the case of nine representative Love wave attenuation data from Table 2.1. If we choose the boundary between layers at 65 km or at 50 km depth, the respective 2-dimensional representation of constraints in solution space are shown in Fig. 2.3, where the solid lines correspond to the case of the 65 km depth boundary and the dashed lines correspond to the case of the 50 km depth boundary. As we can see, the family of solid lines (constraints) provides a set of converging points in the domain of positive x_1 and x_2 (first quadrant) while the other family does not. This exercise implies that a bad choice of the layer thickness will make the hyperplanes nearly parallel and the solution domain empty. In Fig. 2.3 we have a clear choice between two-layer parameterizations. Graphic representation is impossible for

Fig. 2.3. Constraints in two-dimensional solution space. A two-layer Q^{-1} model is assumed. The boundary is at 65 km depth for the constraints shown as solid lines, 50 km depth for those shown as dashed lines. The number beside each line indicates the selected datum from Table 2.1 (Q_L^{-1}, western United States). (Insert) An amplified view of the dotted region. The shaded area represents the solution domain. It may be seen that constraints 1 and 2, and constraints 5, 7, 8 and 9 are correlated; constraint 6 is incompatible.

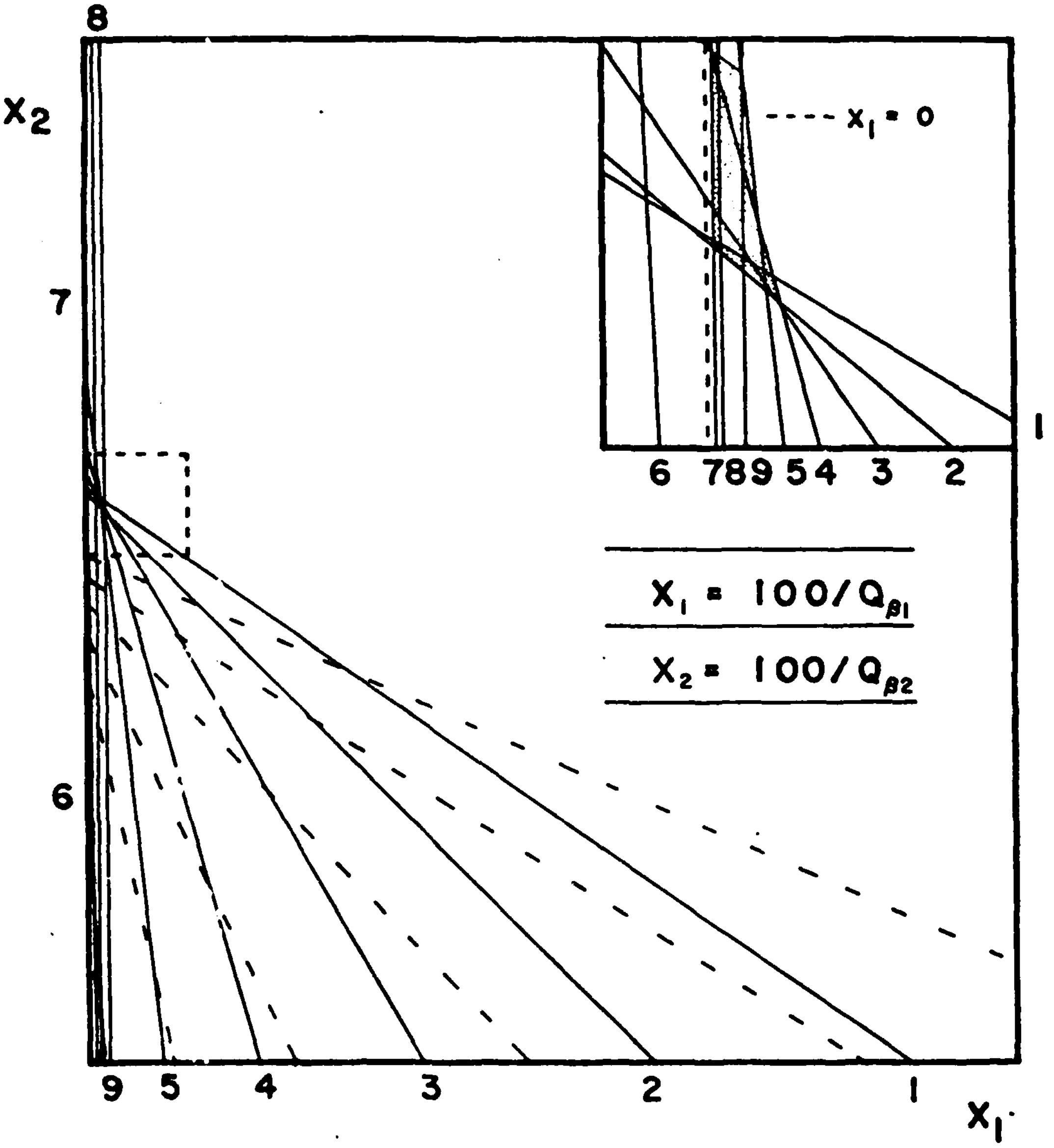
8
X_2
7
6
9
5
4
3
2
1
X_1
$X_1 = 0$
6
7
8
9
5
4
3
2
1
$X_1 = 100/Q_{\beta 1}$
$X_2 = 100/Q_{\beta 2}$

the M-dimensional case, but we can in analogous fashion optimize the M layer thicknesses by use of the square matrix inverse. That is, by choosing an appropriate set of layer thicknesses, hyperplanes can be focused in solution space. As a measure of focusing, we define a focusing index $f_o = p_j/q_j$, where p_j is the percentage of acceptable solutions from the square matrix inverse and thus is related to how well models with such layering can fit the data, and q_j is the volume of the solution domain in M-dimensional solution space. The index j loops over all possible choices of the set of layer thicknesses. Some examples of the dependence of f_o on the layering in the Q^{-1} model are given in Table 2.3; the highest value of f_o is the preferable layer parameterization.

2.6.3 Correlation and Incompatibility

Generally, each observation does not contribute independent information about the model. This is because of the high correlation of the partial derivatives of surface wave phase velocity at near frequencies. Correlation gets even higher when the observational error is large. According to the resolution analysis in the preceding section, the number of layers allowed in the model is few (three or four). Therefore, our problem is overdetermined, i.e. N is 20 or more and M is three or four. Somehow, we need a criterion that two data are independent or uncorrelated for a 'simple' co-variance matrix to be constructed. The meaning of 'simple'

TABLE 2.3 Use of the square matrix inverse to fix layer thicknesses for a 3-layered Q^{-1} model: Love wave data, western United States

Layer interface depths, km	Focusing index f
17, 64	235
15, 74	122
21, 69	202
21, 74	71
21, 64	418
25, 64	290

matrix is a weighting matrix chosen by reasonable judgement to utilize the weighted least square inverse. On the other hand, if the observational value of $Q^{-1}(f)$ is contaminated by effects other than the anelasticity of the Earth or by rough measurements, some data will be incompatible. To be more precise, we define 'correlated' and 'incompatible' data in terms of square matrix resolution:

Two data are correlated if their corresponding hyperplanes in solution space do not intersect inside the feasible solution domain but do contribute to build the domain. A datum is incompatible if its hyperplane does not contribute to build the domain of feasible solutions. These definitions are illustrated in Fig. 2.3.

We may pursue the geometric picture of each datum as a constraint somewhat further. Equation 1.3 represents a set of M-1 dimensional hyperplanes. A pertinent geometrical parameter of a pair of hyperplanes is the angle between them. The angle between hyperplanes is defined as

$$\cos \theta_{ik} = \frac{\sum_{j}^{M} a_{ij} a_{jk}}{\sqrt{\left(\sum_{j}^{M} a_{ij}^{2} \sum_{j}^{M} a_{jk}^{2} \right)}}$$

This angle is the coefficient of correlation if observations are error free. With observational errors in consideration, we define the correlation length (in the same units as the x_j) as

$$D_{ij} = \left\{ \left(\frac{\sigma_i}{\sin \theta_{ij}} \right)^2 + \left(\frac{\sigma_j}{\sin \theta_{ij}} \right)^2 + 2 \frac{\sigma_i}{\sin \theta_{ij}} \frac{\sigma_j}{\sin \theta_{ij}} \cos \theta_{ij} \right\}^{1/2}$$

where θ_{ij} is the angle between ith and jth hyperplane, and σ_i and σ_j are the standard deviations of ith and jth observations (see Fig. 2.4). The same value of error in an observation will cause a relatively different error in the solution space, in proportion to the correlation length. This is the geometrical meaning of our definition of correlation (refer to Table 2.4).

As an example, for the same selected Q_L^{-1} data in western United States, square matrix resolution gives the following results with a three-layer model (boundaries at 20 and 65 km; see Table 2.3).

(1) Twenty-one feasible solutions exist among 84(=${}_9C_3$) possible solutions.

(2) Data 1 and 2, and data 8 and 9 are correlated.

(3) Data 6 and 7 are incompatible with the remaining data.

The incompatible data lie in the range of surface-wave periods where a 'minimum' in Q^{-1} has been noted (Trggvason 1965; Tsai and Aki 1969). Tsai and Aki (1969) explained this minimum as due to frequency-dependent Q^{-1} in the lithosphere.

Fig. 2.4. Correlation length D_{ij} between ith and jth constraints. σ_i and σ_j are the standard deviations for the ith and jth observations, respectively.

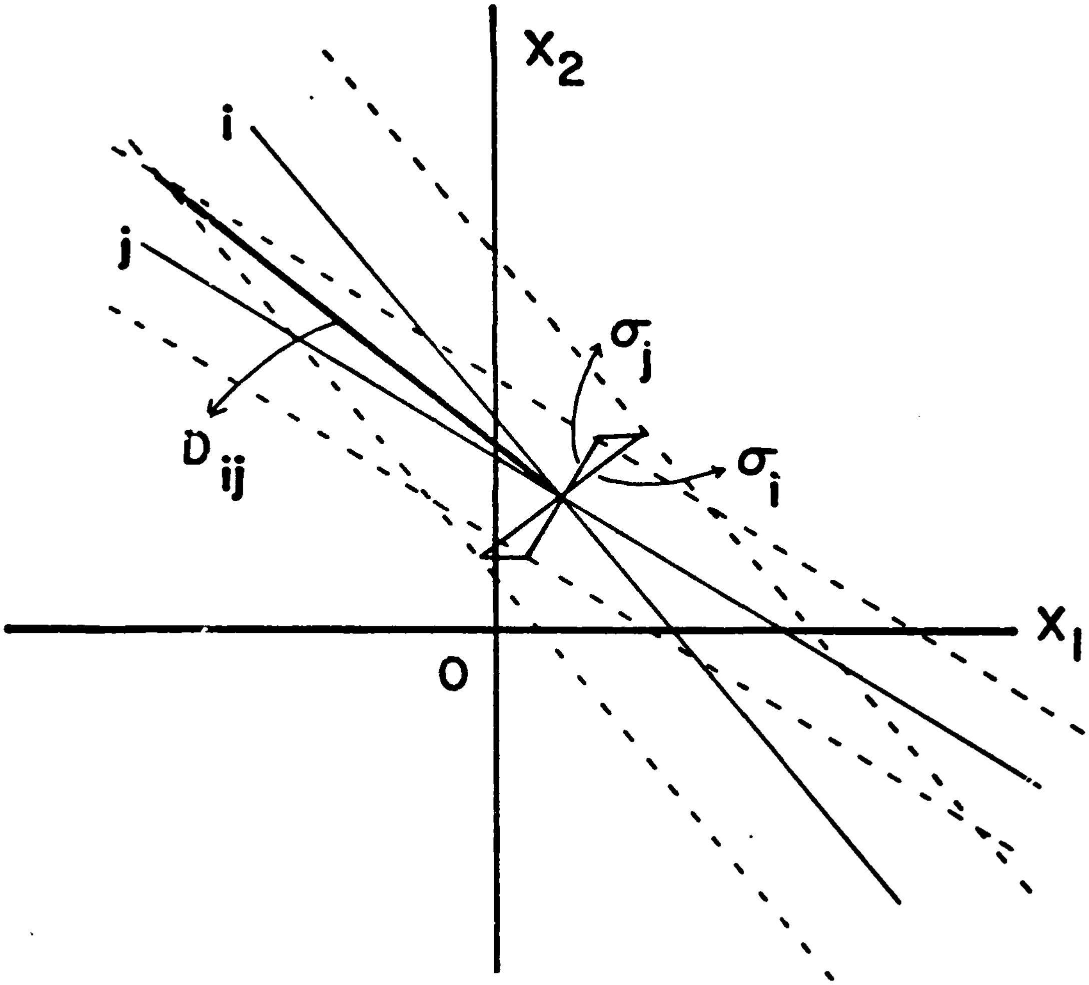
X₂
i
j
σ_j
σ_i
D_ij
O
X₁

TABLE 2.4 Correlation length D_{ij} between selected Q_L^{-1} data, western United States.

2	3	4	5	6	7	8	9	i/ j
20.57	3.68	1.12	0.58	1.22	0.30	0.28	0.27	1
	8.65	1.64	0.74	1.46	0.34	0.32	0.31	2
		6.36	1.79	2.70	0.66	0.57	0.54	3
			7.67	7.37	1.24	0.97	0.86	4
				56.23	2.99	1.89	1.55	5
					15.89	7.93	5.99	6
						29.87	12.92	7
							109.46	8

However, the question is still open because no model can explain nearly zero attenuation. One possible explanation may be a constructive interference in the period range of minimum Q^{-1} due to scattering. At any rate, the occurrence of incompatible data in this period range (20-25s) is not accidental. Therefore, we can assume that data 1, 3, 4, 5 and 9 are independent (uncorrelated) and we could apply the weighted least square inverse using the co-variance matrix, $\underline{\underline{R}}$:

$$\underline{\underline{R}} = \begin{pmatrix} \sigma_1^2 & 0 & 0 & 0 & 0 \\ 0 & \sigma_3^2 & 0 & 0 & 0 \\ 0 & 0 & \sigma_4^2 & 0 & 0 \\ 0 & 0 & 0 & \sigma_5^2 & 0 \\ 0 & 0 & 0 & 0 & \sigma_9^2 \end{pmatrix}$$

2.6.4 Linear programming procedure

The essence of the linear programming problem is composed of four parts: 1) a set of M independent variables; 2) a priori bounds on those variables; 3) a set of constraints, cast in terms of linear equations and inequalities; 4) a linear function, called the object function, which is to be minimized subject to these constraints. The independence of the variables (solution parameters) as discussed above in terms of resolution analysis indicates that

1) By square matrix resolution with Love wave or Rayleigh wave data, the optimum layer boundaries are at 20 km and 85 km depth for western US (data set 1), 135 km depth for data set 2 (east-central US) and 25 km and 135 km depth for data set 3. Hereafter we refer to these as major boundaries. Note these depths are uncertain by several kilometers.

2) The resolution of Rayleigh wave and Love wave data together is improved over that using either set of data separately.

Therefore the number of degrees of freedom, or the number of independent variables, are flexible to a certain extent due to the relaxation of constraints using extremal hyperplanes and the above result 2. We will increase the number of boundaries carefully until the fit to the data is no longer improved over that using only the major boundaries. The result of this procedure is a 6 layer Q_β^{-1} model in western US and 4 and 5 layer models in east-central US (data sets 2 and 3, respectively). During the process of increasing the number of layers, the original 2 or 3 layer model with major boundaries is used as a guide to reduce large fluctuations in Q_β^{-1} between successive layers. If the 3 layer model parameter x_i is split into two others, x_i' and x_i'', then

$$lo_i < x_i < up_i$$

$$lo_i < a_i x_i' + b_i x_i'' < up_i$$

where lo_i and up_i are lower and upper bounds of the model parameter x_i, derived from the linear programming procedure using only major boundaries, and a_i and b_i are the fractions of the original layer allotted to the two new layers. The a priori bounds used for the initial linear programming inversion, are defined as $0 < x_i < 100$ (where $x_i = 100/Q_i$). The object function is defined as

$$z = \pm x_i$$

where + is for the minimum and - is for the maximum of the envelope. Data indicated to be incompatible by square matrix resolution analysis are not included in the linear programming inversion.

2.6.5 Result and discussion

The envelopes of the attenuation models $Q_\beta^{-1}(z)$ resulting from the final linear programming inversion and illustrated in Fig. 2.5 are given in Table 2.5. The corresponding envelopes $Q_L^{-1}(f)$ and $Q_R^{-1}(f)$ are shown in Fig. 2.6 together with all data used in the inversion.

For Love wave attenuation in western United States, the greatest disagreement between observed and predicted values comes from the period range 15-25 s. For Rayleigh wave attenuation in the same region, on the other hand, the disagreement comes from the period range between 30 and 40 s. These two mismatches mean that a frequency independent Q_β^{-1}

Fig. 2.5. Envelopes of attenuation models for (a) data set 1 (western United States), (b) data set 2 (east-central United States), (c) data set 3 (east-central United States).

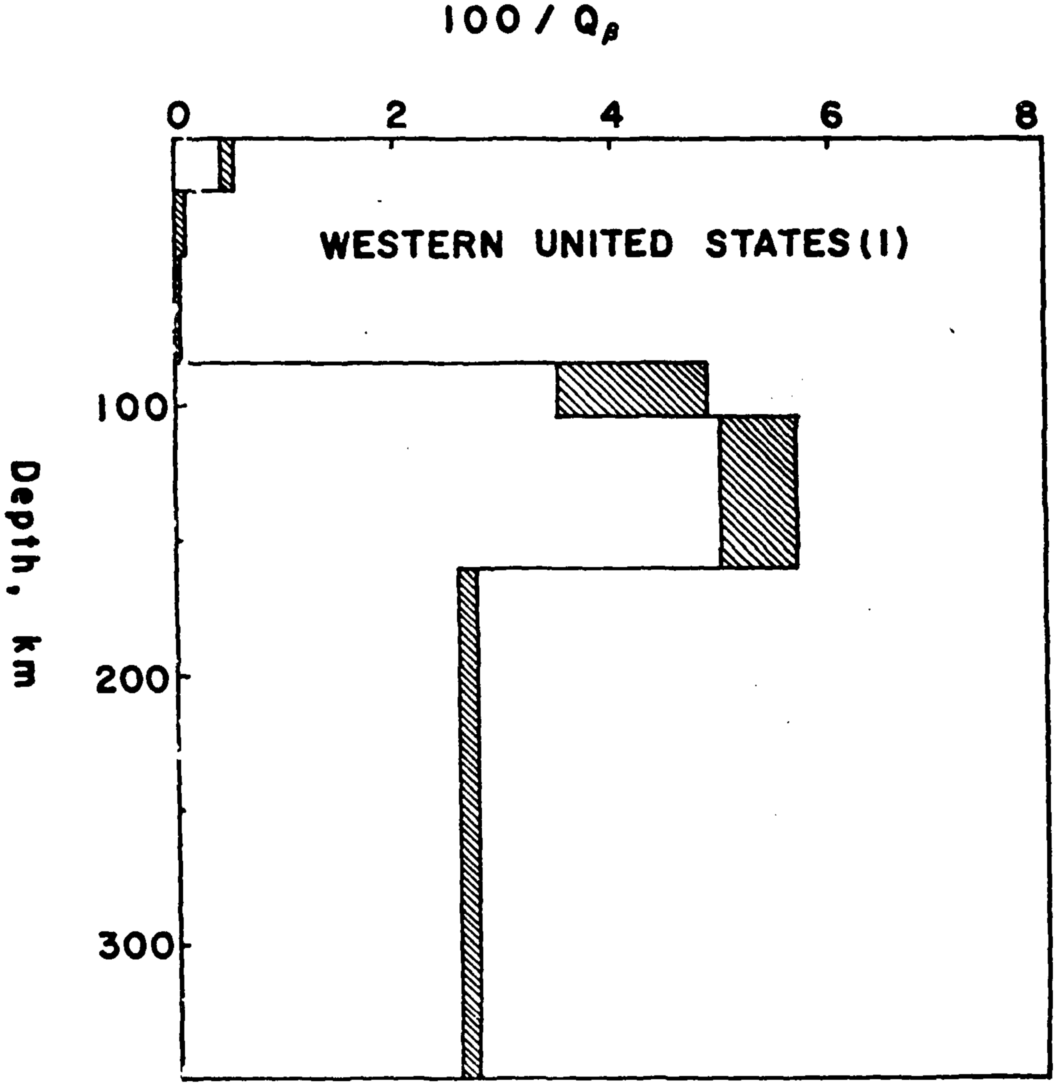
100 / Q_β
0
2
4
6
8
WESTERN UNITED STATES (1)
100
200
300
Depth, km

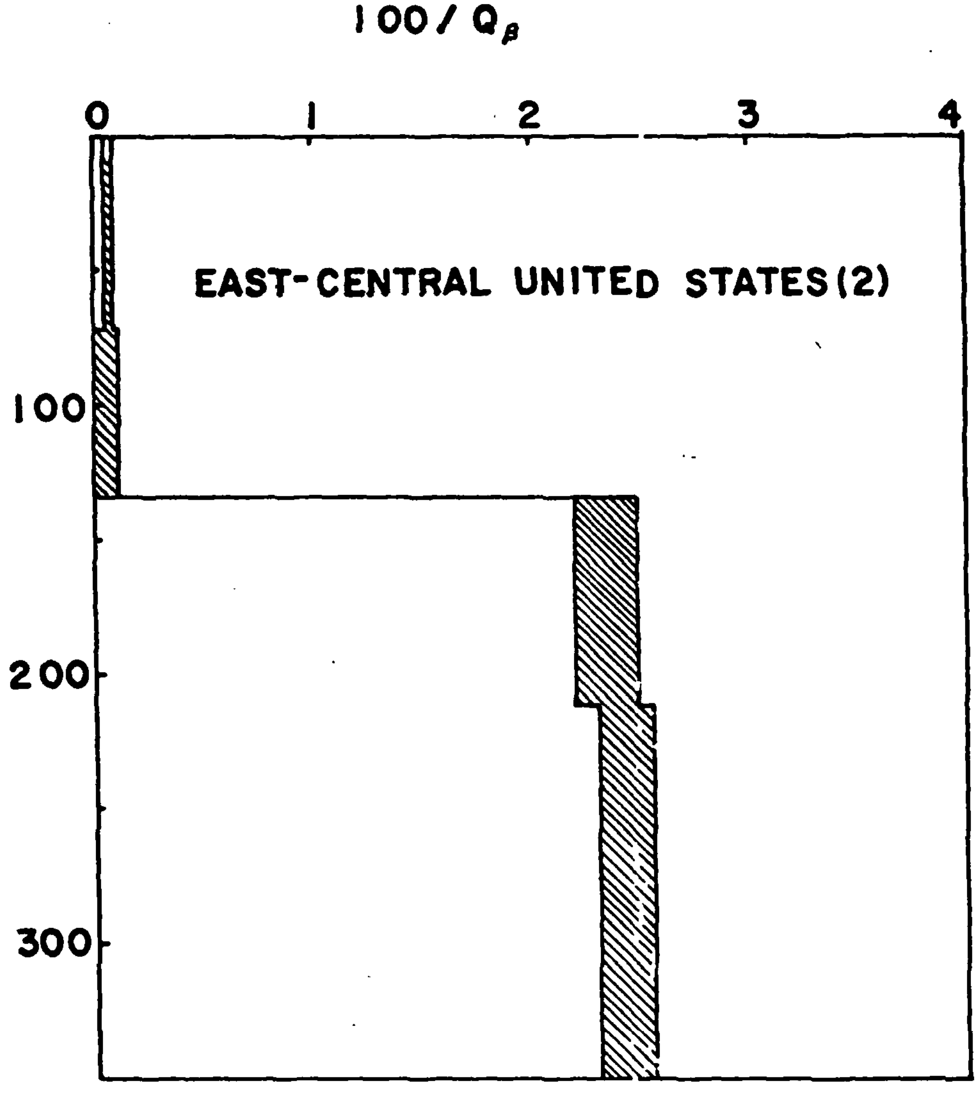
100 / Q_β
0
1
2
3
4
EAST-CENTRAL UNITED STATES (2)
100
200
300
Depth, km

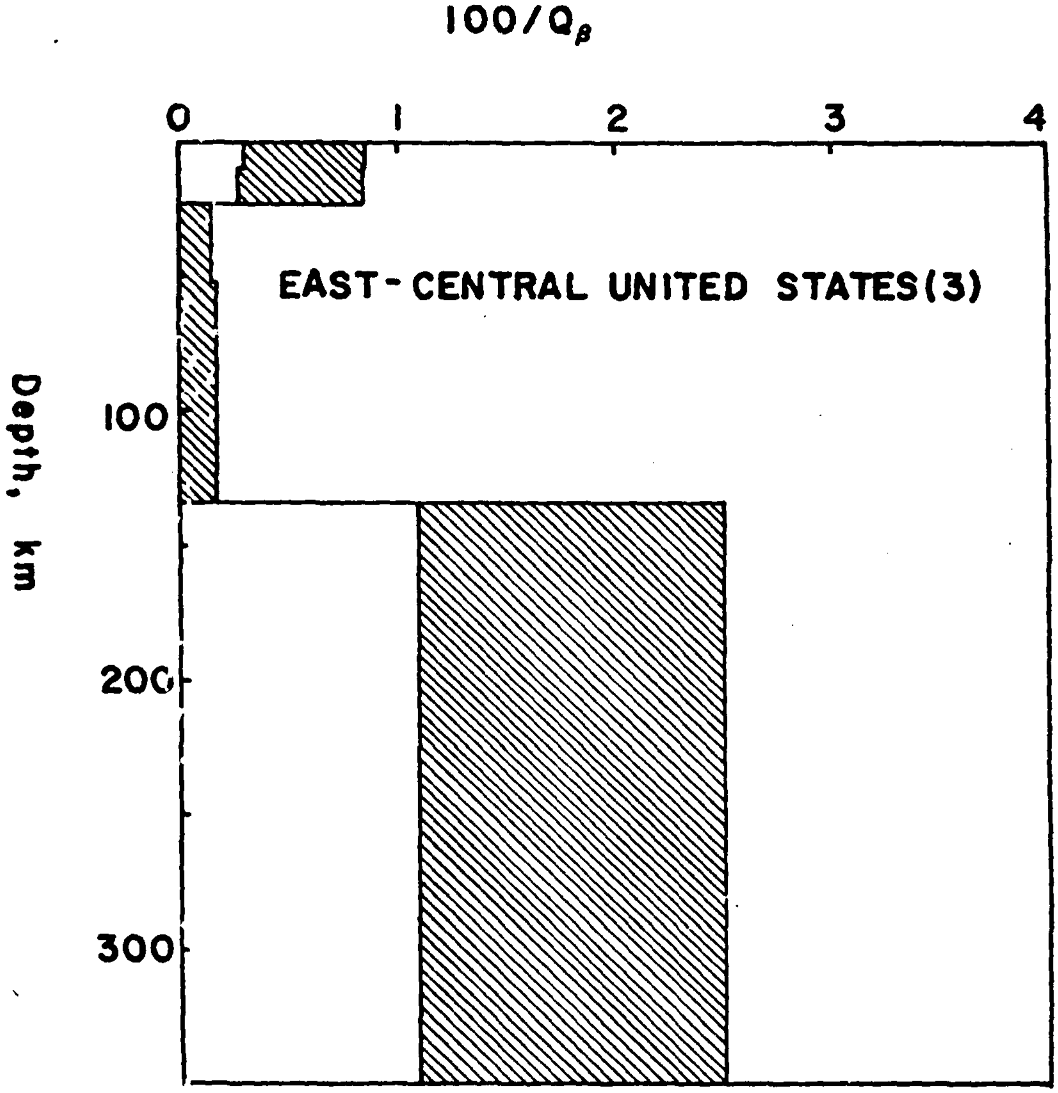
$100/Q_\beta$
0
1
2
3
4
EAST-CENTRAL UNITED STATES(3)
Depth, km
100
200
300

TABLE 2.5a Envelope of attenuation model, $100/Q_\beta$, western United States

Depth, km	min	max
0-21	0.43	0.54
22-45	0.0	0.05
46-84	0.0	0.03
85-104	3.50	4.87
105-160	4.95	5.73
161-350	2.60	2.69

TABLE 2.5b Envelope of attenuation model, $100/Q_\beta$, east-central United States (data set 2)

Depth, km	min	max
0-72	0.06	0.08
73-134	0.0	0.09
135-212	2.19	2.48
213-350	2.29	2.57

TABLE 2.5c Envelope of attenuation model, $100/Q_\beta$, east-central United States (data set 3)

Depth, km	min	max
0-9	0.29	0.86
10-23	0.25	0.84
24-52	0.0	0.15
53-134	0.0	0.17
135-350	1.09	2.51

Fig. 2.6. Surface wave attenuation predicted by envelope of models in Fig. 2.5 (solid lines). Triangles and circles represent the observed values (Table 2.1 and 2.2); open symbols are for incompatible data. Love and Rayleigh wave Q^{-1} are given in (a) and (b) for data set 1, (c) and (d) for data set 2 and (e) and (f) for data set 3.

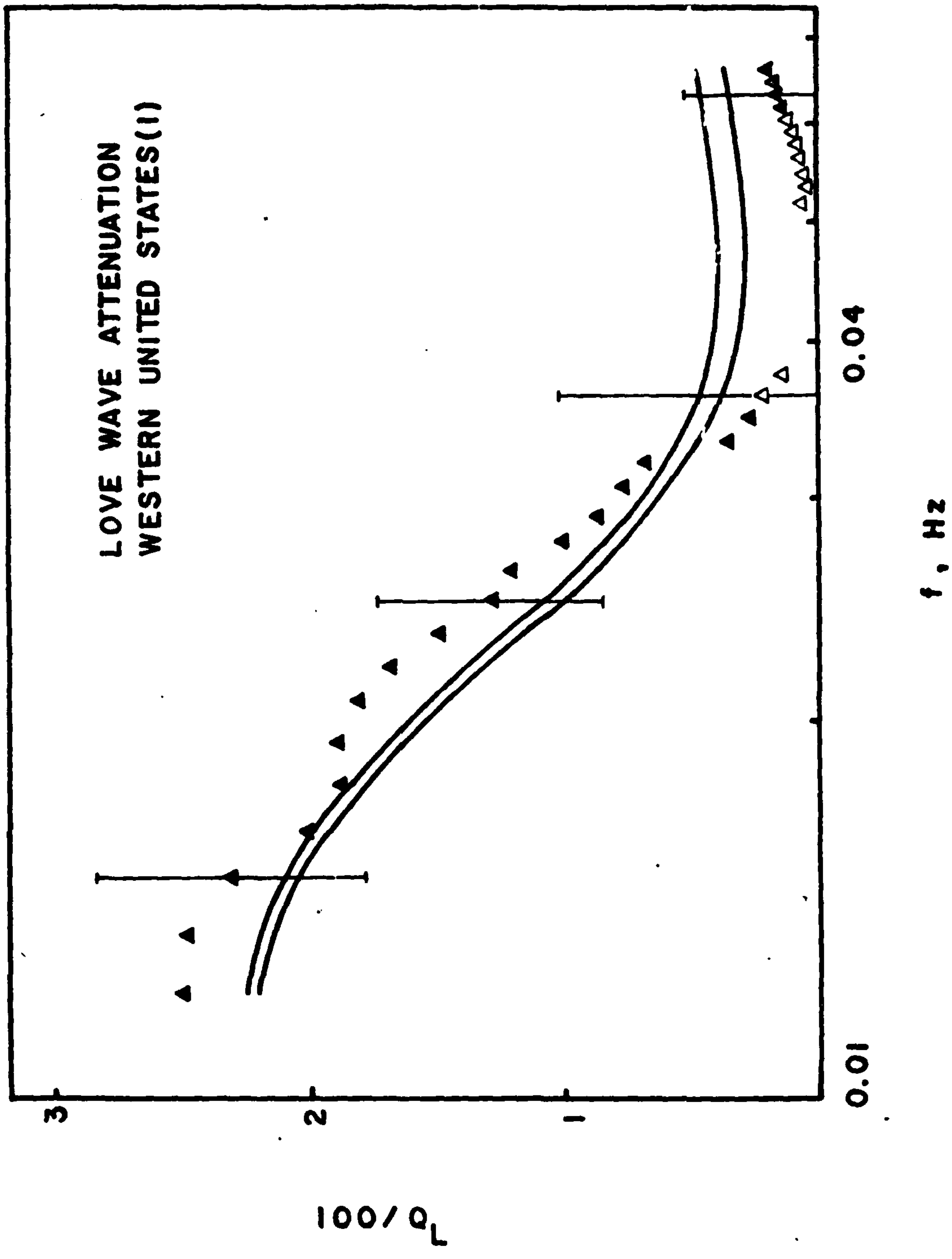
LOVE WAVE ATTENUATION
WESTERN UNITED STATES(1)
100/Q_L
3
2
1
0.01
0.04
f , Hz

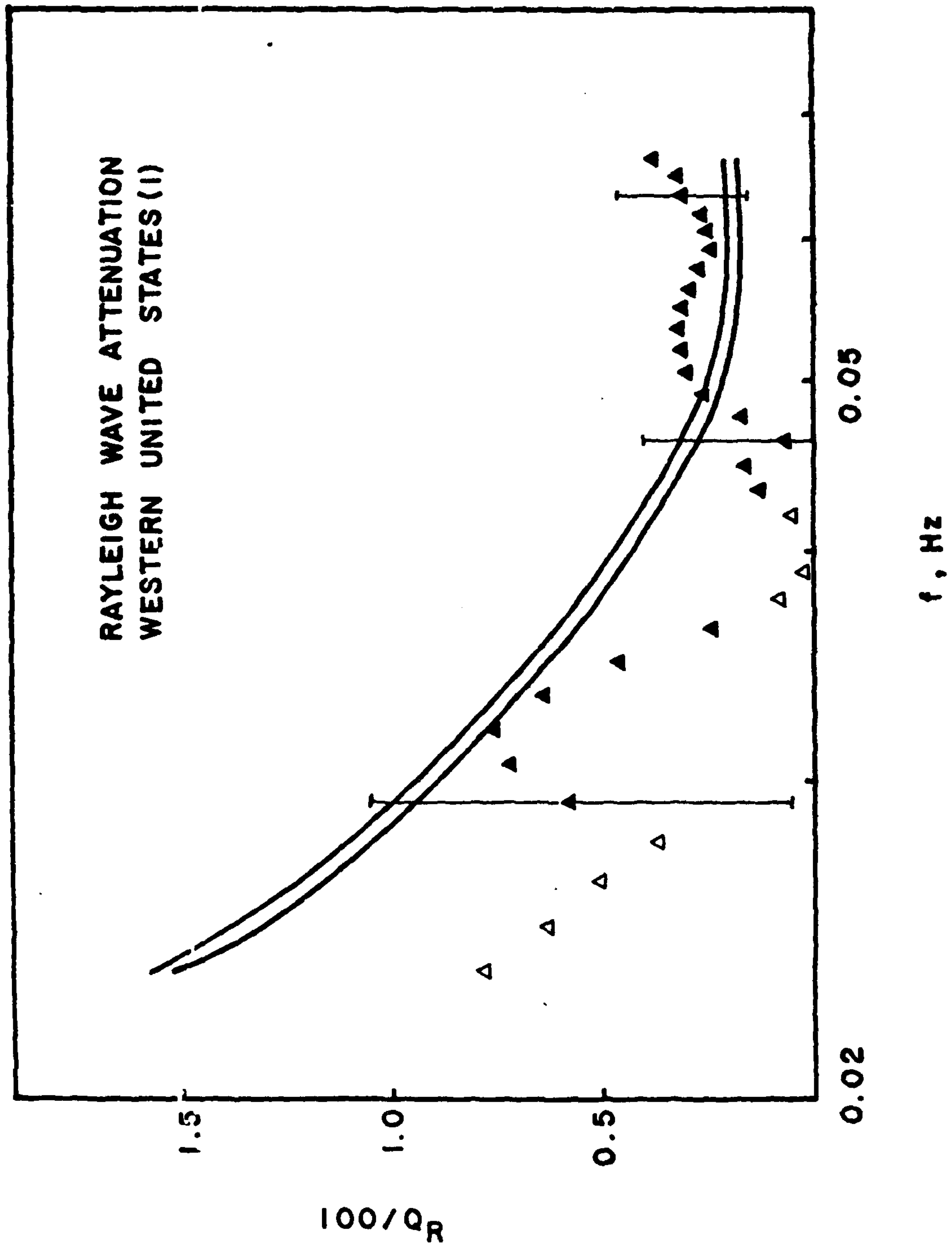
RAYLEIGH WAVE ATTENUATION
WESTERN UNITED STATES (I)
100/Q_R
1.5
1.0
0.5
0.02
0.05
f, Hz

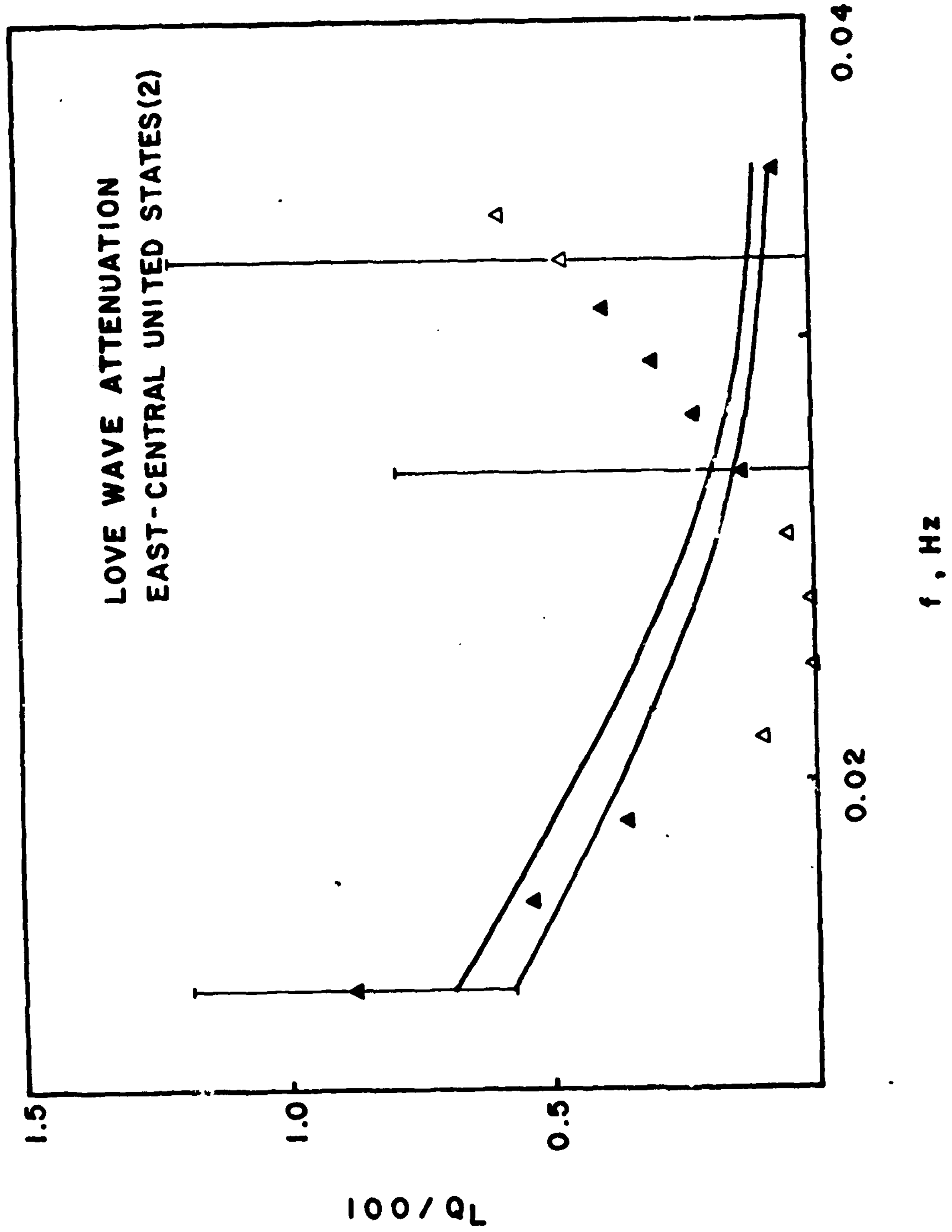
LOVE WAVE ATTENUATION
EAST-CENTRAL UNITED STATES(2)
1.5
1.0
0.5
100/QL
0.02
0.04
f, Hz

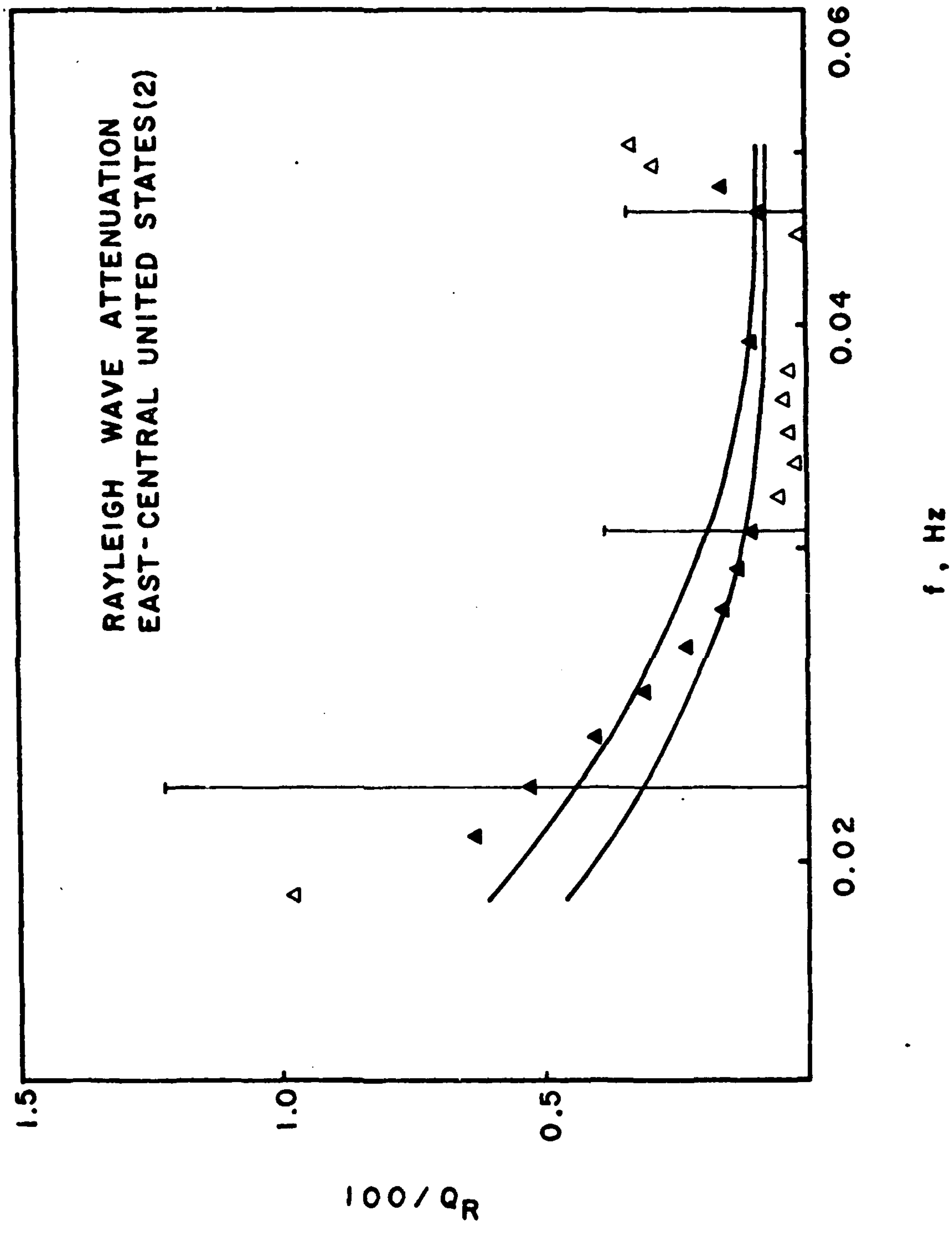
RAYLEIGH WAVE ATTENUATION
EAST-CENTRAL UNITED STATES(2)
1.5
1.0
0.5
$100/Q_R$
0.02
0.04
0.06
f, Hz

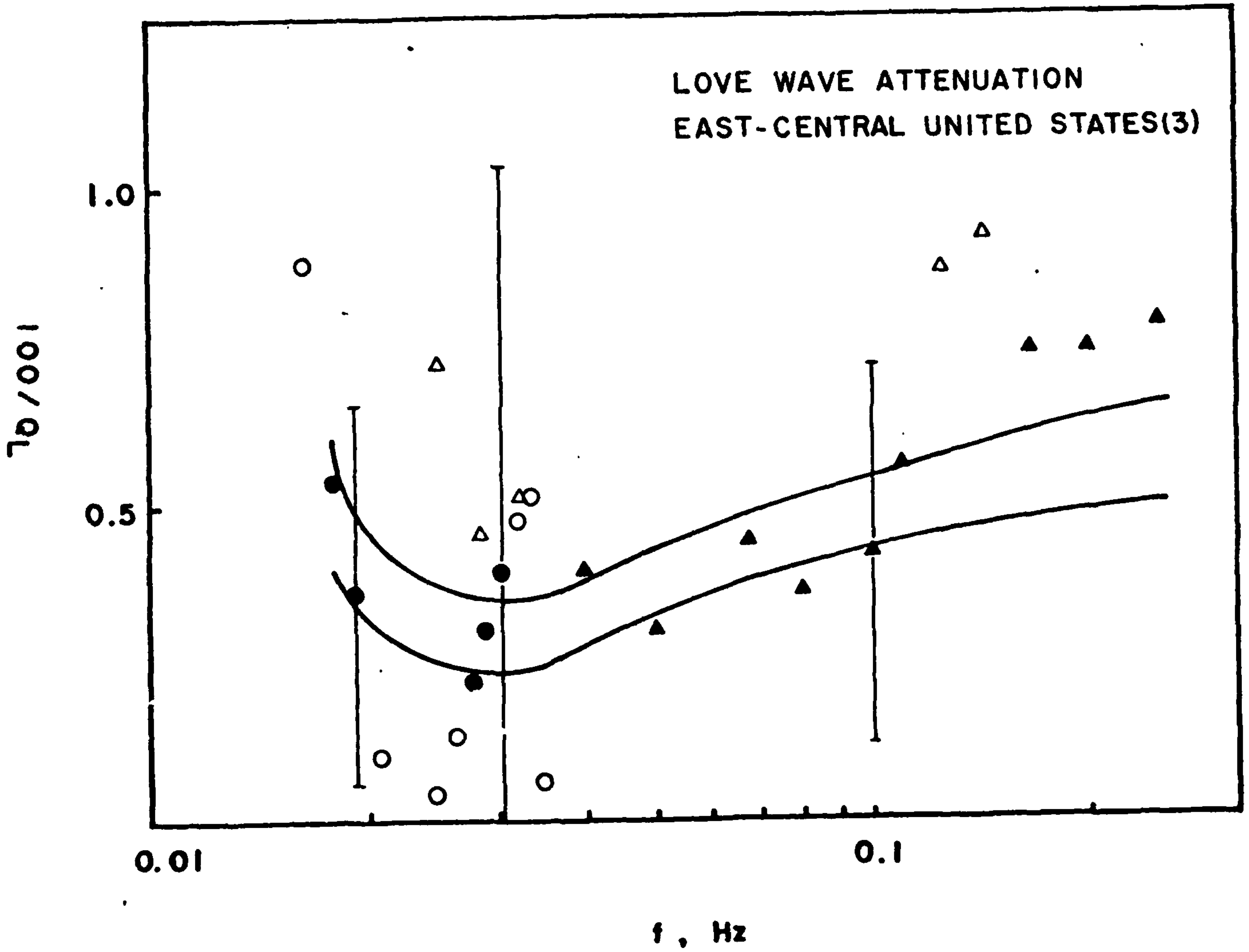
LOVE WAVE ATTENUATION
EAST-CENTRAL UNITED STATES(3)
100/Q_L
1.0
0.5
0.01
0.1
f , Hz

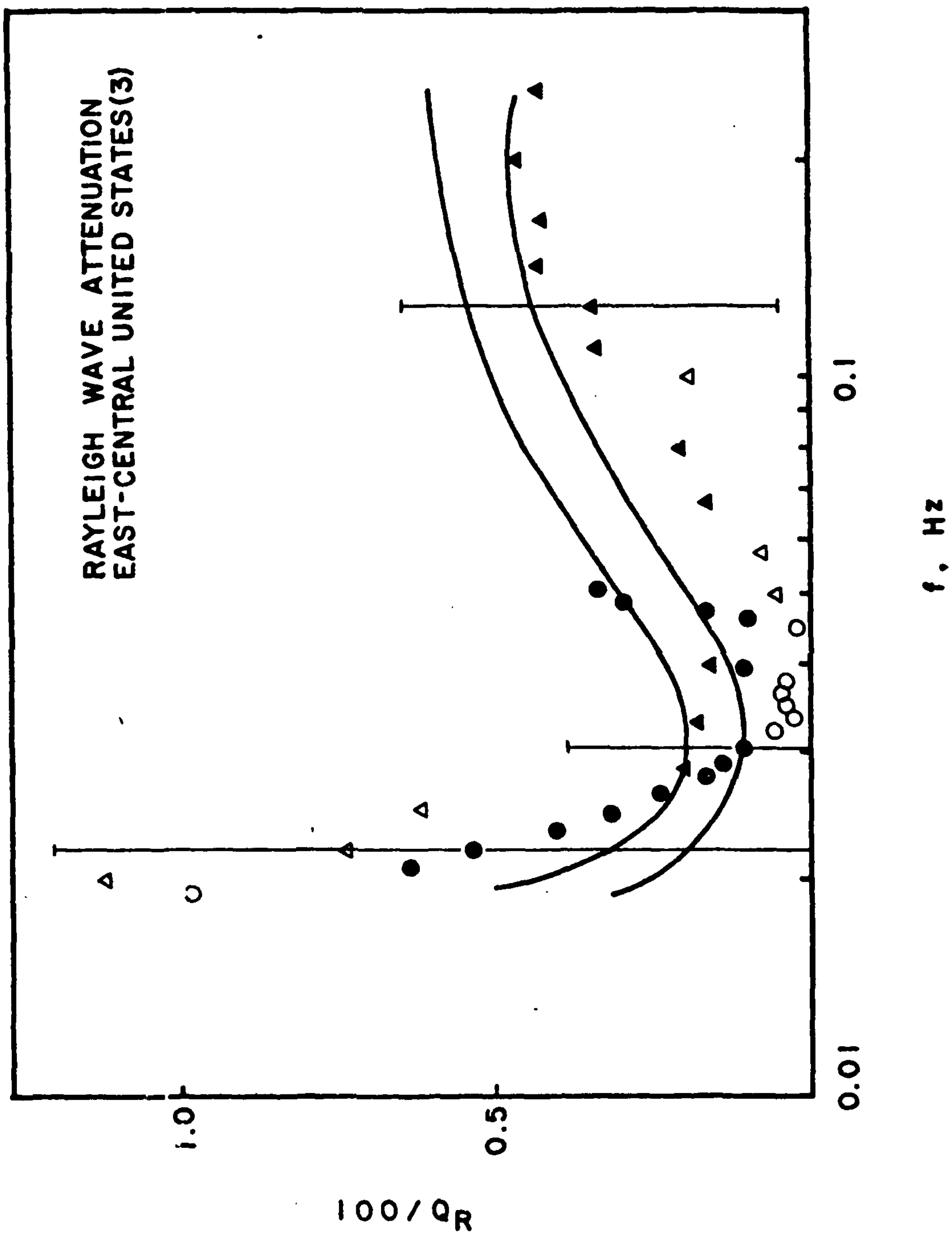
RAYLEIGH WAVE ATTENUATION
EAST-CENTRAL UNITED STATES(3)
100/Q$_R$
1.0
0.5
0.01
0.1
f, Hz

model can never simultaneously approach a perfect fit to both sets of data. The same statement is true of plausible frequency-dependent Q_β^{-1} models (Solomon 1972a), e.g. models obtained by inverting equation 1.5. This difficulty is related to the minimum in Q_L^{-1} and Q_R^{-1} versus period noted earlier (Tryggvason 1965; Tsai and Aki 1969) and to other wiggles in the attenuation curves. The wiggles in Q_R^{-1}, which are especially pronounced, may possibly be a scattering effect. The total travel length L is 2000 km and the wavelength λ is 60-150 km, so kL = 80-200, where k is the wave number. For scattering from weak heterogeneities in elastic properties and density to be negligible, ka must be less than 0.4, where a is the correlation length or, roughly, the characteristic dimension of the heterogeneities (Chernov 1960). Since $ka < 0.4$ would require $a < 4$-10 km, scattering is not likely to be a negligible effect.

For east-central United States, the frequency independent model provides an acceptable fit to the data except for a discrepancy between Q_L^{-1} and Q_R^{-1} in the period range 30-36s. The high attenuation of Love waves in that period range may either be due to higher mode interference, more likely for Love waves than Rayleigh, or due to anisotropy of the attenuation mechanism.

Several results of the Q_β^{-1} models in Table 2.5 and Figure 2.5 are worthy of comment. It is clear that the lithosphere, identified with low Q^{-1}, and the asthenosphere, identified as a deeper zone of high Q^{-1}, both differ between western and central or eastern North America. The lithosphere is thicker and Q_β^{-1} in the asthenosphere is significantly less in east-central than in western United States.

We obtain lithosphere thicknesses of 80±20 km and 130±30 km for western and east-central United States, respectively. The range in thicknesses comes from separate inversions of Love and Rayleigh wave attenuation and is conservative in that inversion using both sets of data gives a narrower range of thicknesses for both regions. These values for lithosphere thickness are not out of line with those inferred from the distribution of seismic velocity with depth using either refraction results (Green and Hales 1968; Julian 1970) or dispersion data (Biswas and Knopoff 1974).

The value for Q_β^{-1} in the asthenosphere differs by a factor of about 2 between the two regions, in agreement with the results of Solomon (1972a). Both this difference in Q_β^{-1} and the different lithosphere thickness can be explained by a modest temperature contrast in the upper mantle between the two areas (Solomon 1972a).

Some fine structure is notable in the models. A decrease in Q_β^{-1} with depth in the lithosphere is resolvable from data sets 1 and 3, a result also obtained by Mitchell (1973b). The interpretation of this conclusion depends on the seismic loss mechanisms, but the models are consistent with a closing of fluid-filled cracks or a decrease of volatile content with depth in the lithosphere. It also appears that a decrease in Q_{β}^{-1} below about 160 km is resolvable in western United States.

In summary, there are difficulties in modelling the attenuation of surface waves that arise from an assortment of reasons: 1) the loss mechanism at high pressure and temperature in the Earth is imperfectly known; 2) the measurement error is large and data are sparse; and 3) attenuation by mechanisms other than anelasticity is not negligible and not always separable. At this stage, under the assumption that the interference to the true anelastic attenuation is localized to some period range, our rules of data correlation and incompatibility are a reasonable filter to sort out which measurements are suitable for inversion. The Q_{β}^{-1} models that result from the inversion offer several insights into the nature of the lithosphere and asthenosphere.

In the next three chapters, we will formulate the simultaneous inversion of not only surface wave attenuation but also surface wave phase velocity. A major justification for this approach is because the anelastic dispersion from linearity seems to be important in the inversion process of surface waves. The validity of linearity is first reviewed in terms of the possible mechanisms for seismic-wave damping in the earth's mantle.

CHAPTER III

Attenuation Mechanisms in the Upper Mantle

3.1 Resume

The deviations from perfect elastic behavior of a sample material in the laboratory have yet to be understood. The situation in the earth's mantle is expected to be at least as complicated. A stress wave propagating through a non-elastic medium experiences an attenuation of amplitude due to various processes. These processes have not been well understood in terms of atomic or ionic (microscopic) properties of the material; rather they have been lumped under the heading internal friction.

Standard models have been used to describe internal friction in terms of various combinations of springs (perfect elasticity) and dashpots (Newtonian fluid). The Maxwell solid, the Kelvin-Voigt solid and the standard linear solid are examples of such models. Surely, these standard models do not explain reality most times. Orowan (1967) suggested that in a composite material, such as the earth's mantle, it is necessary to invoke the more general arrangement of springs and dashpots for each molecular constituent; the standard linear solid with an additional dashpot corresponding to the viscous deformation. Such a general arrangement does not explain the direct observations regarding the non-elastic properties of the earth: the attenuation of seismic waves.

However, it provides a diagrammatic convenience and a way of thinking macroscopically. Although most laboratory experiments are performed at conditions different from the earth's mantle, they may provide sound bases for a 'thought experiment'. The possible theoretical mechanisms of seismic attenuation have been reviewed at length by Jackson and Anderson (1970). Among the many suggested, the possible mechanisms in the asthenosphere are of greatest interest since most absorption occurs there. Solomon (1971, 1972) thoroughly examined partial melting in terms of Walsh's model (1968, 1969) and Jackson examined a grain boundary relaxation model (1969, 1971). In this chapter, we are going to review some aspects of the attenuation mechanism which will be important in the following chapters.

3.2 Seismic and laboratory observations

One of the earliest and most important observations in the laboratory was that Q is substantially independent of frequency in a solid at low pressures and temperature. Since Linsay (1914) first made this observation, many investigators have verified the fact with different materials (composite non-metals) over a broad range of frequencies. For earth materials, the conclusion is the same. Knopoff and Porter (1963) showed that in granite the attenuation of Rayleigh waves over the frequency range 50-400 kHz appears to have a Q nearly independent of frequency. At higher frequencies, a fourth power law of attenuation becomes dominant in their observations, which suggests a Rayleigh scattering process. Similar results have been observed in limestone by Peselnick and Outerbridge (1961). Born (1941) studied sandstone which had varying amounts of interstitial water injected into the sample. The interesting result is that the dry rock has a frequency-independent Q while the wet rock has a Q increasing linearly with frequency. Another important observation is that Q for rock, again, at low pressure and temperature, is an order of magnitude lower than for single crystal materials. Peselnick and Zietz (1959) indicate that Q for calcite is about 1900, a factor of 10 greater than in limestone, which is polycrystalline calcite. This suggests that grain boundary effects are likely important and show the same frequency dependence of Q for single crystals and composite materials.

Few observations on the behavior of Q at near melting temperatures have been performed. Mizutani and Kanamori (1964) measured the elastic and anelastic properties of a Pb-Bi-Sn-Cd alloy of melting point 72°C from 10 to 130°C at near MHz frequencies. They observed that the elastic velocity decreases with temperature. The decrease accelerates near the melting point and is most pronounced for shear waves. The quality factor, Q, for P-waves increases almost linearly with frequency between 0.5 and 3.0 MHz. Kuroiwa (1964) and Spetzler and Anderson (1968) studied attenuation in the various forms of ice at temperatures near the melting point.

They found that the introduction of NaCl into the ice broadened the peaks, shifted them to lower temperatures and increased the peak damping. The background damping, attributed to grain boundary effects, increased with increasing content of an impurity. Goetze (1969) discussed the behavior of metals at near melting temperature.

The intrinsic attenuation of rocks as a function of temperature and pressure is not known. Some laboratory measurements of hysteresis loops for strains no less than 10^{-6} shows that the attenuation is dependent on the amplitude of the strain (McKavanagh and Stacey, 1964). This suggests that linear theories are valid only at strain amplitude less than 10^{-6}.

For seismic observations, the most common difficulty is that the influence of scattering due to heterogeneity cannot be removed. Earlier observations by Collins and Lee (1956) and by McDonal et al. (1958) were measured at a small number of stations in relatively homogeneous short range of less than 30 feet. By no surprise, their observations in the field gave results comparable to those obtained in the laboratory on homogeneous rocks. Their main finding was that Q is nearly independent of frequency over the frequency range 100 to 1000 Hz (50-550 Hz for McDonal et al.). Among many observations by other investigators, Anderson and Kovach (1964) observed multiple reflections from deep focus earthquake in Brazil recorded in

Peru. They indicated that for the upper mantle Q in shear is about 160 and for the lower mantle about 1450, and Q is roughly independent of frequency over the range 11 to 25 seconds for the entire mantle.

Since that time, the observations of Love and Rayleigh wave attenuation has been considered to be more reliable than body wave observations, because the surface waves are less subject to the effects of scattering by inhomogeneity. However, the interpretation is more complicated due to strong dispersion. Benioff et al. (1961) measured the attenuation of Rayleigh waves from the Chilean earthquake and summarized that there is significantly more attenuation in Love waves than in Rayleigh waves. This may be an indication that the attenuation due to pure compressive modulus is negligible. The presently available surface wave attenuation data covers North America (Solomon, 1971; Mitchell, 1973, 1975), Eurasia (Yacoub and Mitchell, 197?; Burton, 1974), the Pacific Ocean (Mitchell et al., 1976) the Atlantic Ocean (mostly) (Tsai and Aki, 1969). Also there are many useful great-circle path data (e.g., Kanamori, 1970; Dziewonski and Landisman, 1970). These data clearly show a regional variation over much of the common period range. One cause is the varying lithospheric thicknesses regionally. For example, the lithosphere thickness in western U.S. (a tectonic region) is about 80 km while that in eastern U.S. (a stable shield region) is about 130 km (see Chapter II) and that of the average Pacific ocean is 60 km (Mitchell et al., 1976). Recent body wave observations (Solomon, 1972b; Der and McElfresh, 1977) suggest that Q increases with frequency above 1 Hz.

3.3 Nonlinear or linear attenuation process?

Knopoff and McDonald (1958) argued that the observed 'constant Q' for seismic wave attenuation is incompatible with linear theory. They developed a non-linear wave equation in which dry friction is the attenuation mechanism. McKavanagh and Stacey (1974) suggested that a cusp at the end of stress-strain hysteresis loops at strain amplitudes down to 10^{-6} may be evidence of non-linearity. The question of linearity vs. non-linearity is very important because the linear theory makes the general problem of attenuation of non-sinusoidal waveforms mathematically tractable. In other words, waves can be superposed by Fourier components without modifying one another. Kogan (1966) criticized the non-linear theory based on experimental evidence. Savage and Hasegawa (1967) presented similar criticism. Lomnitz (1957, 1962) suggested a linear theory which attributes the attenuation of elastic waves in polycrystalline materials to logarithmic creep. The theory predicts both the magnitude of Q and its frequency independence. McDonal et al. (1958) and Knopoff and Porter (1963) have investigated the attenuation of a seismic pulse rather than the usual harmonic waves. The procedure employed in both experiments was to analyze the pulse into its Fourier components and then determine Q as a function of frequency from the attenuation of various Fourier components. The magnitude of Q determined from the Fourier components and insensitive frequency dependence suggest that the superposition principle was applicable and therefore, the mechanism of attenuation linear. Orowan (1967) and Liu et al. (1976) suggested 'constant Q' observation can be explainable in the linear theory assuming the presence of a continuous distribution of linear visco-elastic elements. Above all, non-linearity becomes apparent in waves of extremely large amplitudes and so has little relevance to seismic waves. For example, a wave of displacement amplitude 1 mm and wavelength 10 km gives its strain amplitude of 6×10^{-7} ($= 2\pi A/\lambda$). One more possible argument for non-linearity is the non-existence of body wave dispersion since dispersion due to absorption is a characteristic of the linear theory. Although this question will be addressed in the next chapter, the frequency dependence of Q may provide the answer to such an argument, a point also suggested by many others.

3.4 Solid friction and viscous damping

Perfectly dry rock is not expected to occur in the earth because of the presence of ground water, of hydrothermal solution or, at greater depth, of partial melting. As Born's experiment (1941) shows, the presence of a fluid phase in rock causes substantially lower Q and a Q of increasing linear dependence on frequency. Solid ('dry') friction was described by Walsh (1966) as crack surfaces in contact slide relative to one another. It is rather insensitive to temperature but highly pressure dependent. Solid friction is independent of velocity and therefore is intrinsically frequency independent but depends on amplitude. It cannot be described in terms of viscoelasticity but may be of the static hysteresis type. The amplitude-insensitive crack surface friction is not well explained on the basis of Amonton's Law (according to which $\tau = \mu . p$ where τ is the frictional drag, μ the coefficient of friction, and p the normal pressure between the rubbing surfaces). Solid friction may be limited to describe the non-elastic behavior near the surface of the earth where temperature is not a main factor.

A conspicuous feature of seismic velocity profiles for certain parts of the upper mantle is the upper mantle low velocity zone (LVZ). Is the LVZ in the upper mantle a strong indication of the presence of fluid phase, probably partial melting? Or can a composition change or a phase change be hypothesized to explain the LVZ? Gordon and Davis (1968) suggested that the LVZ is principally due to interface inelasticity, which can persist to great depth due to the presence of fluid phase. They claimed that this is a unique explanation of the simultaneous occurrence of the LVZ and the low Q zone (LQZ) due to modulus defect. In such a case, low Q results from interface friction rather than from the fluid itself. However, according to Born (1941), a small amount of water injected into the interstitial region in sandstone increases substantially the internal friction. Therefore, the presence of the fluid itself should be an important factor in increasing the internal friction. Many authors suggested that the low velocity zone may be due to partial melting of mantle materials. Partial melting in the earth's mantle is likely to have the character of an interstitial fluid embedded in a host matrix, since shear waves are transmitted through. A more pronounced minimum of shear velocity than that of P-wave velocity in the low velocity zone indicates the presence of melting. Various melt models of damping have been suggested for the earth's mantle by Mavko and Nur (1975) and O'Connell and Budiansky (1977). Isolated penny-shaped cracks with melt (short time-scale damping), interconnected cracks with short range melt flow (intermediate time-scale damping), and large scale melt diffusions (large time-scale damping) are considered by Mavko and Nur (1975).

3.5 Hysteresis, resonance, scattering and relaxations

The mechanisms likely to be responsible for the attenuation of seismic waves are classified in four categories.

Quickly we may rule out hysteresis, resonance and scattering, for the dissipation mechanism in the earth mantle. Although scattering does not reflect the anelastic properties of medium, it is quite important to recognize the scattering effect when inhomogeneities are comparable in scale to the wavelength of the seismic waves. Ultimately, it will be very important to remove the scattering effect to improve the quality of seismic amplitude data. However, we may avoid this difficulty when we choose rather homogeneous structures and use longer wavelength (longer period) data for a study of the damping mechanism at greater depth (the mantle).

Granato and Lücke (1956) proposed that a pinned edge dislocation may act as a violin string with a damping force proportional to its velocity. This type of resonance internal friction is strongly dependent on average loop length and proportional to the dislocation density. The internal friction will increase with temperature, as thermal unpinning will increase loop length, even though the dislocation density will decrease with temperature by annealing. However this type of internal friction due to resonance appears only at high frequencies and is irrelevant to the seismic problem.

Solid friction across cracks was considered by Walsh (1966) as mentioned in the previous section. This mechanism adequately explains measurements at low pressure (Birch and Bancroft, 1938) including the frequency independence of internal friction and its decrease with pressure. However, most cracks in dry rocks would be closed under modest pressure (less than about 10 kbar). In wet (partially molten) rocks, fluid might persist to keep cracks open under mantle pressures. However, at high pressure, the internal friction due to solid friction likely will be minimized, and viscous stress relaxation may dominate internal friction. As discussed in section 3.4, this type of mechanism due to static hysteresis may depend on amplitude and belongs to the class of non-linear theories, which are not favored by seismic amplitudes, though not ruled out.

Most linear attenuation mechanisms are a form of relaxation process. A relaxation process is a characteristic of viscoelastic material (standard linear solid), in which no irreversible deformation is undergone. In such a material, internal friction has the form:

$$Q^{-1} = \frac{M_u - M_r}{M_u} \frac{\omega\tau}{1 + (\omega\tau)^2} \qquad (3.1)$$

where M_u is an unrelaxed elastic modulus, M_r is a smaller relaxed modulus, ω is angular frequency, and τ is a relaxation time. Notice that the peak internal friction occurs at $\omega\tau = 1$. Zener (1948) considered a relaxation in a two component system where a viscous phase is embedded in an elastic matrix. The remarkable feature of such a two component system is the large anelastic effects due to a small amount of viscous material. Another feature is the wide variety of types of relaxation spectra. If all the localized viscous regions had the same size and shape, we would expect a concentrated relaxation spectrum. Rather, observed behavior indicates a distribution of the size and shape of the viscous regions. Walsh (1969) made more specific assumptions for two phase media. Solomon (1971) applied this theory to partial melting for the upper mantle of western United States.

The importance of grain boundary effects in seismic attenuation was stressed by Peselnick and Zietz (1959), Jackson (1969) and Jackson and Anderson (1970). Also important is high temperature background relaxation (Jackson, 1969; Jackson and Anderson, 1970). Most physical mechanisms proposed for seismic attenuation in the earth's mantle are of the form of a thermally activated relaxation and all these mechanisms are distributed with a largely unknown distribution function.

3.6 Distribution function of relaxation times

The 'standard linear solid' gives a Debye peak (bell-shaped) absorption spectrum with peak at the frequency determined by $\omega\tau = 1$, where τ is a relaxation time. For most materials, it is too simple to represent physically meaningful viscoelastic behavior. As Orowan (1967) explained, in the case of soda glass, the elementary process of relaxation (or viscoelastic creep) is the jump of a sodium ion from one cell to another. This cannot be described by a dashpot. A different ion may be activated with a different energy by a different stress. Therefore, there may be various activation energies and strain contributions which can be represented by different viscoelastic schemes. To satisfy a frequency independent Q, the activation energy spectrum, or the relaxation time spectrum, should be distributed. Various distribution functions have been proposed to explain empirical curves by metallurgists and polymer scientists. To understand the usefulness of these distribution functions, the most simple and frequently used functions are given in the following.

3.6a Box distribution

According to Becker (1925) if the distribution function of activation energies is constant, then viscoelastic creep is logarithmic and Q^{-1} is frequency insensitive over a wide range of frequency (Becker theorem). Orowan (1967) interpreted Becker's theorem in terms of the 'standard linear solid'. Recently, Liu et al. (1976) demonstrated that a continuous distribution of relaxations could be superposed to produce a frequency independent Q over seismic frequencies using a linear viscoelastic model. In all of the above cases, a relaxation function $\psi(t)$ is expressed as a superposition of the elementary relaxation functions e^{-st} with distribution density N(s),

$$\psi(t) = \int_0^\infty N(s)\, e^{-st}\, ds \qquad (3.2)$$

$$N(s) = \begin{cases} A / s & \text{for } s_1 < s < s_2 \\ 0 & \text{otherwise} \end{cases}$$

where A is a constant, s is the relaxation frequency (Becker used the term 'relaxance' for s). Liu et al. (1976) chose s_1 and s_2 in such a way that the frequency range of seismic interest is completely covered between s_1 and s_2. Becker was rather in the position of explaining empirical logarithmic creep functions in terms of relaxations which have been shown by numerous creep experiments. Becker mentioned s_1 as 'the lower limit below which no observable relaxation is contributed by the volume element within the duration of the experiment' and s_2 as 'the upper limit above which an element is completely relaxed before measurements can begin'. The above mentioned N(s) is generally known as a box distribution function (Gross, 1953). A so-called Becker material, or the result of a band-limited superposition of elementary relaxations, shows a creep curve (Orowan, 1967; Kanamori and Anderson, 1977)

$$\psi(t) = \ln(s_2 t) - Ei(-s_1 t) + \gamma \qquad (3.3)$$

where

$$Ei(x) = \int_{-\infty}^{x} \frac{e^{-u}}{u} du$$

is the 'exponential integral', and the constant γ (= 0.5772) is the limit value of $Ei(-x) - \ln x$ for $x \to 0$. At $t = 0_+$ the exponential integral dominates. However, after a small time (when $s_2 t$ exceeds 3), the creep becomes logarithmic. The logarithmic creep leads to an approximately constant Q (Lomnitz, 1957). Most observations of logarithmic creep have been for metals and long-chain polymers (viscoelastic material) at low temperature. However, the effect of pressure is opposite that of temperature so that the discrepancy between laboratory temperatures and temperatures in the mantle may not be as serious as we usually consider.

3.6b Log-normal distribution

The 'box distribution' which is constant and finite over a limited range of $\ln \tau$ and zero elsewhere has been discussed in the previous section. A different relaxation spectrum, a log-normal distribution, has been studied at length (Norwick and Berry, 1961) to explain broad regions of nearly constant Q in metals. A log-normal distribution of relaxation times is a Gaussian distribution in the logarithm of the relaxation times, in which the absorption can be specified by three parameters. These are the mean relaxation time, τ_m, the width of the distribution, ω, and the magnitude of relaxation, Δ. For the 'box distribution', the clear advantage is its possible evaluation of integral (3.2) in terms of known functions; nevertheless, it has the distinctive disadvantage that it is a physically arbitrary distribution, and for the limits s_1 and s_2 to fall just outside the seismic frequency band is unreasonably convenient. The Gaussian distribution more likely represents the physical situation in which a distribution of relaxation times arises due to the distribution of atomic environments about a mean value. The relaxation process controlled by atomic movement is strongly temperature dependent (Jackson and Anderson, 1970):

$$\tau = \tau_o e^{H/RT} \qquad (3.4)$$

where H is an activation energy, τ_o and R are constants, and T is temperature. In equation (3.4), if the value of H is distributed with a distribution parameter $\zeta°$ according to

Gaussian distribution, then the value of ln τ is also distributed with parameter ζ in a Gaussian manner,

$$\zeta = \zeta^{o} / RT$$

If we assume that ζ° is independent of temperature, then ζ varies inversely as T. That means, if temperature is low, the absorption spectrum becomes broader and goes to the 'box distribution' in the limit. On the other hand, as temperature goes higher, the absorption peak becomes sharper and shows frequency dependence. The apparent disadvantage of the log-normal distribution is that the integral (3.2) cannot be evaluated in terms of explicit functions.

3.7 Q frequency dependent or independent?

The frequency dependence in Q in the earth's mantle from most seismic evidence is ambiguous at best. Solomon (1971) reviewed elaborately the contradicting evidence. One of the main sources of ambiguity is the large uncertainties in seismic measurements. The main obstacles in seismic amplitude measurements are geometrical effects, such as scattering, multipathing and mode conversion. Jackson (1971) assumed a frequency dependent model based on the mechanism of grain boundary relaxation and showed a reasonable fit to the intermediate range of Love wave and toroidal oscillation data (40-200 sec). However, Jackson's model (57-31-010) seems not to have good agreement with longer period data

(>200s). Jackson (1971) indicated that the assumption of frequency independent Q resulted in negative values of the Q model in some depth. Solomon (1971, 1972a) suggested a relaxation model due to partial melting in the upper mantle of western United States. Solomon's (1971, 1972a) frequency dependent model showed a good agreement with Love and Rayleigh wave attenuation data in the period range 15 to 82 seconds. However, the same data set is still in good agreement with frequency independent models (Solomon, 1971; Lee and Solomon, 1975). Archambeau et al. (1969) concluded that Q_α (P-wave attenuation) in the upper mantle of western United States increases with increasing frequency over the period range 0.75 to 1.5 Hz based on their observations of the attenuation of P_n waves. However, a frequency independent Q has been usually assumed. Recent observations of body wave attenuation (Solomon, 1972b; Der and McElfresh, 1977) suggest that Q increases with increasing frequency above 1 Hz. Russian investigators, Fedotov and Boldyrev (1969), Khalturin and Rautian (personal communication with Aki) expressed the same opinion. From an observational standpoint, it is fair to say that no conclusion can be made one way or the other for periods longer than 1 sec and there seems to be growing evidence of Q increasing with frequency for shorter periods (< 1 sec). From the theoretical point of view, individual relaxation mechanisms may be thermally activated processes and are strongly frequency dependent. However, a certain distribution function of these relaxation mechanisms could show a frequency independent spectrum of Q over a limited frequency band (Orowan, 1967; Liu et al., 1976). If extensive melting is possible in the earth's mantle, Q will become more frequency dependent because of the charactersitic of liquid state for Q to increase with ω (Knopoff, 1964). Such an explanation may have something to do with the frequency dependent observations (or related interpretations) in western U.S. (Archambeau et al., 1969; Solomon, 1972a) and the Atlantic Ocean (Tsai and Aki, 1969).

For partial melting, Walsh (1968, 1969) considered the earth's mantle as a two-phase medium. If we think of a two phase medium in terms of a matrix embedded with viscous inclusions, relaxation due to either viscosity of the inclusions or viscous fluid flow through connected cavities may be responsible for damping. For distributed cavity sizes and shapes such inclusions will lead to a distributed absorption spectrum. We could not say anything more until either we measure accurately attenuation of long period body waves or we improve our knowledge on the attenuation mechanism in the earth's mantle. Therefore, the box distribution of relaxation mechanisms, which may possibly occur in the earth's mantle and which leads to a logarithmic creep function, often observed in the laboratory, may be a reasonable first guess.

On the other hand, the gap between the laboratory and the earth's mantle may be less serious than we usually assume, since temperature and pressure effects may work against each other. Finally, with the recent more widespread appreciation of the importance of anelastic dispersion, the more accurate phase information as well as inaccurate amplitude information can be a strong constraint to discriminate among some of the assumptions about frequency dependence of Q.

CHAPTER IV

Anelastic Dispersion

4.1 Resume

In the previous chapter, we discussed attenuation mechanisms and distribution functions to explain the gap between individual mechanisms and observations. In this chapter, we are going to take an alternative approach, in which we postulate basic principles like superposition and causality, and write the consequent mathematical relations between physical parameters. Ultimately we want to use these relations for inversion problems in the following chapter. Kolsky (1956), Futterman (1962), Lamb (1962), Strick (1967) and Azimi et al. (1968) used this approach in one way or another. The principles of superposition and causality provide relationships between the real component and imaginary component of the complex elastic modulus (phase velocity v and attenuation coefficient χ), given the observed frequency dependence of Q. Some other dispersion-attenuation relations also can be provided from a finite or infinite superposition of relaxation mechanisms using a certain distribution function. Solomon (1972a) and Liu et al. (1976) showed examples of these. Others arise from the empirical equations like Lomnitz's Law (1957) and the Jeffreys-Lomnitz law (1958). All of these relations, however, are indistinguishable mathematically for a given frequency dependence of Q. Therefore, they are classified in two general categories, frequency independent Q and frequency dependent Q.

4.2 Superposition and causality

We have discussed the validity of the linear theory of seismic wave propagation in anelastic media in the previous chapter. Linear theory provides Fourier analysis and the superposition principle. Therefore, the attenuation problem of non-sinusoidal waveforms is mathematically manageable. A wave form may be decomposed into its Fourier components, each component as a sinusoidal wavelet being attenuated and recomposed into the damped form of the complex wave. The causality principle, 'no signal before stimulus', is a must-be-obeyed condition in any physical system. However, causality often seems to be violated when we approximate a theory or an equation for numerical calculation, or when we try to fit a small piece of spectral data. The violation of causality sometimes causes disastrous consequences. In seismology, we have an example of causality violation. We used to make three simultaneous but incompatible assumptions based on limited pieces of observations. We used to assume: 1) frequency independent Q, which is approximately indicated by observation, 2) non-dispersiveness, which is indicated by body wave observations (surface wave observation is complicated by its own dispersion due to penetration depth), and 3) linearity.

Therefore, among the three, one or more is necessarily wrong. The causality violation due to these three assumptions can be easily demonstrated in the following example of a delta function pulse $\delta(t-x/c)$. The Fourier transform of the pulse $\delta(t-x/c)$ is

$$F(\omega) = \frac{1}{2\pi}\int_{-\infty}^{\infty} \delta(t-T)\, e^{i\omega t}\, dt = e^{i\omega T}/2\pi \quad (4.1)$$

Allowing the pulse to travel for a time T in the medium of constant Q, we obtain the attenuated spectrum

$$F_T(\omega) = \frac{1}{2\pi}\int_{-\infty}^{\infty} \delta(t-T)\, e^{i\omega t} e^{-\frac{\omega t}{2Q}}\, dt = e^{i\omega T} e^{-\frac{\omega T}{2Q}}/2\pi \quad (4.2)$$

Transforming back to the time domain,

$$f_T(t) = \int_{-\infty}^{\infty} F_T(\omega) e^{-i\omega t}\, d\omega = 2\left[\frac{T/2Q}{(T/2Q)^2+(T-t)^2}\right] \quad (4.3)$$

The result of equation (4.3) shows that the pulse peaks at t=T and spreads symmetrically to both earlier and later times. The fundamental unacceptable feature is that the disturbance begins before t=T.

A moderate frequency dependence of Q may be introduced with an associated dispersion to cancel the Fourier component which travels faster than its signal velocity. Assuming certain types of frequency dependence of Q, the corresponding dispersion relations are given by Kramers-Krönig relations (Hilbert transforms). A detailed discussion on causality and Kramers-Krönig relations is given in Appendix I.

4.3 Anelastic dispersion

In a linear theory of attenuation, dissipation must accompany dispersion. Such dispersion due to anelasticity is known as 'anelastic dispersion'. This notion is the by-product of principles of superposition and causality. Futterman (1962) derived a dispersion relation from the Kramers-Krönig causality relations. An important consequence of anelastic dispersion is that it is of first order in Q^{-1} and the dispersion between two decades of frequency in the earth's mantle is about [illegible] which is nearly an order of magnitude larger than the uncertainties in the data. We will discuss the significance of this statement. Although the effect of anelastic dispersion has been discussed by a number of authors for nearly two decades, the significance of this effect has been either neglected or widely thought to be minimal in the seismological community until quite recently. For the point of historical interest, we will discuss the reason for the neglect of anelastic dispersion.

4.3a Importance of anelastic dispersion in seismic studies

Ever since long period surface wave velocities and free oscillation periods were first interpreted to derive earth structure, the result has not been compatible with the classical models of Jeffreys and Gutenberg derived from body waves. The so-called 'baseline discrepancy' is the travel time difference of P and S waves from such a velocity model for long period data with reference to Jeffreys-Bullen travel times, for example. This baseline discrepancy is known to be more pronounced for S wave than P waves. According to Sen-Gupta (1975), his observed travel times of body waves from deep focus earthquakes, compared with the travel times computed from the B1 model of Jordan and Anderson (1974), an inversion model based on 80 percent free oscillation data and 20 percent body wave data, are 0.3 seconds early for P, 6.4 seconds early for S, and 5.7 seconds early for ScS. Sipkin and Jordan (1975) suggested there may be a continental bias in observed travel time of S waves while free oscillation data represent the average earth mantle. However, by any explanation, the S wave travel time difference of 6.4 seconds is too big. Carpenter and Davies (1966) and Davies (1967) pointed out the importance of dispersion in surface wave inversion and discussed the compatibility of body wave and surface wave observations. Hart et al. (1976), Anderson et al. (1977), and Kanamori and Anderson (1977) discussed the anelastic effect in the inversion of surface waves and free oscillation data. The significance of the anelastic dispersion effect is that the baseline discrepancy can be removed. Non-dispersive earth models from surface wave and free oscillation predict the phase velocities around 50 second period with about 1 percent error (Carpenter and Davies, 1966; Liu et al., 1976).

4.3b Reasons for neglect of anelastic dispersion

As explained in the previous section (4.2) and also by Stacey et al. (1975), it has been a mistake to use three incompatible assumptions which lead to causality violation, namely, linearity, constant Q, and non-dispersiveness of the medium. Knopoff (1956, 1959) discussed a linearized equation of motion of the form,

$$c_o^2 \left\{ \left(1 + \frac{1}{|\omega| Q} \frac{\partial}{\partial t} \right) \frac{\partial^2 u}{\partial x^2} \right\} = \frac{\partial^2 u}{\partial t^2}$$

where u is the particle displacement and c_o is the wave velocity in the absence of attenuation ($Q \to \infty$). Here we can see the same mistake of constant elastic modulus being assumed (non-dispersiveness). Because of a similar error, Ricker (1953) and Knopoff (1956) reported that the waveforms propagating through media with solid friction are not changed but spread out symmetrically.

Other reasons for the historical neglect of anelastic dispersion are given by Kanamori and Anderson (1977). (1) For a simple damped linear oscillator the inclusion of an infinitesimal attenuation ϵ changes the natural frequency of the system from ω to $\omega(1-C\epsilon^2)$, where C is a constant. Since $\epsilon \sim Q^{-1}$, the effect can be ignored for Q greater than 100, a typical value in the earth's mantle. 2) Knopoff and MacDonald

(1958) showed that the inclusion of infinitesimal attenuation in a linear system results in Q which is proportional to odd powers of frequency; therefore a constant Q model is inconsistent with a linear system. This led Knopoff and MacDonald to introduce a non-linear model. 3) Futterman's (1962) dispersion theory has been challenged by some investigators (Stacey et al., 1975) because the propagation velocity is increased by inclusion of anelasticity. (Futterman's theory has been defended by Savage (1976) and Kanamori and Anderson (1977) in that Futterman's mistake is not a real physical implausibility but rather is a result of the arbitrary assumption that phase velocity at zero frequency is the elastic velocity). These arguments can be given for historical interest. Some confusions due to arguments between linear or non-linear theory, and between frequency dependent or independent Q should not prevent us from seeing the significance of anelastic dispersion.

4.4 Dispersion-attenuation relations

Dispersion-attenuation relations can be given in two different ways. (1) In the frequency domain, for a given frequency dependence of Q, Kramers-Krönig relations provide a dispersion-attenuation relation. A frequency dependence (either dependent or independent) of Q can be given by superposition of a certain individual relaxation mechanism or of viscoelastic elements, or by empirical observations.

(2) In the time domain, Boltzmann's after-effect equation will provide a complex modulus and a dispersion relation for a given creep function or relaxation function. A creep (or relaxation) function can be given in a similar way, by superposing the relaxation (or creep) function of each viscoelastic element using a distribution function or by empirical observations. No matter which procedure we go through, the same dispersion-attenuation relations are given for the same frequency dependence of Q. Therefore, we will discuss two categories of frequency dependent and independent Q.

4.4a Frequency independent Q

Various attempts have been made to explain the nearly constant Q in the seismic frequency band (Futterman, 1962; Lomnitz, 1957; Azimi et al., 1968; Liu et al., 1976). Futterman (1962) and Azimi et al. (1968) derived dispersion relations in the frequency domain.

$$\chi(\omega) = C\omega \qquad \text{(Futterman)}$$

$$\chi(\omega) = \frac{\chi_0 \omega}{1 + \chi_1 \omega} \qquad \text{(Azimi et al.)} \qquad (4.4)$$

where $\chi(\omega)$ is attenuation coefficient and C, χ_0, χ_1 are constants. Relations (4.4) give the following dispersion relations (Appendix II)

$$v(\omega) = v_\omega \left[1 - \frac{1\omega}{\pi Q_o}\right]^{-1} \qquad \text{(Futterman)}$$

$$v(\omega) = v_\infty \left[1 + \frac{2\chi_o\omega}{\pi(1-\chi_1^2\omega^2)} \ln \frac{1}{\chi_1\omega}\right]^{-1} \qquad \text{(Azimi et al.)} \tag{4.5}$$

where χ_1 is chosen so that $\chi(\omega)$ is almost linear in some finite frequency range $0 \leq \omega \leq \omega_{lim}$ (Azimi et al. used the value of constant χ_1 as $\sim 10^{-7}$ sec).

For attenuation

$$Q^{-1}(\omega) = Q_o^{-1} \qquad \text{(Futterman)}$$

$$Q^{-1}(\omega) = \frac{Q_o^{-1}}{1 + \chi_1\omega} \qquad \text{(Azimi et al.)}$$

Since χ_1 is very small (10^{-7}), the two above expressions are vertually identical.

Lomnitz (1957) and Liu et al. (1976) instead derived dispersion relations in the time domain. The creep function was given as follows

$$\phi(t) = \begin{cases} q \ln(1 + at) & \text{(Lomnitz)} \\ C\,(1 - e^{-t/\tau}) & \text{(Liu et al.)} \end{cases} \tag{4.6}$$

where q, a, C, are constants and τ is a relaxation time constant. These creep functions will give the following dispersion relations (Appendix III)

$$v(\omega) = \begin{cases} v_\infty\{1 + \frac{1}{\pi Q_o}[\gamma + \ln\frac{\omega}{a}]\} \text{(Lomnitz)} \\ \\ v_\infty\{1 - \frac{1}{\pi Q_o} \ln\left(\frac{s_2}{\omega}\right)\} \quad \text{(Liu et al.)} \end{cases} \tag{4.7}$$

where γ, a, s_2, are constants, v_∞ is the velocity at infinite frequency, and Q is approximately constant at the value Q_o. From (4.5) and (4.7), when Q_o^{-1} is small,

$$v(\omega_1)/v(\omega_2) = 1 + \frac{1}{\pi Q_o} \ln\left(\frac{\omega_1}{\omega_2}\right) \tag{4.8}$$

This is a good approximation for various attenuation laws of constant Q.

4.4b Frequency dependent Q

Jeffreys (1958) modified Lomnitz's law (1957) to the Jeffreys-Lomnitz law which also represents an empirical law (Andrade, 1911). The creep function for the Jeffreys-Lomnitz law is

$$\phi(t) = \frac{q}{\nu}\left[(1 + at)^{\nu} - 1\right] \tag{4.9}$$

where q and a are constants and ν is a number between 0 and 1. As ν goes to zero, (4.9) tends toward the original Lomnitz law. In the time domain, this creep function (4.9) gives the following dispersion relations (Appendix III)

$$\left.\begin{aligned} Q^{-1}(\omega) &= q\, a^{\nu}\, (\nu-1)!\ \omega^{-\nu}\ \sin\frac{\pi\nu}{2} \\ v(\omega) &= v_{\infty}\cdot\left[1+\frac{Q^{-1}}{2}\cot\frac{\pi\nu}{2}\right]^{-1} \end{aligned}\right\} \qquad (4.10)$$

(Jeffreys et al., 1960; Jeffreys, 1965, 1975). For ν, a number of suggestions have been made by Jeffreys ($\frac{1}{4}$, $\frac{1}{5}$) and Andrade ($\frac{1}{3}$). Lamb (1962), Strick (1967) and Azimi et al. (1968) considered the following frequency dependence of the attenuation coefficient $\chi(\omega)$,

$$\chi(\omega) = \chi_{o}\,\omega^{1-\nu} \qquad (4.11)$$

where ν is a number between 0 to 1.,

The frequency domain approach (Appendix II) will give the following dispersion relations,

$$\left.\begin{aligned} Q^{-1}(\omega) &= C\,\omega^{-\nu} \\ v(\omega) &= v_{\infty}\left[1+\chi_{o}v_{\infty}\,\omega^{-\nu}\ \tan\frac{\pi\nu}{2}\right]^{-1} \end{aligned}\right\} \qquad (4.12)$$

Lamb (1962) used $\nu = \frac{1}{2}$ and Strick (1967) and Azimi et al. (1968) rather try to explain nearly constant Q with $\nu = 0.078$ (Strick) and $\nu = 0.1$ (Azimi et al.).

Equations (4.10) and (4.12) give

$$\left.\begin{aligned} Q^{-1}(\omega_1)/Q^{-1}(\omega_2) &= (\omega_1/\omega_2)^{-\nu} \\ \frac{v(\omega_1)}{v(\omega_2)} &= \left[1 + \frac{Q_o^{-1}}{2}\cot\frac{\pi\nu}{2}\left(1 - \frac{\omega_1}{\omega_2}\right)^{-\nu}\right]^{-1} \end{aligned}\right\} \quad (4.13)$$

where Q_o^{-1} is Q^{-1} at $\omega = \omega_2$.

Solomon (1972a)considered a frequency dependent Q model for western United States with the assumption of partial melting. Solomon (1972a)used a couple of relaxation times for the asthenosphere. For such a superposition of a finite number of relaxations, dispersion relations can be written as (Solomon, 1972a)

$$\left.\begin{aligned} Q^{-1}(\omega) &= \sum_i \frac{\Delta\mu_i}{(1 - \Delta\mu_i)^{1/2}} \frac{\omega\tau_i}{1 + (\omega\tau_i)^2} \\ v(\omega) &= v_\infty\left[1 - \sum_i \frac{\Delta\mu_i}{1 + (\omega\tau_i)^2}\right]^{1/2} \end{aligned}\right\} \quad (4.14)$$

where $\Delta\mu_i$ and τ_i are the strength and the characteristic time of the i-th relaxation.

CHAPTER V

Formulation of Simultaneous Inversion of Surface Wave Phase Velocity and Attenuation

5.1 Resume

In this chapter, we describe a formalism for simultaneous inversion of surface wave phase velocity and attenuation. The forward problem of surface waves in an anelastic medium and the subsequent inverse procedure are developed. Basically, a complex formulation is developed first and treated component-wise for computational purposes. Resolution analysis is extended to the complex case using Der and Landisman's (1972) two-variable concept. A comparison between the simultaneous formulation and Anderson and Hart's (1976) treatment is included.

5.2 Forward problem

The problem of surface wave propagation through perfectly elastic multilayered media can be treated by Haskell's matrix formulation. In each layer, with boundary conditions of the free surface and of continuity of stress and displacement at the interfaces, a set of equations hold:

$$\begin{aligned} (\lambda_j + 2\mu_j)\ \nabla_t^2\ \phi_j &= \rho_j \frac{\partial^2 \phi_j}{\partial t^2} \\ \mu_j\ \nabla_t^2\ \psi_j &= \rho_j \frac{\partial^2 \psi_j}{\partial t^2}. \end{aligned} \tag{5.1}$$

$$\mu_j \; \nabla_t^2 \, v_j = \rho_j \frac{\partial^2 v_j}{\partial t^2} \qquad (5.1b)$$

where $$\nabla_t^2 = \frac{\partial}{\partial x^2} + \frac{\partial}{\partial z^2}$$

$$u_j = \frac{\partial \phi_j}{\partial x} + \frac{\partial \psi_j}{\partial z} , \quad w_j = \frac{\partial \phi_j}{\partial z} - \frac{\partial \psi_j}{\partial x}$$

where x (propagation direction) and z are the horizontal and vertical axes, respectively, λ_j, μ_j and ρ_j are Lame parameters and density in the j-th layer, ψ_j, ϕ_j are scalar and vector potentials of the elastic field of the jth layer, and u_j, v_j, w_j are the displacements in the x-, y-, and z-directions. For an anelastic (or viscoelastic) medium, the wave equation (5.1) and the solution have the same form in the frequency domain as for an elastic medium except that the elastic modulus is replaced with a complex quantity according to the '*correspondence* principle' (Christensen, 1971). The Fourier transform of equation (5.1) with complex modulus is

$$E^*(\omega) \; \nabla_t^2 \, \bar{F}_j = \rho_j \; \omega^2 \, \bar{F}_j(x,z,\omega) \qquad (5.2)$$

$$\bar{F}_j(x,z,\omega) = \frac{1}{2\pi} \int_{-\infty}^{\infty} F_j(x,z,t) \, e^{i\omega t} \, dt$$

where $E^*_j(w)$ represents either $\lambda_j + 2\mu_j$ or μ_j and F_j

represents ϕ_j, ψ_j or v_j. $E_j^*(\omega)$ depends on frequency in general. The frequency dependence can be specifically defined by the creep function (or relaxation function) of the medium. As an example, the solution of $F_j = v_j$ (for Love waves) of equation (5.2) with the boundary conditions mentioned above is

$$\bar{v}_j(x,z,\omega) = \bar{F}_j(x,z,\omega) = 2\pi A e^{-bz} e^{ikx} \delta(\omega - \omega_o)$$

where A is a constant, δ is a Dirac delta function, and where

$$k = \omega/c$$

$$b = k\sqrt{1 - c^2/\beta^2}$$

$$\beta^2 = \mu^*/\rho$$

and the phase velocity c is found from the solution to equation (5.1). The inverse transform of $\bar{v}_j$ is

$$v_j(x,z,t) = \underline{A}\, e^{-bz} e^{ik_o(x-ct)}$$

where $k_o = \omega_o/c$

$$b_o = k_o \sqrt{1 - (c/\beta)^2}_{\omega_o}$$

$$c_o = (c_1 + ic_2)_{\omega_o}$$

$$\beta_o = (\beta_1 + i\beta_2)_{\omega_o}$$

Therefore, Haskell's (1953) matrix formulation may be extended to lossy media by implementing complex velocities and a dispersion relation between the real and imaginary parts of the intrinsic velocity. Similarly, for Rayleigh waves, the above extension of Haskell's matrix formulation can be achieved.

5.3 Inverse problem

The phase velocity and attenuation of surface waves on a multilayered, anelastic earth are obtained from the roots of the complex dispersion-attenuation functions (Schwab and Knopoff, 1971) f_L (Love) and f_R (Rayleigh):

$$f_L(T_i, c_i^L, \beta_j, \rho_j, d_j) = 0$$

$$f_R(T_i, c_i^R, \beta_j, \alpha_j, \rho_j, d_j) = 0 \qquad (5.3)$$

$$i = 1, 2, \ldots, m; \quad j = 1, 2, \ldots . n$$

where T_i, c_i^L, and c_i^R are ith period and Love and Rayleigh wave phase velocities and α_j, β_j and d_j are, respectively, the P- and S-wave velocities, density and thickness for the jth layer. The velocities c^L, c^R, α and β are complex quantities.

The inverse problem can be stated as the problem of finding an anelastic (complex) earth model from given observational data pairs, phase velocities and phase attenuations. We start with an initial anelastic earth model and a set of observed dispersion-attenuation data pairs. The phase velocity and attenuation for the initial complex model are then calculated theoretically by Haskell's (1953) method at the period of each observed data pair. The generalized Haskell formulation is for a flat earth, whereas the observations are for a spherical earth. The flat-to-spherical transformation of Biswas and Knopoff (1970), as amended by Schwab and Knopoff (1971) to include anelasticity, is used for sphericity corrections for Love waves. For Rayleigh waves, a similar transform is given in Schwab and Knopoff (1971). However, it is difficult to use in a computer code. In this study, Bolt and Dorman's (1961) empirical correction has been used for sperioity and gravity corrections. Although North and Dziewonski (1976) improved such a correction, a minimal change is expected at periods less than 100 sec.

From the dispersion-attenuation calculations we can also obtain the partial derivatives of complex phase velocity c with respect to each complex parameter p of the layered earth model. Then the linear perturbation equation can be written relating the desired parameter corrections to the differences between the corresponding theoretical and observed phase velocity values:

$$\Delta c_i^{L,R} = \frac{\partial c_i^{L,R}}{\partial p_j} \Delta p_j \qquad (5.4)$$

where the repeated indices imply summation for n layers. A similar equation for each period can be formed.

Because the physical significance of a complex quantity is more easily understood by decomposition into real and imaginary parts, we write equation (5.4) as two real equations, rather than one complex equation.

$$\begin{pmatrix} \Delta c_1^{L,R} \\ \Delta c_2^{L,R} \end{pmatrix} = \begin{pmatrix} \frac{\partial c_1^{L,R}}{\partial p_1} & \frac{\partial c_1^{L,R}}{\partial p_2} \\ \frac{\partial c_2^{L,R}}{\partial p_1} & \frac{\partial c_2^{L,R}}{\partial p_2} \end{pmatrix} \begin{pmatrix} \Delta p_1 \\ \Delta p_2 \end{pmatrix} \qquad (5.5)$$

where $c_1^{L,R}$ and $c_2^{L,R}$ are the real and imaginary parts of $c^{L,R}$ and p_1 and p_2 are the real and imaginary parts of p.

It is assumed that all the dissipation is due to imperfect elasticity. By requiring the density to be real we ignore the possibility of losses due to imperfect inertia

(Anderson and Archambeau, 1964). For Love waves we can write equation (5.5) in more familiar terms:

$$\begin{pmatrix} \Delta c_1^L \\ \\ \Delta c_2^L \end{pmatrix}_i = \begin{pmatrix} \dfrac{\partial c_1^L}{\partial \beta_1} & \dfrac{\partial c_1^L}{\partial \beta_2} \\ \dfrac{\partial c_2^L}{\partial \beta_1} & \dfrac{\partial c_2^L}{\partial \beta_2} \end{pmatrix}_{ij} \begin{pmatrix} \Delta\beta_1 \\ \\ \Delta\beta_2 \end{pmatrix}_j \qquad (5.6)$$

where β_1 and β_2 are the real and imaginary parts of the shear wave velocity in the jth layer. For Rayleigh waves, eq.(5.5) can be written as,

$$\begin{pmatrix} \Delta c_1^R \\ \\ \Delta c_2^R \end{pmatrix}_i = \begin{pmatrix} \dfrac{\partial c_1^R}{\partial \beta_1} & \dfrac{\partial c_1^R}{\partial \beta_2} & \dfrac{\partial c_1^R}{\partial \alpha_1} & \dfrac{\partial c_1^R}{\partial \alpha_2} & \dfrac{\partial c_1^R}{\partial \rho} \\ \\ \dfrac{\partial c_2^R}{\partial \beta_1} & \dfrac{\partial c_2^R}{\partial \beta_2} & \dfrac{\partial c_2^R}{\partial \alpha_1} & \dfrac{\partial c_2^R}{\partial \alpha_2} & \dfrac{\partial c_2^R}{\partial \rho} \end{pmatrix}_{ij} \begin{pmatrix} \Delta\beta_1 \\ \Delta\beta_2 \\ \Delta\alpha_1 \\ \Delta\alpha_2 \\ \Delta\rho \end{pmatrix}_j \qquad (5.7)$$

Since one or both of $\Delta\beta_1$ and $\Delta\beta_2$ depend upon frequency (as do $\Delta\alpha_1$ and $\Delta\alpha_2$ for Rayleigh waves), the right hand sides of eq. (5.6) and (5.7) should be standardized at a single reference frequency for inversion (see below). Generalizing equation (5.4) to m complex observations and using matrix notation gives:

$$\underline{\underline{A}}^{L,R}\,\underline{x}^{L,R} = \underline{y}^{L,R} \qquad (5.8)$$

where $\underline{y}$ is an m x 1 matrix of differences between observed and predicted phase velocities and attenuations, $\underline{\underline{A}}$ is an mx n matrix of partial derivatives, and $\underline{x}$ is an n x 1 matrix of perturbations to the starting anelastic earth model. The elements of $\underline{y}^L$, $\underline{\underline{A}}^L$ and $\underline{x}^L$ are real 2 x 1, 2 x 2 and 2 x 1 matrices, respectively and the elements of $\underline{y}^R$, $\underline{\underline{A}}^R$ and $\underline{x}^R$ are real 2 x 1, 2 x 5 and 5 x 1 matrices, respectively.

The partial derivatives of phase velocity with respect to shear velocity are obtained by implicit function theory (Schwab and Knopoff, 1972):

$$\frac{\partial c^{L,R}}{\partial \beta} = -\frac{\partial f_{L,R}}{\partial \beta} \Big/ \frac{\partial f_{L,R}}{\partial c^{L,R}}$$

$$\frac{\partial c^{R}}{\partial \alpha} = -\frac{\partial f_{R}}{\partial \alpha} \Big/ \frac{\partial f_{R}}{\partial c^{R}} \qquad (5.9)$$

where

$$f_L = (s, -i)a_{n-1}a_{n-2} \cdots \quad a_1 \begin{pmatrix} 1 \\ 0 \end{pmatrix}$$

$$f_R = T^{(o)}\overline{\overline{F}}^{(1)}F^{(2)} \quad \cdots \quad \left[\begin{array}{ll} F^{(n-2)}\overline{\overline{F}}^{(n-1)}T^{(n)} & \text{even } n \\ \overline{\overline{F}}^{(n-2)}F^{(n-1)}\overline{\overline{T}}^{(n)} & \text{odd } n \end{array} \right.$$

are the dispersion-attenuation functions for Love and Rayleigh waves and where

$$a_j = \begin{pmatrix} \cos Q_j & i\,\mu_j^{-1} r_{\beta_j}^{-1} \sin Q_j \\ i\,\mu_j r_{\beta_j} \sin Q_j & \cos Q_j \end{pmatrix}, \quad j=1,2, \ldots, n-1$$

$$s = - \mu_n \sqrt{1 - c^2/\beta_n^2}$$

$$T^{(o)} = [- \zeta_1(\zeta_1-1),\ 0,\ (\zeta_1-1)^2,\ \zeta_1^2,\ q/c^2\rho_1,\ \zeta_1(\zeta_1-1)]$$

$$T^{(n)} = \begin{pmatrix} 0 \\ -r_{\alpha_n} \\ r_{\alpha_n} r_{\beta_n} \\ 1 \\ -r_{\beta_n} \\ 0 \end{pmatrix} , \quad \bar{T}^{(n)} = \begin{pmatrix} 0 \\ r_{\beta_n} \\ 1 \\ r_{\alpha_n} r_{\beta_n} \\ r_{\alpha_n} \\ 0 \end{pmatrix} \epsilon$$

$$F^{(j)} = \begin{pmatrix} F_{1212}^{(j)} & F_{1213}^{(j)} & F_{1214}^{(j)} & F_{1223}^{(j)} & F_{1224}^{(j)} & F_{1234}^{(j)} \\ F_{1312} & F_{1313} & F_{1314} & F_{1323} & F_{1324} & F_{1334} \\ F_{1412} & F_{1413} & F_{1414} & F_{1423} & F_{1424} & F_{1434} \\ F_{2312} & F_{2313} & F_{2314} & F_{2323} & F_{2324} & F_{2334} \\ F_{2412} & F_{2413} & F_{2414} & F_{2423} & F_{2424} & F_{2434} \\ F_{3412} & F_{3413} & F_{3414} & F_{3423} & F_{3424} & F_{3434} \end{pmatrix}$$

$$\bar{F}^{(j)} = \begin{pmatrix} F_{3434}^{(j)} & -F_{3424}^{(j)} & F_{3423}^{(j)} & F_{3414}^{(j)} & -F_{3413}^{(j)} & F_{3412}^{(j)} \\ -F_{2434} & F_{2424} & -F_{2423} & -F_{2414} & F_{2413} & -F_{2412} \\ F_{2334} & -F_{2324} & F_{2323} & F_{2314} & -F_{2313} & F_{2312} \\ F_{1434} & -F_{1424} & F_{1423} & F_{1414} & -F_{1413} & F_{1412} \\ -F_{1334} & F_{1324} & -F_{1323} & -F_{1314} & F_{1313} & -F_{1312} \\ F_{1234} & -F_{1224} & F_{1223} & F_{1214} & -F_{1213} & F_{1212} \end{pmatrix}$$

TABLE 5.1

EXPRESSIONS FOR THE QUANTITIES $F_{ijkl}^{(m)}$

ij \ kl	12	13	14	23	24	34
12	$-\epsilon_8^{(m)}$	0	$\epsilon_{13}^{(m)}$	$\epsilon_6^{(m)}$	0	$\epsilon_{10}^{(m)}$
13	$-i(\epsilon_{11}\eta_9 + \epsilon_7\eta_{10})$	$\epsilon_{15}\eta_{14}$	$i(\epsilon_{14}\eta_9 + \epsilon_{12}\eta_{10})$	$i(\epsilon_9\eta_9 + \epsilon_5\eta_{10})$	$-\epsilon_{15}\eta_7$	$i(\epsilon_{11}\eta_9 + \epsilon_7\eta_{10})$
14	$\epsilon_{11}\eta_7 - \epsilon_7\eta_{12}$	$i(\epsilon_{15}\eta_{10})$	$-\epsilon_{14}\eta_7 + \epsilon_{12}\eta_{12}$	$-\epsilon_9\eta_7 + \epsilon_5\eta_{12}$	$i(\epsilon_{15}\eta_8)$	$-\epsilon_{11}\eta_7 + \epsilon_7\eta_{12}$
23	$-\epsilon_{11}\eta_{15} + \epsilon_7\eta_7$	$i(\epsilon_{15}\eta_9)$	$\epsilon_{14}\eta_{15} - \epsilon_{12}\eta_7$	$\epsilon_9\eta_{15} - \epsilon_5\eta_7$	$i(\epsilon_{15}\eta_{11})$	$\epsilon_{11}\eta_{15} - \epsilon_7\eta_7$
24	$-i(\epsilon_{11}\eta_{11} + \epsilon_7\eta_8)$	$-\epsilon_{15}\eta_7$	$i(\epsilon_{14}\eta_{11} + \epsilon_{12}\eta_8)$	$i(\epsilon_9\eta_{11} + \epsilon_5\eta_8)$	$\epsilon_{15}\eta_{13}$	$i(\epsilon_{11}\eta_{11} + \epsilon_7\eta_8)$
34	ϵ_{10}	0	$-\epsilon_{13}$	$-\epsilon_6$	0	$-\epsilon_6$

$\epsilon_0^{(m)} = \rho_m + 1/\rho_m$
$\epsilon_1 = \zeta_m - \epsilon_0\zeta_m + 1$
$\epsilon_2 = \epsilon_1 - 1$
$\epsilon_3 = \epsilon_1 + \epsilon_0$
$\epsilon_4 = \epsilon_2 + \epsilon_0$
$\epsilon_5 = \epsilon_1^2$
$\epsilon_6 = \epsilon_1\epsilon_2$
$\epsilon_7 = \epsilon_1\epsilon_3$

$\epsilon_1^{(m)} = \epsilon_1^{(m)}\epsilon_4^{(m)}$
$\epsilon_9 = \epsilon_2^2$
$\epsilon_{10} = \epsilon_2\epsilon_3$
$\epsilon_{11} = \epsilon_2\epsilon_4$
$\epsilon_{12} = \epsilon_3^2$
$\epsilon_{13} = \epsilon_3\epsilon_4$
$\epsilon_{14} = \epsilon_4^2$
$\epsilon_{15} = -\epsilon_0$
$\epsilon_{16} = \epsilon_8 + \epsilon_{10}$

$\eta_1^{(m)} = \cos P_m$
$\eta_2 = \cos Q_m$
$\eta_3 = r_m \sin P_m$
$\eta_4 = \sin P_m / r_m$
$\eta_5 = r_{\alpha m} \sin Q_m$
$\eta_6 = \sin Q_m / r_{\beta m}$
$\eta_7 = \eta_1\eta_2$
$\eta_8 = \eta_1\eta_5$

$\eta_9^{(m)} = \eta_1^{(m)}\eta_6^{(m)}$
$\eta_{10} = \eta_2\eta_3$
$\eta_{11} = \eta_2\eta_4$
$\eta_{12} = \eta_3\eta_5$
$\eta_{13} = \eta_4\eta_5$
$\eta_{14} = \eta_3\eta_6$
$\eta_{15} = \eta_4\eta_6$

where

$$r_{\beta_j} = \begin{cases} \sqrt{(c^{L,R}/\beta_j)^2 - 1} & \text{if Re } c^{L,R} > \text{Re } \beta_j \\ -i\sqrt{1 - (c^{L,R}/\beta_j)^2} & \text{if Re } c^{L,R} < \text{Re } \beta_j \end{cases}$$

$$r_{\alpha_j} = \begin{cases} \sqrt{(c^R/\alpha_j)^2 - 1} & \text{if Re } c^R > \text{Re } \alpha_j \\ -i\sqrt{1 - (c^R/\alpha_j)^2} & \text{if Re } c^R < \text{Re } \alpha_j \end{cases}$$

$$Q_j = \omega\, r_{\beta_j}\, d_j / c^{L,R}$$

$$P_j = \omega\, r_{\alpha_j}\, d_j / c^R$$

$$q = \begin{cases} 0 & \text{for continental paths} \\ i\,\rho_o c^2 \tan\,[P_o/r_{\alpha_o}] & \text{for oceanic paths} \end{cases}$$

$$\epsilon = (-1)^{n-1}\, \rho_1^2\, c^2 / \zeta_n\, r_{\alpha_n} r_{\beta_n}\, \rho_n^2\, \alpha_n^2$$

$$\zeta_j = 2\,(\beta_j/c)^2$$

and where the square root operation is performed so as to make Re $r_{\beta_j} > 0$, Re $r_{\alpha_j} > o$ for all j. The partial derivatives required to evaluate equation (5.9) are given for Love waves, by

$$\frac{\partial f_L}{\partial c} = \left[\frac{\partial s}{\partial c}, 0\right] a_{n-1} a_{n-2} \cdots a_1 \binom{1}{0}$$

$$+ [s, -i] \sum_j a_{n-1} a_{n-2} \cdots \frac{\partial a_j}{\partial c} \cdots a_1 \begin{pmatrix} 1 \\ 0 \end{pmatrix}$$

$$\frac{\partial f_L}{\partial \beta_j} = [s, -i]\, a_{n-1} a_{n-2} \cdots \frac{\partial a_j}{\partial \beta_j} \cdots a_1 \begin{pmatrix} 1 \\ 0 \end{pmatrix}$$

$$\frac{\partial f_L}{\partial \beta_n} = \left[\frac{\partial s}{\partial \beta_n}, 0\right] a_{n-1} a_{n-2} \cdots a_1 \begin{pmatrix} 1 \\ 0 \end{pmatrix}$$

For Rayleigh waves,

define

$$\bar{\Delta}^{(n-1)} = \bar{F}^{(1)} F^{(2)} \bar{F}^{(3)} \ldots F^{(n-2)} \bar{F}^{(n-1)}$$

$$\Delta^{(n-1)} = \bar{F}^{(1)} F^{(2)} \bar{F}^{(3)} \ldots \bar{F}^{(n-2)} F^{(n-1)}$$

then

$$f_R = \begin{cases} T^{(o)}\, \bar{\Delta}^{(n-1)} T^{(n)} & \text{for even } n \\ T^{(o)}\, \Delta^{(n-1)} \bar{T}^{(n)} & \text{for odd } n \end{cases}$$

For even n,

$$\frac{\partial f_R}{\partial c^R} = \frac{\partial T^{(0)}}{\partial c^R} \bar{\Delta}^{(n-1)} T^{(n)} + T^{(0)} \frac{\partial \bar{\Delta}^{(n-1)}}{\partial c^R} T^{(n)} + T^{(0)} \bar{\Delta}^{(n-1)} \frac{\partial T^{(n)}}{\partial c^R} \quad (5.10b)$$

where

$$\frac{\partial \bar{\Delta}^{(n-1)}}{\partial c^R} = \sum_{j=1}^{n-1} F^{(1)} \bar{\bar{F}}^{(2)} \; - - - \; \frac{\partial F^{(j)}}{\partial c^R} \; - - \; \bar{\bar{F}}^{(n-1)} T^{(n)}$$

$$\frac{\partial f_R}{\partial p_j} = T^{(0)} \bar{\bar{F}}^{(1)} F^{(2)} \; - - - \; \frac{\partial F^{(j)}}{\partial p_j} \; - - \; \bar{F}^{(n-1)} T^{(n)}$$

$$\frac{\partial f_R}{\partial p_n} = T^{(0)} \bar{\bar{F}}^{(1)} F^{(2)} \; - - - \; \bar{\bar{F}}^{(n-1)} \frac{\partial T^{(n)}}{\partial p_n}$$

$$\frac{\partial f_R}{\partial p_1} = T^{(0)} \bar{\bar{F}}^{(1)} F^{(2)} \; - - - \; \bar{\bar{F}}^{(n-1)} \frac{\partial T^{(n)}}{\partial p_1}$$

where p can be either α or β .

For odd n, similar formulae hold. From equation (5.11), only two of the elements of the 2 x 2 real matrix in equation (5.6) are independent for Love waves and only six of the elements of the 2 x 5 real matrix in equation (5.7) are independent for Rayleigh waves. Thus the matrices can be completely specified from the real and imaginary parts of $\partial c^{L,R}/\partial \beta$ and $\partial c^R/\partial \alpha$.

Since $c^L = c^L(\beta)$ and $c^R = c^R(\alpha, \beta)$ are analytic, single-valued functions their first derivative are unique and independent of the direction along which the derivative is taken), the Cauchy-Riemann condition is satisfied for

$$c^{L,R} = c_1^{L,R} + i c_2^{L,R} , \quad \beta = \beta_1 + i\beta_2 , \quad \alpha = \alpha_1 + i\alpha_2$$

(Morse and Feshbach, 1953, p. 357), and

$$\left.\begin{array}{ll} \dfrac{\partial c_1^{L,R}}{\partial \beta_1} = \dfrac{\partial c_2^{L,R}}{\partial \beta_2} , & \dfrac{\partial c_1^{L,R}}{\partial \beta_2} = - \dfrac{\partial c_2^{L,R}}{\partial \beta_1} \\ \dfrac{\partial c_1^{R}}{\partial \alpha_1} = \dfrac{\partial c_2^{R}}{\partial \alpha_2} , & \dfrac{\partial c_1^{R}}{\partial \alpha_2} = - \dfrac{\partial c_2^{R}}{\partial \alpha_1} \end{array}\right\} \quad (5.11)$$

5.4 Resolution

To assess a criterion for stability of the inversion process, we should examine the averaging kernel or resolving length at various depths. In Lee and Solomon (1975), we determined the resolving length for surface wave attenuation data with errors using the idea of Der et al. (1970) of minimizing simultaneously both the variance of a physical parameter of interest in a layer and the deviation from a δ-function of the averaging kernel for the same layer. Der et al. and others have shown that the resolution of layer parameters can be improved by combining two independent observations, such as Love and Rayleigh wave dispersion or fundamental mode and first higher mode Love waves. Der and Landisman (1972) extended their theory to the case of two variables, namely shear velocity and density in the crust and mantle. In the extended theory, separation of the two unknown variables, depth resolution, and accuracy of the parameter estimates are three competing objectives. A similar theoretical discussion was given by Backus (1970) in an abstract form. Dziewonski (1970) noted that the strong correlation between the partial derivatives of free oscillation periods with respect to density and shear velocity makes the inversion process highly non-unique. Derr (1969) showed that the addition of free oscillation overtones of low radial order to the set of fundamental mode observations does not greatly improve the depth resolution of shear velocity but facilitates the separation of shear velocity from density. Similar conclusions were also given by Der and Landisman (1972).

The simultaneous inversion of phase velocity and attenuation, however, differs in two important respects from the above cases:

1) The relative errors associated with phase velocity and attenuation data are generally very different, much larger for Q^{-1} observations than for phase velocity measurements.

2) The two variables β and Q_{β}^{-1} are expected to be well separated by the Der and Landisman (1972) treatment because

the real and imaginary parts of the data are more closely related to the two unknown variables (real and imaginary parts, respectively, of an earth model) than is the case for the two-variable problems mentioned above.

We follow the treatment of Der and Landisman (1972) for parameter resolution for a two-parameter earth model. The linear combination of data $y_i^{L,R}$ used as the estimator of a desired parameter $x_k^{L,R}$ in layer k is

$$x_k^{L,R} = \sum_i r_{ik} y_i^{L,R} = \sum_i^N \sum_j^M r_{ik} S_{ij}^{L,R} x_j^{L,R} \qquad (5.12)$$

where r_{ik} is a coefficient to be determined, N is the number of data, M is the number of layers in the model, and where $S_{ij} = \dfrac{\partial y_i^{L,R}}{\partial x_j^{L,R}}$, normalized by the layer thickness in km.

The three quantities to be minimized are (Der and Landisman, 1972)

1) the variance of the desired variable $x_k^{L,R}$
2) S_1, the resolution for $x_k^{L,R}$
3) S_2, the dependence on the undesired variable $\bar{x}_k^{L,R}$ for the same layer.

If we assume that the observational errors are independent

$$\text{var } x_k^{L,R} = \sum_i^N r_{ik}^2 \text{ var } y_i^{L,R} \qquad (5.13)$$

$$(s_1^{L,R})^2 = \sum_{j=k}^M d_j (E_{kj}^{L,R})^2$$

$$(s_2^{L,R})^2 = \sum_j^M d_j (F_{kj}^{L,R})^2$$

where d_j is the layer thickness and

$$E_{kj}^{L,R} = \sum_{i}^{N} r_{ik} S_{ij}^{L,R}$$

$$F_{kj}^{L,R} = \sum_{i}^{N} r_{ik} T_{ij}^{L,R} , \quad T_{ij}^{L,R} = \frac{\partial y_i^{L,R}}{\partial \bar{x}_j} \qquad (5.15)$$

These three objectives can be accomplished by minimizing the function

$$\varepsilon_k^{L,R} = \sin\xi \text{ var } x_k^{L,R} + \cos\xi\sin\eta (s_1^{L,R})^2 + \cos\xi\cos\eta (s_2^{L,R})^2 + 2\,\theta (E_{kk}^{L,R} - 1) \qquad (5.16)$$

where θ is a Lagrange multiplier. The parameters ξ and η $(0 \leq \xi, \eta \leq \frac{\pi}{2})$ are adjusted so as to balance the three desired minimizations. As ξ is increased, the approximation to the delta function becomes worse, the variances of $x_k^{L,R}$ become smaller and separation between $x_k^{L,R}$ and $\bar{x}_k^{L,R}$ improves.

5.5 Inversion Procedure

For the dispersion-attenuation relations discussed in section 4.4, Q_β^{-1}, Q_α^{-1}, β and α are related to β_1, β_2, α_1 and α_2 such that

$$Q_\beta^{-1} = 2\,\beta_2 / \beta_1$$

$$Q_\alpha^{-1} = 2\,\alpha_2 / \alpha_1 \qquad (5.17a)$$

$$\beta = (\beta_1^2 + \beta_2^2) / \beta_1$$

$$\alpha = (\alpha_1^2 + \alpha_2^2) / \alpha_1 \qquad (5.17b)$$

For each of these relations, β_1, α_1 or all $\beta_1, \beta_2, \alpha_1$ and α_2 depend on frequency

$$\beta_{1j}(\omega_i) = \bar{\beta}_{1j} + g(\omega_i)\bar{\beta}_{2j}$$

$$\beta_{2j}(\omega_i) = \bar{\beta}_{2j}\, h(\omega_i)$$

$$\alpha_{1j}(\omega_i) = \bar{\alpha}_{1j} + g(\omega_i)\bar{\alpha}_{2j} \qquad (5.18)$$

$$\alpha_{2j}(\omega_i) = \bar{\alpha}_{2j}\, h(\omega_i)$$

where g and h are specified functions of frequency and $\bar{\beta}_{1j}$, $\bar{\beta}_{2j}$, $\bar{\alpha}_{1j}$ and $\bar{\alpha}_{2j}$ are values of β_{1j}, β_{2j}, α_{1j} and α_{2j} at a reference frequency respectively. In general, the inverse problem to equation (5.8) is conducted at the reference frequency, the partials in (5.4) are with respect to β_1, β_2, α_1 and α_2, and the earth structure at any other frequency follows from (5.18) (see Appendix IV).

CHAPTER VI

Applications

We now apply the formalism for the forward and inverse dispersion-attenuation problem that we discussed in the previous chapters to (1) Love waves in western North America, (2) Love and Rayleigh waves in western North America, (3) Love and Rayleigh waves in east-central North America, (4) Rayleigh waves in the central Pacific. We tried to test various dispersion-attenuation relations in each region. In western North America (1), the dispersion-attenuation relations for Q independent of frequency ($\nu=0$), Q varying as powers of 1/2, 1/3 and 1/5 of frequency ($\nu = 1/2, 1/3, 1/5$, where ν is the power of Q^{-1} of frequency dependence) and Q for a superposition of shear relaxations were assumed in various inversion trials. In western North America (2), the dispersion-attenuation relations for $\nu = 0$, 1/2 and 1/5 were tested. In east-central North America (3), $\nu = 0$, 1/2 were tested. In the central Pacific (4), $\nu = 0$ was applied in the inversion process.

6.1 Data

a. North America

The data sets for $Q^{-1}_{L,R}$ of North America are described and tabulated in Lee and Solomon (1975) and in Chapter II; the accompanying phase velocity measurements are given in Solomon (1971).

Since this data set, derived from records of events in the years 1964-1968, includes no Rayleigh wave data in western North America at periods longer than 40 seconds, we made an effort to search for events in the years 1969-1975 for which energy at periods longer than 40 seconds was visible on the vertical component. A requirement of the search is that events must be nearly on the great circle connecting the two stations LON and TUC. 'Nearly' great circle path is taken to include a flexibility of 10° in azimuth from precise great circles.

We picked and digitized five events (Table 6.1) whose magnitudes ranged between 5.8 and 6.5 and which are located in China, Alaska and Indochina at distances between 40 and 130 degrees from the stations. After we went through the standard procedure, described in Solomon (1971), we realized that we could not obtain any new information, because of several reasons: (1) Suitably long period (Rayleigh waves) are poorly generated unless an earthquake has a magnitude of near 6 or greater. (2) The path from an event to the stations should not cross geologically complex regions. (3) If the event is too large in magnitude or too close to one or both stations, the records are usually complicated or unreadable. (4) In our case, the great circles connecting each of the five events to the stations LON and TUC pass through a part of the Asian continent and Alaska, where the geology is not simple. Further, three of the five events are too far

Table 6.1. Events examined for long period Rayleigh waves, LON to TUC

Events	Depth km	m_b	Distance,		$\Delta\phi$	Date	Origin time	Lat.	Long.	Region
			LON	TUC						
A	7	6.0	24.1	42.9	3.3	29 Oct '68	22:16:15.6	65.4°N	152.8°W	Alaska
B	59	6.5	100.1	116.9	0.9	29 Jul '70	10:16:19.3	26.02N	95.4°E	Burma
C	33	5.8	50.2	66.9	0.6	18 May '71	22:44:43.8	63.95°N	146.11°E	Eastern Siberia
D	33	5.9	118.9	135.6	5.1	7 Apr '73	3:0:58.8	6.97°N	91.38°E	Nicobar Islands
E	11	6.2	94.6	111.3	5.4	10 May '74	19:25:15.0	28.24°N	104.12°E	China

Source of data: U.S. Geological Survey

$\Delta\phi$ = distance in back azimuth at TUC between LON to TUC path and actual path away from the stations (more than 100° away). As a consequence, we were not able to add to our knowledge of long period Rayleigh wave propagation in western North America.

b. Central Pacific Ocean

The data set for Q_R^{-1} for the central Pacific ocean has been measured by Mitchell et al. (1976). They determined Q_R^{-1} from the records of three earthquakes at WWSSN stations distributed around the west coast of America, the Far East and the Pacific. These measurements represent a weighted average of the entire Pacific ocean region. Such an average model does not strictly represent the structure in any particular location because of the lateral variation of oceanic structure according to the age of the sea floor (Forsyth, 1975).

We particularly have chosen one event among the three for which the data sample paths predominantly across the relatively old (80-90 m.y. old average) central Pacific. The location of this event (April 26, 1973, $20^h26^m30.8^s$, latitude 19.9°N, longitude 155.13°W, $m_b = 6.0$), stations and paths are shown in Figure 6.1. The corresponding phase velocities, also a weighted average of 'pure path' velocities, are calculated using the magnetic anomaly map (Pitman et al. 1974) of the Pacific and the results of Forsyth (1975, 1977) on the variation of phase velocity with increasing age of the sea floor. We divided the Pacific into eleven age

Fig. 6.1. Pacific area map showing paths between the April 26, 1973 earthquake and stations (ALQ, ANP, ARE, BAG, BOG, CHG, COL, COR, DAV, HKC, JCT, LPB, NIL, RAR, RIV, SNG, TAU, TUC, WEL) used in the Q^{-1} measurements of Mitchell *et al.* (1976).

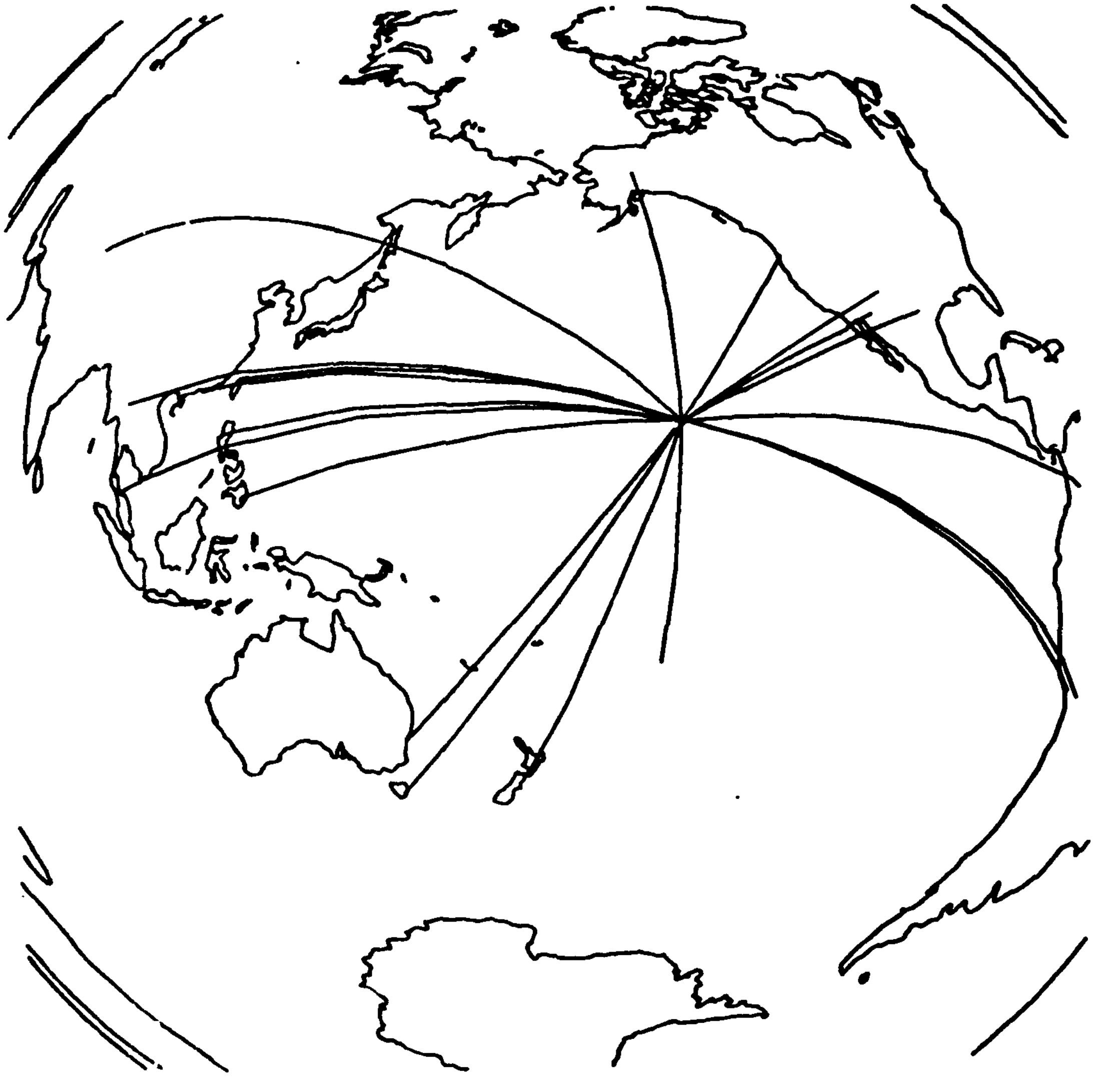

age regions (0-5 m.y., 5-10 m.y., 10-20 m.y., 20-38 m.y., 38-53 m.y., 53-65 m.y., 65-83 m.y., 83-100 m.y., 100-135 m.y., 135-190 m.y., greater than 190 m.y.) and continental paths. Each great circle path from event to station is plotted on the map of age zone boundaries, from which we can calculate the total path length in each age group for the sum of all the paths (see Table 6.2). Then we can determine the weighted average of phase velocity and group velocity at each period using the results of Forsyth (1975, 1977) and the weights shown in the Table 6.2. The resultant weighted phase velocity and group velocity curves for the eastern Pacific are shown in Figures 6.2 and 6.3.

The magnetic anomaly map on the basis of which seafloor ages were estimated does not include the marginal basins of the western Pacific, across which pass many of the surface wave paths used here. Additional age information for these basins have been taken from Weissel (1977) for the Lau Basin, from Weissel _et al._ (1977) for the Coral Sea and New Hebrides Basin, from Watts and Weissel (1977) for the south Fiji Basin and from Sclater _et al._ (1976) for the Philippine Sea. Details of the adopted basin ages are listed in Table 6.3.

Table 6.2 Great circle paths in each age group for the 26 April 1973 Pacific event

Path	Distance (°)	Percentage
0-5 m.y. ocean	19.987	1.535
5-10 "	33.963	2.608
10-20 "	98.864	7.593
20-38 "	26.058	2.001
38-53 "	205.869	15.812
53-65 "	137.222	10.539
65-83 "	22.999	1.766
83-100 "	303.729	23.327
100-135 "	179.768	13.807
135-190 "	150.167	11.533
GT. 190	5.859	0.45
North American* continent	32.569	8.273
South American continent	9.827	0.755
Total	1302.042	100

*Continental paths in southeast Asia are included in this group.

Fig. 6.2. Envelopes of Rayleigh wave phase velocity predicted by model S21P for the central Pacific. Circles are data points, which are calculated as a weighted average of 'pure path' velocities (Forsyth, 1975, 1977) using the magnetic anomaly map of Pitman et al. (1974).

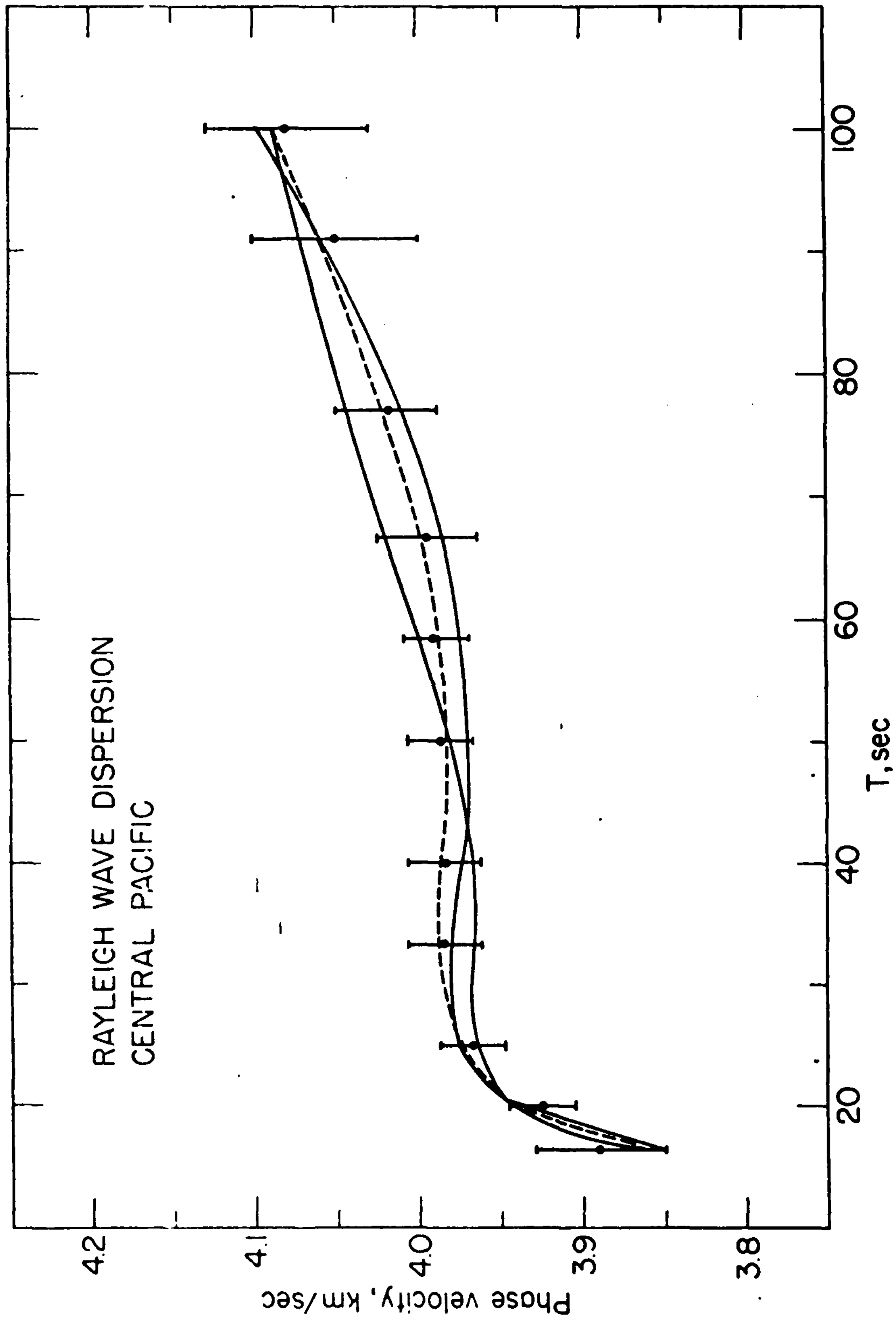
RAYLEIGH WAVE DISPERSION
CENTRAL PACIFIC
Phase velocity, km/sec
4.2
4.1
4.0
3.9
3.8
T, sec
20
40
60
80
100

Fig. 6.3. Rayleigh wave group velocity for the central Pacific. Data points are calculated as a weighted average of 'pure path' group velocities (Forsyth, 1975, 1977) using the magnetic anomaly map of Pitman *et al.* (1974).

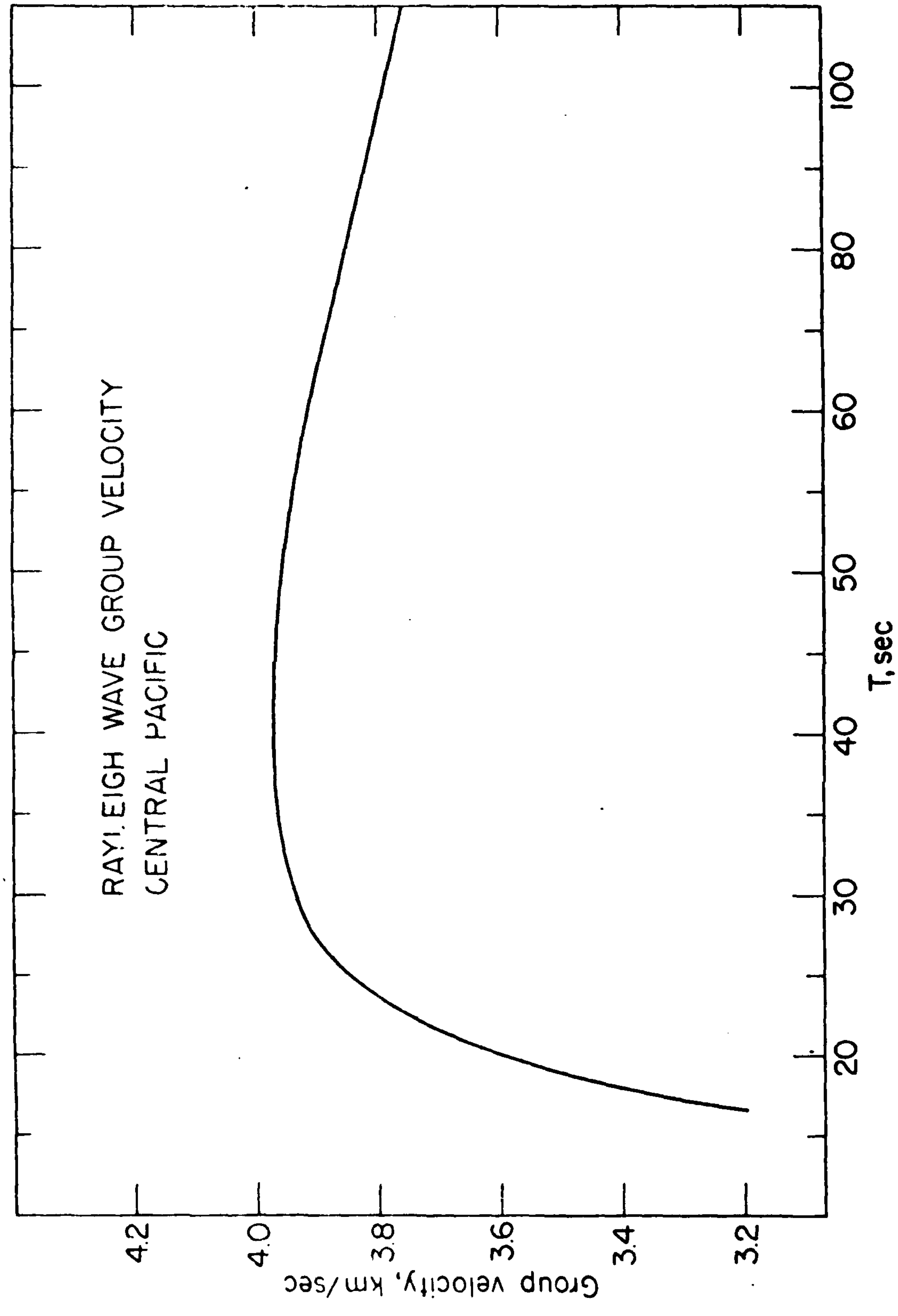
RAYLEIGH WAVE GROUP VELOCITY
CENTRAL PACIFIC
Group velocity, km/sec
4.2
4.0
3.8
3.6
3.4
3.2
T, sec
20
30
40
50
60
80
100

Table 6.3. Ages of Marginal Basins in the Pacific

Area	Age Range m.y.	Magnetic Anomaly
Central Basin Fault, Philippine Sea[1]	49-43	17
Southwest Philippine Basin[1]	49-53	21
Northeast Philippine Basin[1]	49-53	21
Lau Basin[2]	0-3.5	1-2
Coral Sea Basin[3]	60-65	24-26
New Hebrides Basin[3]	45-52	18-21
South Fiji Basin[4]	28-35	7a

---

1. Sclater *et al.*, 1976.
2. Weissel, 1977.
3. Weissel *et al.*, 1977.
4. Watts and Weissel, 1977.

6.2 Inversion: a. Love waves in western North America

The starting model for calculation of partial derivatives is shown in Figure 6.4. The model was chosen so that the real part (β, ρ) satisfies the real (elastic) inverse problem for the dispersion data in Figure 6.5 and the imaginary part (Q^{-1}) satisfies the imaginary (Q^{-1} only) inverse problem for the attenuation data in Figure 6.6. The velocity-density model shares features with models of Alexander (1963), Anderson and Julian (1969), Kovach and Robinson (1969) and Biswas and Knopoff (1974). The density model in Figure 6.4 remains fixed and real in the inversion process since phase velocity is generally more sensitive to changes in β than in ρ and since inertial losses are neglected. The starting Q^{-1} model for the constant-Q inversion is from Lee and Solomon (1975) and from Chapter II. The starting Q^{-1} models for inversion using a power law dependence of Q on frequency are given in Table 6.4. The starting Q^{-1} model for inversion using relaxation mechanisms after Solomon (1972a), is also shown in Table 6.4.

For purposes of calculating partials, the equivalent flat model to that in Figure 6.4 was divided into 28 homogeneous layers and an underlying half-space.

The diagonal elements ($\partial c_1^L/\partial\beta_1 = \partial c_2^L/\partial\beta_2$) in the partial derivative matrix in equation (5.5) are comparable

Fig. 6.4. The initial model of density, shear wave velocity and shear attenuation for the inversion of Love wave data in western North America.

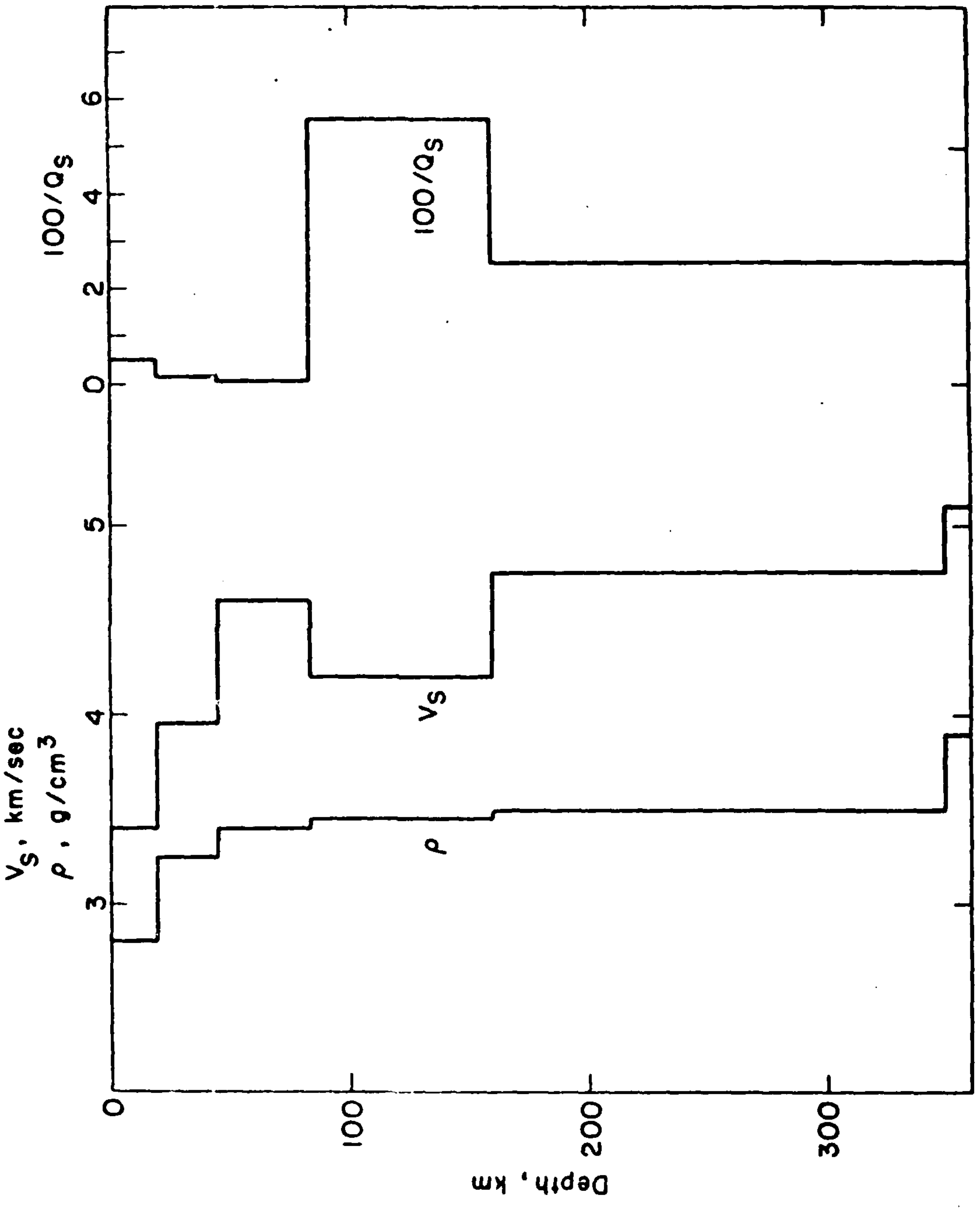
100/Q_S
0
2
4
6
100/Q_S
V_S, km/sec
ρ, g/cm^3
3
4
5
V_S
ρ
0
100
200
300
Depth, km

TABLE 6.4 Starting Q^{-1} models for inversion

Layer No.	Depth	Thickness km	S1 $100/Q_\beta$	S2 $q\ a^\nu$ $\alpha=1/5$	S3 $q\ a^\nu$ $\alpha=1/3$	S4 $q\ a^\nu$ $\alpha=1/2$	S5 $100/Q$
1	21.	21.	0.50	0.003	0.0025	0.002	0.1
2	45.	24.	0.10	0.002	0.0015	0.001	0.01
3	84.	39.	0.05	0.002	0.0015	0.001	0.01
4	160.	76.	5.60	0.07	0.05	0.035	Rx(0.1,0.008) + Rx(0.1,20)
5	350.	190.	2.60	0.03	0.025	0.015	Rx(0.1,2)

For model S1, Q is constant over seismic frequencies; for S2, S3, and S4, $Q^{-1}(\omega) = q\ a^\nu \omega^{-\nu}(\nu-1)!\ \sin \pi\nu/2$.

Rx($\Delta\mu,\tau$) indicates that attenuation is given by $Q^{-1} = \frac{\Delta\mu}{\sqrt{1-\Delta\mu}} \frac{\omega\tau}{1+(\omega\tau)^2}$ where $\Delta\mu$ is the dimensionless relaxation strength. τ is the relaxation time in sec, and ω is the angular frequency in radians/sec [Solomon, 1972a].

Fig. 6.5. Love wave phase velocity, western North America. Observations are shown by circles; vertical bars represent standard deviations. The envelope (solid lines) is that associated with the extremal earth model bounds from inversion S4.

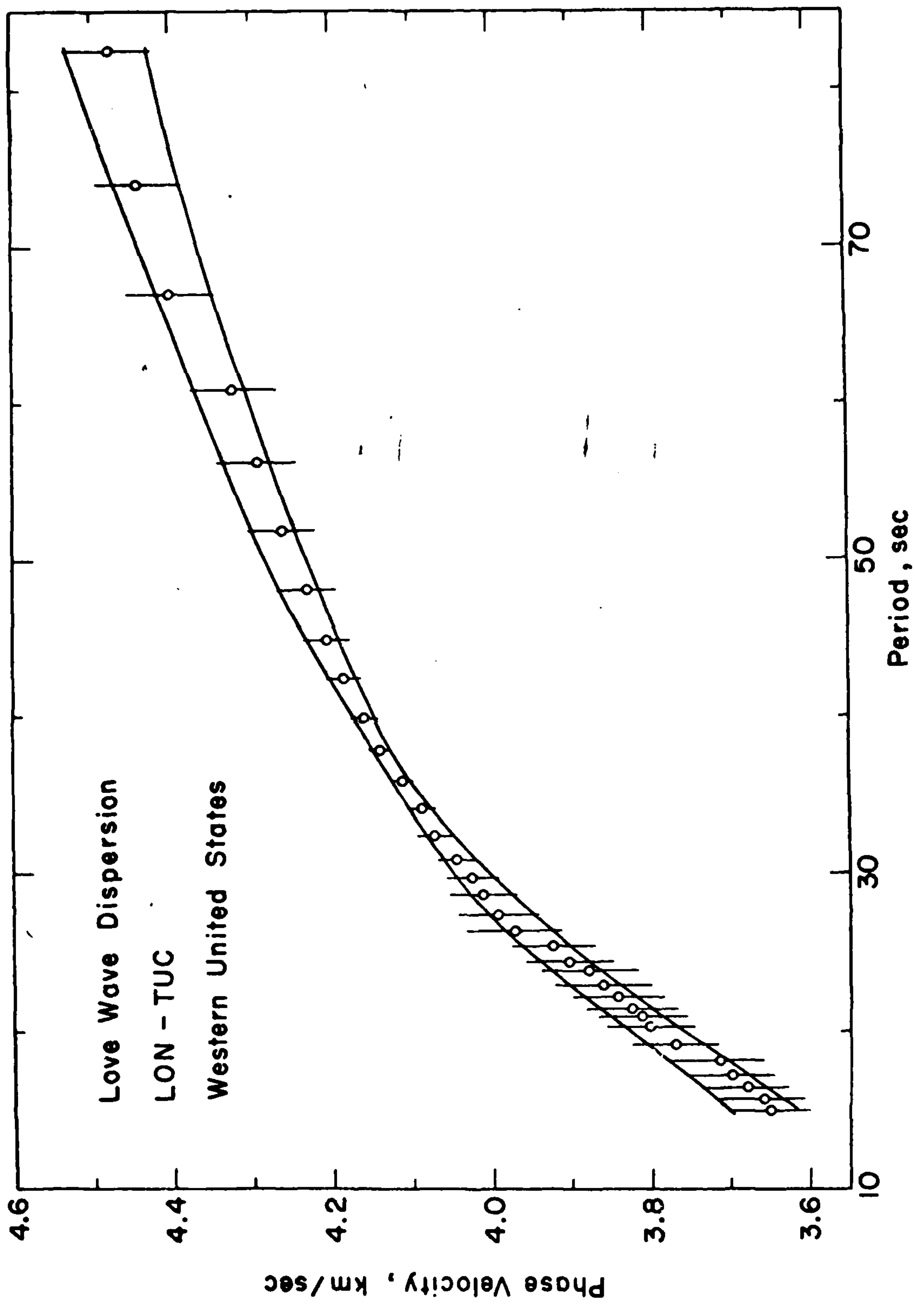
Love Wave Dispersion
LON - TUC
Western United States
Phase Velocity, km/sec
4.6
4.4
4.2
4.0
3.8
3.6
Period, sec
10
30
50
70

Fig. 6.6. Love wave attenuation, western North America. Circles are observations, vertical bars represent standard deviations. The solid lines represent the envelope associated with extremal earth models for inversion S1, the dashed lines for S4.

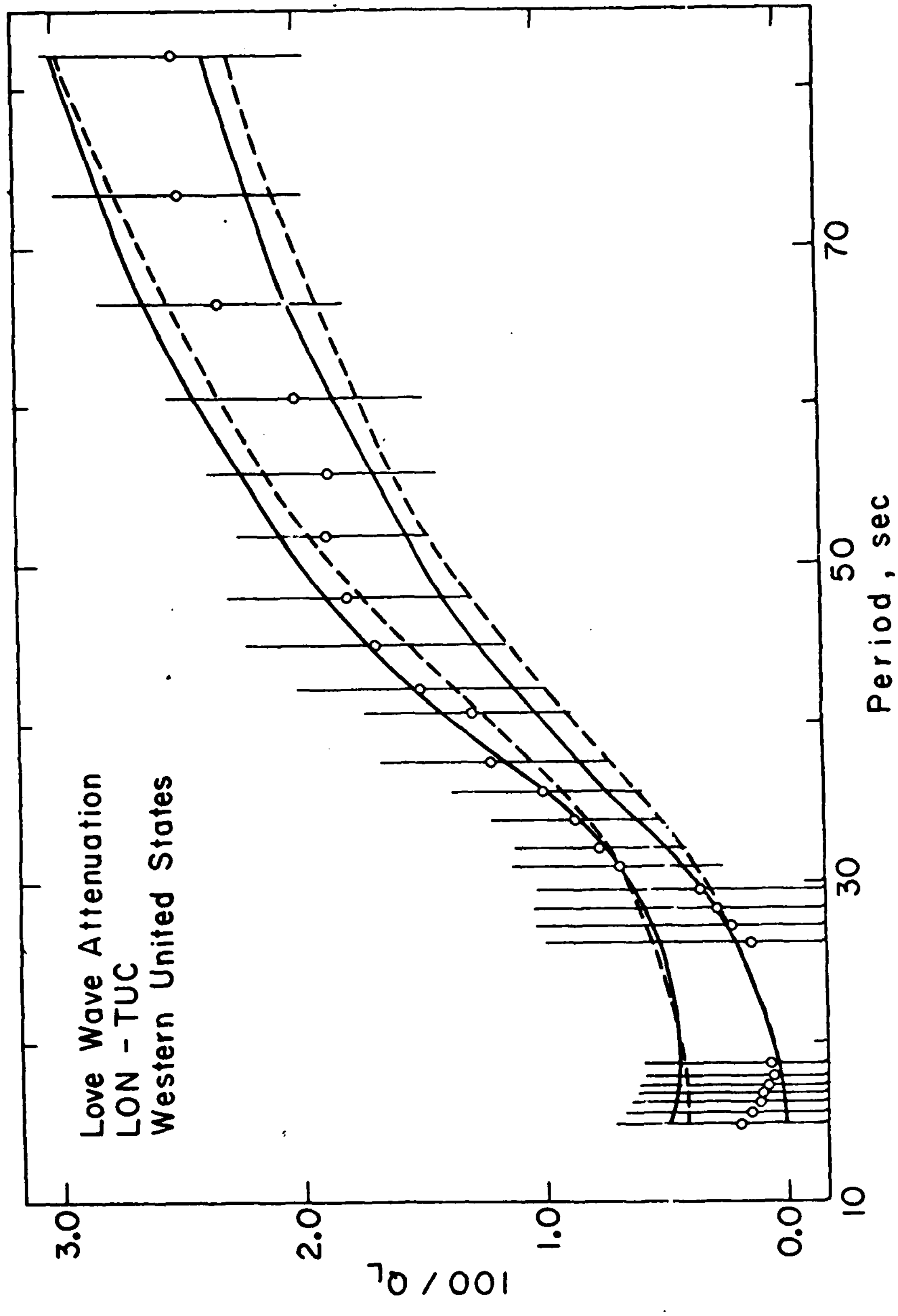
Love Wave Attenuation
LON - TUC
Western United States
3.0
2.0
1.0
0.0
100 / Q_L
10
30
50
70
Period , sec

to those determined by many workers for separate inversions of phase velocity and Q^{-1}; these partials are shown for selected frequencies in Figure 6.7. The 'off-diagonal' elements ($\partial c_1^L/\partial\beta_2 = -\partial c_2^L/\partial\beta_1$) have a more complicated sign structure, as shown in Figure 6.7. For Love waves with periods between 25 and 80 sec, the sign of $\partial c_1/\partial\beta_2$ changes at 60 to 80 km depth. Thus the phase lag due to anelasticity above that depth would give a decreasing phase velocity for increasing attenuation ($\partial c_1/\partial\beta_2 < 0$) whereas below such a depth the phase advances with increasing Q^{-1}($\partial c_1/\partial\beta_2 > 0$). For shorter periods ($T \leq 20$ sec), there is an additional zero crossing at about 20 km depth. These sign changes are closely related to the phase structure of the displacement-depth function as described by Schwab and Knopoff (1971).

An important consequence of the sign structure of $\partial c_1/\partial\beta_2$ in Figure 6.7 is that quite different $\beta_2(Q^{-1})$ models can produce comparable changes in the dispersion curve because of trade-offs between the contributions from different depth intervals.

Resolution analysis was conducted as described in section 5.4. The optimal averaging kernels E_{kj} obtained by minimization of ϵ_k in equation (5.16) are shown in Figure 6.8a and 6.8b for five layers. The vertical depth resolution can be defined as the width of the peak where the value of the approximate delta function is close to unity ($\gtrsim 0.8$).

Fig. 6.7a. Selected partial derivatives of the real part of Love wave phase velocity with respect to the real part of shear velocity ($\partial c_1/\partial\beta_1$, solid lines), and the imaginary part ($\partial c_1/\partial\beta_2$, dashed lines) per unit layer thickness for the initial model in Figure 6.4. The partials shown are for frequency-independent Q^{-1} at the frequency indicated; for frequency-dependent Q^{-1} relations the partial derivatives have a similar structure. Discontinuities in the partials occur at discontinuities in the initial model.

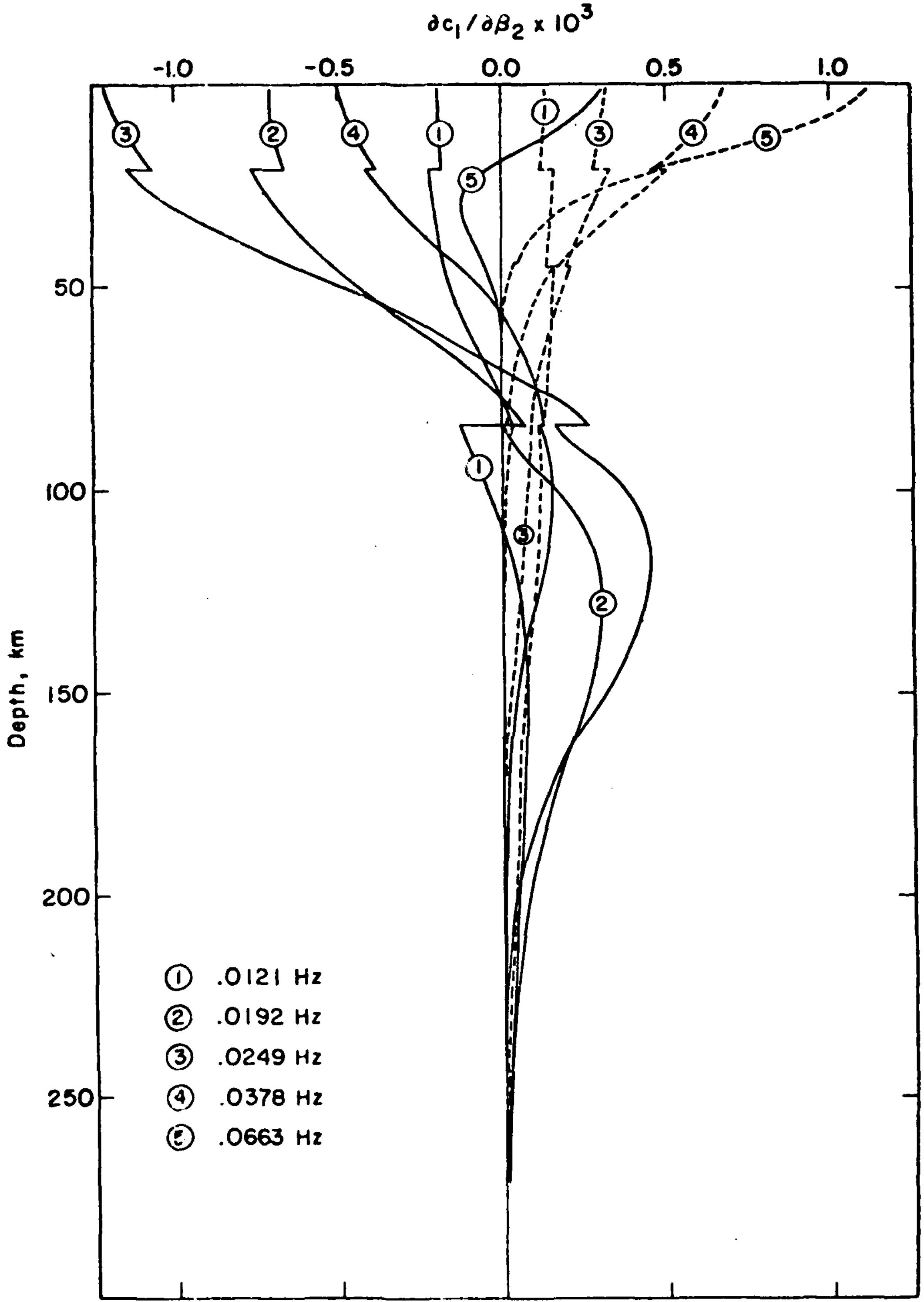
$\partial c_1/\partial\beta_2 \times 10^3$
-1.0
-0.5
0.0
0.5
1.0
Depth, km
50
100
150
200
250
-5.0
-2.5
0.0
2.5
5.0
$\partial c_1/\partial\beta_1 \times 10^2$
①
②
③
④
⑤
① .0121 Hz
② .0192 Hz
③ .0249 Hz
④ .0378 Hz
⑤ .0663 Hz

Fig. 6.7b Selected partial derivatives of the real part of Rayleigh wave phase velocity with respect to the imaginary part of shear velocity ($c_1^R/\partial\beta_2$, solid lines), and the imaginary part of compressive wave velocity ($c_1^R/\partial\alpha_2$, dashed lines) per unit layer thickness for the initial model in Table 6.9. The partials shown are for frequency-independent Q^{-1} at the frequency indicated; for frequency-dependent Q^{-1} relations the partial derivatives have a similar structure. Discontinuities in the partials occur at discontinuities in the initial model.

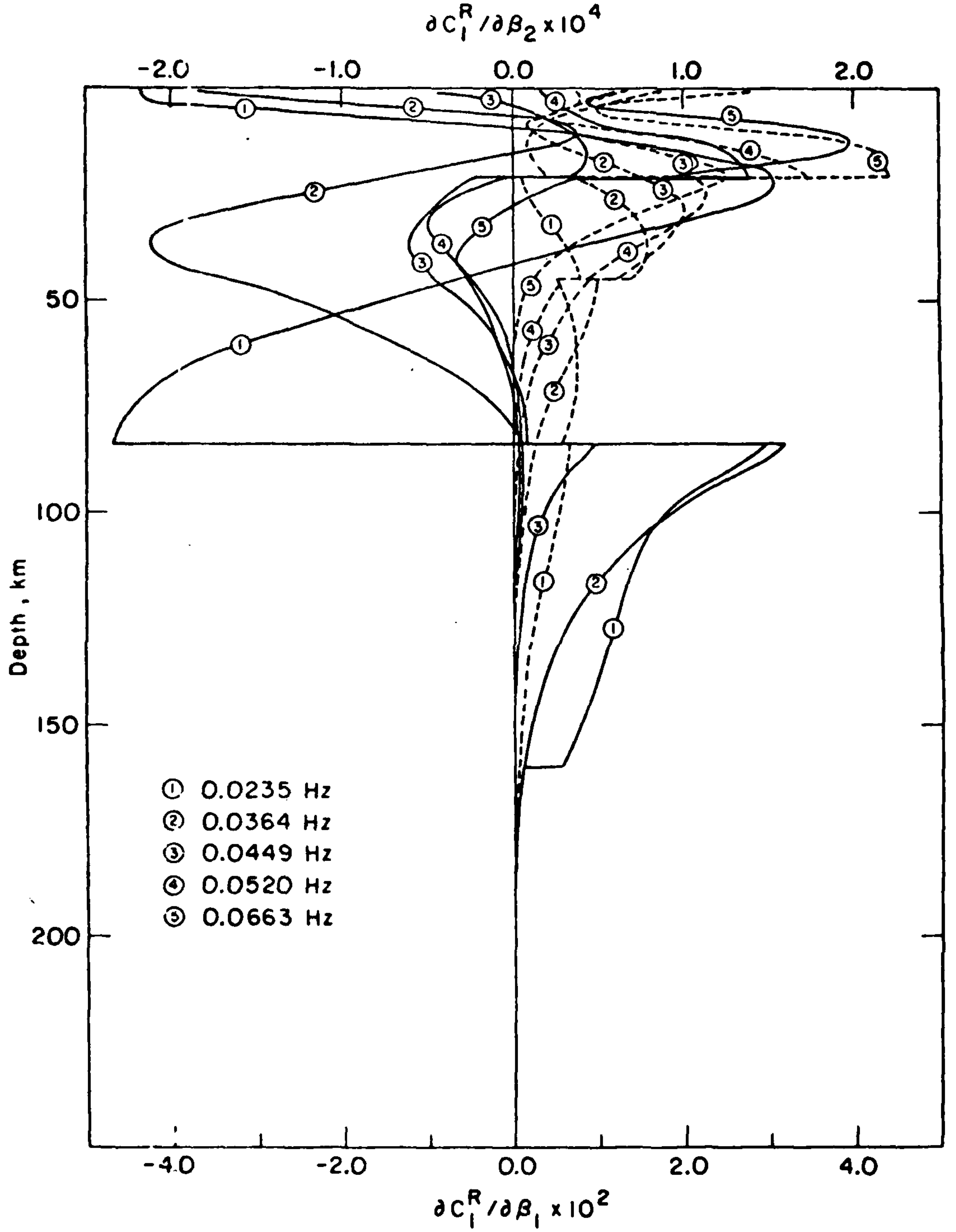
$\partial C_1^R / \partial \beta_2 \times 10^4$
-2.0
-1.0
0.0
1.0
2.0
Depth, km
50
100
150
200
① 0.0235 Hz
② 0.0364 Hz
③ 0.0449 Hz
④ 0.0520 Hz
⑤ 0.0663 Hz
-4.0
-2.0
0.0
2.0
4.0
$\partial C_1^R / \partial \beta_1 \times 10^2$

For comparison, separate 'one variable' cases are drawn in the same figure. The model standard deviation for the two cases are given as σ_{β_o}, σ_{β_s} (or σ_{Q_o}, σ_{Q_s}), calculated for a unit layer thickness, where the subscripts β and Q denote shear velocity and Q^{-1} and the subscripts o and s denote separate inversion and simultaneous inversion, respectively. Based on the resolving lengths of the averaging kernels, a five-layer earth was adopted for the inverse problem. The mid-depths of each layer are approximately those shown in Figure 6.8.

The inversion scheme follows the set theoretical approach of Lee and Solomon (1975) and of Chapter II. Envelopes in model space of shear velocity and shear attenuation are determined from the data set and associated error estimates by linear programming. The reference frequency for all inversions is 1 Hz. The envelopes for shear velocity β and attenuation Q_β^{-1} are given in Tables 6.5 to 6.8 for a dispersion model (S1) with Q independent of frequency, for models (S2 to S4) with Q varying as a power of the frequency, and for a model (S5) based on a superposition of shear relaxations. The relaxation times, relative relaxation strengths, and depth intervals for model S5 are as in Table 6.4 and remain fixed during inversion. (The S class of models all result from simultaneous inversion; an E class consists of models

TABLE 6.5 Envelopes of shear velocity and shear attenuation at 0.01 Hz for selected simultaneous inversions.

Layer no.	Depth (km)	minimum β, km/sec				maximum β, km/sec			
		S1	S2	S3	S4	S1	S2	S3	S4
1	0-21	3.241	3.242	3.245	3.248	3.386	3.382	3.404	3.416
2	21-45	3.715	3.589	3.696	3.697	4.310	4.346	4.350	4.358
3	45-84	4.220	4.169	4.123	4.103	4.822	4.842	4.828	4.826
4	84-160	3.796	3.762	3.710	3.701	4.327	4.370	4.510	4.561
5	160-350	4.811	4.783	4.740	4.699	5.144	5.402	5.430	5.545

Layer no.	Depth (km)	minimum $100/Q_\beta$				maximum $100/Q_\beta$			
		S1	S2	S3	S4	S1	S2	S3	S4
1	0-21	0.0	0.0	0.0	0.0	0.667	0.882	1.063	1.192
2	21-45	0.0	0.0	0.0	0.490	0.268	0.396	0.500	0.538
3	45-84	0.0	0.0	0.020	0.390	0.207	0.303	0.400	0.413
4	84-160	4.525	4.769	5.196	6.338	7.384	7.774	8.268	8.512
5	160-350	2.628	1.699	1.610	1.554	3.783	4.440	4.387	4.087

TABLE 6.6 Envelopes of shear velocity and shear attenuation at 0.1 Hz for selected simultaneous inversions.

Layer no.	Depth (km)	minimum β , km/sec				maximum β km/sec			
		S1	S2	S3	S4	S1	S2	S3	S4
1	0-21	3.251	3.253	3.255	3.256	3.399	3.399	3.416	3.425
2	21-45	3.723	3.705	3.716	3.703	4.317	4.362	4.364	4.364
3	45-84	4.227	4.177	4.133	4.109	4.829	4.850	4.837	4.833
4	84-160	4.019	3.957	3.863	3.820	4.562	4.598	4.653	4.678
5	160-350	4.919	4.866	4.786	4.729	5.291	5.361	5.465	5.572

Layer no.	Depth (km)	minimum $100/Q_\beta$				maximum $100/Q_\beta$			
		S1*	S2	S3	S4	S1*	S2	S3	S4
1	0-21		0.0	0.0	0.0		0.560	0.496	0.378
2	21-45		0.0	0.0	0.155		0.250	0.232	0.171
3	45-84		0.0	0.007	0.123		0.191	0.185	0.131
4	84-160		3.088	2.469	2.047		5.110	3.983	2.770
5	160-350		1.082	0.753	0.494		2.870	2.078	1.310

*S 1 limits are the same as those listed in Table 6.5

TABLE 6.7 Envelopes of shear velocity and shear attenuation at 1 Hz for selected simultaneous inversions.

Layer no.	Depth (km)	minimum β , km/sec				maximum β , km/sec			
		S1	S2	S3	S4	S1	S2	S3	S4
1	0-21	3.263	3.264	3.260	3.259	3.411	3.415	3.423	3.428
2	21-45	3.730	3.713	3.710	3.705	4.325	4.369	4.369	4.367
3	45-84	4.235	4.185	4.137	4.111	4.837	4.838	4.840	4.835
4	84-160	4.243	4.122	3.940	3.861	4.796	4.768	4.725	4.717
5	160-350	5.028	4.940	4.807	4.739	5.438	5.456	5.484	5.581

Layer no.	Depth (km)	minimum $100/Q_\beta$				maximum $100/Q_\beta$			
		S1*	S2	S3	S4	S1*	S2	S3	S4
1	0-21		0.0	0.0	0.0		0.354	0.231	0.120
2	21-45		0.0	0.0	0.050		0.158	0.117	0.054
3	45-84		0.0	0.013	0.039		0.121	0.090	0.041
4	84-160		1.982	1.159	0.652		3.314	1.882	0.884
5	160-350		0.687	0.351	0.156		1.840	0.974	0.416

*S 1 limits are the same as those listed in Table 6.5.

TABLE 6.8 Envelopes of shear velocity and shear attenuation for simultaneous inversion for Solomon [1972a]-type relaxation model.

Layer	β, km/sec		$100/Q_\beta$	
f=0.01Hz	min	max	min	max
1	3.263	3.416	0.0	0.537
2	3.715	4.261	0.0	0.269
3	4.109	4.697	0.0	0.213
4	3.816	4.430	1.218	4.719
5	4.615	5.147	0.268	1.313
f=0.1 Hz				
1	3.271	3.428	0.0	0.537
2	3.717	4.264	0.0	0.259
3	4.112	4.701	0.0	0.213
4	3.880	4.449	0.210	0.814
5	4.645	5.177	1.054	5.170
f=1 Hz				
1	3.283	3.441	0.0	0.537
2	3.720	4.267	0.0	0.269
3	4.115	4.704	0.0	0.213
4	3.889	4.450	0.145	0.562
5	4.664	5.196	0.171	0.839

Fig. 6.8. Resolving kernels for shear wave (a) phase velocity and (b) attenuation at selected depths (arrows) at the reference frequency of 1 Hz. Model standard deviations are shown at the right for both simultaneous (S) and separate (0) inversion results, shown as solid and dashed lines, respectively.

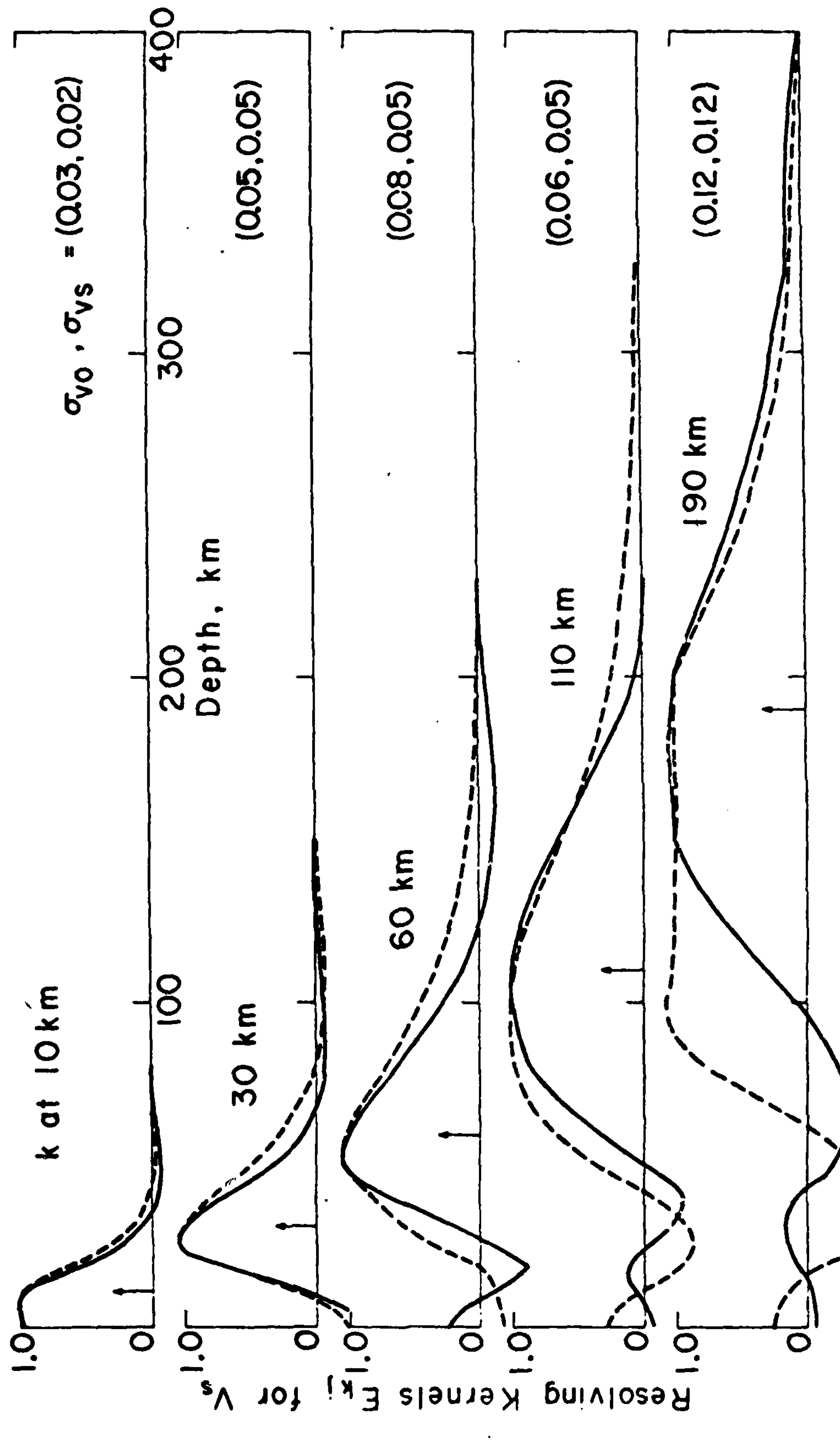
σvo , σvs = (0.03, 0.02)
(0.05, 0.05)
(0.08, 0.05)
(0.06, 0.05)
(0.12, 0.12)
k at 10 km
30 km
60 km
110 km
190 km
100
200
300
400
Depth, km
1.0
0
1.0
0
1.0
0
1.0
0
1.0
0
Resolving Kernels Ekj for Vs

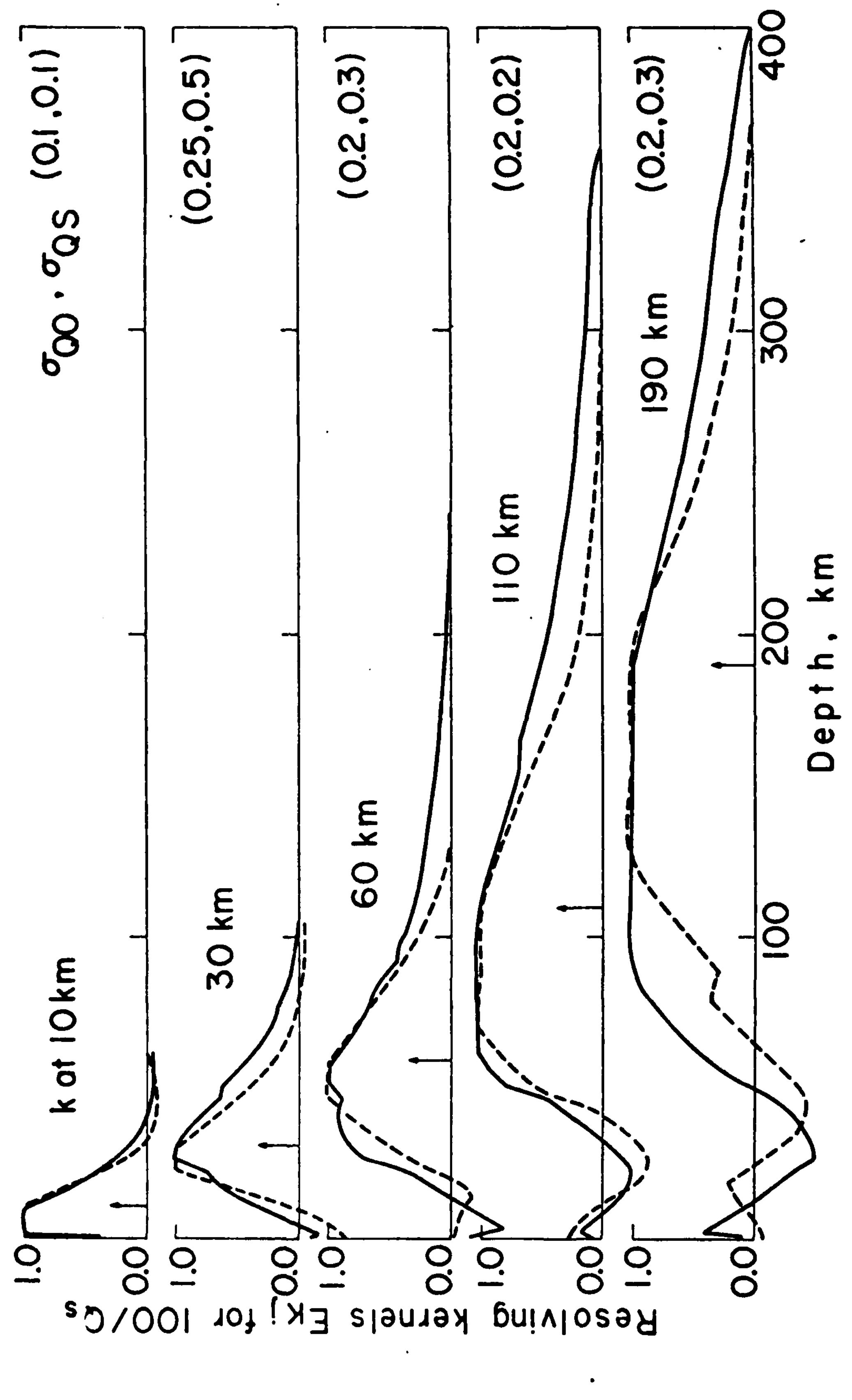
σQO · σQS (0.1,0.1)
k at 10km
30 km
(0.25,0.5)
60 km
(0.2,0.3)
110 km
(0.2,0.2)
190 km
(0.2,0.3)
1.0
0.0
1.0
0.0
1.0
0.0
1.0
0.0
1.0
0.0
100
200
300
400
Depth, km
Resolving kernels EKj for 100/Gs

resulting from separate inversions). The corresponding envelopes in data space are illustrated for some of these models in Figures 6.5 and 6.6. As with all extremal inversions of this sort, the envelopes include all acceptable models but not every model falling within the envelopes is acceptable.

In general, both β and Q_β^{-1} (except for model S1) are functions of frequency. The intrinsic dispersion for β is very sensitive to the assumed frequency dependence of Q_β^{-1}. The effect of the frequency dependence on the envelopes for β and Q_β^{-1} are illustrated for two models in Figures 6.9 and 6.10.

The result of weighted least-square inversion (Lee and Solomon, 1975) on the same data set is shown in Figure 6.11. The β and Q_β^{-1} profiles (S11) are 'best' models in the least squares sense for the layering shown. The initial model for the inversion was chosen from S1 by averaging two extreme models which have no low velocity zone. Note that the presence of a modest low velocity zone in model S11 does not depend on a low velocity zone in the starting model.

b. Love and Rayleigh waves in western North America

The starting models for calculation of partial derivatives in this case are listed in Table 6.9 for Q independent of frequency. The models for β and Q_β^{-1} are taken from the results of the previous section and are

Fig. 6.9. Envelopes of shear wave velocity and attenuation, models S1 and E1. Envelopes of S1 are shown at three different frequencies. Long-dashed lines represent envelopes of E1, solid lines are for S1 at 0.01 Hz, short-dashed lines for S1 at 0.1 Hz and dot-dashed lines for S1 at 1 Hz.

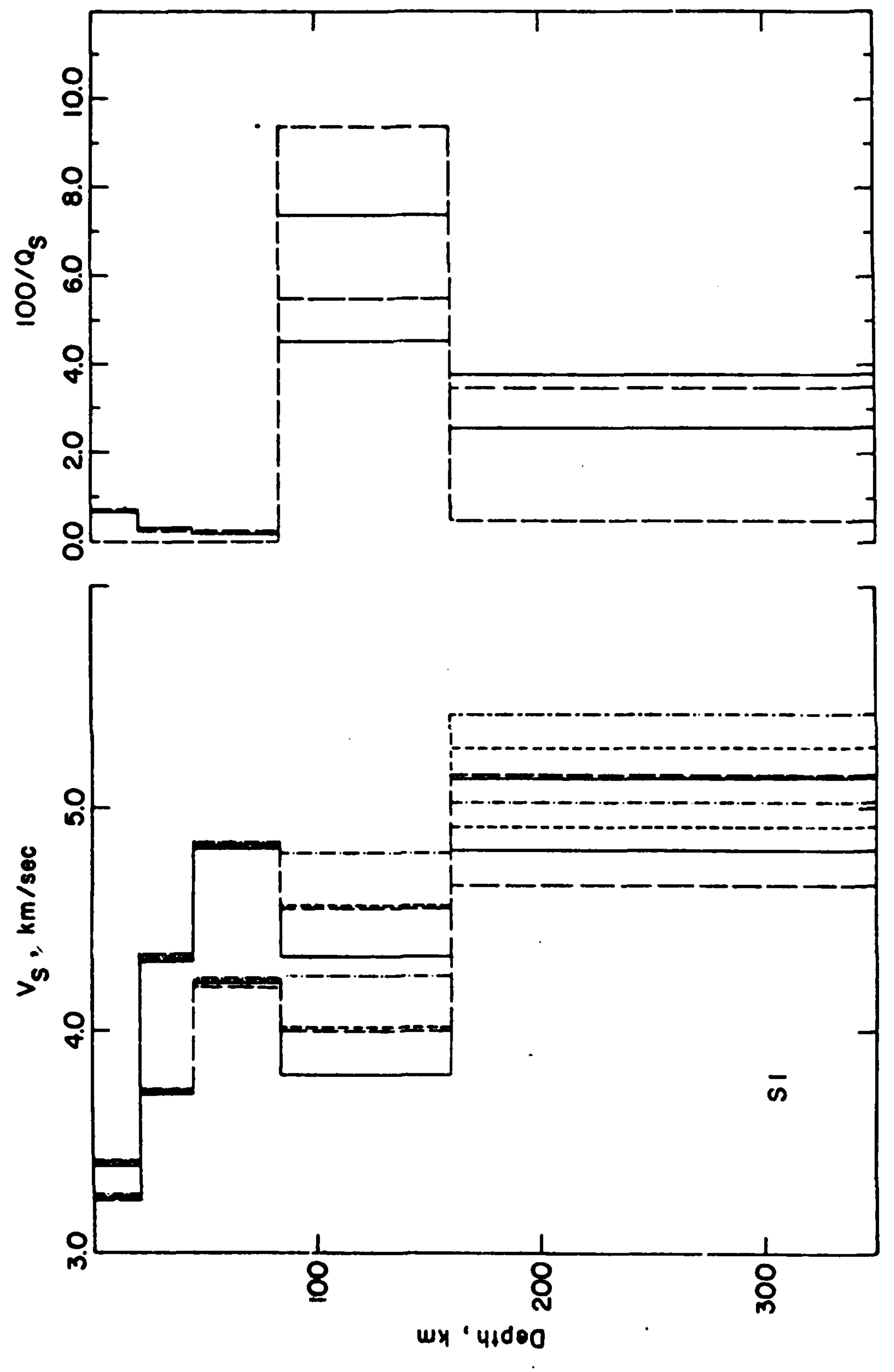
100/Q_S
0.0
2.0
4.0
6.0
8.0
10.0
V_S, km/sec
3.0
4.0
5.0
100
200
300
Depth, km
SI

Fig. 6.10. Envelopes of shear wave velocity and attenuation, models S4 and E1. Envelopes of S4 are shown at three different frequencies. Long-dashed lines represent envelopes of E1, solid lines are for S4 at 0.01 Hz, short-dashed lines for S4 at 0.1 Hz and dot-dashed lines for S4 at 1 Hz.

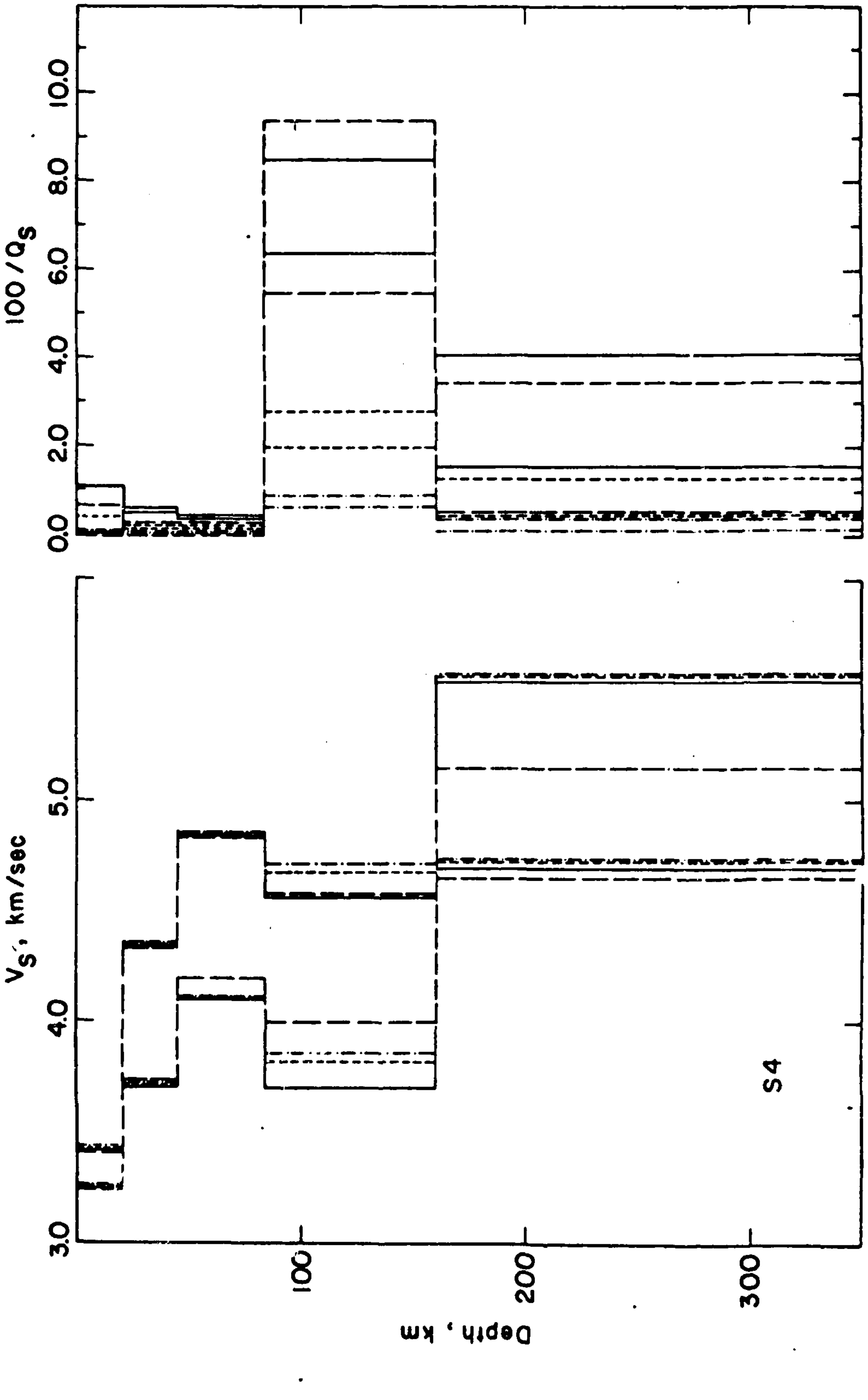
0.0
2.0
4.0
6.0
8.0
10.0
100/Q_S
3.0
4.0
5.0
V_S, km/sec
100
200
300
Depth, km
S4

Fig. 6.11. 'Best' fitting earth models from weighted least-square inversion. Model S11 is from simultaneous inversion, model QC11 is derived from the technique of Anderson _et al._ (1977). The models are shown at the reference frequency of 1 Hz.

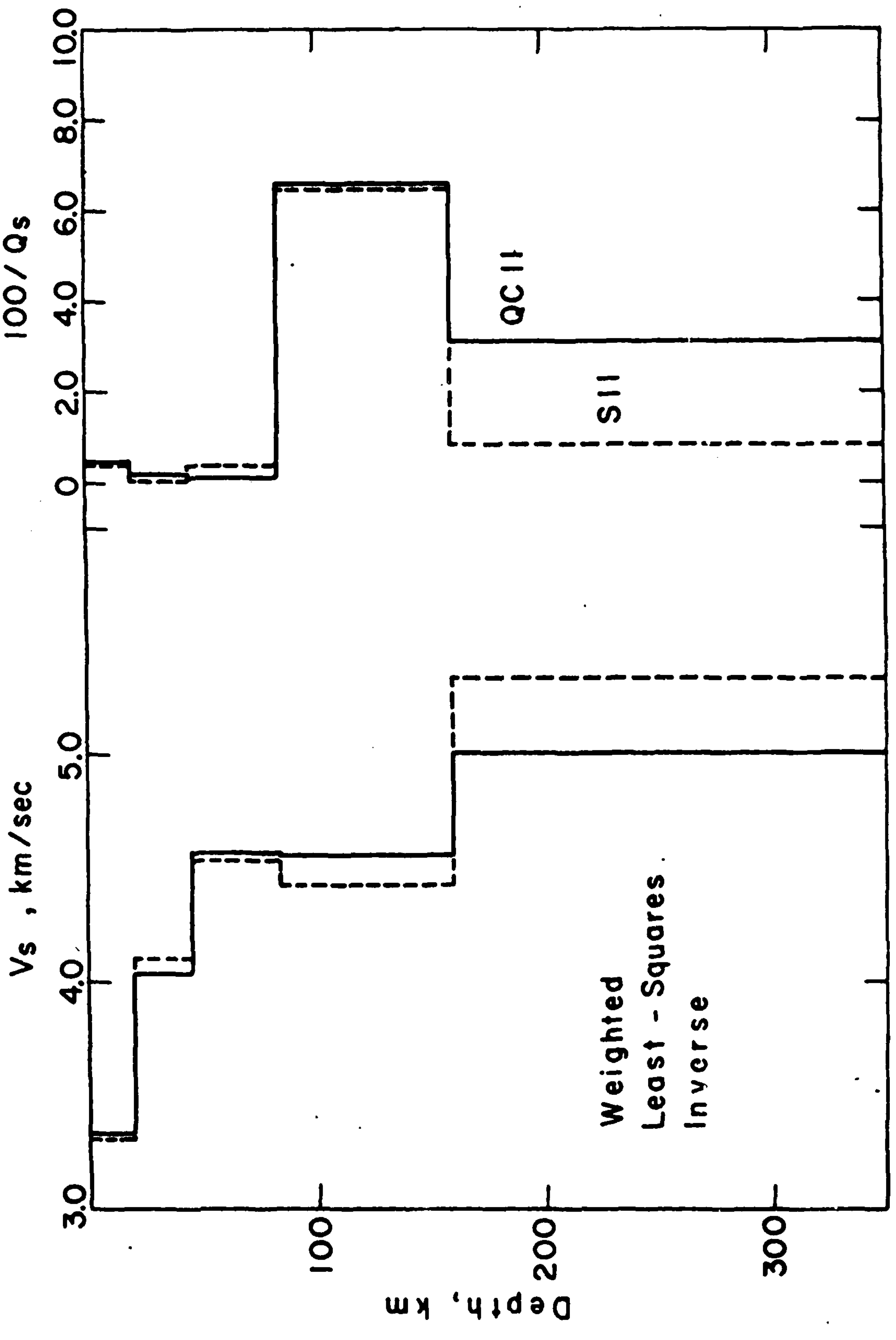
100/Qs
0
2.0
4.0
6.0
8.0
10.0
QC11
S11
Vs , km/sec
3.0
4.0
5.0
Weighted
Least - Squares
Inverse
100
200
300
Depth, km

Table 6.9: Starting model for inversion of combined Love and Rayleigh phase velocity and attenuation in western North America.

Depth, km	β, km/sec	α, km/sec	ρ, g/cm^3	$100/Q_\beta$
0-2	1.72	4.00	2.21	.32
2-13	3.58	6.00	2.80	.32
13-21	3.58	6.20	2.80	.32
21-45	3.96	6.50	3.25	.13
45-64	4.54	7.619	3.40	.13
64-84	4.54	7.615	3.40	.13
84-94	4.48	7.615	3.45	5.926
94-128	4.49	7.619	3.45	5.926
128-160	4.49	7.622	3.45	5.926
160-180	5.266	7.90	3.50	2.96
180-220	5.266	8.23	3.50	2.96
220-260	5.266	8.25	3.50	2.96
260-300	5.266	8.27	3.50	2.96
300-350	5.266	8.43	3.50	2.96
∞	5.266	8.53	3.90	2.96

determined by averaging the extreme models of β and Q_β^{-1} for each case of a given frequency dependence of Q_β. The initial density model is taken as in Figure 6.4 and is varied (but remains real) in the inversion process. The P-wave velocity is chosen to have features similar to C11 model of Archambeau et al. (1969) and is held fixed since phase velocity is least sensitive to changes in α among (α,β,ρ) and thus the resolution of the inverse problem is poor for α. Because of the large uncertainties in measured Q^{-1}, we will assume that losses under purely compressive stress are negligible, i.e. $Q_\alpha^{-1} = 4/3(\beta/\alpha)^2 Q_\beta^{-1}$. Finally, a 2 km sedimentary layer has been added to improve the fit for Rayleigh wave phase velocity.

The 'off-diagonal' elements of the partial derivative matrix for Rayleigh waves, $\partial R_1/\partial\beta_2$, are an order of magnitude smaller than those for Love waves (Figure 6.7b). In other words, the difference between simultaneous inversion and the data corrected Anderson-Hart treatment is less significant for Rayleigh waves than for Love waves. However, the advantage of simultaneous inversion still remains because the changes in the Q^{-1} model itself are sensitive to the result of the velocity model inversion.

Resolution analysis was conducted as before. The optimal averaging kernels E_{kj} for both Love and Rayleigh waves are shown in Figures 6.12 for five layers. During

Fig. 6.12a. Resolving kernels for shear velocity at selected depths (arrows) at the reference frequency 1 Hz, using both Love and Rayleigh wave data in western North America. Model standard deviations are shown at the right.

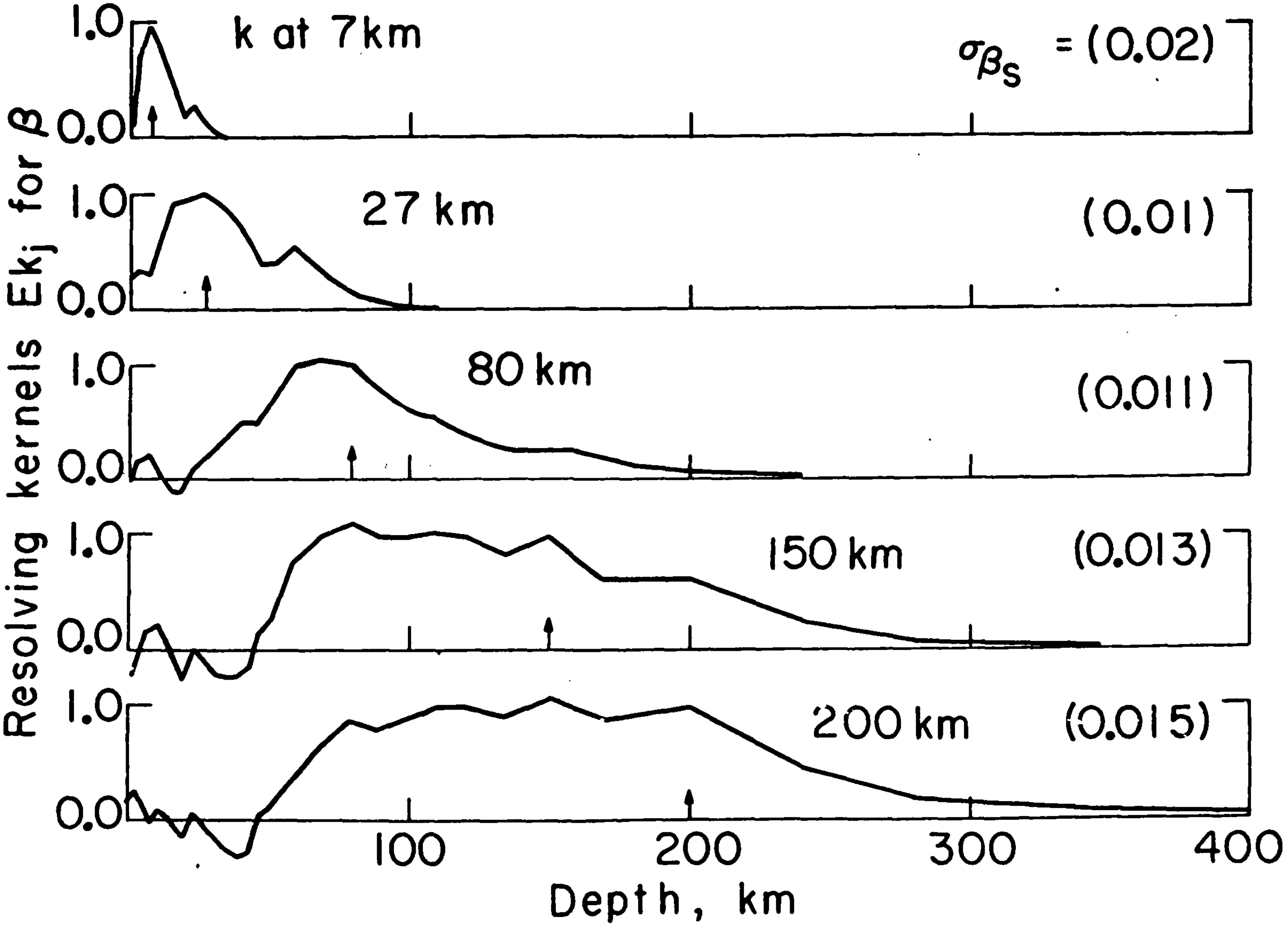
Resolving kernels Ek$_j$ for β
1.0
0.0
k at 7km
σ_{β_S} = (0.02)
27 km
(0.01)
80 km
(0.011)
150 km
(0.013)
200 km
(0.015)
100
200
300
400
Depth, km

Fig. 6.12b. Resolving kernels for shear attenuation at selected depths (arrows), using both Love and Rayleigh wave data in western North America. Model standard deviations are shown at the right.

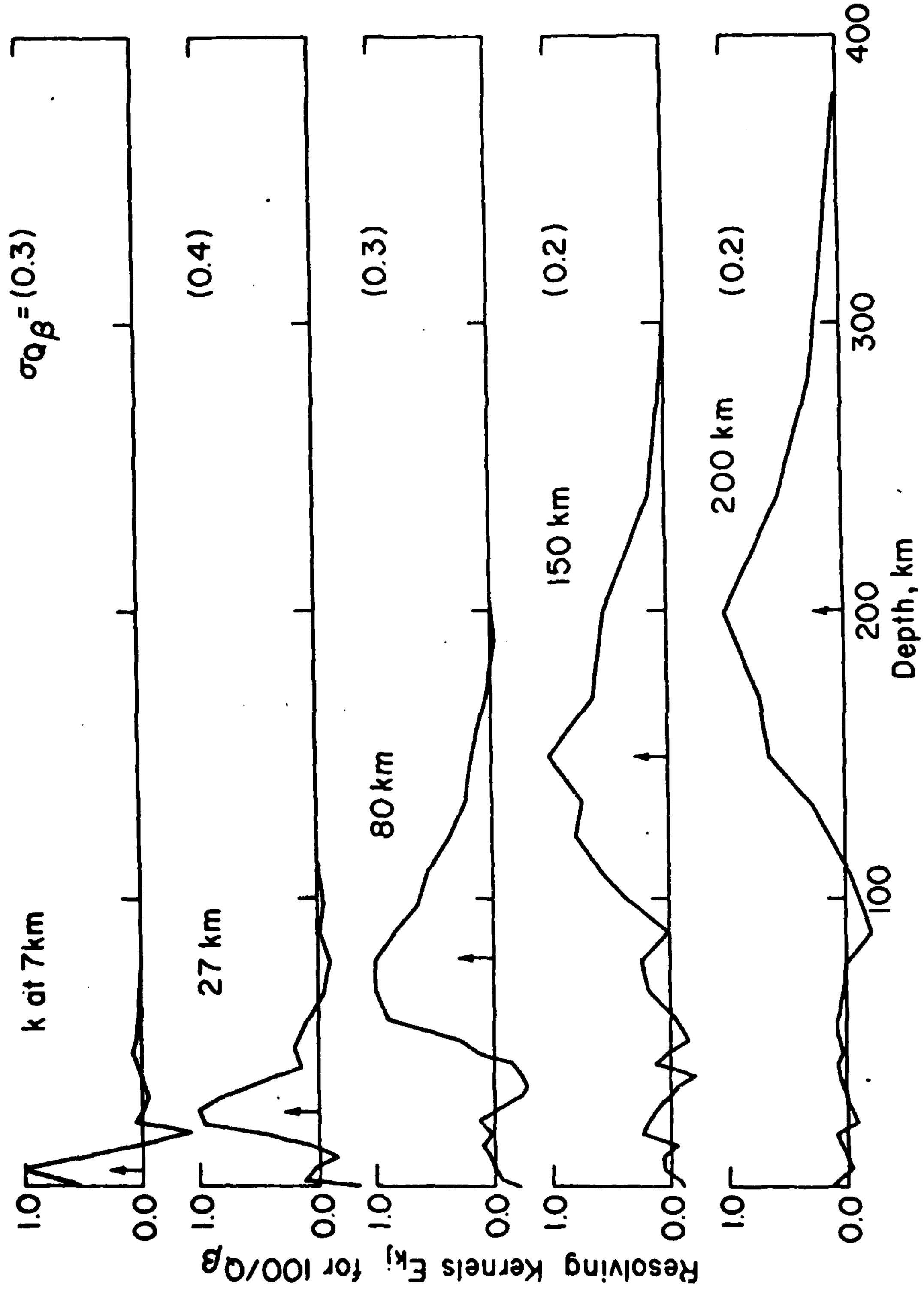
σ_{Q_β} = (0.3)
(0.4)
(0.3)
(0.2)
(0.2)
k at 7km
27 km
80 km
150 km
200 km
1.0
0.0
1.0
0.0
1.0
0.0
1.0
0.0
1.0
0.0
100
200
300
400
Depth, km
Resolving Kernels E_{kj} for $100/Q_\beta$

inversions, the velocities and density in the top sedimentary layer and the half space have been fixed. As in the previous section, the reference frequency for inversion is chosen at 1 Hz and a 5-layer model is adopted. The envelopes of shear velocity β, attenuation Q_β^{-1}, and density ρ are given in Tables 6.10 and Figure 6.13 for a dispersion model (S31W) with Q independent of frequency, and for models (S32W, S33W) with Q varying as a power of the frequency. The corresponding envelopes in data space are illustrated for these models in Figures 6.14, 6.15, 6.16 and 6.17.

c. Love and Rayleigh waves in east-central North America

The starging models of α, β, ρ and Q_β^{-1} are listed in Table 6.11. The models of α, β and ρ are adapted from the results of McEvilly (1964) and the Q_β^{-1} model for the constant-Q inversion is from Lee and Solomon (1975) or from Chapter II. The initial model Q_β^{-1} for inversion using a power law dependence of Q on frequency is chosen to be an acceptable solution to the separate Q inversion. The averaging kernels E_{kj} from resolution analysis for both Love and Rayleigh waves are shown in Figures 6.18, for five layers. The envelopes of shear velocity β attenuation Q_β^{-1} and density ρ are given in Tables 6.12 and Figure 6.19 for a dispersion model (S31E) with Q independent of frequency and for a model (S32E) with Q

Fig. 6.13. Envelopes of shear velocity and shear attenuation, at a frequency of 1 Hz, and density for models S31W, S32W and S33W. Solid lines represent envelopes of S31W (ν = o), short-dashed lines are for S32W (ν = 1/5) and long-dashed lines are for S33W (ν = 1/2).

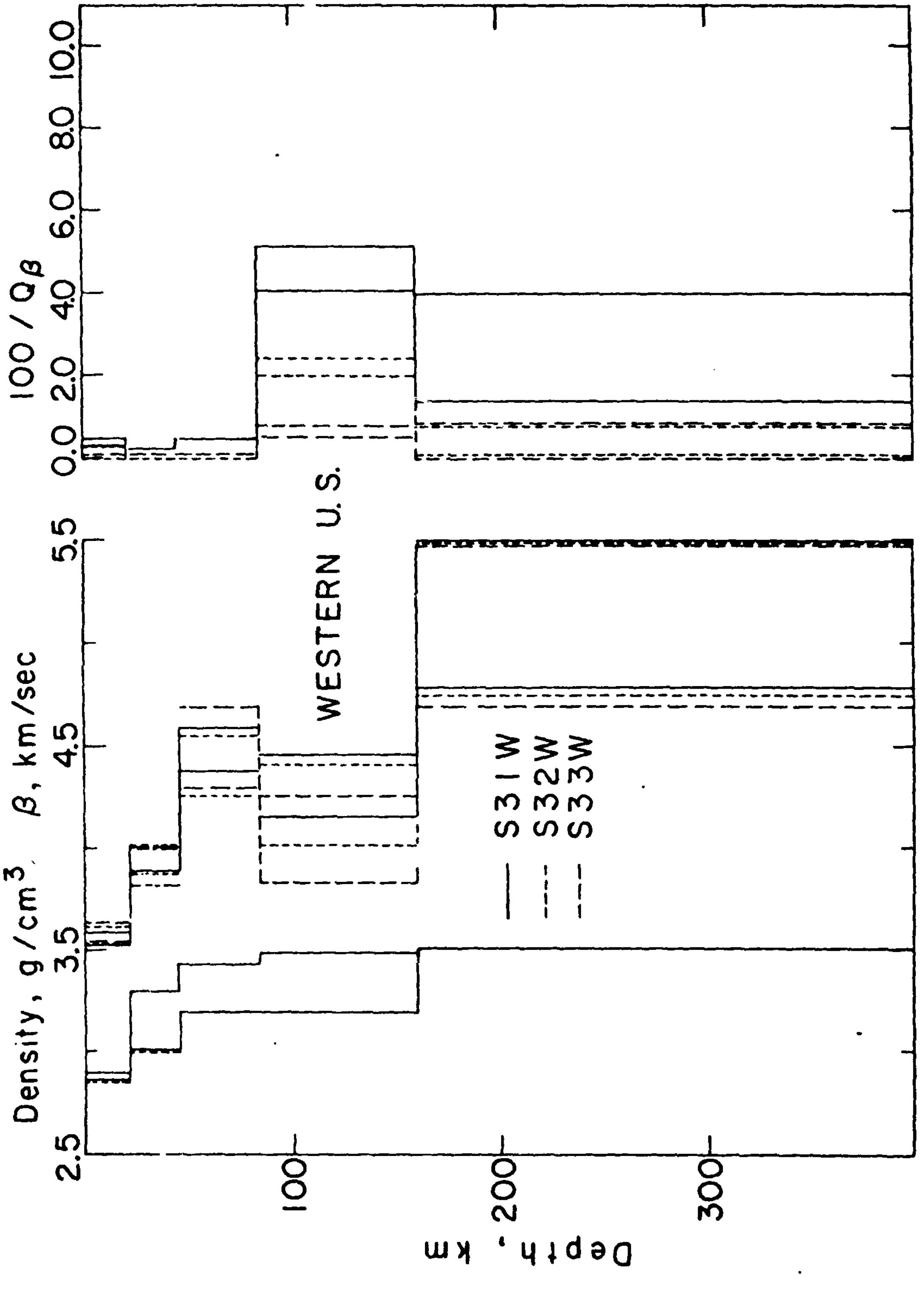
Density, g/cm^3
β, km/sec
2.5
3.5
4.5
5.5
100 / Q_β
0.0
2.0
4.0
6.0
8.0
10.0
WESTERN U.S.
S31W
S32W
S33W
100
200
300
Depth, km

Fig. 6.14. Love wave phase velocity, western North America. Observations are shown by Circles; vertical bars represent standard deviations. The envelope (solid lines) is associated with the extreme earth model bounds from inversion S31W. Open circles are incompatible data for this inversion.

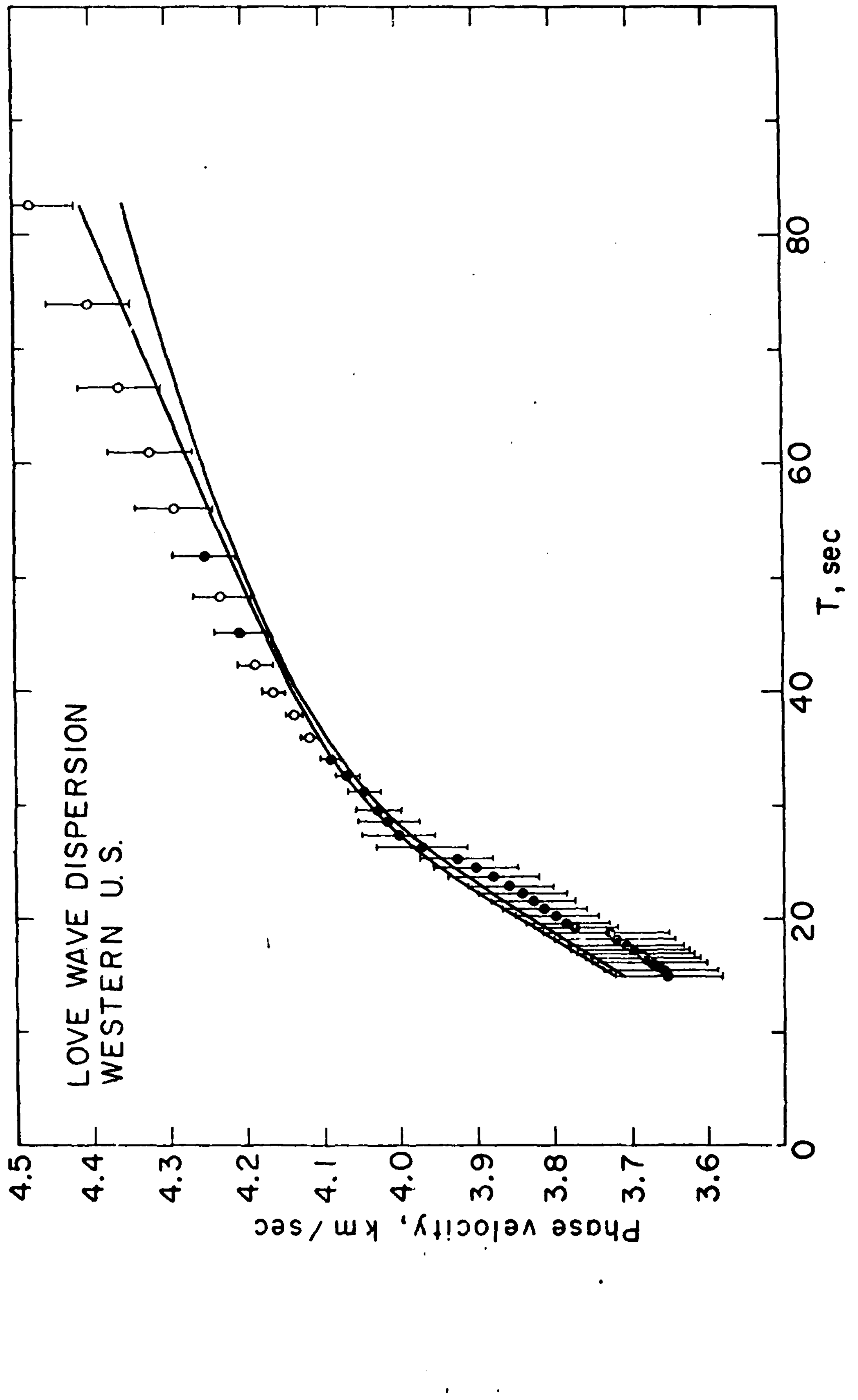
LOVE WAVE DISPERSION
WESTERN U.S.
T, sec
0
20
40
60
80
Phase velocity, k m / sec
4.5
4.4
4.3
4.2
4.1
4.0
3.9
3.8
3.7
3.6

Fig. 6.15. Rayleigh wave phase velocity, western North America. Observations are shown by circles; vertical bars represent standard deviations. The envelope (solid lines) is associated with the extreme earth model bounds from inversion S31W. Open circles are incompatible data for this inversion.

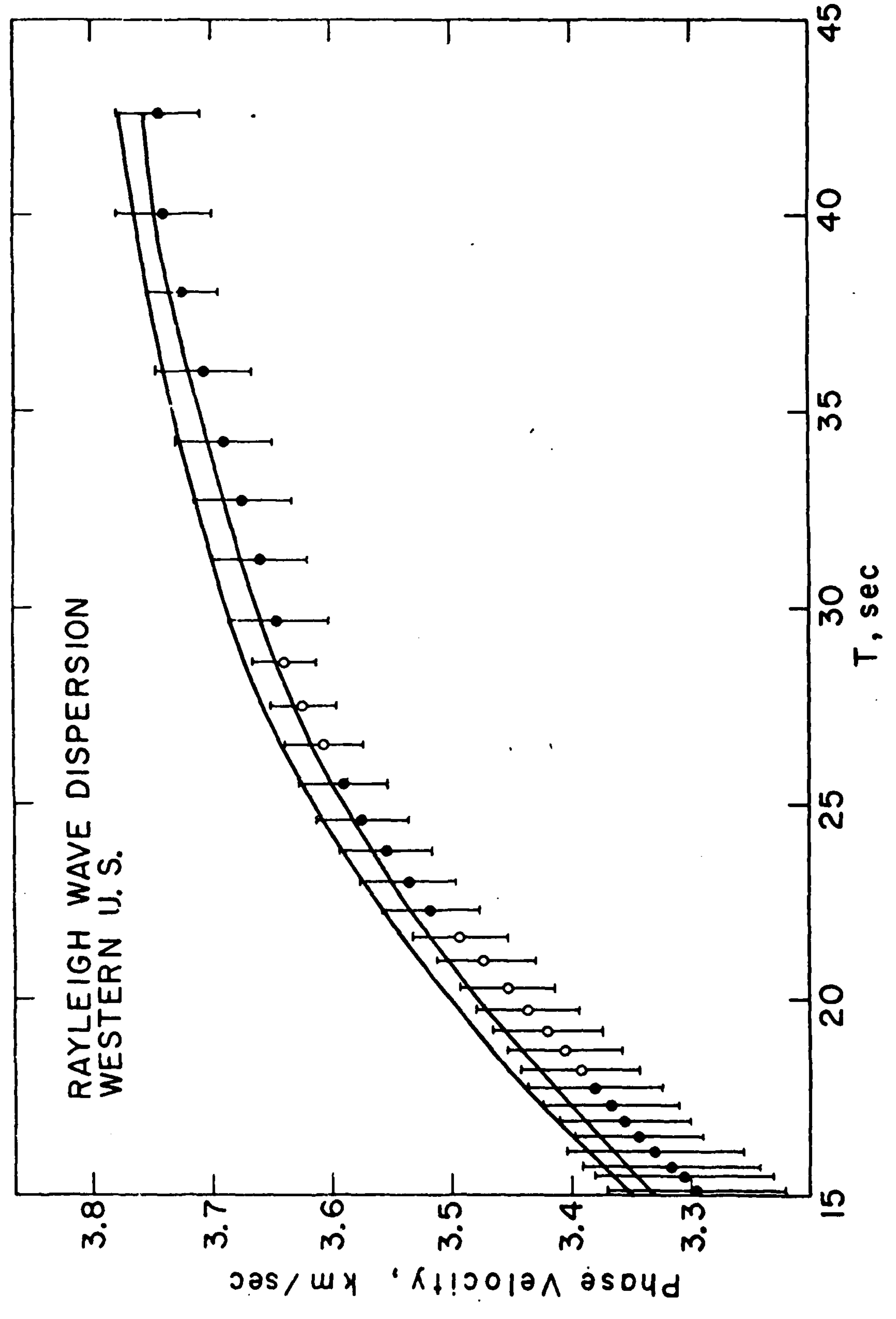
RAYLEIGH WAVE DISPERSION
WESTERN U. S.
Phase Velocity, km/sec
3.8
3.7
3.6
3.5
3.4
3.3
T, sec
15
20
25
30
35
40
45

Fig. 6.16. Love wave attenuation, western North America. Circles are observations; vertical bars represent standard deviations. The solid lines represent the envelope associated with extremal earth models for inversion S31W. Open circles are incompatible data for this inversion.

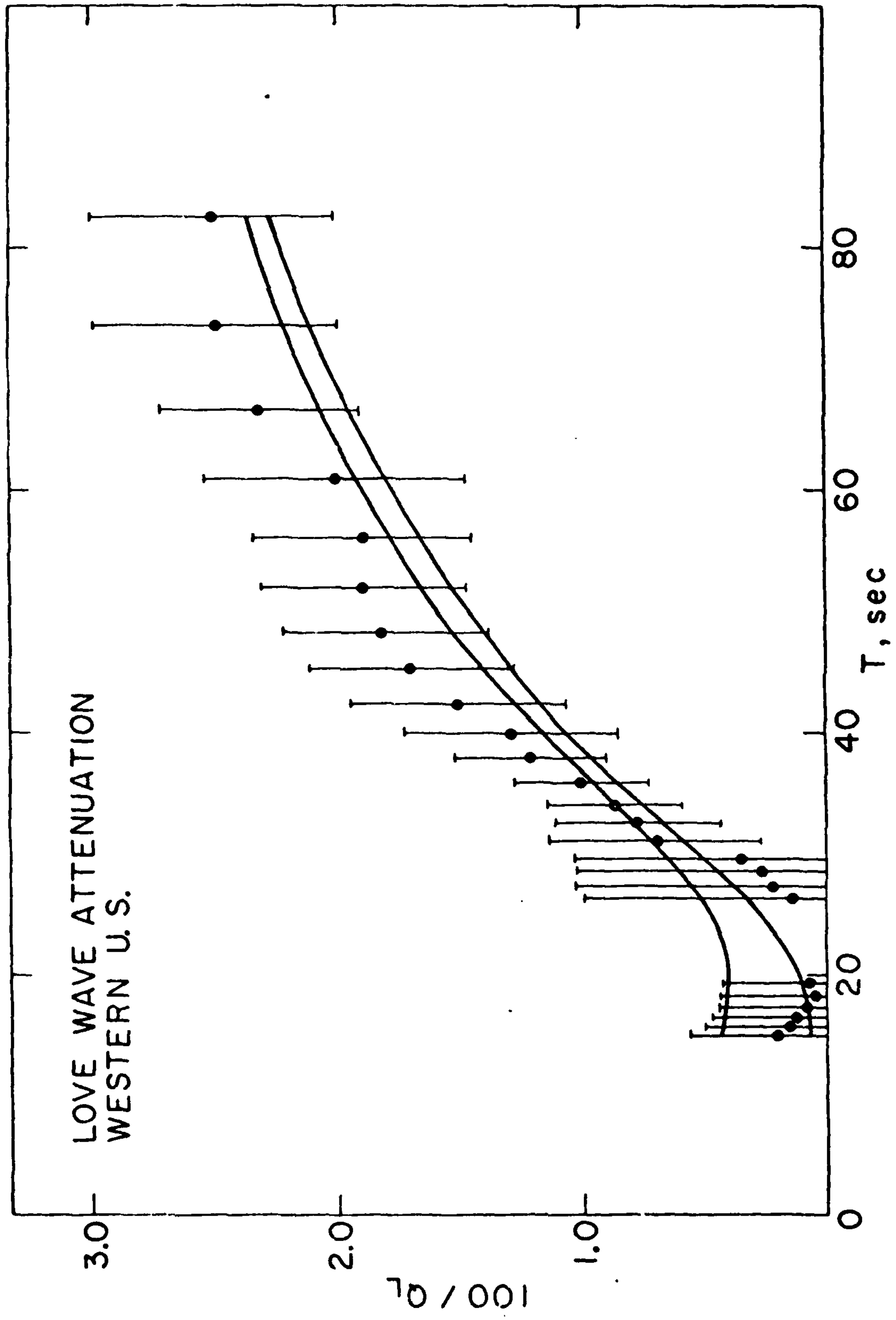
LOVE WAVE ATTENUATION
WESTERN U.S.
3.0
2.0
1.0
100 / Q_L
0
20
40
60
80
T, sec

Fig. 6.17. Rayleigh wave attenuation, western North America. Circles are observations; vertical bars represent standard deviations. The solid lines represent the envelope associated with extremal earth models for inversion S31W. Open circles are incompatible data for this inversion.

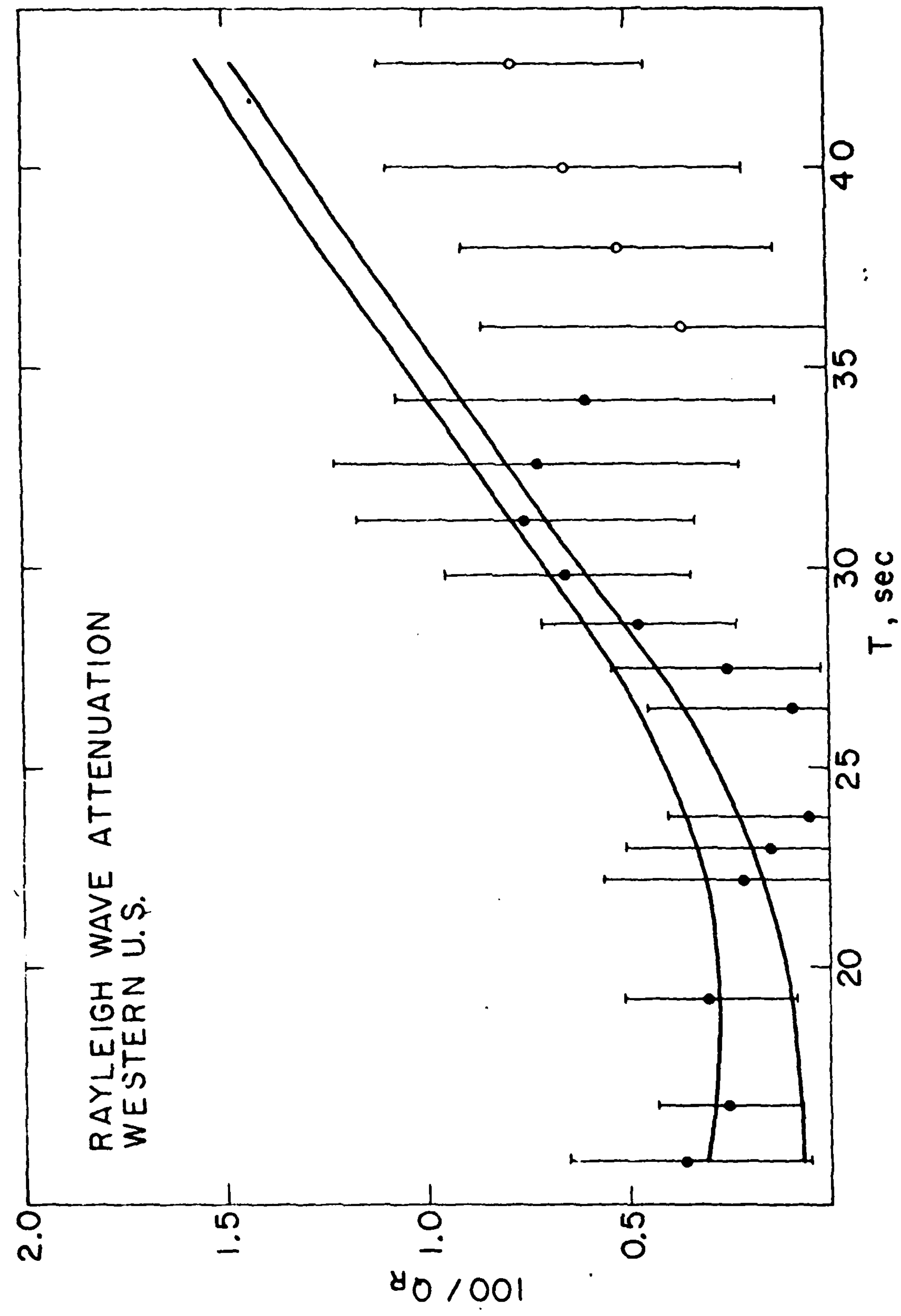
RAYLEIGH WAVE ATTENUATION
WESTERN U.S.
T, sec
20
25
30
35
40
100 / Q_R
2.0
1.5
1.0
0.5

Fig. 6.18a. Resolving kernels for shear velocity at selected depths (arrows) at the reference frequency 1 Hz, using both Love and Rayleigh wave phase velocity and attenuation in east-central North America. Model standard deviations are shown at the right.

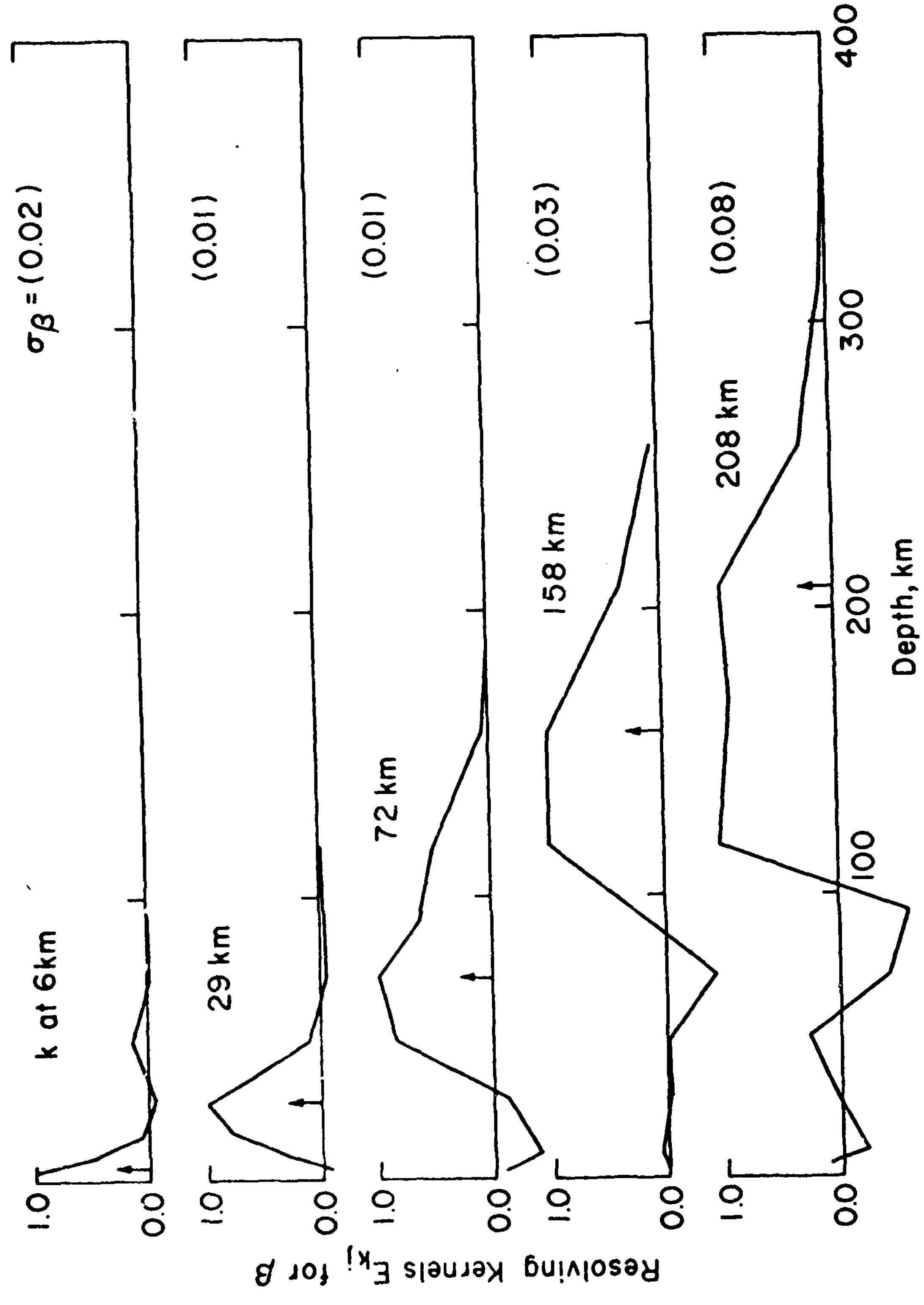
σβ = (0.02)
(0.01)
(0.01)
(0.03)
(0.08)
k at 6km
29 km
72 km
158 km
208 km
1.0
0.0
1.0
0.0
1.0
0.0
1.0
0.0
1.0
0.0
Resolving Kernels E_kj for β
100
200
300
400
Depth, km

Fig. 6.18b. Resolving kernels of shear attenuation at selected depth (arrows) at the reference frequency 1 Hz, using both Love and Rayleigh wave data in east-central North America. Model standard deviations are shown at the right.

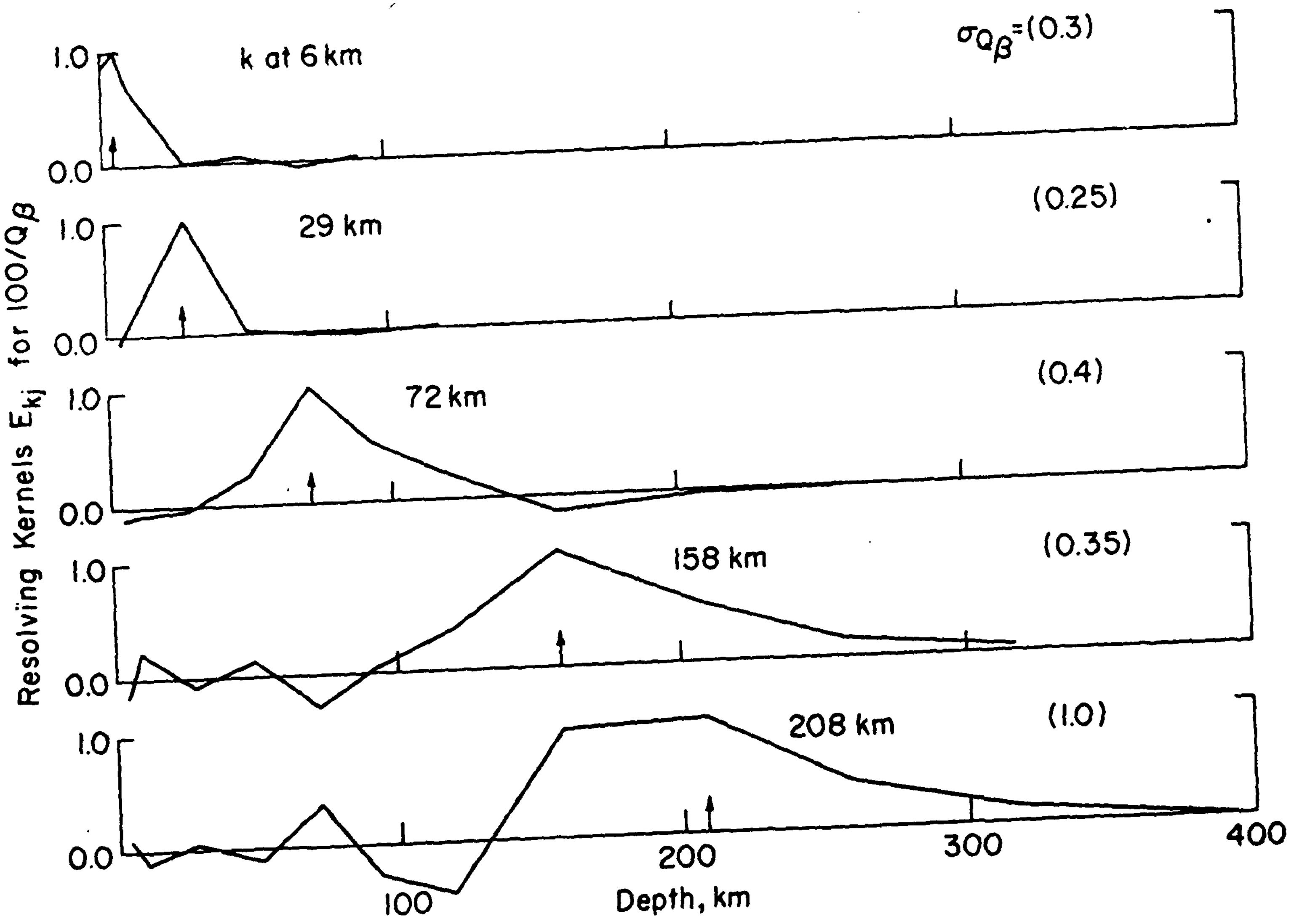
Resolving Kernels E_{kj} for $100/Q_\beta$
σ_{Q_β}=(0.3)
k at 6 km
(0.25)
29 km
(0.4)
72 km
(0.35)
158 km
(1.0)
208 km
1.0
0.0
100
200
300
400
Depth, km

Fig. 6.19. Envelopes of shear velocity and shear, attenuation at a frequency of 1 Hz, and density for models S31E and S32E. Solid lines represent envelopes of S31E ($\nu = o$), and dashed lines are for S32E ($\nu = 1/2$).

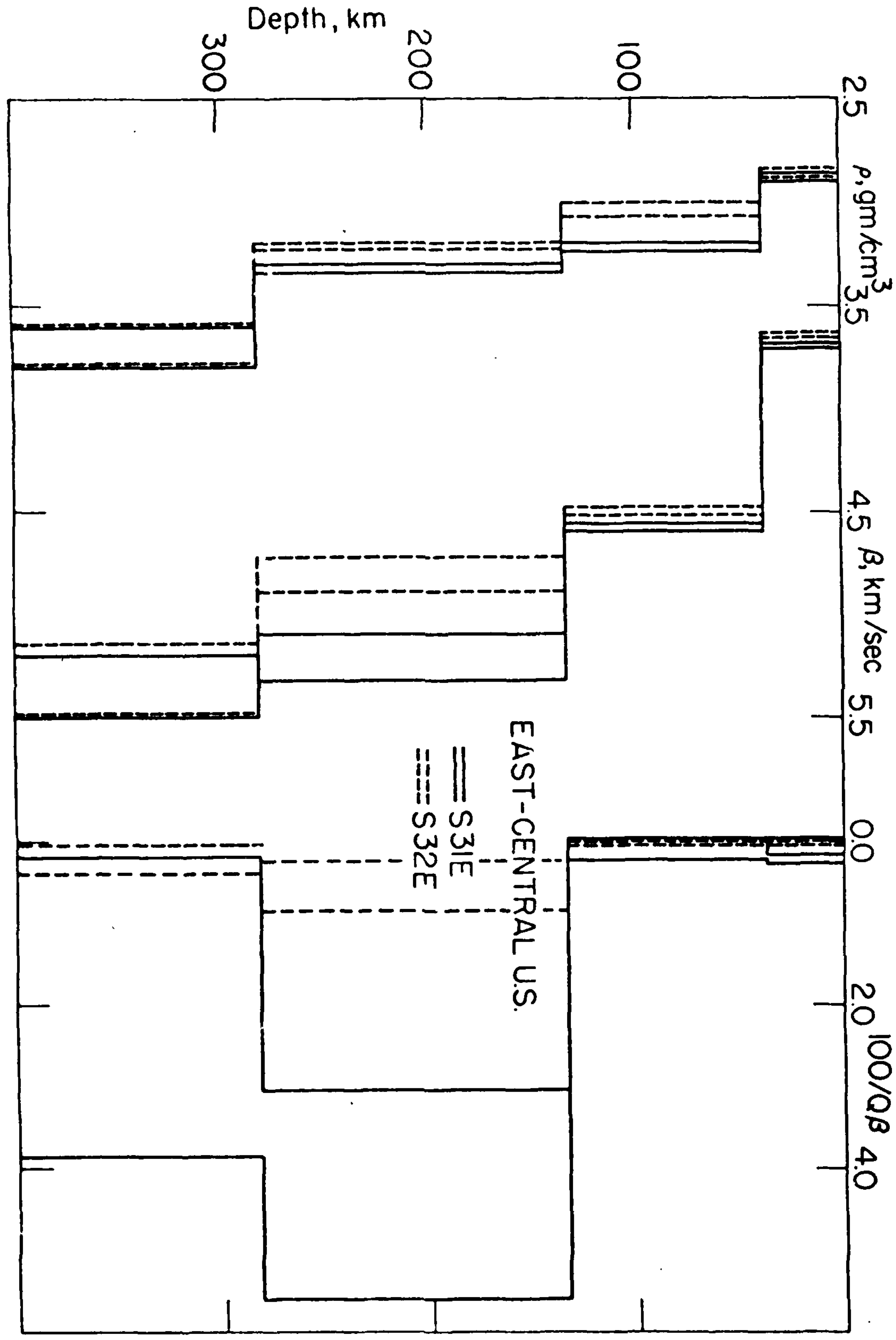
Depth, km
100
200
300
2.5
ρ, gm/cm³
3.5
4.5
β, km/sec
5.5
0.0
2.0
100/Qβ
4.0
EAST-CENTRAL U.S.
S31E
S32E

Table 6.10. Envelopes of shear velocity and shear attenuation at 1 Hz and density; simultaneous inversion results of Love and Rayleigh wave phase velocity and attenuation in western North America.

Layer no.	Depth (km)	minimum β, km/sec			maximum β, km/sec		
		S31W	S32W	S33W	S31W	S32W	S33W
2	2-21	3.527	3.529	3.533	3.492	3.621	3.637
3	21-45	3.897	3.886	3.812	4.012	4.052	4.029
4	45-84	4.382	4.259	4.293	4.583	4.549	4.690
5	84-160	4.105	4.012	3.823	4.463	4.412	4.263
6	160-350	4.782	4.750	4.702	5.500	5.500	5.500

Layer no.	Depth (km)	minimum $100/Q_\beta$			maximum $100/Q_\beta$		
		S31W	S32W	S33W	S31W	S32W	S33W
2	2-21	0.274	0.148	0.051	0.490	0.282	0.118
3	21-45	0.059	0.0	0.0	0.250	0.149	0.105
4	45-84	0.0	0.0	0.0	0.447	0.137	0.087
5	84-160	4.200	2.000	0.453	5.33	2.337	0.783
6	160-350	1.350	0.119	0.084	3.64	0.782	0.860

Layer no.	Depth (km)	minimum ρ, g/cm^3			maximum ρ, g/cm^3		
		S31W	S32W	S33W	S31W	S32W	S33W
2	2-21	2.807	2.846	2.850	2.900	2.90	2.90
3	21-45	3.070	3.042	3.000	3.300	3.30	3.30
4	45-84	3.200	3.200	3.200	3.434	3.50	3.50
5	84-160	3.200	3.200	3.200	3.491	3.441	3.50

Table 6.11. Starting model for inversion of phase velocity and attenuation in east-central North America (case $\nu = o$)

Depth, km	β, km/sec	α, km/sec	ρ, g/cm^3	100/Q_β
0-11	3.5	6.1	2.9	0.1
11-20	3.68	6.2	2.9	0.1
20-38	3.94	6.4	2.9	0.1
38-62	4.75	8.15	3.3	0.1
62-102	4.61	8.20	3.3	0.1
102-135	4.45	8.20	3.4	0.1
135-212	4.45	8.20	3.4	2.3
212-350	4.45	8.20	3.4	2.3
∞	4.80	8.70	3.6	2.3

Table 6.12. Envelopes of shear velocity and shear attenuation at 1 Hz, and density in east-central North America

Layer no.	Depth (km)	Minimum β, km/sec		Maximum β, km/sec	
		S31E	S32E	S31E	S32E
1	0-38	3.684	3.659	3.692	3.666
2	38-82	4.557	4.478	4.594	4.513
3	82-134	5.092	4.719	5.321	4.890
4	134-350	5.200	5.147	5.500	5.500

Layer no.	Depth (km)	Minimum $100/Q_\beta$		Maximum $100/Q_\beta$	
		S31E	S32E	S31E	S32E
1	0-38	0.165	0.037	0.263	0.055
2	38-82	0.0	0.0	0.222	0.048
3	82-134	3.056	0.241	5.630	0.831
4	134-350	0.182	0.036	3.846	0.364

Layer no.	Depth (km)	Minimum ρ, g/cm^3,		Maximum ρ, g/cm^3	
		S31E	S32E	S31E	S32E
1	0-38	2.896	2.895	2.900	2.900
2	38-82	3.200	3.000	3.241	3.010
3	82-134	3.200	3.200	3.327	3.220
4	134-350	3.600	3.600	3.800	3.800

varying as a power of the frequency ($\nu=1/2$). The corresponding envelopes in data space are illustrated for these models in Figures 6.20, 6.21, 6.22 and 6.23.

d. Rayleigh waves in the central Pacific

The starting models of α, β, ρ and Q_β^{-1} are listed in Table 6.13. The starting model of the crust is modified from the 'standard crustal section' of Forsyth (1975a), in which 5 km of water layer, 0.2 km of sedimentary layer and 6.8 km of crustal layer are assumed. For the starting model of the mantle, the density is 3.4 - 3.5 g km^3, the S-wave velocity β is 4.35 km/sec in the LVZ (50-220 km) and 4.60 km/sec in the high velocity lid. P wave velocities are basically from the assumption of a Poisson solid, $\alpha \sim 1.7\beta$ (<220 km depth) and $\alpha \sim 1.8\beta$ (>220 km depth). The starting model for Q_β^{-1} is taken from Mitchell (1976).

No extensive test for the frequency dependence of Q has been performed since the Q_R^{-1} data are relatively poor. The averaging kernels E_{kj} for Rayleigh waves are shown in Figure 6.24 for four layers. The envelopes of shear velocity β and shear attenuation Q_β^{-1} are given in Table 6.14 and in Figure 6.25 for a dispersion model (S21P) with Q independent of frequency. The corresponding envelopes in data space are illustrated for these models in Figures 6.2 and 6.26. Dotted lines in Figures 6.25, 6.2 and 6.26 are the averaged best model and its predicted data, respectively.

Fig. 6.20. Love wave phase velocity, east-central North America. Observations are shown by circles; vertical bars represent standard deviations. The envelope is associated with the extreme earth model bounds from inversion S31E. Open circles are incompatible data for this inversion.

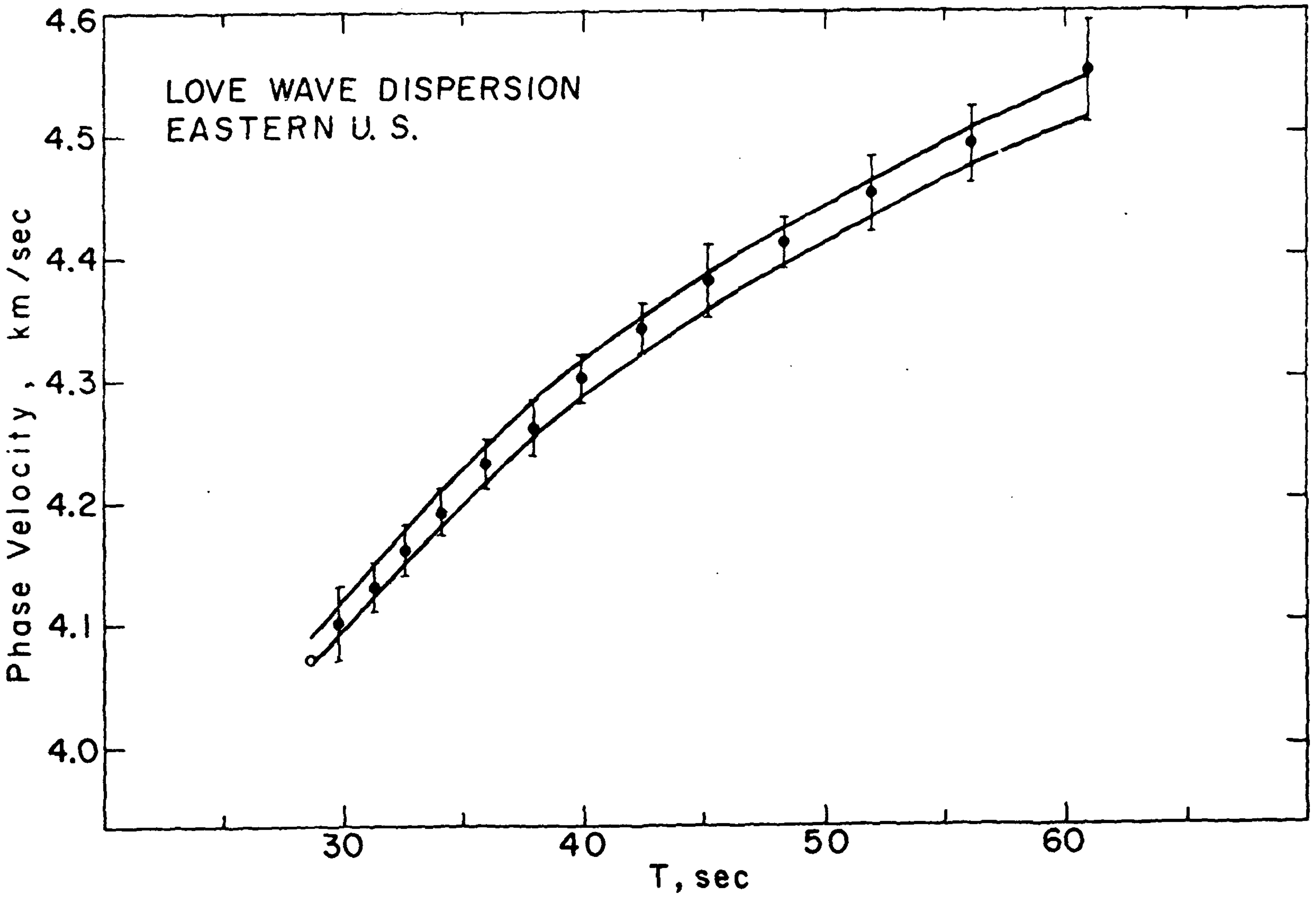
LOVE WAVE DISPERSION
EASTERN U. S.
Phase Velocity , km/sec
4.6
4.5
4.4
4.3
4.2
4.1
4.0
T, sec
30
40
50
60

Fig. 6.21. Rayleigh wave phase velocity, east-central North America. Observations are shown by circles; vertical bars represent standard deviations. The envelope is associated with the extreme earth model bounds from inversion S31E. Open circles are incompatible data for this inversion.

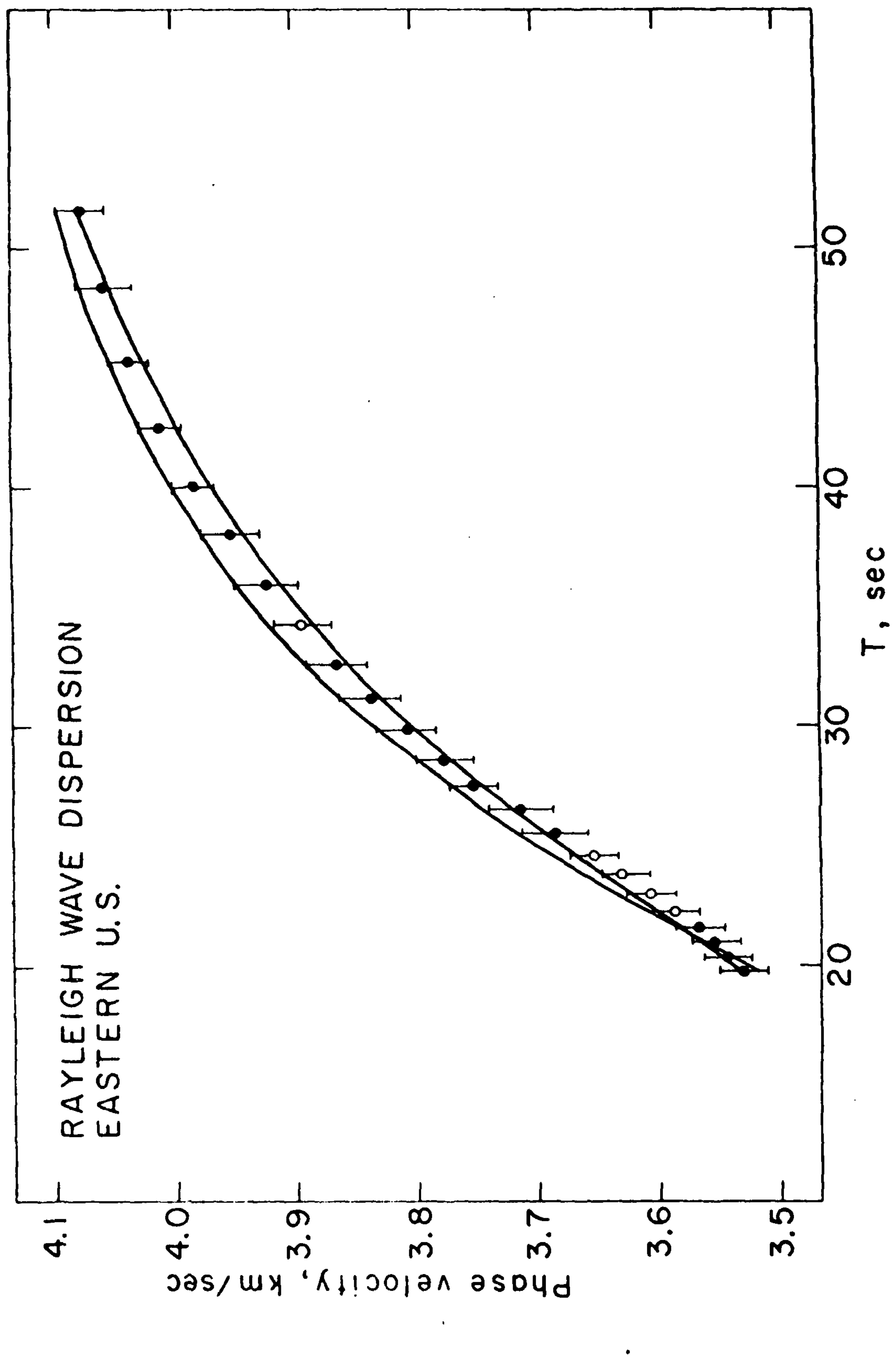
RAYLEIGH WAVE DISPERSION
EASTERN U.S.
T, sec
20
30
40
50
Phase velocity, km/sec
4.1
4.0
3.9
3.8
3.7
3.6
3.5

Fig. 6.22. Love wave attenuation, east-central North America. Circles are observations; vertical bars represent standard deviations. The solid lines represent the envelope associated with extremal earth models for inversion S31E. Open circles are incompatible data for this inversion.

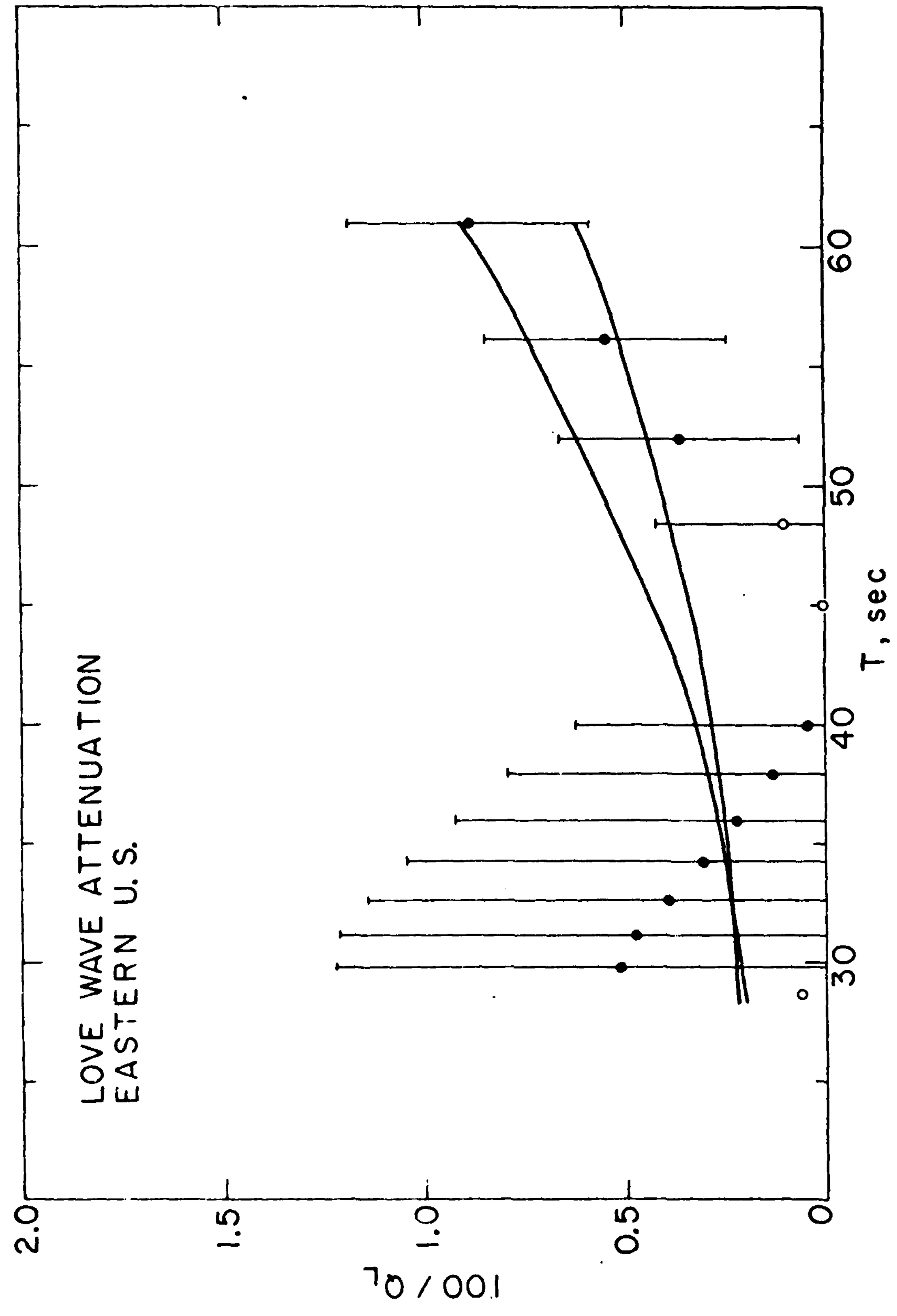
LOVE WAVE ATTENUATION
EASTERN U.S.
100 / Q_L
2.0
1.5
1.0
0.5
0
T, sec
30
40
50
60

Fig. 6.23. Rayleigh wave attenuation, east-central North America. Circles are observations; vertical bars represent standard deviations. The solid lines represent the envelope associated with extremal earth models for inversion S31E. Open circles are incompatible data for this inversion.

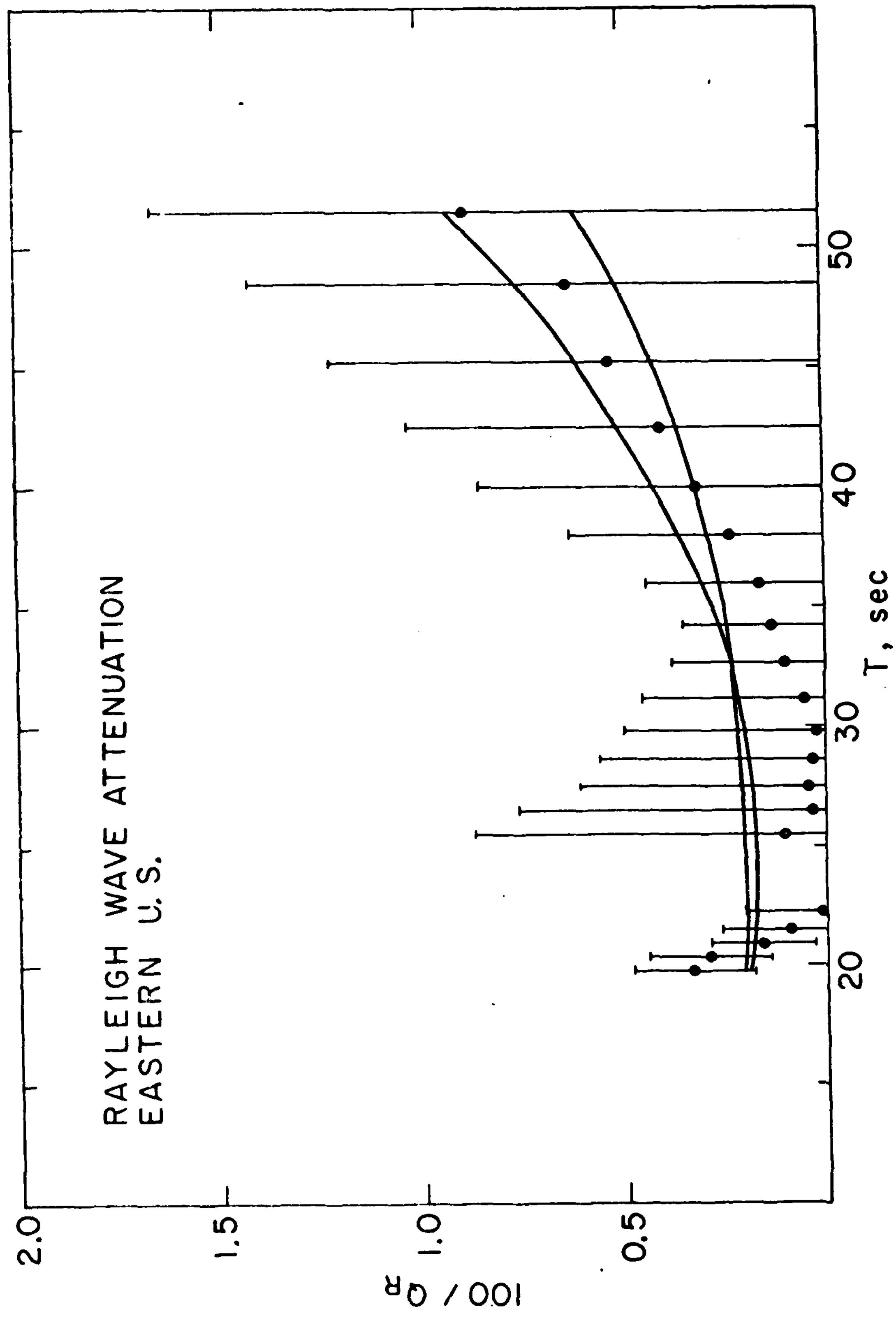
RAYLEIGH WAVE ATTENUATION
EASTERN U.S.
T, sec
20
30
40
50
2.0
1.5
1.0
0.5
100 / Q_R

Fig. 6.24a. Resolving kernels for shear velocity at selected depths (arrows), using Rayleigh wave data in the central Pacific. Model standard deviations are shown at the right.

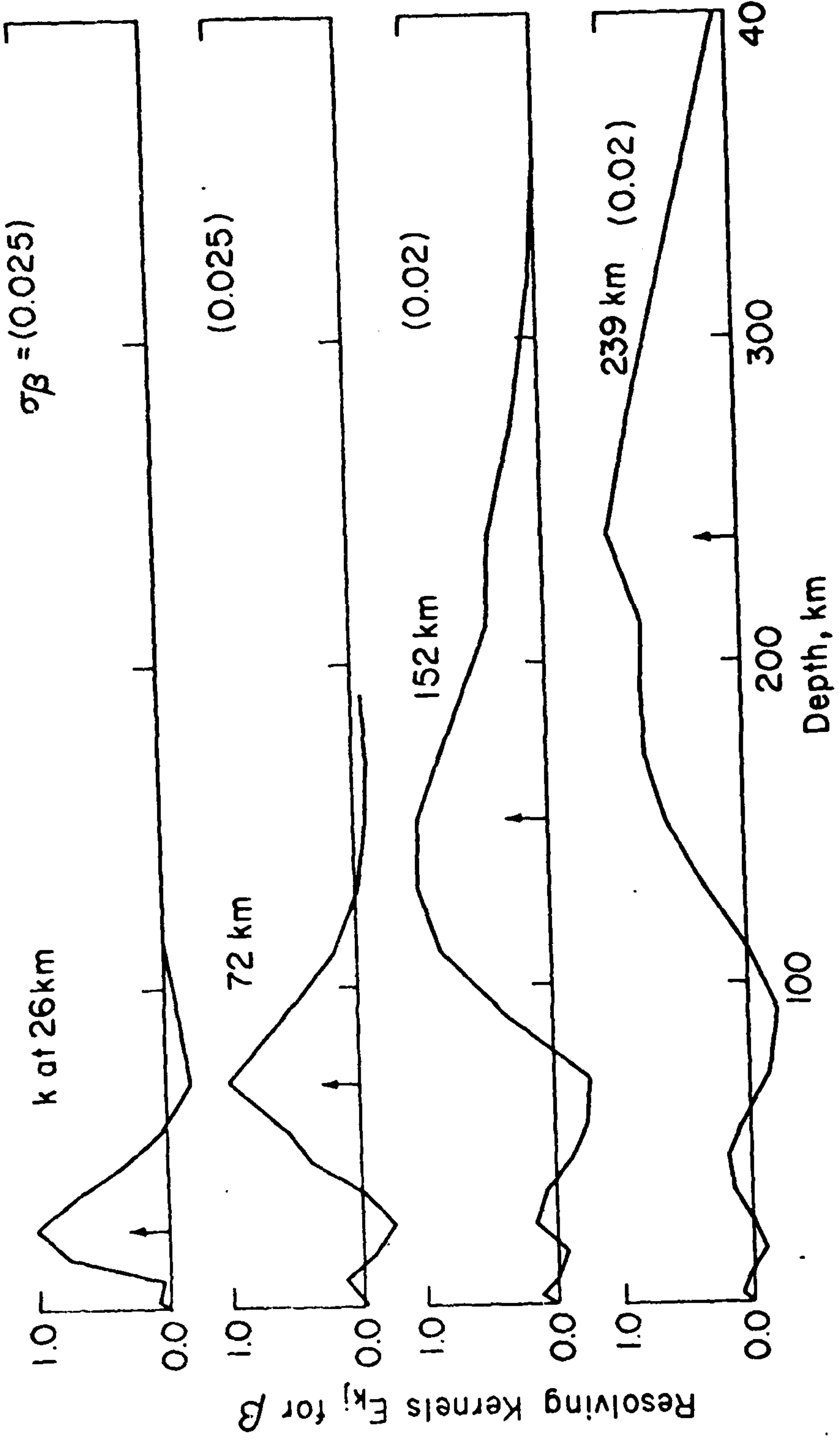
σβ = (0.025)
k at 26km
(0.025)
72 km
(0.02)
152 km
239 km (0.02)
1.0
0.0
1.0
0.0
1.0
0.0
1.0
0.0
100
200
300
400
Depth, km
Resolving Kernels E_kj for β

Fig. 6.24b. Resolving kernels for shear attenuation at selected depths (arrows), using Rayleigh wave data in the central Pacific. Model standard deviations are shown at the right.

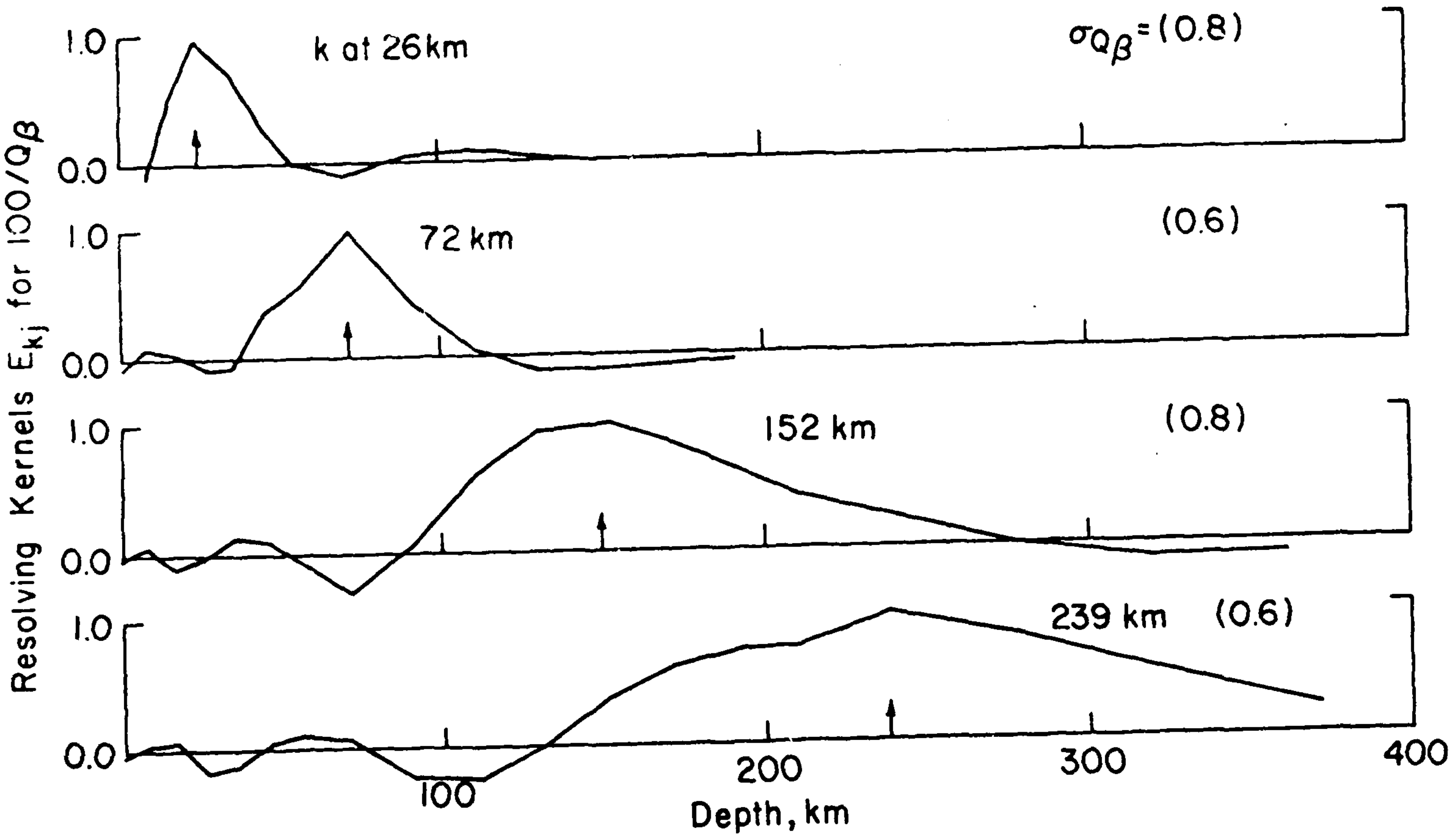
Resolving Kernels E_{kj} for $100/Q_\beta$
1.0
0.0
k at 26km
σ_{Q_β}=(0.8)
72 km
(0.6)
152 km
(0.8)
239 km
(0.6)
100
200
300
400
Depth, km

Fig. 6.25. Envelopes of shear velocity (at 1 Hz) and attenuation for the central Pacific, model S21P. Solid lines represent envelopes of S21P.

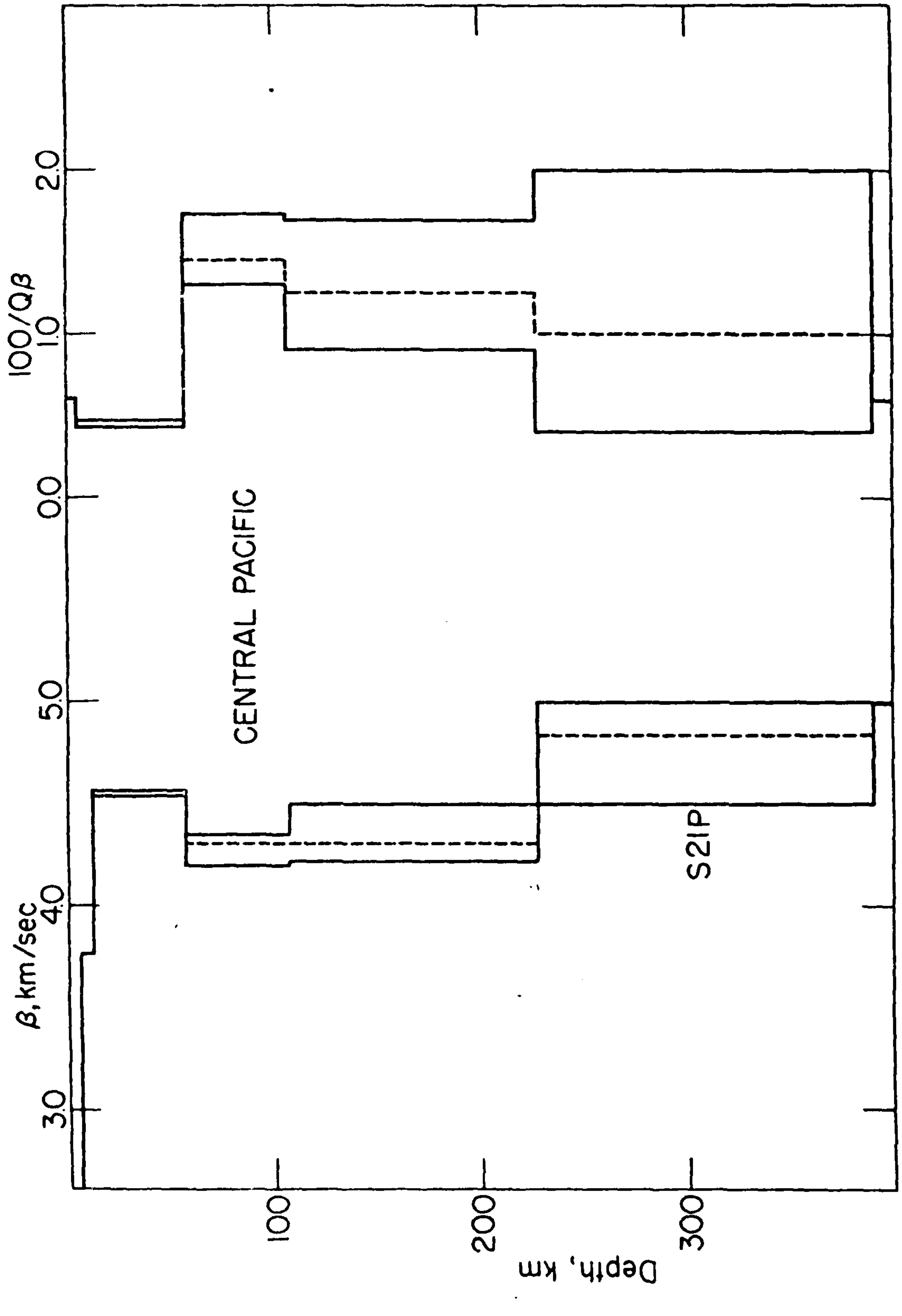
CENTRAL PACIFIC
S21P
100/Qβ
β, km/sec
Depth, km
0.0
1.0
2.0
3.0
4.0
5.0
100
200
300

Fig. 6.26. Rayleigh wave attenuation, central Pacific circles are observations; vertical bars represent standard deviations. The solid lines represent the envelope associated with extremal earth models for inversion S21P. Open circles are incompatible data for this inversion.

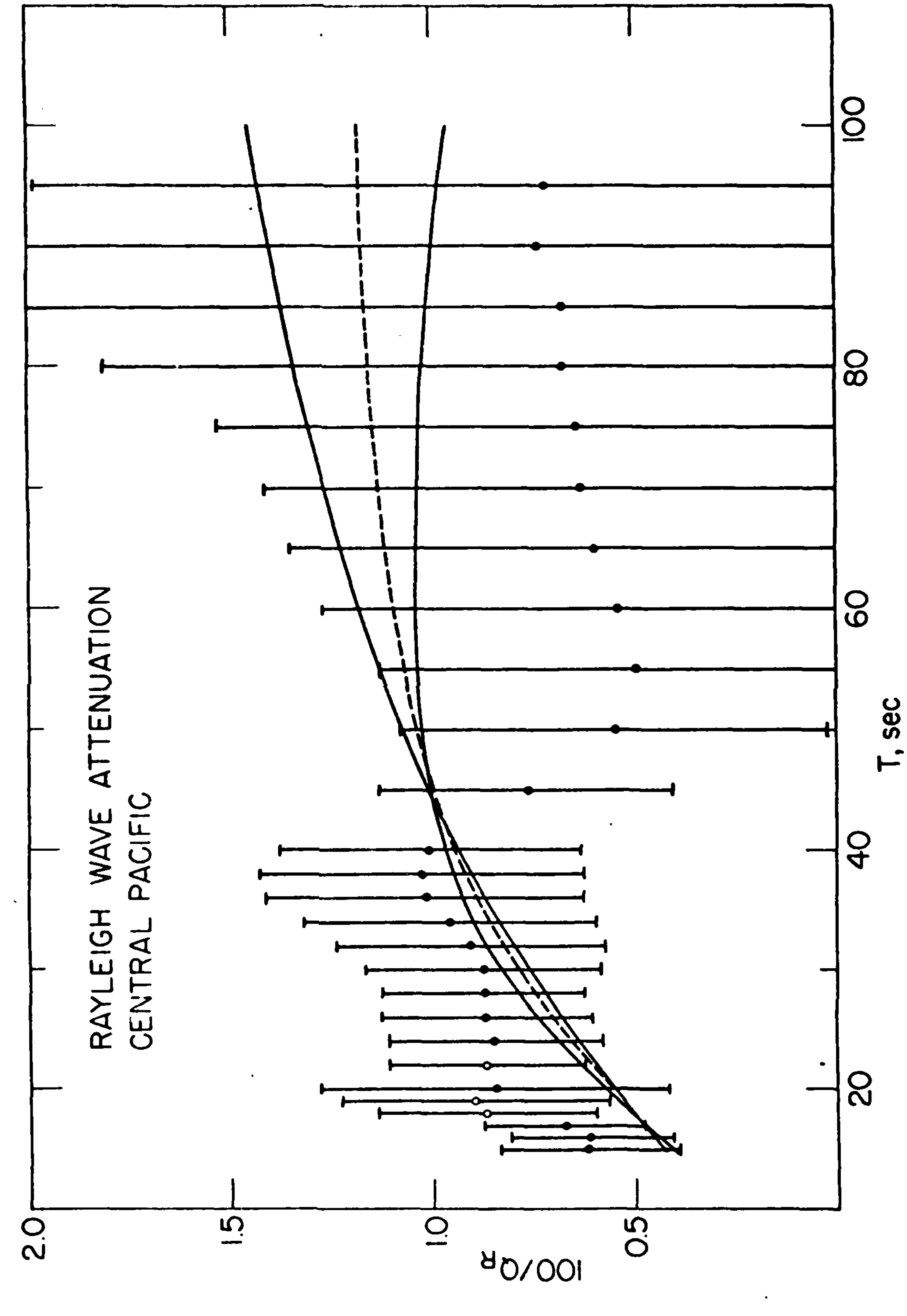
RAYLEIGH WAVE ATTENUATION
CENTRAL PACIFIC
2.0
1.5
1.0
0.5
100/Q_R
20
40
60
80
100
T, sec

Table 6.13. Starting model for the central Pacific

Depth, km	β, km/sec	α, km/sec	ρ, g/cm^3	$100/Q_\beta$
0-5	0.0	1.52	1.03	0.80
5-5.2	1.0	1.70	2.20	0.80
5.2-12	3.76	6.53	3.00	0.60
12-16	4.60	8.17	3.34	0.60
16-27	4.60	8.17	3.34	0.60
27-37	4.60	8.17	3.34	0.60
37-47	4.60	8.17	3.34	0.60
47-57	4.35	7.70	3.40	0.50
57-67	4.35	7.70	3.40	0.50
67-87	4.35	7.70	3.44	1.00
87-107	4.35	7.70	3.44	1.00
107-127	4.35	7.70	3.44	1.20
127-147	4.35	7.70	3.44	1.20
147-167	4.35	7.70	3.44	1.00
167-187	4.35	7.70	3.44	1.00
187-207	4.35	7.70	3.44	1.00
207-227	4.35	7.70	3.44	1.00
227-262	4.60	8.49	3.50	0.60
262-302	4.60	8.49	3.50	0.60
302-352	4.80	8.81	3.50	0.40
352-402	4.80	8.81	3.50	0.40
∞	5.00	9.00	3.76	0.40

Table 6.14. Envelopes of shear velocity and shear attenuation at 1 Hz in the Pacific

Layer no.	Depth (km)	Minimum β	Maximum β
4	12-59	4.542	4.571
5	57-107	4.195	4.350
6	107-227	4.212	4.516
7	227-402	4.50	5.00

Layer no.	Depth (km)	Minimum $100/Q_\beta$	Maximum $100/Q_\beta$
4	12-57	0.413	0.44
5	57-107	1.295	1.742
6	107-227	0.90	1.695
7	227-402	0.404	2.00

6.3 Discussion: a. Love waves in western North America

An important result of the simultaneous inversion is that the low velocity zone and the low Q zone coincide beneath western North America, at least for the surface wave frequency band (Figures 6.9 and 6.10). The mechanisms that contribute to a decreased shear wave velocity must also account for enhanced attenuation in shear.

A second immediate conclusion from these inversion results is that the envelopes of earth models derived by simultaneous inversion of phase velocity and attenuation are not identical to the envelopes of β and Q_β^{-1} models obtained from separate inversion of velocity and Q^{-1} data (Figures 6.9 and 6.10); see Appendix V. While the envelopes show a broad similarity for the two approaches, there are significant differences, particularly within depth intervals over which Q^{-1} and the accompanying intrinsic dispersion are relatively large. At short-period body wave frequencies, the shear wave velocities below 80 km depth for both individual earth models and envelopes of models are substantially higher than those determined without regard for anelasticity.

The simultaneous inversion results in two improvements for the attenuation problem over inversion of Q^{-1} data alone. One improvement is in the resolution in Q_β^{-1} versus depth. As shown in Table 6.15 for frequency independent Q models,

TABLE 6.15 Envelopes of shear velocity (at 1 Hz) and shear attenuation for frequency independent Q models by various inversion procedures, for Love waves in western North America

Layer no.	Depth (km)	minimum β , km/sec			maximum β , km/sec		
		E1	QC1	S1	E1	QC1	S1
1	0-21	3.238	3.236	3.263	3.403	3.407	3.411
2	21-45	3.725	3.711	3.730	4.329	4.398	4.325
3	45-84	4.196	4.144	4.235	4.325	4.873	4.837
4	84-160	4.000	4.117	4.243	4.561	4.935	4.796
5	160-350	4.666	4.953	5.028	5.151	5.742	5.438

Layer no.	Depth (km)	minimum $100/Q_\beta$		maximum $100/Q_\beta$	
		E1	S1	E1	S1
1	0-21	0.0	0.0	0.65	0.67
2	21-45	0.0	0.0	0.25	0.27
3	45-84	0.0	0.0	0.25	0.21
4	84-160	5.51	4.53	9.41	7.38
5	160-350	0.50	2.63	3.50	3.78

the bounds on Q_β^{-1} in the low Q zone are narrower by roughly a factor of 2 in Q^{-1} for model S1 than for model E1 obtained by inversion only of Love wave attenuation data. The second improvement is in the fit of predicted and observed Q_L^{-1} data, especially in the period range 20 to 25 sec where observations of nearly zero Q_L^{-1} occur in the data set for western North America and commonly in other areas as well (e.g. Tsai and Aki, 1969). In Lee and Solomon (1975), the data in this period range were concluded to be incompatible by set theoretical inversion. Such an apparent incompatibility does not arise in the complete formulation of complex earth model and observations.

It is of interest to compare the simultaneous inversion of this paper with the approach recently used by Anderson et al. (1977), Anderson and Hart (1976) and Hart et al. (1976, 1977). The technique adopted by these workers has been to correct the real part of their data for the effect of anelasticity, using equation (4.8) and the Anderson and Archambeau (1964) theory, and then to invert their corrected (real) data to obtain an elastic (real) earth model. The method of Anderson, Hart and others is not mathematically equivalent to the complete anelastic earth problem, equation (5.8); a comparison of the two approaches is given in Appendix V. Because of the complicated dependence of $\partial c_1/\partial\beta_2$ on depth (Figure 6.7a), and because of the significant coupling of $\partial c_1/\partial\beta_2$ with anelastic dispersion, the two approaches do not yield identical results, particularly when the observational frequencies are far from the reference frequency or when the observational frequency band is wide (see Appendix V). For some earth structures, the two sets of results can differ substantially.

A comparison of the two inversion approaches for the Love wave data set for western North America illustrates some of the differences in their predictions. The bounds on β and Q_β^{-1} in the earth for S1 are compared in Table 19 with those for model QC1 (for Q-corrected), obtained by first correcting the observed phase velocities following Liu _et al._ (1976) and Anderson _et al._ (1976) for the Q^{-1} model of Figure 6.4 and then performing an inversion of the corrected real data. The 'best' model for the two different approaches (S11 and QC11) characterize well the differences between the two techniques (see Figure 6.11). The Anderson-Hart approximation yields a monotonically increasing velocity structure while the simultaneous inversion yields a β model with a slight low velocity zone.

All of the proposed dispersion-attenuation relations lead to earth models that can fit the phase velocity and Q^{-1} data, but the various models have very different frequency dependences. The intrinsic dispersion in β within the low Q zone varies from about 10 percent for S1 to 1 percent for S5 between frequencies of .01 and 1 Hz. For frequency independent Q, the need for a low velocity zone disappears for frequencies near 1 Hz and above, though low velocity zones for shear waves are required at that frequency for the other dispersion-attenuation relations. The frequency dependence of Q^{-1} is also obviously different for the various dispersion-attenuation relations, varying from constant to a slowly decreasing function of frequency to a complicated frequency dependence for relaxation models. The inversion in this thesis for relaxation model S5 is of course not general because only a few isolated relaxation peaks and only fixed relaxation times and relative relaxation strengths were considered. The surface wave data alone do not contain enough independent information to regard the spectrum of relaxation times and relaxation strengths to be free parameters that vary with depth.

Broad band observations of body wave velocities and amplitudes offer the greatest promise for narrowing the range of possible dispersion-attenuation relations. Probably, a constant Q model can be discarded at present, at least for frequencies near 1 Hz and above, because of the prediction of such a model that a low velocity zone in western North America may disappear at such frequencies, clearly untrue (Archambeau et al., 1969), and because the lateral variation in amplitudes predicted for short period P and S waves from Q^{-1} models fit to long period surface wave and body wave data are much larger than observed (Solomon et al., 1970; Der et al., 1975). To discriminate among the other proposed models or to test more complicated relaxation models, phase and amplitude spectra of P and S waves that have passed through the low Q, low velocity zone should ideally be obtained over a frequency band spanning .001 to 10 Hz.

When such tests are conducted, it will be important to explore fully the assumption that the measured amplitude losses for surface waves are due only to anelasticity. If a scattering mechanism is an important contributor to the losses, then both the inferred Q_β^{-1} structure and the associated dispersion in β may differ considerably from the results reported here.

b. Love and Rayleigh waves in western North America

The most serious problem here may be SV/SH anisotropy in western North America. Love and Rayleigh wave phase velocities are incompatible for almost the entire common frequency range. Also as indicated in Chapter II, Rayleigh wave attenuation Q_R^{-1} in the period range 35-40 seconds shows disagreement with Love wave attenuation Q_L^{-1}. This is not a consequence of simultaneous inversion but appears to be a consequence either of anisotropy or of some interference effects in the waveforms analyzed. The measurements of Rayleigh wave phase velocity in Solomon (1971) are comparatively lower than other reported measurements in the western United States (Biswas and Knopoff, 1974). However, if we look at the contour map of P_n velocity in western United States (Archambeau et al., 1969) the path between LON and TUC lies in a low P_n velocity 'valley'. To fit the phase velocity curve for Rayleigh waves, a LVZ seems to be necessary contrary to the result of separate Love wave inversion in the previous section. This particular path may be complicated by multiplying effects and/or mode conversions.

c. Love and Rayleigh waves in east-central North America

The simultaneous inversion results for east-central North America give a thick lithosphere and a monotonically increasing velocity model at 1 Hz. A LVZ may not be required at 1 Hz. However, a LQZ is probably present at depths greater than 130 km.

A second result of simultaneous inversion is that the S-wave velocities in other than the crust are increased considerably and density is decreased compared to the results of separate inversion of phase velocity. At the same time, for Q independent of frequency, Q_β^{-1} in the asthenosphere seems to be greater than predicted by the results of separate inversion.

The frequency dependent Q_β^{-1} models are also satisfactory for predicting observations. To discriminate among the possible dependences of Q_β^{-1}, more precise measurements of Q^{-1} must be made.

Similarly, as described in the previous section, the data incompatibility in some period range which occurred in the separate inversion for Q^{-1} does not arise in the simultaneous inversion. The incompatibilities which are indicated in Figures 2.6c and d did not occur in the simultaneous inversion.

d. Rayleigh waves in the central Pacific

The results of simultaneous inversion for β and Q_β^{-1} in the central Pacific are shown in figure 6.25. The LVZ and LQZ coincide and are extensive (60 and 225 km depth). The lithospheric thickness is less than in western North America (tectonic) and east-central North America (shield).

Compared to the Forsyth's models (Table 9, 1975a; Figure 9, 10, and 11, 1977), the result of simultaneous inversion, model S21P, shows a similar shear velocity profile to 135 m.y. old ocean even though model S21P represents 80-90 m.y. old ocean on the average. Forsyth suggested 80-90 km as the starting depth of partial melting. Model S21P suggests a shallower asthenosphere at 60 km depth, which agrees with Mitchell's (1976) model. This is probably because Q^{-1} profile may give a different result from that by velocity profile. Shear velocity at depths greater than 220km may be much higher than any of Forsyth's models. Otherwise the LVZ will terminate at much shallower depth.

Compared with Mitchell's Q model (1976), the noticeable differences are that the LQZ may extend deeper than 220 km and that the LQZ is more pronounced. The Q structure deeper than 220 km is not resolved very well. At around 100 sec period, Mitchell's Q_R^{-1} data were incompatible.

CHAPTER VII

Conclusions

Determining the variation of anelastic properties such as seismic attenuation within the earth's interior both vertically and laterally can be a useful tool to study the physical state of the earth's interior. This is particularly true of the upper mantle, where seismic energy absorption is highest. A precise determination of such properties will help many seismic studies, including those on seismic sources, path effects and seismic discrimination. Also the anelastic properties provide valuable hints on the tectonic history of the earth. For example, zones of active continental-continental collision may be characterized by unusually high attenuation such as under Tibet (Bird, 1976). The thickness of the lithosphere, or high-Q lid, is closely related to lithosphere age and deeper lateral variations may reflect sub-lithospheric convection flow patterns.

However, we have seen several negative aspects of the seismic attenuation studies. First, the anelastic behavior of materials under such high temperature and pressure conditions as in the earth's mantle is poorly known, because such conditions are very difficult to reproduce in the laboratory. At present we must rely mostly on seismic data. Secondly, much of the seismic data available now are determined by few samples with large uncertainties. Moreover, the seismic amplitudes often have been subject to geometrical complications, such as scattering, mode conversion and multipathing effects. Because of all these difficulties, many of the seismic attenuation studies have produced either inconclusive results or even physically implausible results.

One area where most such complications can be overcome is the study of surface wave attenuation. Many advantages of the surface wave attenuation method are reviewed by Anderson et al. (1965). Surface wave amplitudes are often the most prominent feature of the seismogram. The geometrical spreading factor for surface waves can be easily corrected. Surface waves have been less subject to scattering because of their long periods, and, most importantly, surface waves penetrate deep into the earth's upper mantle, where the LQZ exists.

The relatively long period data of surface wave attenuation are still not free of geometrical effects, as are discussed in section 2.6.5. For example, when a seismic wave with wavelength 100 km travels 2000 km distance, an inhomogeneity larger than 10 km could cause non-negligible scattering effects. These kind of geometrical complications have been observed by Tryggvason (1965), Tsai and Aki (1969) and Solomon (1971).

The contamination of seismic surface wave attenuation measurements by such effects causes problems in the inversion of such data. For contaminated and uncertain data, an L_1 norm type of inversion has clear advantages compared to L_2 norm approaches (see details in section 2.3). L_2 norm inversions (least-square type) have often produced physically impossible negative Q^{-1} solutions. L_1 norm inversion, developed as the set theoretical approach, which includes the square matrix inverse and the linear programming technique, and applied to North America and the Pacific in this thesis, gives a number of advantages. The geometrical visualization of the square matrix inverse can be useful to select the proper layering. By choosing proper layer thicknesses, the solution domain can move into the physically meaningful positive domain and be more strongly focussed. A bad layering can either lead the solution domain into the negative domain or widely spread it out. Also we can sort out incompatible data, defined as data which do not contribute to build the solution domain in L_1 norm inversions, a phenomenon noted for data from the minima in Q^{-1} at 20-25 second period in Solomon's data (1971). The linear programming technique can define the lower and upper bounds of the solution domain. Because of the poor statistics of attenuation data, it is often not meaningful to pursue a single best model.

The question of whether linearity of seismic attenuation mechanisms is justifiable is important. In the past, non-linearity was considered from several aspects. First, Knopoff (1956, 1959) argued that the observations of Q independent of frequency are incompatible with linear mechanisms, which show a strong frequency dependence. Second, laboratory experiments of stress-strain hysteresis show a cusp in the hysteresis curve (non-linearity) for strain amplitudes greater than 10^{-6}. Seismic strain amplitudes are small but marginal in this regard. Another aspect of the argument comes from the fact that body waves do not show dispersion, which is a main characteristic of linearity.

However, Orowan (1967) and Liu et al. (1976) showed that a band-limited superposition of linear mechanisms can explain the first argument. Also a slight frequency dependence, which has not been fully tested with still largely uncertain and limited observations, could explain a limited dispersion at short body wave periods. Efforts to search for the effects of such body wave dispersion should be continued. Because the second argument against linearity is marginal, we prefer to retain linearity for the clear computational advantages arising from the superposition principle.

Linearity is controlled by the causality principle as well as the superposition principle. The causality principle, 'no signal before stimulus', requires accompanying dispersion (anelastic dispersion) if there is absorption. The causality principle has often been violated in seismic studies. The assumptions of Q independent of frequency and of perfect elasticity (no dispersion) under linearity are incompatible.

The consequence of neglecting anelastic dispersion is tremendous. The existing perfectly elastic earth models are either misrepresented or cannot be compared fairly with each other. Intrinsic dispersion of shear velocity is an important consequence of anelasticity, particularly within the low-Q zone beneath oceanic and tectonically active regions. Beneath western North America, dispersion can be as great as 10 percent over two decades in frequency, depending on the frequency dependence of Q^{-1}.

One of the important consequences of anelastic dispersion is that the 'baseline discrepancy' question is resolved (Anderson et al., 1977). Sipkin and Jordan (1975) suggested a 'continental bias' might be the cause of this 'base line discrepancy'. If anelastic dispersion is considered, no deep continent-ocean differences are necessary.

Simultaneous inversion is a proper approach to consider the effect of anelastic dispersion which is a first order correction to anelastic velocity models compared to a second order effect in perfectly elastic models. The simultaneous inversion approach is formally different from the approximate inversion scheme of Anderson and Hart (1976) and gives different results. The differences can be amplified when the observational frequency range is wide and/or the reference frequency is far from the observational frequencies. No matter how the observational frequency band is spread, no matter where we choose a reference frequency, a given dispersion-attenuation relationship may be used to extrapolate models to any frequencies.

The difference between the simultaneous inversion approach and the approximate approach of Anderson and Hart (1976) is larger for Love waves than for Rayleigh waves, simply because the partial derivatives of off-diagonal terms for Rayleigh waves are much smaller than for Love waves (see Appendix V). However, most of the advantages are still retained for Rayleigh waves by use of simultaneous inversion.

Other consequences of simultaneous inversion are that the incompatibility in the attenuation data set decreases substantially and the resolution in Q^{-1} versus depth in the earth is improved for a given dispersion-attenuation relation over the separate inversion of Q^{-1} data alone.

The most interesting results of the inversions are the lateral variations of mantle structure. A distinctive LQZ seems to exist everywhere we have data, including western North America (tectonic), east-central North America (stable platform) and the central Pacific (oceanic). However, the thicknesses of the high-Q lid varies from place to place: 60±20 km in the central Pacific, 80±20 km in western North America and 130±30 km in east-central North America. These results are related to the differing tectonic history of each region. In east-central North America, a thick lithosphere has grown over time, and the asthenosphere shows relatively mild attenuation as well as the possibility of no LVZ at a frequency of 1 Hz. In western North America, a thinner lithosphere with substantially higher attenuation in the asthenosphere is characteristic. Many authors have suspected there is substantial partial melting in the asthenosphere of this region. The excess heat necessary to produce melting may have been related to the recent subduction of oceanic lithosphere along western North America.

The LVZ and LQZ coincide in western North America. The inversion of Love wave data alone shows that the assumption of Q independent of frequency over the entire seismic band leads to the removal of the requirement for a LVZ for shear waves at frequencies above 1 Hz. The LVZ persists at these frequencies, however, in the results of the combined inversion of Love and Rayleigh wave data. However, a possible anisotropy problem in western North America may have contributed to an inability to discriminate among various dispersion-attenuation relations. In the Pacific, the LVZ and LQZ coincide as in western North America. The Pacific shows a thinner lithosphere (60 km thick) but lower shear attenuation Q_β^{-1} in the asthenosphere than in the tectonically active western North America.

Widening the period range of attenuation data, conducting more accurate measurements of Q, and confirming or disproving dispersion of body waves will be a good direction to pursue answers to some of the questions raised by this study.

References

Alexander, S.S., 1963. Surface wave propagation in the western United States, Ph.D. Thesis, California Institute of Technology, Pasadena, California, 242 pp.

Anderson, D.L., and C.B. Archambeau, 1964. The anelasticity of the earth, J. Geophys. Res., 69, 2071-2084.

Anderson, D.L. and R.L. Kovach, 1964. Attenuation in the mantle and rigidity of the core from multiply reflected core phases, Proc. Nat. Acad. Sci., 51, 168-172.

Anderson, D.L., and R.S. Hart, 1976. Absorption and the low velocity zone, Nature, 263, 397-398.

Anderson, D.L., and B.R. Julian, 1969. Shear velocities elastic parameters of the mantle, J. Geophys. Res., 74, 3281-3286.

Anderson, D.L., A. Ben-Menahem and C.B. Archambeau, 1965. Attenuation of seismic energy in the upper mantle, J. Geophys. Res., 70, 1441-1448.

Anderson, D.L., H. Kanamori, R.S. Hart, and H.-P. Liu, The earth as a seismic absorption band, 1977. Science, 196, 1104-1106.

Andrade, E.N. daC., 1911. On the viscous flow in metals, and allied phenomena, Proc. Roy. Soc. Lond., A84, 1-12.

Archambeau, C.B., E.A. Flinn, and D.G. Lambert, 1969. Fine structure of the upper mantle, J. Geophys. Res., 74, 5825-5865.

Azimi, Sh.A., A.Y. Kalinin, V.B. Kalinin and B.L Pivovarov, 1968. Impulse and transient characteristics of media with linear and quadratic absorption laws, Izv. Earth Phys., English Trans., No. 2, 88-93.

Backus, G.E., 1970. Inference from inadequate and inaccurate data I, Proc. Nat. Acad. Sci., 65, 1-7.

Backus, G.E., 1970. Inference from inadequate and inaccurate data II, Proc. Nat. Acad. Sci., 65, 281-287.

Backus, G., 1970. Inference from inadequate and inaccurate data III, Proc. Nat. Acad. Sci., 67, 282-289.

Backus, G. and F. Gilbert, 1967. Numerical applications of a formalism for geophysical inverse problems, Geophys. J. R. Astro. Soc., 13, 247-276.

Backus, G. and F. Gilbert, 1968. The resolving power of gross earth data, Geophys. J. R. Astr. Soc., 16, 169-205.

Backus, G. and F. Gilbert, 1970. Uniqueness in the inversion of inaccurate gross earth data, Phil. Trans. R. Soc. (London) A, 266, 123-213.

Becker, R., 1925. Elastiche nachwirkung und plastizität, Z. Phys., 33, 185-213.

Benioff, H., F. Press, and G. Smith, 1961. Excitation of the free oscillations of the earth by earthquakes, J. Geophys. Res., 66, 605-519.

Birch, F., and D. Bancroft, 1938. The effect of pressure on the rigidity of rocks, J. Geol., 1, 46-59.

Bird, P.G., 1976. Thermal and mechanical evolution of continental convergence zones: Zagros and Himalayas, Ph.D. Thesis, Mass. Inst. of Technology, Cambridge, Mass., 423 pp.

Biswas, N.N. and L. Knopoff, 1970. Exact earth-flattening calculation for Love waves, Bull. Seismol. Soc. Amer., 60, 1123-1137, 1970.

Biswas, N.N. and L. Knopoff, 1974. The structure of the upper mantle under the United States from the dispersion of Rayleigh waves, Geophys. J. R. Astr. Soc., 36, 515-539.

Bolt, B.A. and J. Dorman, 1961. Phase and group velocities of Rayleigh waves in a spherical gravitating earth, J. Geophys. Res., 66, 2965-2981.

Born, W.T., 1941. The attenuation constant of earth materials, Geophysics, 6, 132-148.

Budiansky, B. and R.J. O'Connell, 1977. Viscoelastic properties of fluid saturated cracked solids, J. Geophys. Res., in press.

Burton, P.W., 1974. Estimations of Q^{-1} from seismic Rayleigh waves, Geophys. J. R. Astr. Soc., 36, 167-189.

Burton, P.W., 1977. Inversions of high frequency $Q^{-1}(f)$, Geophys. J. R. Astr. Soc., 48, 29-51.

Burton, P.W. and B.L.N. Kennett, 1972. Upper mantle zone of low Q, Nature (London), 238, 87-90.

Carpenter, E.W. and D. Davies, 1966. Frequency dependent seismic phase velocities, an attempted reconciliation between the Jeffreys/Bullen and the Gutenberg models of the upper mantle, Nature, 212, 134-135.

Chernov, L.A., 1960. Wave Propagation in a Random Medium, Chapt. 13, McGraw-Hill, New York.

Christensen, R.M., 1971. Theory of Viscoelasticity, Academic Press, New York.

Claerbout, J.F. and F. Muir, 1973. Robust modelling with erratic data, Geophysics, 38, 826-844.

Collins, F. and C.C. Lee, 1956. Seismic wave attenuation characteristics from pulse experiments, Geophysics, 21, 16-39.

Daly, R.A., 1940. Strength and Structure of the Earth, Hafner Publishing Co., New York.

Dantzig, G., 1963. Linear Programming and Extensions, Princeton University Press.

Davies, D., 1967. On the problem of compatibility of surface wave data, Q, and body wave travel times, Geophys. J. R. Astr. Soc., 13, 421-424.

Der, Z.A. and M. Landisman, 1972. Theory for errors, resolution, and separation of unknown variables in inverse problems, with application to the mantle and the crust in southern Africa and Scandinavia, Geophys. J. R. Astr. Soc., 27, 137-178.

Der, Z.A. and T.W. McElfresh, 1977. The relation between anelastic attenuation and regional amplitude anomalies of short-period P waves in North America, Bull. Seismol. Soc. Amer., in press.

Der, Z.A., R.P. Masse, and M. Landisman, 1970. Effects of observational errors on the resolution of surface waves at intermediate distances, J. Geophys. Res., 75, 3399-3409.

Der, Z.A., R.P. Masse, and J.P. Gurski, 1975. Regional attenuation of short-period P and S waves in the United States, Geophys. J. R. Astr. Soc., 40, 85-106.

Derr, J.S., 1969. Free oscillation observations through 1968, Bull. Seismol. Soc. Amer., 59, 2079-2100.

Dziewonski, A.M., 1970. Correlation properties of free period partial derivatives and their relation to the resolution of gross earth data, Bull. Seismol. Soc. Amer., 60, 741-768.

Dziewonski, A. and M. Landisman, 1970. Great circle Rayleigh and Love wave dispersion from 100 to 900 seconds, Geophys. J. R. Astr. Soc., 19, 37-41.

Forsyth, D.W., 1975a. The early structural evolution and anisotropy of the oceanic upper mantle, Geophys. J. R. Astr. Soc., 43, 103-162.

Forsyth, D.W., 1975b. A new method for the analysis of multimode surface wave dispersion: application to Love wave propagation in the Earth Pacific, Bull. Seism. Soc. Amer., 65, 323-342.

Forsyth, D.W., 1977. The evolution of the upper mantle beneath mid-ocean ridges, Tectonophysics, 38, 89-118.

Franklin, J.N., 1970. Well-posed stochastic extensions of ill-posed linear problems, J. Math. Anal. Appl., 31, 628-716.

Futterman, W.I., 1962. Dispersive body waves, J. Geophys. Res., 67, 5279-5291.

Gilbert, F., 1971. Ranking and winnowing gross earth data for inversion and resolution, Geophys. J. R. Astr. Soc., 23, 125-128.

Goetze, C., 1971. High temperature elasticity and anelasticity of polycrystalline salts, Ph.D. Thesis, Harvard University, Cambridge, Mass., 90 pp.

Gordon, R.B. and L.A. Davis, 1968. Velocity and attenuation of seismic waves in imperfectly elastic rock, J. Geophys. Res., 73, 3917-3935.

Granato, A. and K. Lücke, 1956. Theory of mechanical damping due to dislocations, J. Appl. Phys., 27, 583.

Green, R.W.E. and A.L. Hales, 1968. The travel times of P waves to 30° in the central United States and upper mantle structure, Bull. Seism. Soc. Amer., 58, 267-289.

Gross, B., 1953. Mathematical Structure of the Theories of Viscoelasticity, Hermann and Cie., Paris.

Hart, R.S., D.L. Anderson, and H. Kanamori, 1976. Shear velocity and density of an attenuating earth, Earth Planet. Sci. Lett., 32, 25-34.

Hart, R.S., D.L. Anderson, and H. Kanamori, 1977. The effect of attenuation on gross earth models, J. Geophys. Res., 82, 1647-1654.

Haskell, N.A., 1953. The dispersion of surface waves on multilayered media, Bull. Seismol. Soc. Amer., 43, 17-34.

Isacks, B., Oliver, J. and Sykes, L.R., 1968. Seismology and the new global tectonics, J. Geophys. Res., 73, 5855-5899.

Jackson, D.D., 1969. Grain-boundary relaxations and the attenuation of seismic waves, Ph.D. Thesis, Mass. Inst. of Technology, Cambridge, Mass., 136 pp.

Jackson, D.D., 1971. The attenuation of Love waves and toroidal oscillations of the earth, Geophys. J. R. Astr. Soc., 25, 25-34.

Jackson, D.D., 1973. Marginal solutions to quasi-linear inverse problems in geophysics: the Edgehog method, Geophys. J. R. Astr. Soc., 35, 121-136.

Jackson, D.D. and D.L. Anderson, 1970. Physical mechanisms of seismic-wave attenuation, Rev. Geophys. Space Phys., 8, 1-63.

Jeffreys, J., 1958. A modification of Lomnizt law of creep in rocks, Geophys. J. R. Astr. Soc., 1, 92-95.

Jeffreys, H., 1965. Damping of S waves, Nature, 208, 675.

Jeffreys, H., 1975. Importance of damping in geophysics, Geophys. J. R. Astr. Soc., 40, 23-27.

Jeffreys, H. and S. Crampin, 1960. Rock creep: a correction, Mon. Not. Roy. Astron. Soc., 121, 571-577.

Johnson, C.E., 1972. Regionalized earth models from linear programming methods, M.S. Thesis, Mass. Inst. of Techn., Cambridge, Mass.

Jordan, T.H. and J.N. Franklin, 1971. Optimal solutions to a linear inverse problem in geophysics, Proc. Nat. Acad. Sci., 68, 291-293.

Jordan, T.H. and D.L. Anderson, 1974. Earth structure from free oscillations and travel times, Geophys. J. R. Astr. Soc., 36, 411-459.

Julian, B.R., 1970. Regional variations in upper mantle structure beneath North America, Ph.D. Thesis, Calif. Inst. of Techn., Pasadena, Calif.

Kanamori, H., 1970. Velocity and Q of mantle waves, Phys. Earth Planet. Int., 2, 259-275.

Kanamori, H. and D.L. Anderson, 1977. Importance of physical dispersion in surface waves and free oscillation problems: a review, Rev. Geophys. Space Phys., 15, 105-112.

Keilis-Borok, V.I. and T.B. Yanovskaya, 1967. Inverse seismic problems (structural review), Geophys. J. R. Astr. Soc., 13, 223-233.

Knopoff, L., 1956. The seismic pulse in materials possessing solid friction, I: plane waves, Bull. Seism. Soc. Amer., 46, 175-183.

Knopoff, L., 1959. The seismic pulse in materials possessing solid friction, II: Lamb's problem, Bull. Seism. Soc. Amer., 49, 403-413.

Knopoff, L., 1964. Q, Rev. Geophys., 2, 625-660.

Knopoff, L. and G.J.F. MacDonald, 1958. Attenuation of small amplitude stress waves in solids, Rev. Mod. Phys., 30, 1178-1192.

Knopoff, L. and L.D. Porter, 1963. Attenuation of surface waves in a granular material, J. Geophys. Res., 68, 6317-6321.

Kogan, S.Ya., 1966. A brief review of seismic wave absorption theories II, Izv. Earth Phys., English Trans, No. 11, 678-683.

Kolsky, H., 1956. The propagation of stress pulses in visco-elastic solids, Phil. Mag., (8), 1, 693-710.

Kovach, R.L. and R. Robinson, 1969. Upper mantle structure in the Basin and Range province, western North America, from apparent velocities of S waves, Bull. Seismol. Soc. Amer., 59, 1653-1665.

Kuriowa, D., 1954. Contributions from the Institute of Low Temperature Sciences, A(18), 1.

Lamb, G.L., Jr., 1962. The attenuation of waves in a dispersive medium, J. Geophys. Res., 67, 5273-5277.

Lancsoz, C., 1961. Linear Differential Operators, D. Van Nostrand, 564 pp.

Landau, L.D. and E.M. Lifshitz, 1960. Electrodynamics of Continuous Media, Pergamon Press, London, 417 pp.

Lee, W.B. and S.C. Solomon, 1975. Inversion schemes for surface wave attenuation and Q in the crust and the mantle, Geophys. J. R. Astron. Soc., 43, 47-71.

Lee, W.B. and S.C. Solomon, 1977. Simultaneous inversion of surface wave phase velocity and attenuation: Love waves in western North America, J. Geophys. Res., in press.

Leeds, A., 1975. Lithospheric thickness in the western Pacific, Phys. Earth Planet. Int., 11, 61-64.

Linsay, G., 1914. A study of the longitudinal vibration of waves, Phys. Rev., 3, 397-438.

Liu, H.-P., D.L. Anderson, and H. Kanamori, 1976. Velocity dispersion due to anelasticity; implications for seismology and mantle composition, Geophys. J. R. Astr. Soc., 47, 41-58, 1976.

Lomnitz, C., 1957. Linear dissipation in solids, J. Appl. Phys., 57, 201-205.

Lomnitz, C., 1962. Application of the logarithmic creep law to stress wave attenuation in the solid earth, J. Geophys. Res., 67, 365-368.

Marquart, D.W., 1963. An algorithm for least square estimation of non-linear parameters, J. Soc. Indust. Appl. Math., 11, 421-441.

Mavko, G. and A. Nur, 1975. Melt squirt in the asthenosphere, J. Geophys. Res., 80, 1444-1448.

McDonal, F.J., F.A. Angona, R.L. Mills, R.L. Sengbush, R.G. Van Nostrand, and J.E. White, 1958. Attenuation of shear and compressional waves in Pierre Shale, Geophysics, 23, 421-439.

McEvilly, T.V., 1964. Central United States crust-upper mantle structure from Love and Rayleigh wave phase velocity inversion, Bull. Seism. Soc. Amer., 54, 1997-2015.

McKavanagh, B. and F.D. Stacey, 1974. Mechanical hysteresis in rocks at low strain amplitudes and seismic frequencies, Phys. Earth Planet. Int., 8, 246-250.

Mitchell, B., 1973a. Radiation and attenuation of Rayleigh waves from the southeastern Missouri earthquake of October 21, 1965, J. Geophys. Res., 78, 886-899.

Mitchell, B., 1973b. Surface wave attenuation and crustal anelasticity in central North America, Bull. Seism. Soc. Amer., 63, 1057-1071.

Mitchell, B.J., 1975. Regional Rayleigh wave attenuation in North America, J. Geophys. Res., 80, 4904-4916.

Mitchell, B.J., 1976. Anelasticity of the crust and upper mantle beneath the Pacific Ocean from the inversion of observed surface wave attenuation, Geophys. J. R. Astr. Soc., 46, 521-533.

Mitchell, B.J., L.W.B. Leite, Y.K. Yu, and R.B. Herrmann, 1976. Attenuation of Love and Rayleigh waves across the Pacific at periods between 15 and 110 seconds, Bull. Seism. Soc. Amer., 66, 1189-1201.

Mizutani, H. and H. Kanamori, 1964. Vibration of elastic wave velocity and attenuative property near the melting temperature, J. Phys. Earth, 12, 43-49.

Morse, P.M. and H. Feshbach, 1953. Methods of Theoretical Physics, McGraw-Hill Co., New York, 1953.

North, R.G. and A.M. Dziewonski, 1976. A note on Rayleigh wave flattening corrections, Bull. Seism. Soc. Amer., 66, 1873-1879.

Norwick, A.S. and B.S. Berry, 1961. Log normal distribution function for describing anelastic and other relaxation processes, 1.2, IBM J. Res. Develop., 5, 297-320.

Nur, A., 1971. Viscous phase in rocks and the low-velocity zone, J. Geophys. Res., 76, 1270-1277.

Oliver, J. and B. Isacks, 1967. Deep earthquake zones, anomalous structures in the upper mantle and the lithosphere, J. Geophys. Res., 72, 4259-4275.

Orowan, E., 1967. Seismic damping and creep in the mantle, Geophys. J. R. Astr. Soc., 14, 191-218.

Papoulis, A., 1962. The Fourier Integral and Its Applications, McGraw-Hill, 318 pp.

Parker, R.L., 1972. Inverse theory with grossly inadequate data, Geophys. J. R. Astr. Soc., 29, 123-138.

Peselnick, L. and I. Zietz, 1959. Internal friction of fine grained limestones at ultrasonic frequencies, Geophysics, 24, 285-296.

Peselnick, L. and W.F. Outerbridge, 1961. Internal friction in shear and shear modulus of Solenhofen limestone over a frequency range of 10^7 cycles per second, J. Geophys., Res., 66, 581-588.

Pitmann, W.C., III, R.L. Parson, and E.M. Herron, 1974. Magnetic lineations of the oceans (Map), Lamont-Doherty Geological Obs., Columbia University, Palisades, N.Y.

Press, F., 1968. Earth models obtained by Monte Carlo inversion, J. Geophys. Res., 73, 5223-5234.

Press, F., 1970. Earth models consistent with geophysical data, Phys. Earth Planet. Int., 3, 3-22.

Randall, M.J., 1976. Attenuative dispersion and frequency shifts of the earth's free oscillations, Phys. Earth Planet. Int., 12, P1-P4, 1976.

Ricker, N., 1953. The form and laws of propagation of seismic wavelets, Geophysics, 18, 10-40.

Riez, R. and B. Nagy, 1965. Functional Analysis, Ungar, New York.

Sabatier, P.C., 1977a. Positivity constraints in linear inverse problems - I. General theory, Geophys. J. R. Astr. Soc., 48, 415-442.

Sabatier, P.C., 1977b. Positivity constraints in linear inverse problems - II. Applications, Geophys. J. R. Astr. Soc., 48, 443-460.

Savage, J.C., 1976. Anelastic degradation of acoustic pulses in rock - comments, Phys. Earth Planet. Int., 11, 284-285.

Savage, J.C. and H.S. Hasegawa, 1967. Evidence for a linear attenuation mechanism, Geophysics, 32, 1003-1014.

Savage, J.C. and M.E. O'Neil, 1975. The relation between the Lomnitz and Futterman theories of internal friction, J. Geophys. Res., 80, 245-251.

Schwab, F. and L. Knopoff, 1970. Surface-wave dispersion computations, Bull. Seism. Soc. Amer., 60, 321-344.

Schwab, F. and L. Knopoff, 1971. Surface waves on multilayered anelastic media, Bull. Seismol. Soc. Amer., 61, 893-912.

Schwab, F. and L. Knopoff, 1972. Fast surface wave and free mode computations, in Methods in Computational Physics, 11, B.A. Bolt (ed.), Academic Press, New York, 87-180.

Schwab, F. and L. Knopoff, 1973. Love waves and the torsional free modes of a multilayered anelastic sphere, Bull. Seismol. Soc. Amer., 63, 1107-1117.

Sclater, J.G., D. Karig, L.A. Lawver, and K. Louden, 1976. Heat flow, depth, and crustal thickness of the marginal basins of the south Philippine Sea, J. Geophys. Res., 81, 309-318.

Sen-Gupta, M.K., 1975. The structure of the earth's mantle from body wave observations, Sc.D. Thesis, Mass. Inst. of Techn., Cambridge, Mass. 542 pp.

Sipkin, S.A. and T.H. Jordan, 1975. Lateral heterogeneity of the upper mantle determined from the travel times of ScS, J. Geophys. Res., 80, 1474-1484.

Solomon, S.C., 1971. Seismic-wave attenuation and the state of the upper mantle, Ph.D. Thesis, Mass. Inst. of Techn., Cambridge, Mass., 321 pp.

Solomon, S.C., 1972a. Seismic-wave attenuation and partial melting in the upper mantle of North America, J. Geophys. Res., 77, 1483-1502.

Solomon, S.C., 1972b. On Q and seismic discrimination, Geophys. J. R. Astr. Soc., 31, 163-177.

Solomon, S.C., R.W. Ward, and M.N. Toksöz, 1970. Earthquake and explosion magnitudes: the effect of lateral variation of seismic attenuation, copy of paper presented at Woods Hole Conference on Seismic Discrimination, Vol. 1, Advanced Research Projects Agency, July 20-23.

Spetzler, H. and D.L. Anderson, 1968. The effect of temperature and partial melting on velocity and attenuation in a single binary system, J. Geophys. Res., 73, 6051-6060.

Stacey, F.D., M.T. Gladwin, B. McKavanagh, A.T. Linde, and L.M. Hastie, 1975. Anelastic damping of acoustic and seismic pulses, Geophys. Surv., 2, 133-151.

Strick,E., 1967. The determination of a dynamic viscosity and transient creep curves from wave propagation measurements, Geophys. J. R. Astr. Soc., 13, 197-218.

Tryggvason, E., 1965. Dissipation of Rayleigh wave energy, J. Geophys. Res., 70, 1449-1455.

Tsai, Y.B. and K. Aki, 1969. Simultaneous determination of the seismic moment and attenuation of seismic surface waves, Bull. Seism. Soc. Amer., 59, 275-287.

Utsu, T., 1966. Regional differences in absorption of seismic waves in the upper mantle as inferred from abnormal distributions of seismic intensities, J. Fac. Sci. Hokkaido Univ., Ser. 7, 2, 359-374.

Walsh, J.B., 1966. Seismic attenuation in rock due to friction, J. Geophys. Res., 71, 2591-2599.

Walsh, J.B., 1968. Attenuation in partially melted material, J. Geophys. Res., 73, 2209-2216.

Walsh, J.B., 1969. A new analysis of attenuation in partially melted rock, J. Geophys. Res., 74, 4333-4337.

Watts, A.B. and J.K. Weissel, 1977. Tectonic evolution of the south Fiji marginal basis, Island Arcs, Deep Sea Trenches and Back-Arc Basins, Maurice Ewing Series, Vol. 1, American Geophysical Union, 419-427.

Weissel, J.K., 1977. Evolution of the Lau Basin by the growth of small plates, Island Arcs, Deep Sea Trenches and Back-Arc Basins, Maurice Ewing Series, Vol, 1, American Geophysical Union, 429-436.

Weissel, J.K., A.B. Watts, A. Lapouille, G. Karner, and D. Jongsma, 1977. Preliminary results from recent geophysical investigations in marginal basins of Melanesia, EOS, Tran. Am. Geophys. Un., 58, 504.

Whittaker, E.T. and G.N. Watson, 1973. A Course in Modern Analysis, Cambridge University Press, Cambridge, England.

Wiggins, R.A., 1972. The general linear inverse problem: implication of surface waves and free oscillations for Earth structure, Rev. Geophys. Space Phys., 10, 251-285.

Zener, C.M., Elasticity and Anelasticity of Metals, Univ. of Chicago Press, Chicago, 180 pp, 1948.

Appendix I. Kramers-Krönig Relations (Ref: Landau and Lifschitz, 1960; Futterman, 1962; Papoulis, 1962)

A direct consequence of the causality principle, Kramers-Krönig relations relate the real and imaginary parts of the refractive index of the medium by integral transforms in the frequency domain. The causality principle states that no signal can travel faster than the signal velocity:

$$u(r,t) = 0 \qquad \text{for } t < \frac{r}{v_\infty} \equiv \tau \qquad \text{(A.I.1)}$$

where $u(r,t)$ is a displacement pulse and v_∞ is the signal velocity at frequencies above a cut-off frequency ω_c, above which it is assumed that no absorption occurs and thus the phase velocity is non-dispersive. Representing the pulse by a Fourier transform,

$$u(r,t) = \int_{-\infty}^{\infty} \bar{u}(r,\omega_1)\, e^{-i\omega_1 t}\, d\omega_1 \qquad \text{(A.I.2)}$$

Here the displacement $u(r,t)$ associated with seismic waves should be zero if $t < \tau$, but the Fourier component $\bar{u}(r,\omega)$ may not be zero at any time. Therefore, causality requires that these Fourier components must be combined in such a way that $u(r,t) = 0$ when $t < \tau$. A destructive interference for $t < \tau$ causes a frequency dependent phase velocity in the medium (dispersion). Now we are going to find a way to integrate equation (A.I.2) to meet causality. Equation (A.I.2) can be written as a superposition of plane waves in a complex representation of the form

$$u(r,t) = \int_{-\infty}^{\infty} \bar{u}(\omega_1)\, e^{ik(\omega_1)r - i\omega_1 t}\, d\omega_1 \qquad \text{(A.I.3)}$$

where $K(\omega_1)$ is the complex wave number. The index of refraction $n(\omega_1)$ of the medium is given as

$$n(\omega_1) = K(\omega_1)/K_o(\omega_1)$$

$$K_o(\omega_1) = \frac{1}{v_\infty}$$

where K_o defines the nondispersive behavior of K at the same frequency. Since we have assumed that no absorption occurs above the cut-off frequency ω_c, Im $n(\omega_c) = 0$ and Re $n(\omega_c) = 1$.

The inversion of the integral (A.I.3) gives

$$\bar{u}(\omega_1)\, e^{ik(\omega_1)r} = \frac{1}{2\pi} \int_{-\infty}^{\infty} u(r,t)\, e^{i\omega_1 t}\, dt$$

Invoking the causality condition (A.I.1)

$$\bar{u}(\omega_1)\, e^{ik(\omega_1)r} = \frac{1}{2\pi} \int_{-\infty}^{\infty} u(r,t)\, e^{i\omega_1 t}\, dt \qquad \text{(A.I.4)}$$

Define $\rho = t - \tau$.

$$\bar{u}(\omega_1)\, e^{ik(\omega_1)r} = \frac{1}{2\pi} \int_0^{\infty} u(r,\rho+\tau)\, e^{i\omega_1\rho} e^{i\omega_1\tau}\, d\rho$$

Using $K(\omega_1) = n(\omega_1)\omega_1/v_\infty$ and $\tau = r/v_\infty$,

$$\therefore\ \bar{u}(\omega_1)\, e^{i\zeta(\omega_1)r} = \frac{1}{2\pi} \int_0^{\infty} u(r,\rho+\tau)\, e^{i\omega_1\rho}\, d\rho \qquad \text{(A.I.5)}$$

where

$$\zeta(\omega_1) = \omega_1/v_\infty[n(\omega_1)-1]$$

Since $\rho \geq 0$, we define a new function $\phi(\omega)$ identical in form with the left hand side of (A.I.5), where ω_1 is replaced by a complex ω, $\omega = \omega_1 + i\omega_2$.

$$\phi(\omega) = \bar{u}(\omega)\, e^{i\zeta(\omega)r} = \frac{1}{2\pi} \int_0^{\infty} u(r,\rho+\tau)\, e^{i\omega\rho}\, d\rho \qquad \text{(A.I.6)}$$

The analyicity of $e^{i\zeta(\omega)r}$ in the upper half plane of frequency for $r \geq 0$ follows easily from (A.I.6), due to the factor $e^{-\omega_2\rho}$. Although we do not go into the rigorous proof here, it is not difficult to show that the exponent $\zeta(\omega)$ itself is analytic in the upper half plane u.h.p. from the analyticity of $e^{i\zeta(\omega)r}$. Because of the analyticity of $\zeta(\omega)$, we can apply Canchy's residue theorem. Now we can write

$$\zeta(\omega) = \frac{\omega}{V_\infty} \Delta n(\omega)$$

where $\Delta n(\omega) = n(\omega) - 1$

Now $\Delta n(\omega)$ is analytic in the u.h.p. of frequency, so that Canchy's residue theorem can be written as

$$\Delta n(\omega) = \frac{1}{i\pi} p \int_{-\infty}^{\infty} \frac{\Delta n(\omega)}{\omega - \omega_1} d\omega \qquad \text{(A.I.7)}$$

where P denotes the Canchy principal value. From eq. (A.I.7.), the expressions for the real and imaginary parts are

$$\mathrm{Re}\ \Delta n(\omega_1) = \frac{1}{\pi} p \int_{-\infty}^{\infty} \frac{\mathrm{Im}\Delta n(\omega)}{\omega - \omega_1} d\omega \qquad \text{(A.I.8)}$$

$$\mathrm{Im}\Delta n(\omega_1) = -\frac{1}{\pi} p \int_{-\infty}^{\infty} \frac{\mathrm{Re}\Delta n(\omega)}{\omega - \omega_1} d\omega \qquad \text{(A.I.9)}$$

Since $\mathrm{Im}\ n(\omega_c) = 0$, Equation (A.I.8) becomes

$$\mathrm{Re}[n(\omega)-1] = \frac{1}{\pi} p \int_{-\infty}^{\infty} \frac{\mathrm{Im}\Delta n(\omega)}{\omega - \omega_1} d\omega \qquad \text{(A.I.10)}$$

From equation (A.I.3), since the displacement is a real function of position and time, the crossing symmetry relationship holds, $K(\omega) = K^*(-\omega)$

and subsequently, $n(\omega) = n^*(-\omega)$

$$\begin{aligned} \text{Re } n(\omega) &= \text{Re } n(-\omega) \\ \text{Im } n(\omega) &= -\text{Im } n(-\omega) \end{aligned} \tag{A.I.11}$$

Using (A.I.11), equation (A.I.10), can be written as

$$\text{Re}[n(\omega_1)] - 1 = \frac{2}{\pi} \, p \int_0^\infty \frac{\text{Im } n(\omega)}{\omega^2 - \omega_1^2} \, d\omega \tag{A.I.12}$$

with the result $p \int_{-\infty}^{\infty} \frac{d\omega}{\omega - \omega_1} = 0$, equation (A.I.9) becomes,

$$\text{Im } n(\omega_1) = -\frac{1}{\pi} \, p \int_{-\infty}^{\infty} \frac{\text{Re } n(\omega)}{\omega - \omega_1} \, d\omega \tag{A.I.13}$$

Similarly using crossing symmetry relations, equation (A.I.13) can be written as

$$\text{Im } n(\omega_1) = -\frac{2\omega_1}{\pi} \, p \int_0^\infty \frac{\text{Re } n(\omega)}{\omega^2 - \omega_1^2} \, d\omega \tag{A.I.14}$$

Equations (A.I.10) and (A.I.13) or (A.I.12) and (A.I.14) are known as Kramers-Krönig relations.

APPENDIX II. Dispersion Relations: Frequency Domain Approach

The complex wave number $K(\omega)$ can be expressed in terms of the phase coefficient k and the attenuation coefficient χ:

$$K(\omega) = k(\omega) + i\chi(\omega) \qquad \text{(A.II.1)}$$

The index of refraction of the medium is

$$n(\omega) = \frac{K(\omega)}{K_\infty} = \frac{k(\omega) + i\chi(\omega)}{\omega/v_\infty} \qquad \text{(A.II.2)}$$

where K_∞, v_∞ are the non-dispersive limits of K and v, respectively, and v is the phase velocity.

Usually for the frequency-domain approach, the attenuation coefficient $\chi(\omega)$ is assumed to have a certain frequency dependence.

$$\chi(\omega) = C_1\omega \text{ or } C_2\omega^{1-\nu} \qquad \text{where } 0 < \nu < 1.$$

$$\text{Therefore } \operatorname{Im} n(\omega) = \frac{\chi(\omega)v_\infty}{\omega}$$

$$= C_1 \text{ or } C_2\omega^{-\nu} \qquad \text{(A.II.3)}$$

From the Kramers-Krönig relations (Appendix I)

$$\operatorname{Re}[n(\omega_1)] - 1 = \frac{2}{\pi} P \int_0^\infty \frac{\operatorname{Im} n(\omega)}{\omega^2-\omega_1^2}\omega d\omega$$

This integral can be evaluated for (A.II.3),

$$\left.\begin{aligned} \mathrm{Re}[n(\omega_1)] - 1 &= -\frac{C_1}{\pi} \ln\omega_1, & \nu = 0 \\ \text{or} \qquad &= C_2\omega_1^{-\nu} \cot\frac{\pi\nu}{2}, & \nu \neq 0 \end{aligned}\right\} \qquad \text{(A.II.4)}$$

(Whittaker and Watson, 1962, p. 117).

The phase velocity and the reciprocal quality factor can be written as

$$\begin{aligned} v(\omega) &= \frac{\omega}{k(\omega)} = \frac{v_\infty}{\mathrm{Re}\; n(\omega)} \\ Q^{-1}(\omega) &= \frac{2\chi(\omega)v_\infty}{\omega} = 2\; \mathrm{Im}\; n(\omega) \end{aligned} \qquad \text{(A.II.5)}$$

Therefore, the dispersion relations are given substituting (A.II.3) and (A.II.4) into (A.II.5). And we obtain,

$$v(\omega)/v_\infty = \begin{cases} \left(1 - \frac{C_1}{\pi} \ln\omega\right)^{-1}, & \nu = 0 \\ \dfrac{1}{1 + C_2\omega^{-\nu}\cot\frac{\pi\nu}{2}}, & \nu \neq 0 \end{cases}$$

In this case $n(\infty) = 1$ because the reference non-dispersive behavior is at infinite frequency.

$$Q^{-1}(\omega) = \begin{cases} 2\; C_1, & \nu = 0 \\ 2\; C_2\omega^{-\nu} & \nu \neq 0 \end{cases}$$

where $C_1 = Q_o^{-1}$, $C_2 = \frac{1}{2} qa^{\nu}(\nu-1)! \sin \frac{\pi\nu}{2}$.

APPENDIX III. Dispersion Relations: Time Domain Approach

(Lomnitz, 1957; Liu *et al*., 1976)

For the time-domain approach, the creep function $\phi(t)$ is furnished to derive dispersion relations. Generally, the one-dimensional stress-strain relation is given by Boltzmann's after-effect equation,

$$\varepsilon(t) = \frac{1}{M_u}\left\{\sigma(t) + \int_{-\infty}^{t} \sigma(\tau)\,\dot{\phi}(t-\tau)\,d\tau\right\} \qquad \text{(A.III.1)}$$

where M_u is an unrelaxed elastic modulus and $\sigma(t)$ is the given loading stress. Since $\dot{\phi} = 0$ for $t < 0$, (A.III.1) can be written as a convolution,

$$\varepsilon(t) = \frac{1}{M_u}\left\{\sigma(t) + \sigma(t) * \dot{\phi}(t)\right\} \qquad \text{(A.III.2)}$$

For a plane wave, $\sigma = \sigma_o e^{i(kx-\omega t)}$ and from (A.III.1)

$$\varepsilon(t) = \frac{\sigma(t)}{M_u}\left\{1 + \int_0^{\infty} \dot{\phi}(\tau) e^{i\omega\tau}\,d\tau\right\} \qquad \text{(A.III.3)}$$

Therefore, a complex modulus $M(\omega)$ is given as

$$M(\omega) = M_u / \left[1 + \int_0^{\infty} \dot{\phi}(\tau) e^{i\omega\tau}\,d\tau\right] \qquad \text{(A.III.4)}$$

From the equation of motion, $\rho\ddot{u} = \frac{\partial\sigma}{\partial x}$

$$\rho\omega^2 = K(\omega)^2 M(\omega) \qquad \text{(A.III.5)}$$

$$K(\omega) = \omega\sqrt{\rho/M(\omega)} \qquad \text{(A.III.6)}$$

using (A.II.1), (A.III.4) and (A.III.6),

$$v(\omega) = v_\infty / \mathrm{Re}\,\{1 + \int_0^\infty \dot{\phi}(t) e^{i\omega t} dt\}^{1/2}$$

$$Q^{-1}(\omega) = \frac{2\mathrm{Im}\, M(\omega)}{\mathrm{Re} M(\omega)} = \frac{2\mathrm{Im}\{\int_0^\infty \dot{\phi}(t) e^{i\omega t} dt\}}{1 + \mathrm{Re}\{\int_0^\infty \dot{\phi}(t) e^{i\omega t} dt\}}$$

where $v_\infty = \sqrt{M_u/\rho}$.

For the case of the Jeffrey-Lomnitz law,

$$\phi(t) = \frac{q}{\nu}\,[(1+at)^\nu - 1]$$

$$\dot{\phi}(t) = qa(1+at)^{\nu-1}$$

Let

$$I \equiv \int_0^\infty \dot{\phi}(t) e^{i\omega t} dt = qa \int_0^\infty (1+at)^{\nu-1} e^{i\omega t} dt$$

Putting $(1+at) = \rho$,

$$I = qa \int_0^\infty \rho^{\nu-1} e^{i\frac{\omega}{a}(\rho-1)} \frac{d\rho}{a}$$

$$\simeq q \int_0^\infty \rho^{\nu-1}\, e^{i\frac{\omega}{a}\rho} \qquad \text{for } \frac{\omega}{a} \text{ small (Jeffreys, 1975).}$$

Putting $k = -i(\frac{\omega}{a})$,

$$I = qk^{-\nu}[k^\nu \int_0^\infty \rho^{\nu-1} e^{-k\rho} d\rho]$$

$$= qk^{-\nu}\Gamma(\nu), \quad \text{where } \Gamma(\nu) \text{ is the Gamma function.}$$

$$I = qa^{\nu}\omega^{-\nu}(-i)^{-\nu}\Gamma(\nu)$$

$$= qa^{\nu}\omega^{-\nu}e^{i\frac{\pi\nu}{2}}\Gamma(\nu)$$

Therefore

$$v(\omega)/v_{\infty} = 1/(1 + qa^{\nu}\omega^{-\nu}(\nu-1)!\cos\frac{\pi\nu}{2}) = 1/(1 + C\omega^{-\nu}\cot\frac{\pi\nu}{2})$$

$$Q^{-1}(\omega) = \frac{2qa\nu\omega^{-\nu}(\nu-1)!\sin\frac{\pi\nu}{2}}{1 + qa^{\nu}\omega^{-\nu}(\nu-1)!\cos\frac{\pi\nu}{2}} \cong 2C\omega^{-\nu} \quad \text{for q small,}$$

where

$$C = qa^{\nu}(\nu-1)!\sin\frac{\pi\nu}{2}$$

APPENDIX IV. Partial Derivatives at a Reference Frequency

Using equation (5.18), partial derivatives at a reference frequency can be given as follows. For convenience, the symbols β_1^o, β_2^o, α_1^o, and α_2^o are used for β_1, β_2, α_1, α_2, respectively, at the reference frequency.

$$\left(\frac{\partial c_1}{\partial \beta_1^o}\right)_{ij} = \left(\frac{\partial c_1}{\partial \beta_1}\right)_{ij} \tag{A.IV.1}$$

$$\left(\frac{\partial c_1}{\partial \beta_2^o}\right)_{ij} = \left(\frac{\partial c_1}{\partial \beta_1}\right)_{ij} g_i + \left(\frac{\partial c_1}{\partial \beta_2}\right)_{ij} h_i \tag{A.IV.2}$$

$$\left(\frac{\partial c_2}{\partial \beta_1^o}\right)_{ij} = \left(\frac{\partial c_2}{\partial \beta_1}\right)_{ij} = -\left(\frac{\partial c_1}{\partial \beta_2}\right)_{ij} \tag{A.IV.3}$$

$$\begin{aligned}\left(\frac{\partial c_2}{\partial \beta_2^o}\right)_{ij} &= \left(\frac{\partial c_2}{\partial \beta_1}\right)_{ij} g_i + \left(\frac{\partial c_2}{\partial \beta_2}\right)_{ij} h_i \\ &= \left(\frac{\partial c_1}{\partial \beta_2}\right)_{ij} g_i + \left(\frac{\partial c_1}{\partial \beta_1}\right)_{ij} h_i\end{aligned} \tag{A.IV.4}$$

$$\left(\frac{\partial c_1}{\partial \alpha_2^o}\right)_{ij} = \left(\frac{\partial c_1}{\partial \alpha_1}\right)_{ij} \tag{A.IV.5}$$

$$\left(\frac{\partial c_1}{\partial \alpha_2^o}\right)_{ij} = \left(\frac{\partial c_1}{\partial \alpha_1}\right)_{ij} g_i + \left(\frac{\partial c_1}{\partial \alpha_2}\right)_{ij} h_i \tag{A.IV.6}$$

$$\left(\frac{\partial c_2}{\partial \alpha_2^o}\right)_{ij} = \left(\frac{\partial c_2}{\partial \alpha_1}\right)_{ij} = -\left(\frac{\partial c_1}{\partial \alpha_2}\right)_{ij} \tag{A.IV.7}$$

$$\begin{aligned}\left(\frac{\partial c_2}{\partial \alpha_2^o}\right)_{ij} &= \left(\frac{\partial c_2}{\partial \alpha_1}\right)_{ij} g_i + \left(\frac{\partial c_2}{\partial \alpha_2}\right)_{ij} h_i \\ &= -\left(\frac{\partial c_1}{\partial \alpha}\right)_{ij} g_i + \left(\frac{\partial c_1}{\partial \alpha_1}\right)_{ij} h_i\end{aligned} \tag{A.IV.8}$$

The last steps of equation (A.IV.3), (A.IV.4), (A.IV.7), and (A.IV.8) are the consequence of Cauchy-Riemann relations (5.11). From dispersion relations (4.8) and (4.10)

$$g_i = \begin{cases} \frac{2}{\pi} \ln\,(\omega/\omega_o) & \text{for constant } Q \\ \cot 1/2\pi\alpha(1-(\omega/\omega_o)^{-\nu}) & \text{for power law } Q \end{cases}$$

$$h_i = \begin{cases} 1 & \text{for constant } Q \\ (\omega/\omega_o)^{-\nu} & \text{for power law } Q \end{cases}$$

For the case of constant Q, with the inversion at a reference frequency, the matrix equation (5.6) for Love waves becomes

$$\begin{pmatrix} \Delta c_1 \\ \\ \Delta c_2 \end{pmatrix}_i = \begin{pmatrix} \frac{\partial c_1}{\partial \beta_1^o} & \frac{\partial c_1}{\partial \beta_2^o} \\ \\ \frac{\partial c_2}{\partial \beta_1^o} & \frac{\partial c_2}{\partial \beta_2^o} \end{pmatrix}_{ij} \begin{pmatrix} \Delta\beta_1 \\ \\ \Delta\beta_2 \end{pmatrix}_{\omega_o,j} \tag{A.IV.9}$$

$$= \begin{pmatrix} \frac{\partial c_1}{\partial \beta_1} & \frac{\partial c_1}{\partial \beta_1} g + \frac{\partial c_1}{\partial \beta_2} h \\ \\ -\frac{\partial c_1}{\partial \beta_2} & \frac{\partial c_1}{\partial \beta_1} h - \frac{\partial c_1}{\partial \beta_2} g \end{pmatrix}_{ij} \begin{pmatrix} \Delta\beta_1 \\ \\ \Delta\beta_2 \end{pmatrix}_{\omega_o,j}$$

$$= \left(\frac{\partial c_1}{\partial \beta_1}\right)_{ij} \begin{pmatrix} 1 & g + \delta h \\ -\delta & h - g\delta \end{pmatrix}_{ij} \begin{pmatrix} \Delta\beta_1 \\ \Delta\beta_2 \end{pmatrix}_{\omega_o, j}$$

where $\delta = \frac{\partial c_1}{\partial \beta_2} / \frac{\partial c_1}{\partial \beta_1}$.

For Rayleigh waves, the matrix equation (5.7) becomes

$$\begin{pmatrix} \Delta c_1 \\ \\ \Delta c_2 \end{pmatrix}_i = \begin{pmatrix} \frac{\partial c_1}{\partial \beta_1^o} & \frac{\partial c_1}{\partial \beta_2^o} & \frac{\partial c_1}{\partial \alpha_1^o} & \frac{\partial c_1}{\partial \alpha_2^o} & \frac{\partial c_1}{\partial \rho} \\ \\ \frac{\partial c_2}{\partial \beta_1^o} & \frac{\partial c_2}{\partial \beta_2^o} & \frac{\partial c_2}{\partial \alpha_1^o} & \frac{\partial c_2}{\partial \alpha_2^o} & \frac{\partial c_2}{\partial \rho} \end{pmatrix}_{ij} \begin{pmatrix} \Delta\beta_1 \\ \Delta\beta_2 \\ \Delta\alpha_1 \\ \Delta\alpha_2 \\ \Delta\rho \end{pmatrix}_{\omega_o, j}$$

$$= \left(\left(\frac{\partial c_1}{\partial \beta_1}\right) \begin{pmatrix} 1 & g+\delta h \\ -\delta & h-g\delta \end{pmatrix}, \left(\frac{\partial c_1}{\partial \alpha_1}\right) \begin{pmatrix} 1 & g+\delta h \\ -\delta & h-g\delta \end{pmatrix}, \begin{pmatrix} \frac{\partial c_1}{\partial \rho} \\ \frac{\partial c_2}{\partial \rho} \end{pmatrix} \right)_{ij} \begin{pmatrix} \Delta\beta_1 \\ \Delta\beta_2 \\ \Delta\alpha_1 \\ \Delta\alpha_2 \\ \Delta\rho \end{pmatrix}_{\omega_o, j}$$

where $\delta = \frac{\partial c_1}{\partial \alpha_2} / \frac{\partial c_1}{\partial \alpha_1}$.

APPENDIX V. Comparison Between Simultaneous Inversion and the Correction Technique of Anderson and Hart

The procedure of Anderson and Hart differs in several fundamental respects from a complete simultaneous inversion.

1) Their procedure adopts as given a Q model determined by a separate inversion based on an elastic velocity model. The adopted Q model is used to correct phase velocity (eigenperiod) data for intrinsic dispersion.

The simultaneous inversion takes both Q and velocity as unknowns.

2) Their procedure neglects the contribution from 'off-diagonal' terms in the partial derivative matrix (5.6). These terms are usually coupled with g_i, a measure of dispersion (Appendix IV). Since g_i can be large when observed frequencies are far from the reference frequency, the contribution from 'off-diagonal' related terms may not be small.

We illustrate these differences with an example: the problem of finding two-layer models of shear velocity and attenuation from two observational pairs (phase velocity and attenuation), under the assumption that Q is independent of frequency. For the Anderson-Hart Q-correction procedure

$$\begin{pmatrix} A & B \\ C & D \end{pmatrix} \begin{pmatrix} (\Delta\beta_1, \Delta\beta_2)_o \\ (\Delta\beta_1, \Delta\beta_2)_q \end{pmatrix} = \begin{pmatrix} (\Delta c_1, \Delta c_2)_m \\ (\Delta c_1, \Delta c_2)_n \end{pmatrix} \qquad \text{(A.V.1)}$$

where $(\Delta\beta_1, \Delta\beta_2)_j$ are the model pairs for the j-th layer and $(\Delta c_1, \Delta c_2)_i$ are the i-th observational pairs. A, B, C, D are an abbreviated notation for partial derivatives; e.g. $A = \frac{\partial(c_1)_m}{\partial(\beta_1)_p}$. For the simultaneous inverse problem, from Appendix IV.

$$\begin{pmatrix} A\begin{pmatrix} 1 & gm-\delta \\ \delta & 1+g_m\delta \end{pmatrix} & B\begin{pmatrix} 1 & g_m+\delta \\ -\delta & 1-g_m\delta \end{pmatrix} \\ & \\ C\begin{pmatrix} 1 & g_n+\delta \\ -\delta & 1-g_n\delta \end{pmatrix} & D\begin{pmatrix} 1 & g_n-\delta \\ \delta & 1+g_n\delta \end{pmatrix} \end{pmatrix} \begin{pmatrix} \begin{pmatrix} \Delta\beta_1 \\ \Delta\beta_2 \end{pmatrix}_p \\ \\ \begin{pmatrix} \Delta\beta_1 \\ \Delta\beta_2 \end{pmatrix}_q \end{pmatrix} = \begin{pmatrix} \begin{pmatrix} \Delta c_1 \\ \Delta c_2 \end{pmatrix}_m \\ \\ \begin{pmatrix} \Delta c_1 \\ \Delta c_2 \end{pmatrix}_n \end{pmatrix}$$

where $\delta = \frac{\partial c_1}{\Delta\beta_2} / \frac{\partial c_1}{\Delta\beta_1}$. Here δ is used as a single value for simplicity, although it may vary in different layers and different frequencies. Thus

$$\begin{aligned}(\Delta\beta_1)_{p,S} = {} & (\Delta\beta_1)_{p,QC} + g\ F_1((\Delta c_2)_i) + g\ \Delta g\delta F_2((\Delta c_2)_i) \\ & + g\delta F_3((\Delta c_1)_i) + \Delta g\delta F_4((\Delta c_1)_i) + O(\delta)\end{aligned}$$

$$\text{(A.V.2)}$$

$$(\Delta\beta_2)_{p,S} = (\Delta\beta_2)_{p,QC} + \delta\Delta g G_1((\Delta c_2)_i) + \delta G_2((\Delta c_1)_i) + O(\delta^2)$$

where

$$\Delta g = g_n - g_m$$

$$F_1((\Delta c_2)_i) = ((\Delta c_2)_m D g_1)/(AD-BC)$$

$$F_2((\Delta c_2)_i) = 2\ \{(\Delta c_2)_n A - (\Delta c_2)_m C\}\ BD/(AD-BC)$$

$$F_3((\Delta c_1)_i) = ((\Delta c_1)_m D - (\Delta c_1)_n B)/(AD-BC)$$

$$F_4((\Delta c_1)_i) = ((\Delta c_1)_m D - (\Delta c_1)_n B)/(AD-BC)$$

$$G_1((\Delta c_2)_i) = 2\ \{(\Delta c_1)_n A - (\Delta c_2)_m C\}\ BD/(AD-BC)$$

$$G_2((\Delta c_1)_i) = ((\Delta c_1)_n B - (\Delta c_1)_m D)$$

and where S stands for simultaneous inversion and QC stands for the Anderson-Hart Q correction technique. Similarly $(\Delta\beta_1, \Delta\beta_2)_q$ can be computed. The correction terms on the right-hand side of equation (A.V.2) are $O(g)$, $O(g\Delta g\delta)$, $O(g\delta)$, $O(\Delta g\delta)$, etc. The δ's are typically 0.05 (see Figure 6.7a) and and g's are 2-3 in our problem. g can be larger when the observational frequencies are even further from the reference frequency, taken as 1 Hz in this work. Δg is 1.1 for the Love wave data of western North America if Q is constant; it can be larger when the observational frequency band is wider.

4. PUBLICATIONS

July 1977 - December 1977

Burr, N. and S.C. Solomon, The relationship of source parameters of oceanic transform earthquakes to plate velocity and transform length, J. Geophys. Res., 83, 1193-1205, 1978.

Johnston, D.H., M.N. Toksöz and A. Timur, Attenuation of seismic waves in dry and saturated rocks, II. Mechanisms, Geophysics, in press, 1978.

Lee, W.B. and S.C. Solomon, Simultaneous inversion of surface wave phase velocity and attenuation: Love waves in western North America, J. Geophys. Res., in press, 1978.

Toksöz, M.N., E. Arpat and F. Saroglu, East Anatolian earthquake of 24 November 1976 - field observations, Nature, 270, 423-425, 1977.

Toksöz, M.N., J. Nabelek and E. Arpat, Source properties of the 1976 earthquake in E. Turkey: A comparison of field data and teleseismic results, Tectonophysics, in press, 1978.

Thesis

Lee, W.B., Simultaneous inversion of surface wave phase velocity and attenuation for continental and oceanic paths, Ph.D. Thesis, M.I.T., 274 pp, 1977.

Abstract

American Geophysical Union, Fall Annual Meeting, December 1977

Toksöz, M.N. and E. Arpat, Studies of premonitory phenomena preceding two large earthquakes in Eastern Turkey.